DECEMBER 2023 M.Sc. in Civil Engineering FETİHHAN UĞUR

REPUBLIC OF TÜRKİYE

GAZİANTEP UNIVERSITY

GRADUATE SCHOOL OF NATURAL & APPLIED SCIENCES

DESIGN AND OPTIMIZATION OF A SPHERICAL HYDROKINETIC TURBINE

M.Sc. THESIS

IN

CIVIL ENGINEERING

BY

FETİHHAN UĞUR

DECEMBER 2023

DESIGN AND OPTIMIZATION OF A SPHERICAL HYDROKINETIC TURBINE

M.Sc.

in

Civil Engineering

Gaziantep University

Supervisor

Prof. Dr. Mehmet İshak YÜCE

By

Fetihhan UĞUR

December 2023

DESIGN AND OPTIMIZATION OF A SPHERICAL HYDROKINETIC TURBINE

submitted by **Fetihhan UĞUR** in partial fulfillment of the requirements for the degree of Master of Science in **Civil Engineering, Gaziantep University** is approved by,

Prof. Dr. Çiğdem AYKAÇ
Director of the Graduate School of Natural and Applied Sciences ………..............

Prof. Dr. Nildem TAYŞİ
Head of the Department of Civil Engineering ………..............

Prof. Dr. Mehmet İshak YÜCE
Supervisor, Civil Engineering
Gaziantep University ………..............

Exam Date: 15 December 2023

Examining Committee Members:

Prof. Dr. Mehmet İshak YÜCE
Gaziantep University ………..............

Prof. Dr. Ali AYTEK
Gaziantep Islam Science and Techology University ………..............

Asst. Prof. Dr. Gökmen ÖZTÜRKMEN
Gaziantep University ………..............

I hereby declare that all information in this document has been obtained and presented in accordance with academic rules and ethical conduct. I also declare that, as required by these rules and conduct, I have fully cited and referenced all material and results that are not original to this work.

Fetihhan UĞUR

ABSTRACT

DESIGN AND OPTIMIZATION OF A SPHERICAL HYDROKINETIC TURBINE

UĞUR, Fetihhan
M.Sc. in Civil Engineering
Supervisor: Prof. Dr. Mehmet İshak YÜCE

December 2023
147 pages

Spherical hydrokinetic turbines are a relatively new technology with the ability to generate energy using fluid motion. The efficiency of these turbines depends greatly on their design. To maximize the performance of turbines, increase their efficiency and ensure environmental sustainability, their designs need to be optimized using simulation techniques. The scope of the thesis aims to increase energy production and improve efficiency by optimizing the design and operating parameters of hydrokinetic turbines. The turbine's geometry, airfoil, number of blades, and other design factors can greatly affect overall performance. Therefore, optimization algorithms and techniques should be used to determine the optimal design parameters. During optimization, the parameters of the spherical hydrokinetic turbine designed using the Computational Fluid Dynamics technique were optimized using certain algorithms. The simulations were used to evaluate energy production and efficiency. In this way, the theoretical performance of the turbines was determined in advance and the necessary optimizations were made. As a result of the research, the turbine model with the best variation among the available parameters was determined.

Keywords: Renewable Energy, Hydrokinetic Energy, Spherical Hydrokinetic Turbines, Computational Fluid Dynamic

ÖZET

KÜRESEL HİDROKİNETİK TÜRBİNİN TASARIMI VE OPTİMİZASYONU

UĞUR, Fetihhan
Yüksek Lisans Tezi, İnşaat Mühendisliği
Danışman: Prof. Dr. Mehmet İshak YÜCE
Aralık 2023

147 sayfa

Küresel hidrokinetik türbinler, akışkan hareketini kullanarak enerji üretme yeteneği olan, görece yeni bir teknolojidir. Bu türbinlerin verimlilikleri, tasarımlarına büyük ölçüde bağlıdır. Türbinlerin performansını en üst düzeye çıkarmak, verimliliklerini artırmak ve çevresel sürdürülebilirliği sağlamak için simülasyon tekniklerini kullanarak tasarımlarının optimize edilmesi gerekmektedir. Tez kapsamında, hidrokinetik türbinlerin tasarım ve işletme parametrelerini optimize ederek enerji üretimini artırmayı ve verimliliğin daha iyi hale getirilmesi amaçlanmıştır. Türbinin geometrisi, kanat profili, kanat sayısı ve diğer tasarım faktörleri, genel performansı büyük ölçüde etkileyebilir. Bu nedenle, en uygun tasarım parametrelerini belirlemek için optimizasyon algoritmaları ve teknikleri kullanılmalıdır. Optimizasyon sırasında, Hesaplamalı Akışkan Dinamiği tekniği kullanılarak tasarlanan küresel hidrokinetik türbinde, parametreler belirli algoritmalar kullanılarak optimize edilmiştir. Yapılan simülasyonlar, enerji üretimini ve verimliliği değerlendirmek için kullanılmıştır. Bu sayede, türbinlerin teorik olarak nasıl performans göstereceği önceden tespit edilmiş ve gerekli optimizasyonlar yapılmıştır. Araştırma sonucunda, elde bulunan parametreler arasından en iyi varyasyona sahip türbin modelini belirlenmiştir.

Anahtar Kelimeler: Yenilenebilir Enerji, Hidrokinetik Enerji, Küresel Hidrokinetik Türbinler, Hesaplamalı Akışkan Dinamiği.

''Dedicated to my dear family''

ACKNOWLEDGEMENTS

I express deep gratitude to my supervisor, Prof. Dr. Mehmet İshak YÜCE, for his sacrifice, high dedication, and valuable guidance in my thesis work and academic progress. The knowledge, sincerity, and constant encouragement of Prof. Dr. YÜCE have played a critical role in the successful completion of this study. Being his student is a great honor and privilege for me. I thank him for his contributions.

I wish to express deep gratitude to my wife, E. Nilüfer Uğur, who has been a constant support throughout the thesis process and stood by my side. Her patience, and courage played a pivotal role in propelling me forward during this journey. I thank her for always being there for me.

TABLE OF CONTENTS

Page

LIST OF TABLES

LIST OF FIGURES

Page

LIST OF SYMBOLS

A Area

Ad Actuator disc area

c Chord length

Cd Drag coefficient

Cl Lift coefficient

Cl/Cd Lift/drag ratio

Cp Power coefficient

D Drag force

k Turbulent kinetic energy

L Lift force

m Mass

P Pressure

P Power

Patm Atmospheric pressure

Q Mass flow rate

R Radius of 2D turbine

Re Reynolds number

RPM Revolutions per minute

Sk Skewness

T Thrust

T	Temperature
U	Velocity
α	Angle of attack
β	Pitch angle
ε	Efficiency
ε	turbulence dissipation rate
η	Overall efficiency
λ	Tip speed ratio
μ	Dynamic viscosity
ν	Kinematic viscosity
ρ	Density
σ	blade solidity
Ω	Angular velocity of rotor

BACKGROUND

Providing a clean and livable environment for future generations has become an increasingly common issue in today's world. The sustainability of natural life and the desire to leave a livable and unpolluted environment to future generations is an idea that most people take for granted. (Fay and Golumb, 2002). As energy demand continues to increase, the need for environmentally friendly and sustainable energy sources increases (Layman, 1998). The search for alternative energy sources has accelerated to meet this demand. It is well known that fossil fuel use contributes to environmental pollution, the greenhouse effect and CO2 emissions. In this context, renewable energies such as hydroelectricity, wind energy and solar energy can be considered as suitable options (Guney, 2005; Güney and Kaygusuz, 2010).

Hydroelectricity can be defined as a renewable energy source in which the kinetic and potential energy of water is converted into electrical energy. This method uses the kinetic energy of water to generate electricity. Hydroelectric energy production occurs by utilizing the kinetic energy of water or the potential energy of water falling from a height. Hydroelectric energy is generated by converting the kinetic energy of water into electrical energy through a turbine. Hydropower leaves a much lower carbon footprint compared to fossil fuels. Hydropower is an important issue in meeting global energy demand, leaving aside its environmental impacts. However, every hydroelectric project must be carefully examined and appropriate measures must be taken to minimize environmental impacts. In addition to playing a vital role in combating climate change, hydropower plays an important role in the transition to renewable sources for energy production and has significant potential for a sustainable energy future.

Hydropower can be divided into two main groups: hydrostatic energy and hydrokinetic energy. While hydrostatic energy means giving a certain potential to water and then proceeding to the energy production phase, hydrokinetic energy does not require giving a certain potential to water. The most well-known example of hydrostatic energy is dams. Dams increase the total mechanical energy by giving potential energy to water and increase the kinetic energy reaching the turbines (Khan et al., 2009). Dams are thought to have a low carbon footprint and are a sustainable energy source. However, there are significant cost and time requirements during construction and there are concerns about their impact on ecosystems.

Hydrokinetic energy stands out as an option that rapidly increases its potential. Hydrokinetic energy, unlike hydrostatic energy methods, converts the kinetic energy of water into electrical energy using certain mechanisms. Hydrokinetic energy, considered a renewable energy source, utilizes the gravitational forces acting on water. There are hydrokinetic energy methods that can use open channel systems, such as tidal movements in rivers and oceans. This type of energy uses turbine devices to convert mechanical energy into electrical energy. Hydrokinetic energy is a type of energy that differs from hydrostatic energy in that it does not need to transfer potential energy to water beyond its available kinetic energy. In addition, hydrokinetic energy takes up less space than other renewable energy sources, and as mentioned, construction costs are relatively lower since it does not require the transfer of potential energy to water. As a result, it has less impact on ecosystems. The issue of sustainability is a very important issue in hydrokinetic energy systems. Water flows and tides provide a constant source of energy, enabling hydrokinetic energy to produce electricity consistently and uninterruptedly. Rivers, streams and tides around the world offer rich potential for hydrokinetic energy. Although the general perception of hydrokinetic energy is not yet fully formed, the widespread use of this technology can be expected considering its advantages. Positive reviews, its renewable nature, minimal environmental impact, ease of installation and relatively low installation costs may lead to further investigation of the technology. However, reasons such as its immaturity, low efficiency and difficulties in location selection can be seen as disadvantages of this technology. Because hydrokinetic energy technology is still in development, some view its costs as high and its efficiency as low. However, as technology progresses, it is inevitable that costs will decrease and efficiency will increase, as in other new technologies. Monitoring the development of hydrokinetic energy and conducting the necessary research will contribute to its better inclusion among renewable energy sources. There are different types of turbines, classified according to their design for specific conditions. For example, the turbines used for tidal movements are significantly different from those used in open channel systems such as rivers. Turbine types are also used in closed and pressurized pipeline systems such as drinking water networks. Due to the differences in the designs of these turbines and their ongoing development stages, efficiency and improvement methods in hydrokinetic turbines are of great importance. Various methods can be used for improvements, with computational fluid dynamics being the most preferred method for hydrokinetic turbines. Computational fluid dynamics uses computer programs and mathematical methods to model and solve for the motion, temperature distribution, pressure, density, and other properties of fluids. Thanks to simulations, changes can be made in the turbines, and with this method, the turbines can be designed and optimized according to certain conditions.

CHAPTER I
INTRODUCTION

Increasing demand for energy, harmful environmental effects of traditional energy production technologies, increasing costs and depletion of fossil fuel reserves have led scientists and engineers to search for alternative, environmentally friendly, cost-effective and sustainable energy production methods (Yüce and Muratoğlu, 2015). Hydrokinetic energy has significant potential as a resource. Therefore, hydrokinetic energy offers one of the least environmentally damaging methods for large-scale electricity production (Bryden et al., 1998).

Hydrokinetic turbines are technologies that convert the kinetic energy of water flow into electrical energy. These turbines used to obtain energy from water flows such as rivers, streams and oceans in water-rich regions, have become an important component of environmentally friendly energy production. Hydrokinetic turbines cause less environmental impact by using the kinetic energy of water flow rather than accumulating potential energy by trapping water. The modularity and scalability of hydrokinetic devices are attractive features, in contrast to the relatively large, economically expensive and ecosystem-disrupting structures of dams (Ben Elghali et al., 2007). This technology could be an especially attractive option for coastal areas and island nations, as sea currents and tidal energy can provide a constant and reliable source of energy. Another advantage of hydrokinetic turbines is that they can minimize environmental impacts on natural aquatic ecosystems during energy production. However, some technical feasibility issues still need to be taken into account before widespread adoption (L.I Lago et al., 2010). Variables such as flow rates, water depths and environmental conditions can affect turbine performance. Therefore, the development and optimization of this technology requires continuous research and development efforts.

Hydrokinetic turbines are emerging as an important renewable energy source that can further contribute to the world's future energy production. This technology, which has the potential to meet energy needs while minimizing environmental impacts, offers an alternative path to a sustainable energy future. The studies carried out within the scope of the thesis are divided into sections and the contents of the sections are as follows;

In Chapter 2, the significance of the energy topic is highlighted. Information is provided about the need for energy, where energy is currently sourced from, and the global distribution of these sources. General overviews of renewable and non-renewable energy sources are presented, with a discussion on the future role of renewable energy.

In chapter 3, information about hydrokinetic turbines has been provided. The classification criteria for turbines have been conveyed. Research on Axial Flow Hydrokinetic turbines and Cross Flow Hydrokinetic turbines has been presented, discussing which types of turbines perform well under specific conditions. An introduction has been made regarding the thesis topic, which focuses on spherical hydrokinetic turbines.

In chapter 4, Information has been provided about airfoils and their types. In the theoretical section, emphasis has been placed on the theories and assumptions to be used in the design, and information has been given on potential issues that may be encountered in turbine design.

In chapter 5, historical milestones of finite element methods have been outlined. The significance and role of finite elements in computational fluid dynamics have been discussed. The purposes and types of methods have been conveyed. Information has been provided on how the examination of mesh particles should occur after their creation.

In Chapter 6, the importance and role of turbulence models in computational fluid dynamics are discussed. Various turbulence model types are introduced, and information related to research conducted on these models is summarized.

Chapter 7 covers the initial stage of the design, including hydrofoil selection and criteria. Various types of hydrofoil profiles have been modeled and analyzed, and the outputs have been examined to focus on selecting the best hydrofoil type.

In Chapter 8, various models have been created based on the best hydrofoil type identified in Chapter 7. The goal in this chapter is to determine the chord length of the hydrofoil and the number of blades constituting the turbine. During the modeling of the hydrofoils, power coefficients have been examined based on different solidity values, and as a result of the comparison, the optimum number of blades and chord length have been determined.

In Chapter 9, the final stage of the design, the twist angle parameter, which plays a significant role in spherical turbines, has been examined, and the appropriate twist angle has been selected. Inputs from Chapter 8 have been utilized, leading to the attainment of the ultimate optimum model.

In Chapter 10, a general overview summarizes the work conducted within the scope of the thesis. The results of the study are analyzed, and some points are highlighted for future research.

CHAPTER II
ENERGY

2.1 Energy

Energy can be defined in many ways, but it is almost impossible to give a precise definition of energy due to the multitude of its forms. The most widely accepted definition is as follows: Energy is the capacity of a system to do work. In physics, work is defined as the product of the displacement of the point of application of a force in the direction of the component of the force acting in that direction, and energy is measured in the same unit as work. From the earliest stages of human infancy stage to the present day, individuals' energy needs have fundamentally changed to become more complex and sophisticated. Ways to meet basic energy needs and the changes this energy shows over time require comprehensive research. Although the rough energy need has always changed throughout human history, these changes have sometimes exceeded expectations in certain periods of history. As seen in Figure 2.1, there has been an increase in the growth rate since 1950. Current energy demand is expected to increase even more in the coming years.

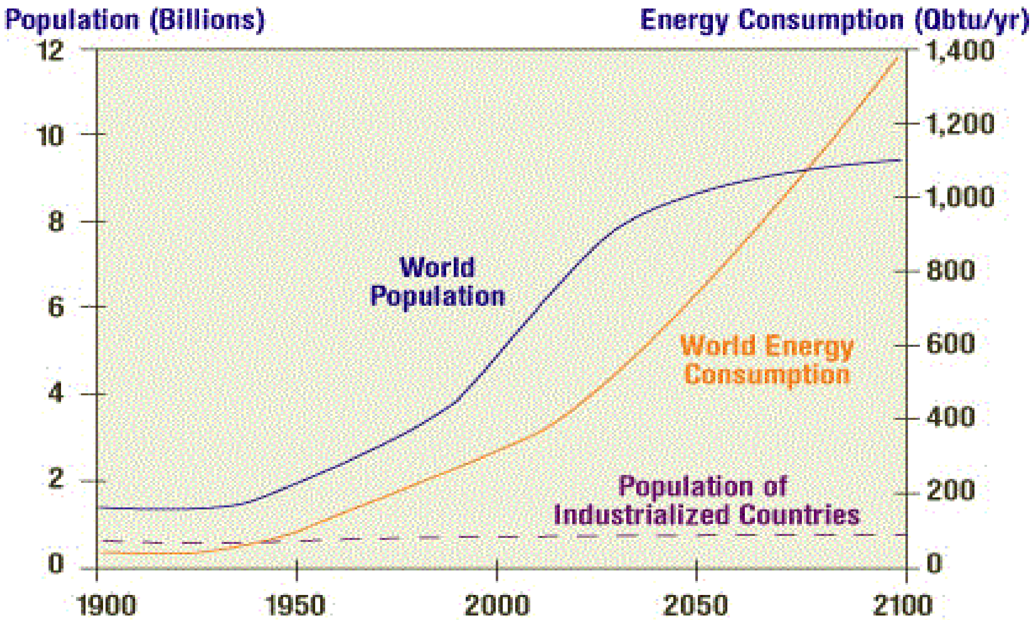

Figure 2.1 World population and energy demand growth (IEA, 2011)

Following the active use of electricity in the late 19th century, the spread of machines that make life easier in society, the changing perception of comfort in people and the resulting energy demand led to the discovery and development of the energy field. Another important issue is the efficiency of the devices used in energy consumption. For example, while the current efficiency of electricity generation in the early 20th century was around 5%, today the average efficiency in developed countries is around 36%, and the best combined cycle natural gas-fired power plants can reach this ratio over 50%. % productivity (Kaygusuz, 1999).

Table 2.1 Countries energy consumption (Stats. Review of World Energy,2022)

Unit:Exajoules	**Years**							
Countries	**1965**	**1975**	**1985**	**1995**	**2005**	**2015**	**2020**	**2021**
Canada	5.00	8.24	10.29	12.17	13.66	14.55	13.82	13.94
Mexico	1.06	2.14	4.08	5.07	6.78	7.72	6.43	6.79
U.S.	51.98	69.55	72.66	87.63	96.88	92.69	88.54	92.97
Brazil	0.99	2.80	4.81	6.89	9.08	12.40	12.00	12.57
Austria	0.68	1.01	1.14	1.32	1.53	1.42	1.44	1.48
France	4.71	7.25	8.67	10.37	11.35	10.11	8.86	9.41
Germany	10.69	13.55	15.45	14.31	14.27	13.60	12.36	12.64
Poland	2.79	4.39	5.28	3.99	3.83	4.00	4.08	4.44
Spain	1.21	2.65	3.32	4.39	6.41	5.67	5.18	5.59
Turkey	**0.33**	**0.84**	**1.39**	**2.56**	**3.59**	**5.77**	**6.44**	**6.83**
U. K	8.34	8.60	8.61	9.19	9.79	8.20	7.06	7.18
Iran	0.35	1.17	2.32	3.81	6.99	9.94	12.02	12.19
Iraq	0.08	0.19	0.52	1.26	1.11	1.57	1.99	2.12
Israel	0.15	0.27	0.35	0.70	0.88	0.99	1.03	1.05
Egypt	0.33	0.45	1.18	1.58	2.52	3.50	3.54	3.79
India	2.23	3.50	5.70	10.67	16.57	28.91	32.19	35.43
Japan	6.56	13.99	16.13	21.49	22.55	19.07	17.13	17.74
Average	5.734	8.270	9.524	11.612	13.399	14.124	13.771	14.480

Over time, the average lifespan of individuals has increased due to developments and increased productivity. Simultaneously, the significant increase in the world population has led to a versatile increase in energy demand (Demirbaş and Balat, 2006). Since life expectancy directly affects the population growth rate, the increasing world population not only increases the total number of individuals but also increases energy demand over time. It is possible to divide the resources required to meet this energy demand into two main groups: renewable energy and non-renewable energy.

2.2 Non-renewable Energy Sources

Non-renewable energy sources can be broadly divided into two main types: nuclear energy and fossil fuels. Fossil fuels are natural resources that contain high amounts of carbon in their structure. These energy sources obtained from the remains of living organisms include oil, coal and natural gas. Fossil fuels such as oil, natural gas and coal are concentrated energy sources that develop over long periods of time from animal and plant remains (Quaschning, 2009). Nuclear energy is obtained from the irregular structure of the atom. This type of energy has various storage requirements and falls into the category of non-renewable energy sources due to its non-renewable nature, limited structure and lack of reuse opportunities. Problems with fossil fuels, increasing interest in environmental protection, as well as social concerns about safety and health, contribute to making new and renewable energy technologies more attractive and attract more attention than non-renewable energy sources (Zhou et al., 2010).

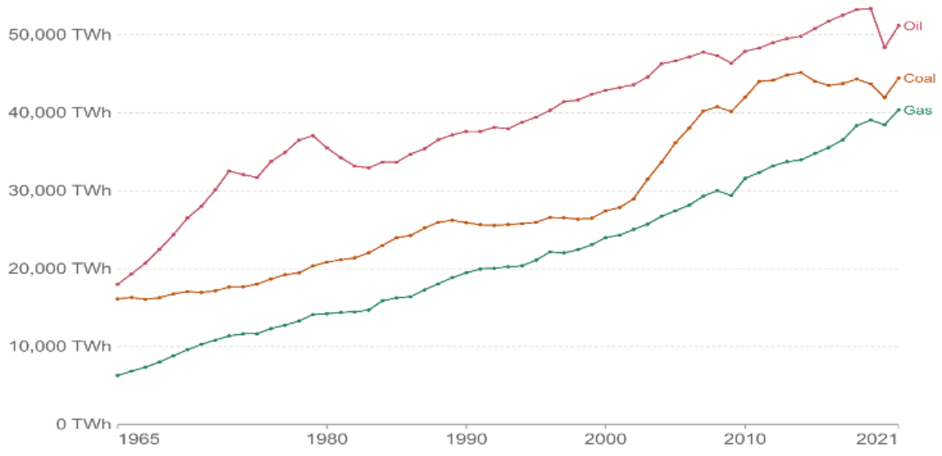

Figure 2.2 Fossil fuel Consumption over years (Our World in Data, 2022)

Non-renewable energy sources face a significant challenge as their production rates are significantly lower than their consumption rates. Additionally, the greenhouse effect and global environmental problems raise concerns for such energy sources (Kagazyo et al., 1997). As energy demand continues to increase, these resources decrease over time and cannot be easily renewed. When the use of fossil fuels is examined from 1965 to 2021, it is seen that there is a general increase in consumption. In those years, the slowdown in production due to the Covid-19 epidemic significantly reduced the use of these resources. When we look at the global distribution of fossil fuel use during this period, it is seen that the highest rate is in China, and the restrictions implemented during the pandemic period led to a decrease in total fossil fuel consumption.

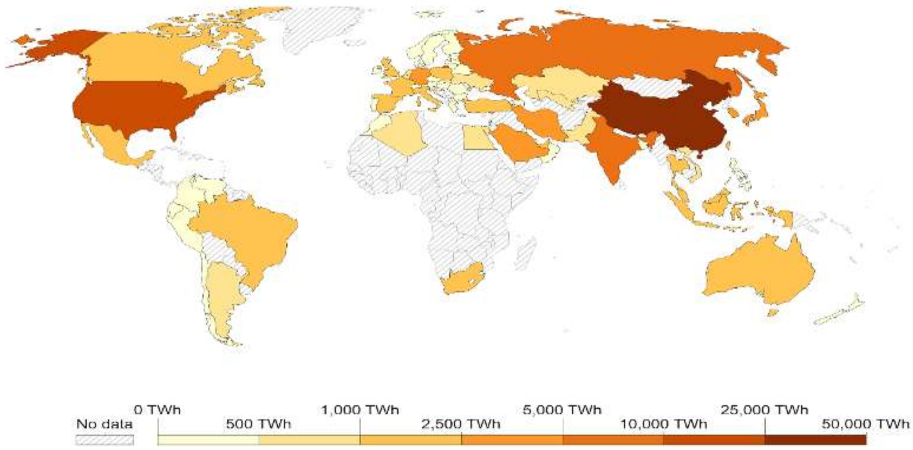

Figure 2.3 Fossil fuel Consumption over countries (Our World in Data, 2022)

2.2.1 Coal

From a content perspective, coal is a non-renewable energy source that consists of relatively low sulfur and nitrogen, containing carbon, hydrogen, and oxygen. It exhibits diversity in its composition based on the conditions of its formation. The majority of the world's reported coal reserves (250.9 billion tons), documented in approximately 80 countries by the World Energy Council, are located in the United States. Russia follows with 160.4 billion tons, and Australia with 144.8 billion tons. Among other coal-rich countries are China (138.8 billion tons), India (97.7 billion tons), Germany (36.1 billion tons), Ukraine (34.4 billion tons), Poland (25.8 billion tons), Kazakhstan (25.6 billion tons), and Indonesia (22.6 billion tons). Therefore, more than 90% of the world's coal reserves are within the borders of these nine countries.

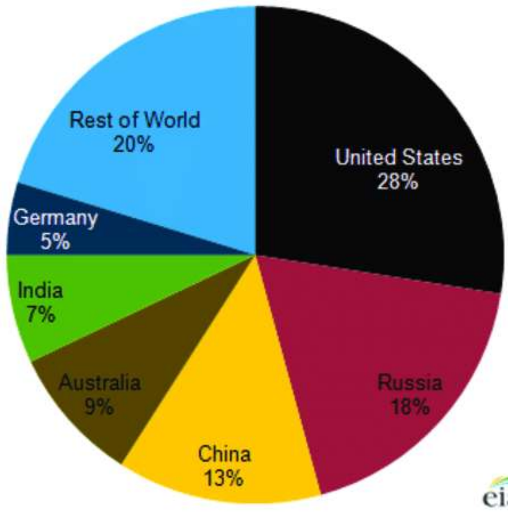

Figure 2.4 Global share of recoverable coal reserves (U.S. EIA, 2008)

2.2.2 Petroleum

Petroleum, a non-renewable resource, is primarily a liquid fossil fuel composed mostly of hydrocarbons. Structurally, it is the result of the burial of marine organisms such as plankton and algae on the seabed of ancient oceans, undergoing millions of years of transformation. This period is identified as the Mesozoic era, occurring between 252 and 66 million years ago. This valuable resource can be found in underground reservoirs like the fractures of sedimentary rocks. Although crude oil is initially black in color, refining processes transform it into products of various colors and viscosities. According to BP's estimates, global petroleum production may have already peaked in terms of petroleum reserves. Considering the finite nature of fossil fuels, if production reaches its peak, it will gradually start to decline, creating an evident gap between supply and demand.

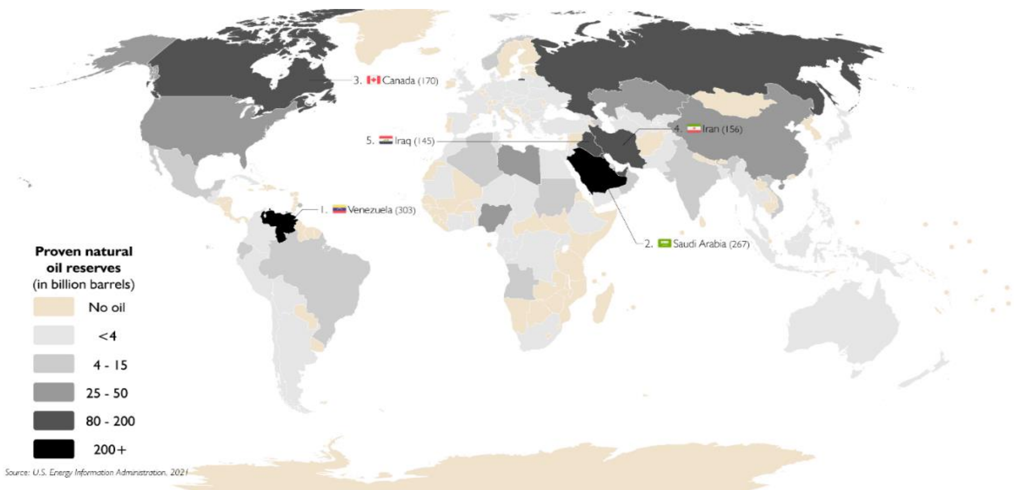

Figure 2.5 Global Proven natural oil reserves. (Our World in Data.,2022)

2.2.3 Natural Gas

Compared to petroleum, natural gas is a fossil fuel that is abundant in reserves and relatively cleaner. Similar to oil, natural gas also originates from the remains of marine microorganisms. It is a more recent energy source when compared to oil and coal. Until the late 1990s, coal was more commonly used as an energy source than natural gas. However, advanced countries have now shifted their preference to natural gas in their energy demand, taking into account its environmental impact to some extent. Natural gas is primarily composed of methane, and, like oil, it is extracted through drilling operations. Unlike petroleum, natural gas is trapped in small volumes but high proportions underground, and its reserves are more evenly distributed globally compared to oil sources. Experts express concerns that the reserves of this resource could be depleted by the middle or end of the 21st century.

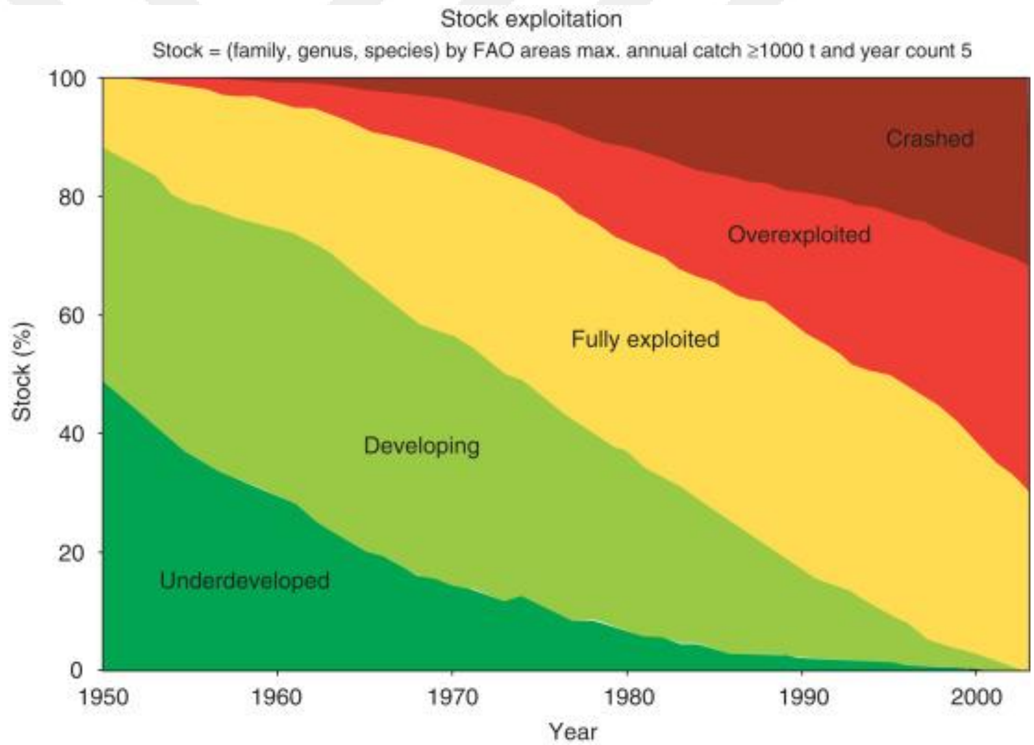

Figure 2.6 Stock (%) and exploitation over the years (Our World in Data ,2022)

2.3 Renewable Energy Sources

Sustainable or recurrently derived energy from the natural environment can be defined as renewable energy. Renewable energies are derived from normally occurring sources such as solar, wind, biomass, geothermal, and wave energy. It is expected that the percentage of renewable energy sources will increase in the future energy mix, while the utilization of petroleum fuels is expected to decrease (Panwar et al., 2011).

Renewable energy technologies and efficient energy usage are identified as the most effective potential solutions to current environmental issues, supported by practical examples (Midilli et al., 2005).

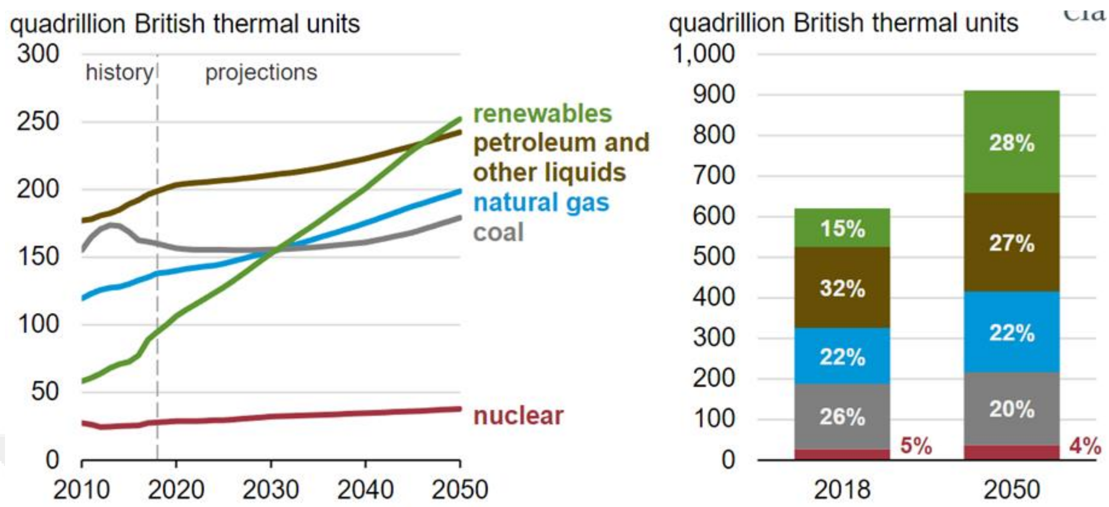

Figure 2.7 Global primary energy consumption (EIA-2018)

Renewable energy sources:

- Solar energy
- Wind power
- Biomass energy
- Geothermal Energy
- Hydraulic energy

2.3.1 Solar energy

It can be defined as the energy obtained from direct sunlight. Just as both heat and electricity can be produced from solar energy using collectors, it is also possible to produce electricity using photovoltaic cells. Solar energy can be an attractive alternative primarily for product drying, as it does not impose additional energy costs beyond the initial investment. However, many products are restricted to use only during daylight hours and require constant cleaning, which limits their use. For this reason, solar energy needs to be stored in the form of heat energy and this stored energy must be used to meet the demand at night or during periods when sunlight is insufficient.

2.3.2 Wind Energy

Humankind's use of wind energy began centuries ago, initially to obtain mechanical energy and power mechanisms through movement. In today's context, the mechanical energy obtained is converted into electrical energy through turbines for practical use (Capik et al., 2012; Yılmaz and Çavuşoğlu, 2012). Since wind energy is a worldwide accessible and easily obtainable energy source, it can be widely used in many regions. It is predicted that wind energy will make a significant contribution to the increase in renewable energy use in the coming years (Kaygusuz, 2010).

2.3.3 Bio-Gas

Biogas obtained from organic waste as a result of the fermentation of living bacteria through anaerobic respiration is a biofuel with a methane content varying between 45% and 70%. It can be used in many areas such as heating, electricity generation and vehicle fuel. Biomass, wind and geothermal energy are commercially competitive and have made relatively rapid progress (Fridleifsson, 2001).

2.3.4 Geothermal Energy

Geothermal energy is a type of energy that can be obtained directly or indirectly in regions where geothermal resources are located. Geothermal energy, with its various applications such as heating, cooling, electricity production, mining production and spa purposes, is also an important renewable energy source for countries with geothermal energy resources, such as Turkey.

2.3.5 Hydro-power

It is believed that the energy potential of water was first used in Egyptian civilization. The aim is to facilitate tasks by transferring the mechanical energy of open channel systems in rivers to grain grinding mechanisms through wheels (Schlager and Weisblatt, 2006). Later, with developing techniques, the height parameter was increased and potential energy was added to the water. Potential energy given to water can be converted into kinetic energy when needed. Today, it still maintains its position as the cheapest renewable energy source (South and Kaygusuz, 2010).

Hydraulic energy can be split into two main groups based on the method used. These are hydrostatic and hydrokinetic systems. Hydrostatic energy systems can deliver potential energy to water and store potential energy. From the stored energy, electricity is generated by releasing water through turbines, with dams being the most common example. To endow water with potential energy, it is necessary to increasing the depth of the water. The construction costs are relatively higher for hydrokinetic energy for these reasons. On the other hand, hydrokinetic energy transforms the kinetic energy inherent in the water's current moment into electricity using turbines. While the mechanisms used in hydrokinetic systems are relatively smaller and less expensive than those in hydrostatic systems, providing stable energy in these systems is more challenging. In addition, due to lower installation costs and relatively smaller mechanisms, displacement (mobilization) is more easily achievable in these systems.

2.4 Hydrokinetic Energy

Hydraulic energy is the clean energy source with the largest share in meeting global energy needs (Güney and Kaygusuz, 2010). Hydroelectric power constitutes 16% of total electricity production and 80% of electricity produced using renewable sources (Bilgili et al., 2018; Hussain et al., 2019). Its superior performance in terms of efficiency among energy types, coupled with the global presence and availability of this type of energy in almost every geography, increases the interest in hydraulic energy (Öztürk et al., 2009). As mentioned earlier, hydraulic energy can be divided into two main groups: hydrostatic energy and hydrokinetic energy. Hydrostatic energy endows water with height potential energy, converting the possessed hydrostatic energy into mechanical energy through turbines. The mechanical energy of turbines is then converted into electrical energy by generators. In terms of resource utilization, hydrostatic energy is more costly than hydrokinetic energy. This is because hydrostatic energy generates height potential energy in water by accumulating water in a specific area, requiring the construction of a dam. Dam constructions are both costly and relatively more complex in design. Large dams cause sedimentation at the riverbed, leading to biological and ecological problems over time (Beck et al., 2012; Chen et al., 2016; Raadal et al., 2011). Since hydroelectric power plants require large reservoirs, providing the necessary space poses certain challenges. If the region where people live enters the reservoir area, many individuals will have to relocate directly or indirectly, potentially facing economic hardships. The placement of displaced individuals by relevant authorities may encounter challenges (Beck et al., 2012; Schafer et al., 2018; Siciliano et al., 2015). Apart from ecological issues for high and large-volume reservoir dams, the presence of dams can create microclimates in the area, induce excessive rainfall in certain regions, affect earthquakes with the created high mass, and influence changes in wind directions and intensities by creating pressure differences in the micro-level atmosphere (Elosegi and Sabater, 2012).

Hydrokinetic turbines are mechanisms that transform the existing kinetic energy in free-flowing water into electrical energy. Primarily utilizing drag and lift forces, they first convert the kinetic energy present in the water into mechanical energy and afterwards convert the mechanical energy into electrical energy. The operating principle is similar to wind turbines, where the fluid is air in wind turbines and water in hydrokinetic energy. Due to the higher density of water compared to air, smaller geometry dimensions can be designed (Killingtveit, 2019).

CHAPTER III
HYDROKINETIC TURBINES

3.1 Hydrokinetic Turbines

Energy demand is increasing day by day. With the limited amount of fossil fuel resources in the world and growing environmental problems, the need for sustainable energy resources is becoming more important day by day. In this context, hydrokinetic turbines, a relatively new technology among renewable energy technologies that produce electrical energy using water flow, have an important place. Hydrokinetic turbines provide a method of energy production that minimizes environmental impacts by utilizing the natural movement of water.

There are studies arguing that the irregularities in river flow caused by dams cause ecological concerns (Berkün et al., 2008). Hydrokinetic turbines are used in rivers, streams, canals, etc. Electrical energy production can be achieved by directly integrating into systems with water flow. Therefore, unlike hydrostatic turbines, they do not require dam construction (Muratoğlu and Yüce, 2015). Its working principle is based on capturing and transforming the kinetic energy of water movement. When the water flow hits the turbine, the blades of the turbine rotate. This rotational motion excites a generator within the hydrokinetic turbine. The generator converts the rotational motion of the turbine into electrical energy. The energy produced by electricity is used as electrical energy by being transmitted to the electrical grid or to a local consumption point.

Hydrokinetic turbines have several advantages, making them attractive for sustainable energy production:

- Environmentally Friendly: Hydrokinetic turbines do not contribute to carbon emissions. It minimizes environmental impacts. They do not create large fluctuations in water flow
- Continuous Energy Production: Hydrokinetic turbines are not affected by daily and seasonal changes due to the steady flow of water. Therefore, they provide continuous energy production.

- Low Maintenance Costs: Hydrokinetic turbines generally have low maintenance and operational costs. The long lifespan of wearing parts like blades reduces the need for maintenance

In addition to the advantages of hydrokinetic turbines, there are also some limitations:

- Location Dependency: Hydrokinetic turbines must be installed in areas where water flow is sufficient. This implies limited location diversity.
- Environmental Impacts: Hydrokinetic turbines must consider their effects on local ecosystems due to water flow. Therefore, project planning and site selection are crucial.

It has been stated in the energy section that hydrokinetic turbines have a significant potential for sustainable energy production. More efficient designs in the future, technological developments that reduce environmental impacts, and increased availability of water resources may lead to more widespread use of hydrokinetic turbines. This technology can play a crucial role in meeting the world's energy needs and supporting environmental sustainability. Using natural water flow is an important component for sustainable energy production. The fact that hydrokinetic energy is environmentally friendly, a system that produces continuous energy and has low maintenance costs paves the way for this technology. However, it should not be forgotten that there are some limitations such as location requirements and environmental impacts. In the future, widespread adoption of hydrokinetic turbines through technological advancements could support global efforts toward sustainable energy and potentially replace fossil fuels.

3.2 Classification of Hydrokinetic Turbines

Because hydrokinetic turbines offer a variety of design options, their classification can be made according to various criteria. Hydrokinetic turbines are generally divided into two main categories based on water flow direction: Axial flow turbines, in which the rotor axis is aligned with the water flow direction; Cross-flow hydrokinetic turbines in which the rotor is placed perpendicular to the water flow. When classifications are divided according to the operating principle of the turbine, classification can also be made according to critical factors affecting turbine performance such as flow type, flow rate and desired energy output. While all hydrokinetic devices operate with the same conversion principles regardless of their application area, there may be subtle differences in design and operating characteristics (Khan et al., 2009). In summary, hydrokinetic turbines can be primarily categorized into two main types: Cross Flow and Axial Flow.

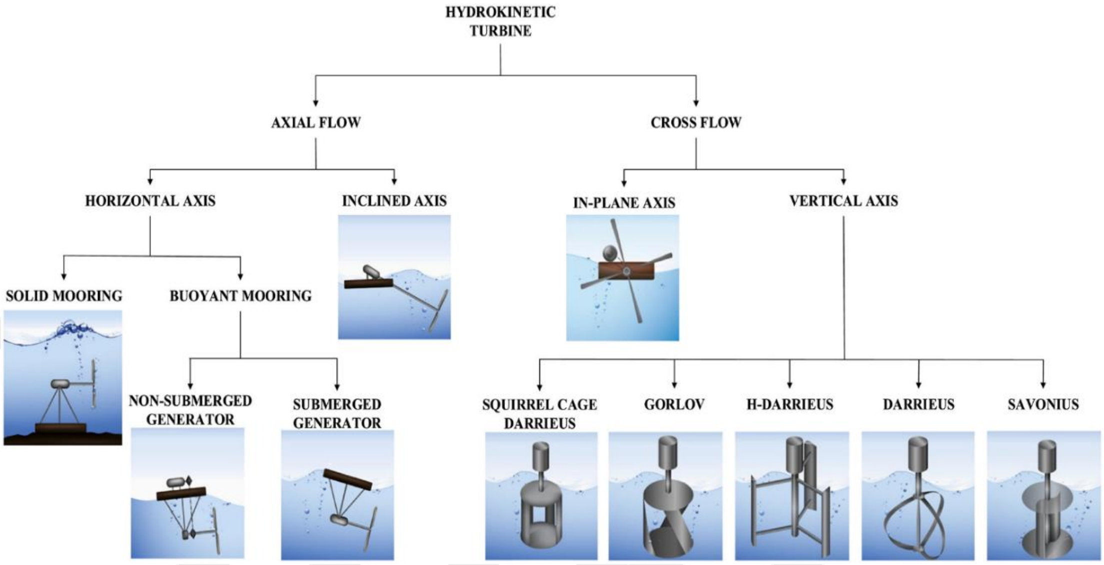

Figure 3.1 Types of hydrokinetic turbines. (Khan et al, 2009)

3.3 Axial Flow Hydrokinetic Turbines

Axial-flow hydrokinetic turbines have a horizontal/inclined rotation axis aligned parallel to the water flow direction (Batten et al., 2007). They are very similar to wind turbines in design and operation, and are sometimes referred to as propeller turbines and have similarities with ship propellers (Saini and Saini, 2019). To achieve high efficiency, it is very important that the turbine rotor is aligned with the water flow. The flow requirements of axial flow turbines make them suitable for applications such as oceans and tides (Guney and Kaygusuz, 2010). The rotor of these turbines may have two, three or more blades and may be open or implicit depending on torque requirements and flow characteristics. They can be positioned anywhere in the water column, but the most common installation is bottom mounted. Turbines may use active or passive measures to yaw or pitch the blades, depending on flow conditions or control settings. They may have curved blades that allow them to vary their hydrodynamic performance based on flow conditions or control settings. Hydrokinetic turbines, especially when used in open channels, may be exposed to unwanted debris carried by water. Regimes in open channels can lead to sudden changes in water speed, causing hydrokinetic turbine rotors to fail over time. Therefore, rotors of hydrokinetic turbines are often made of solid composite materials to ensure durability and prevent corrosion (Marsh, 2004). The use of axial flow turbines in remote areas was first suggested by Peter Garman in 1978 (Khan, 2006). Axial Flow Hydrokinetic Turbines can basically be divided into three groups: "Solid Coupled, Non-submerged Generator, Submerged Generator.

3.3.1 Solid Mooring

These are axial flow hydrokinetic turbines that are fixed to the ground in the deployed area. They are particularly suitable for regions with strong bottom currents. The generator on these turbines is submerged. Isolation issues should be considered for this type of turbine.

3.3.2 Non-Submerged Generator

These are axial flow hydrokinetic turbines that are fixed to the ground in the deployed area. They are particularly suitable for regions with strong bottom currents. The generator on these turbines is submerged. Isolation issues should be considered for this type of turbine.

3.3.3 Submerged Generator

These are axial flow hydrokinetic turbines fixed to the ground in the deployed area, especially suitable for regions with strong surface currents. The generator on these turbines is submerged. Like in Solid Mooring types, isolation issues should be considered for this type of turbine.

3.4 Cross Flow Hydrokinetic Turbines

Cross Flow hydrokinetic turbines are designed with a rotation axis perpendicular to the incoming water flow. The cylindrical shape of these turbines facilitates effective utilization of channel depth. Cross Flow hydrokinetic turbines have the ability to accept water from all directions. The rotor of these turbines can be designed with two, three, or multiple blades, depending on torque requirements and flow conditions (Saini and Saini, 2019).

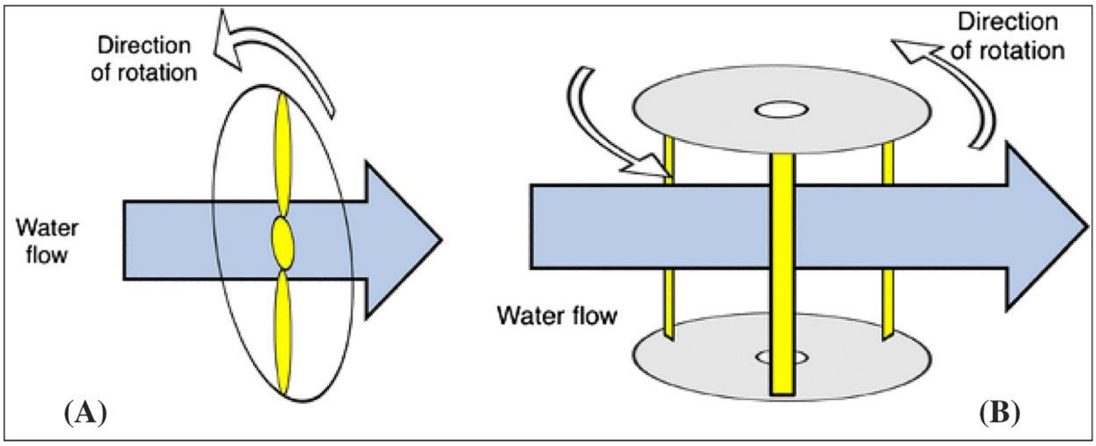

Figure 3.2 (A) Axial-flow, (B) Cross-flow (Roberts A et al. 2016)

3.4.1 In-plane Axis Hydrokinetic Turbines

Horizontal axis hydrokinetic turbines are devices that convert the kinetic energy of water into electrical energy by exposing their bladed rotors to water flow. They are often located over water sources such as rivers, streams or ocean currents. It has been mentioned that hydrokinetic turbines can be divided into two groups according to their operating principles. The first group consists of horizontal axis turbines whose rotation axis is parallel to the main flow direction. Turbines whose rotation axis is perpendicular to the incoming water are called vertical axis turbines (Batten et al., 2006; Meyers et al., 2006). Horizontal-axis hydrokinetic turbines are a subject of ongoing research due to their relatively higher efficiency, lower drag losses, reduced vibrations and gentler lift compared to their vertical-axis counterparts (Khan et al., 2009; Manwell et al., 2002).

3.4.2 Vertical Axis Hydrokinetic Turbines

Vertical axis hydrokinetic turbines are turbine types whose rotation axis is perpendicular to the direction of liquid flow (Eriksson et al., 2006). Basically, vertical axis hydrokinetic turbines can be classified as Savonius, Darrieus, H-Darrieus and Gorlov. They produce energy with a rotor activated by water flow. Since the rotor is positioned vertically in vertical axis hydrokinetic turbines, it is likely to take up less space than in horizontal axis hydrokinetic turbines. Since these turbines are effective even in slow water flows, as stated in detailed studies, they are suitable for water resources such as slow-flowing rivers and canals. The blades of vertical axis hydrokinetic turbines have an adjustable structure, which allows the turbine performance to be optimized for different water conditions. These turbines require minimal maintenance costs due to their high size and accessibility. Vertical axis hydrokinetic turbines can be widely used in small-scale local power generation projects.

3.4.2.1 Savonius Turbines

Savonius turbines were invented in 1920 to convert wind energy into electrical energy. These types of turbines resemble an "S" shape. It consists of two curved-surface hydrofoils connected to a central shaft. One of the blades is called the advancing blade and the other is called the returning blade. The basic principle of Savonius turbines is to convert the kinetic energy of fluids into electrical energy. They are mostly driven by drag force with less lift force (Talukdar et al., 2018; Ostos et al., 2019; Akwa et al., 2012). Due to the predominant use of drag force, they produce the same amount of torque in both directions, making them advantageous for self-starting. Electricity production from Savonius turbines is inefficient due to their low operating speed (Youssef et al., 2019; Talukdar et al., 2018). They can be produced and used for low flows.

3.4.2.2 Darrius Turbines

The Darrieus turbine was patented by Georges Jean Marie Darrieus in 1931. Like Savonius turbines, Darrieus turbines, which convert kinetic energy into electrical energy in a cost-effective manner, have some advantages and disadvantages in their areas of use. While providing torque regardless of fluid direction, a disadvantage is that the term self-starting cannot be fully used in standard designs (Dominy et al., 2007). Darrieus type wind turbines achieve twice the torque per revolution due to their design geometry. Considering that the wind blows from one direction, the power produced by the turbine creates a sinusoidal curve. The power coefficient of Darrieus type turbines is higher than other vertical axis turbines. The blades used in Darrieus type turbines are aerodynamically designed. When liquid flows at right angles around the blades, it creates a pressure difference. This pressure difference causes a net torque on the shaft to which the blades are connected (Zhao et al., 2015).

3.4.2.3 H-Darius Turbines

H-Darrieus type turbines differ slightly from standard Darrieus turbines in terms of geometry. Since the blades of H-Darrieus turbines are vertical, the effect of the fluid in a certain region of this blade will be the same on the vertical axis. H-Darrieus turbines are being investigated for commercial use due to their resistance to wind direction and higher power coefficients than other horizontal axis turbines (Mertens et al., 2003; Noves et al., 2018). Wind tunnel tests of vertical-axis turbines and horizontal-axis turbines show evidence that vertical-axis turbines perform better in flows inclined up to 30 degrees compared to horizontal-axis turbines (Kumar et al., 2019).

3.4.2.4 Gorlov Turbines

The Gorlov helical turbine (GHT) can be classified as a type of Darrieus turbine. In Gorlov turbines, vertical helical blades are used instead of straight blades to increase performance depending on the angle of attack (Jayaram and Bavanish, 2021). Although helical turbines pose some difficulties in the production process, their ability to dampen vibrations in the main shaft of the turbine provides a significant advantage in cross-flow conditions (Bachant and Wosnik, 2015).

3.5 Spherical Hydrokinetic Turbines

Spherical turbines are more similar to Darrieus type turbines. However, due to their spherical shape, they are referred to as spherical Darrieus or spherical turbines in the literature. The turbine has a vertical axis. It can create aerodynamic pressure differences depending on the blade types it has. This pressure difference allows the turbine to rotate, as in other turbine types. While they can be used in open channel systems, they can also be used in pressurized irrigation network pipes and drainage pipes (Schlabach et al., 2011). Pressure reducing valves are used to relieve excess pressure and also remove unnecessary air trapped in the pipe network. Relieving excess pipe pressure by other methods, such as using a turbine, has always been a subject of research. Additionally, the excess energy used by turbines in the pipeline network can be used to operate some measuring devices and sensors connected to the pipeline without external power sources (Kumar and Sarkar, 2023; Kumar and Shahid, 2017). The in-pipe hydroelectric power system is not dependent on weather changes and can be classified as a renewable energy source due to its environmental friendliness (Kumar and Sarkar, 2023).

CHAPTER IV
THEORY

4.1 Aerofoils

Aerofoil is a special hydrofoil geometry that can produce lift (Lissaman, 1983). It is a special shape used in rotating blades, aircraft hydrofoils and aerodynamic surface designs, creating lift and drag force in the air flow. An airfoil typically has a curved upper surface and a flatter lower surface. This structure exploits pressure differences between the upper and lower surfaces, based on Bernoulli's principle and varying air speeds, to create lift and enable aircraft to fly or rotor blades to turn. Existing hydrophiles have been codified and standardized into specific shapes over time.

The types and shapes of hydrofoils used in aviation differ in number and shape from those used in the field of hydrokinetic energy. For example, the blade profiles used in hydrofoils of low-speed aircraft are generally known to be thicker. It also has more curvature or camber. Specifically, hydrofoil profiles for high-speed aircraft use sharper leading edges. Similar considerations can be applied when designing the types of hydrofoils used in hydrokinetic turbines.

4.1.2 History of Aerofoils

Historically, the design of airfoil profiles for specific applications has been done to develop the best hydrofoil profiles for specific aircraft. Different aerofoils have been designed through wind tunnel experiments and theoretical analysis. The earliest known airfoil sections for aircraft concepts were patented by Horatio Phillips in the 1880s, inspired by the hydrofoils of birds, as shown in Figure 4.1. This is the first time Phillips has tested these airfoil profiles in a wind tunnel.

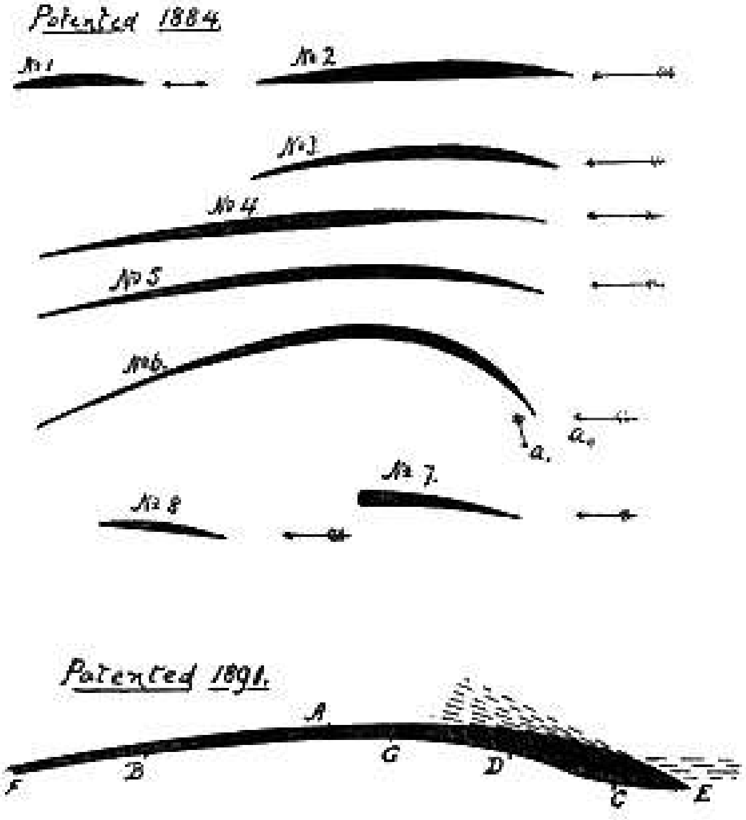

Figure 4.1 Airfoil shapes were patented in the late 1880s

There are typical design requirements for airfoil profiles. For the designed blade, it is important to reach high values of the maximum lift coefficient before flow separation and stalling occur. Having the least friction in the fluid velocity range determined by examining the operating conditions of the blade profiles will minimize the energy losses arising from the hydrofoil geometry. Additionally, having the highest lift-to-drag ratio at varying angles of attack is a factor that increases efficiency.

4.1.3 Airfoil Classification

Hydrofoils can be categorized into various services depending on their design goals, geometry, and various effects. The main hydrofoil use types within the primary scope of research include NACA profiles, Clark-Y profiles, Eppler Profiles, Selig profiles, and supercritical hydrofoil profiles.

4.1.3.1 NACA Hydrofoil Profiles

A series of standardized hydrofoil profiles developed by NACA in the early 20th century. These hydrofoil profiles are identified by a four-digit number that represents a specific parameter related to the hydrofoil shape.

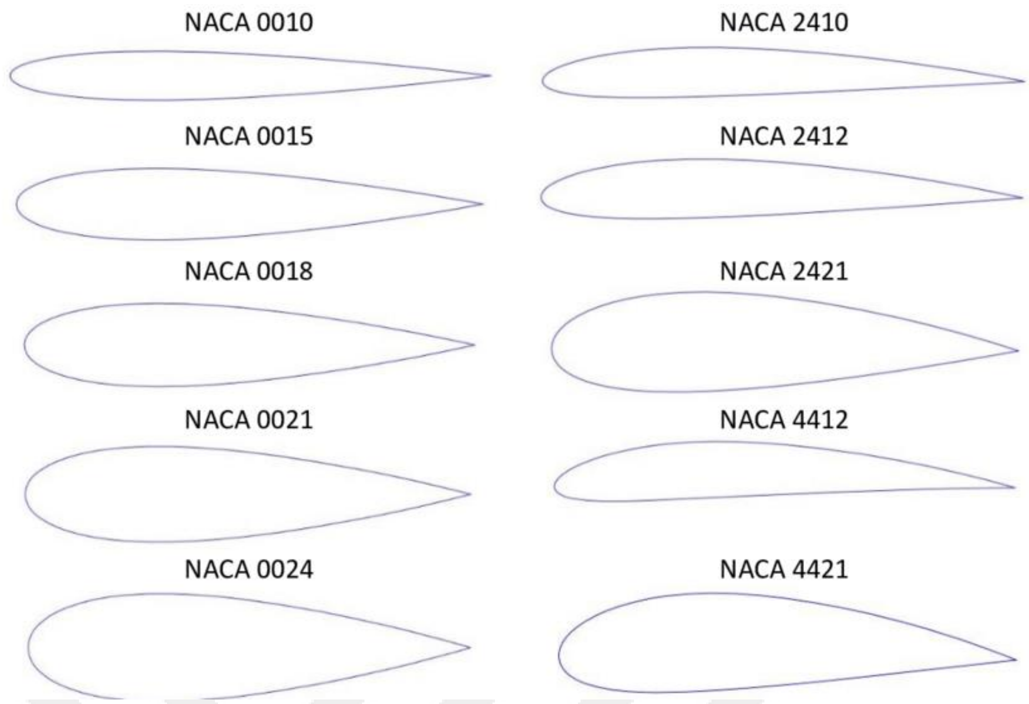

Figure 4.2 Some of NACA aerofoils (Didane et al,2021)

4.1.3.2 Clark-Y Hydrofoil Profiles

The Clark-Y hydrofoil profile is a type of hydrofoil that has been investigated for situations involving high speeds (Xu and Khoo, 2022). It has a medium camber. Good lift characteristics are available at low and medium speeds. The Clark-Y hydrofoil profile has a wide range of applications by providing a balanced relationship between lift and drag.

4.1.3.3 Eppler Hydrofoil Profiles

Eppler hydrofoil profiles are a series of hydrofoil profiles developed by "R.S. Eppler". These hydrofoil profiles are known for their high lift coefficients and good performance at low speeds (Elimelech et al., 2012).

4.1.3.4 Selig Hydrofoil Profiles

Selig hydrofoil profiles are another series of hydrofoil profiles developed by Michael Selig and his team. These hydrophilic profiles are widely used in fields such as radio-controlled aircraft and unmanned aerial vehicles (UAV) due to their stability. Selig hydrofoil profiles have various shapes and provide a balance between lift and drag characteristics (Selig and Gugliemo, 2012).

4.1.3.5 Supercritical Hydrofoil Profiles

Supercritical hydrofoil profiles are specifically designed to delay the formation of shock waves and reduce wave drag at high subsonic speeds. The upper surface of these hydrophilic profiles is flattened and the lower surface has a gentler curve, helping to minimize friction (Sobieczky and Seebass, 1984). Supercritical hydrofoil profiles are widely used in commercial jet aircraft.

4.2 Hydrofoil Section

A hydrofoil can be defined as a lifting surface or strut that operates in water (Molland and Turnock, 2022). Hydrofoils are machines with different geometries that are specially designed to produce the desired forces. Hydrofoil is the name given to the airfoil when aerofoils are used in water. Hydrofoils are used as hydrofoil sections in hydrokinetic turbines designed to take advantage of the physical properties of water. These types of hydrofoils are designed to produce high lift forces and reduce drag. An important feature of hydrofoil hydrofoils is that there are differences in length and angle between the upper and lower surfaces. Hydrofoil hydrofoils generate lift forces by working on an air flow. Hydrofoil hydrofoils typically have a longer and convex surface at the top and a shorter and concave surface at the bottom. According to Bernoulli's principle, fast-moving air creates low pressure, while slow-moving air at the bottom surface creates high pressure. This difference allows the air to travel a longer distance over the hydrofoil, creating a greater pressure difference and thus producing greater lift.

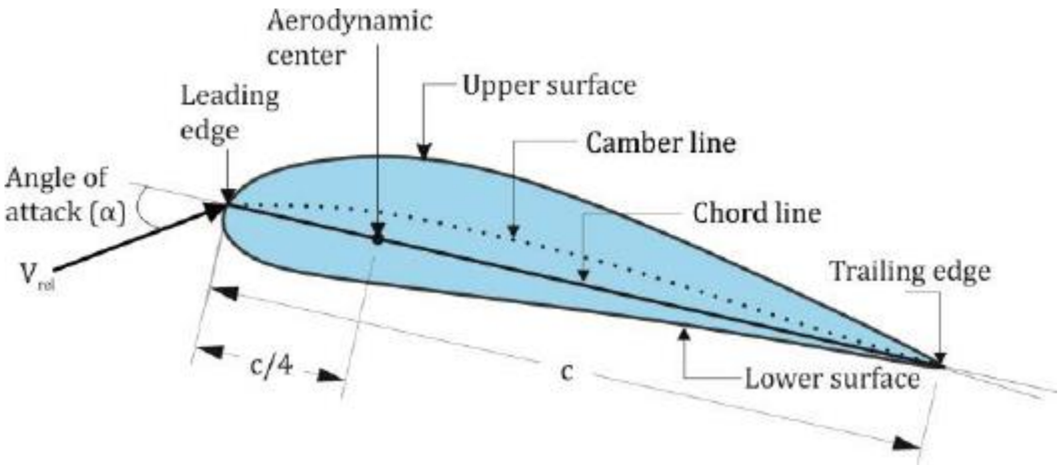

Figure 4.3 Aerofoil (Muratoglu and Yuce, 2015)

Hydrofoils are used in a variety of applications depending not only on aerodynamic design but also on factors such as material selection, surface roughness, hydrofoil profile and hydrofoil cross-section. Hydrofoils are considered an important component that affects the performance, stability and efficiency of the mechanisms used.

4.3 Blade Element Theory

Blade element theory is a theory used to analyze the aerodynamic performance of hydrofoils. It contains various equations and formulas. It is known for providing closed form solutions with relatively simple procedures (Mahmuddin, 2017). These equations are used to describe hydrofoil design, performance and interaction.

4.3.1 Lift Forces & Drag Forces

Lift and drag forces come into play in hydrofoil designs used for aerodynamic purposes. The lift force can be represented as “F_L”, while the drag force can be represented as “F_D”. These two forces are very important in aerodynamic designs. Lifting force is depends some parameters; such as lift coefficient which is directly depends on blade type, the density of the fluid in which the hydrofoil is located, the speed of the fluid and the hydrofoil area.

$$F_L = C_L\left(\frac{1}{2} * \rho * v^2\right) * A \qquad (4.1)$$

In the equation:

F_L: Lift force

P: Density of fluid

v: Velocity of fluid

A: Hydrofoil cross-section area

C_L: Lifting coefficient (Depends on hydrofoil type and angle of attack)

The lift coefficient, denoted by “C_L”, is an experimentally obtained coefficient. It is directly influenced by the geometric design of the hydrofoil being used.

$$C_L = \left(\frac{1}{2} * \rho * v^2\right)^{-1} * \frac{1}{A} * F_L \qquad (4.2)$$

The drag force is another force that occurs depending on the geometry of the hydrofoil being used. It is directly related to the angle of attack of the hydrofoil and is effective even at 0 degrees angle of attack. Although it is dependent on the same parameters as lift force, it is represented by the “C_D” value instead of the “C_L“ value.

$$F_D = C_D\left(\frac{1}{2} * \rho * v^2\right) * A \tag{4.3}$$

In this equation:

F_D: Drag Force

ρ: Density of fluid

v: Velocity of fluid

A: Hydrofoil cross-section area

Cd: Drag coefficient (Depends on hydrofoil type and angle of attack)

The drag force coefficient, denoted by “C_D” is an experimentally obtained coefficient. It is directly influenced by the geometric design of the hydrofoil being used.

$$C_D = \left(\frac{1}{2} * \rho * v^2\right)^{-1} * \frac{1}{A} * F_D \tag{4.4}$$

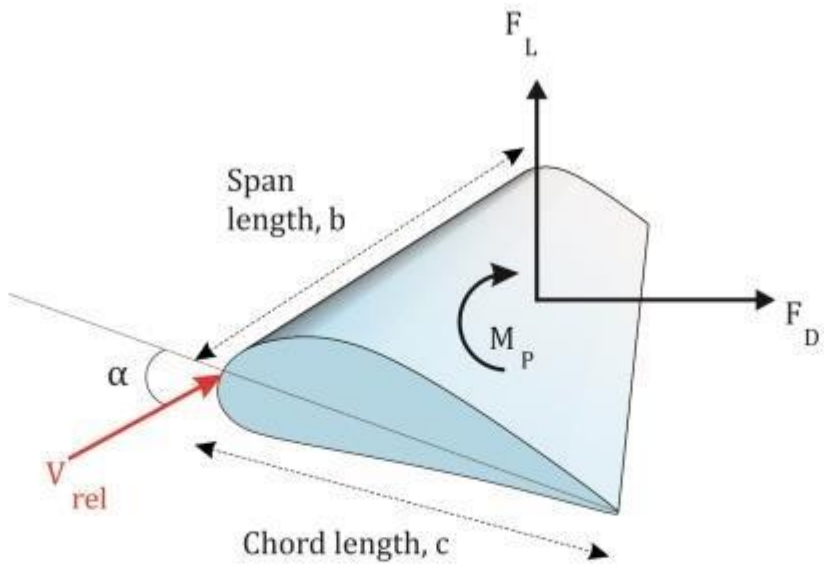

Figure 4.4 Hydrokinetic Turbine Blade Section (Muratoglu and Yuce, 2015).

To measure the lift-to-drag behavior of an airfoil profile, the ratio of the dimensionless lift coefficient to the drag coefficient, represented as C_L/C_D, is utilized. This ratio varies with the angle of attack. The lift coefficient can be defined as follows:

$$C_L = \frac{L}{q} * S \tag{4.5}$$

$$q = \rho * U^2/2 \tag{4.6}$$

Here, L is the lift force, S is the hydrofoil area, ρ is the air density, and U is the fluid velocity. Similarly, it is possible to write the same equation for the drag coefficient. As the numerator and denominator of these two equations have force dimensions, the equation is dimensionless.

In summary, the CL/CD ratio is a measure of the ratio of the lift force to the drag force produced by a hydrofoil when exposed to the fluid passing over it. In hydrofoil designs, achieving the desired lift force increase in turbines is achieved by increasing the CL/CD ratio when necessary. Since the CL/CD ratio depends on the original geometry of the hydrofoil, lift and drag forces are measured by subjecting different geometries to equal fluid velocities. This process is carried out using Computational Fluid Dynamics (CFD) analyses. Then, the most suitable hydrofoil type and angle of attack can be determined by testing different angles of attack on the hydrofoil that produces the maximum CL/CD ratio at equal fluid velocities.

4.3.2 Relationship Between Angle of Attack and Lift Coefficient

Angle of attack (AoA) or angle of attack refers to the angle between the blade surface of a turbine or rotor and the incoming fluid flow. In simple terms, AoA is the inclination of the blade or rotor against the incoming air or liquid flow. For hydrokinetic turbines, angle of attack is an important parameter that determines the performance of the airfoil.

The angle at which the hydrofoil or rotor intersects the air or fluid flow determines the magnitude of aerodynamic lift and drag forces. In many blade types, lift generally increases as angle of attack increases, but at extremely high angles the blades produce more drag than lift. As the drag force increases for turbine types where drag force is required, it increases the possibility of turbulence at high speeds. This causes a phenomenon called "Stall", where the blade suddenly stops working instead of providing the intended effect, causing the lift force and power coefficient to decrease through vibrations.

The design of the Angle of Attack (AoA) for hydrokinetic turbines where effective lift force is desired is found by experimenting with different variations to find the optimum AoA. The determined value varies depending on the design parameters of the turbine and its intended use. There is a relationship between the angle of attack (α) of the blade and the lift coefficient (Cl). This relationship is different for each airfoil and design and can also be determined experimentally.

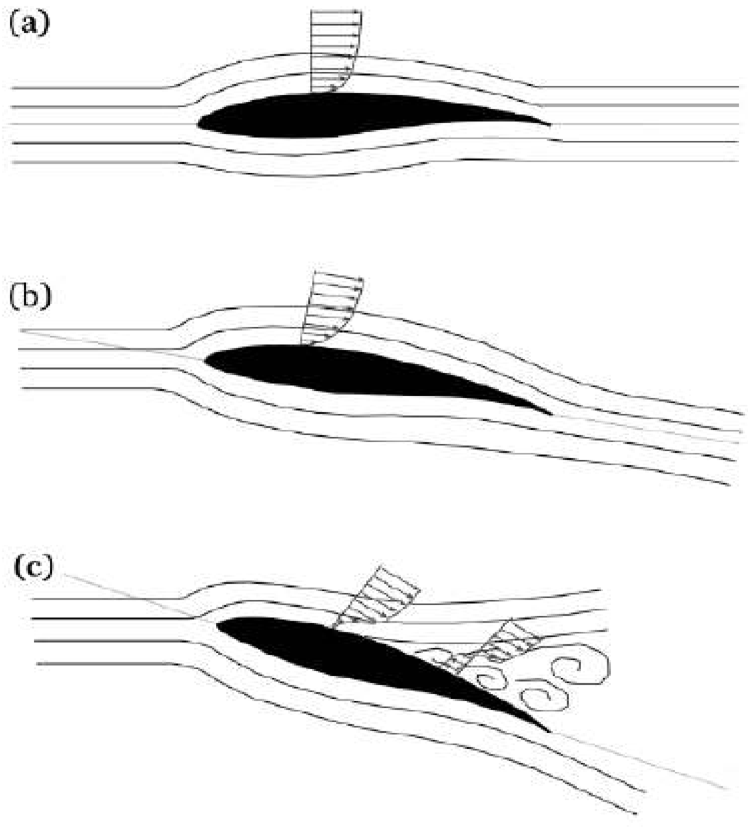

Figure 4.5 Angle of Attack and Lift & Drag Forces. (Abdulrahim, 2014)

4.3.3 Energy Equation

The energy equation is an equation that describes the balance between the input energy and output energy of a blade. This equation is involved in the design of energy converting devices such as turbines or engines. Blade theory is a relatively complex concept and includes various additional equations and analytical methods related to hydrofoil design. Additionally, these equations can be affected by a number of variables such as the blade's shape, size, speed, density, and environmental factors. For this reason, equations and calculation methods specific to each application are used. It is generally used to explain heat transfers, input energy, output energy and the balance between them.

4.4 Actuator Disk Theory

Actuator disk theory, also known as actuator disk model, is a theory that creates equations based on input and output parameters in devices with rotating blades. Classical work on actuator disc theory is still routinely used in its simplest form and with some recent extensions (Chattot, 2014).

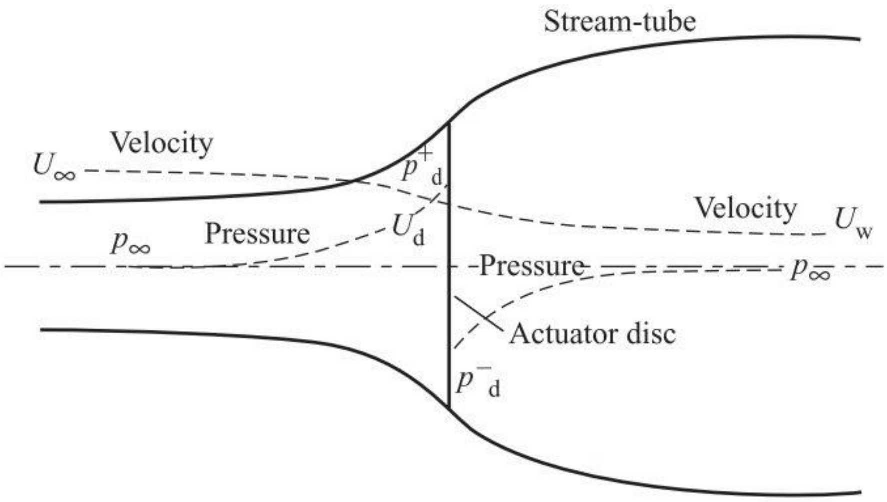

Figure 4.6 Actuator Disk (Quinn et al., 2015)

4.4.1 Idealizing the Rotor

Actuator disk theory simplifies the representation of a rotor as an infinitely thin, two-dimensional disk with a given area and associated aerodynamic properties. When using disk theory, the rotor must be idealized as a disk in the formulation of the formulas.

4.4.2 Total Mass Conservation

It assumes that the mass flow rate through the actuator disk remains constant. Therefore, the mass of the fluid passing through the disk is expected to be equal to the mass entering the disk. This principle is used as a parameter in calculating the velocity of fluid passing through the disc.

4.4.3 Aerodynamic Performance

The theory is used to determine the thrust or lift force produced by the rotor. It also helps determine the aerodynamic performance of the rotor, including the velocity field induced behind the rotor.

4.4.4 Momentum Theory

Actuator disc theory is based on the principles of conservation of momentum. It is based on the assumption that the rotor extracts energy from the flow by slowing the air, leading to a decrease in kinetic energy and an increase in thrust or lift.

4.4.5 Calculation of Power Output

Actuator disc theory can be used to calculate the power output of a hydrokinetic turbine or the thrust produced by a propeller. This is essential for the design and analysis of hydrokinetic turbines and similar devices. While actuator disc theory provides a useful simplification for analyzing the basic aerodynamic performance of rotors, it must be considered that, in practical condition hydrokinetic turbines and other rotating devices are three-dimensional and differ from the ideal actuator disc.

4.5 Betz Law

Betz's Law is a law that sets a limit for maximizing the efficiency of a turbine in extracting energy from the fluid around it. This principle, developed by German engineer Albert Betz, is used to calculate the efficiency of turbine systems such as wind turbines and hydrokinetic turbines. The second law of thermodynamics, known as Carnot efficiency, puts a limit on the conversion of heat to work by converting irregular energy into regular energy. However, for an organized form of energy, there is no limit beyond the limit predicted by the first law of thermodynamics (Energy conservation law). Betz's Law predicts that an ideal turbine operating in a fluid can convert only a certain percentage of the energy of the incoming fluid. According to this law, the maximum energy limit that a turbine can convert corresponds to approximately one-third of the energy of the incoming fluid. That is, according to Betz's Law, an ideal turbine can operate with a maximum efficiency of 59.3%.

Betz's Law plays a very important role in the design and performance calculation of every kind of turbines. It has been reported that a hydrokinetic turbine can only convert a certain percentage of the energy of the fluid flowing towards the turbine inlet. The remaining energy is distributed as heat to the fluid around the turbine. In practice, turbines cannot fully reach this limit due to various losses and interactions. However, systems known as ducted type turbines can achieve energy outputs above this rate with compression.

$$KE = \frac{1}{2}mV^2 \quad (4.7)$$

$$m = \rho A_0 \frac{(V_1+V_2)}{2} \quad (4.8)$$

$$P = \frac{1}{2}m\frac{({V_1}^2-{V_2}^2)}{2} \quad (4.9)$$

KE : Kinetic energy

m:Mass flow rate

$$P = \frac{1}{4}\rho A_0({V_1}^2 - {V_2}^2)(V_1 + V_2) \quad (4.10)$$

$$P_0 = \frac{1}{2}m{V_1}^3 \quad (4.11)$$

$$\frac{P}{P_0} = \frac{1}{2}\left(1 - \left(\frac{V_2}{V_1}\right)^2\right)\left(1 + \left(\frac{V_2}{V_1}\right)\right) \quad (4.12)$$

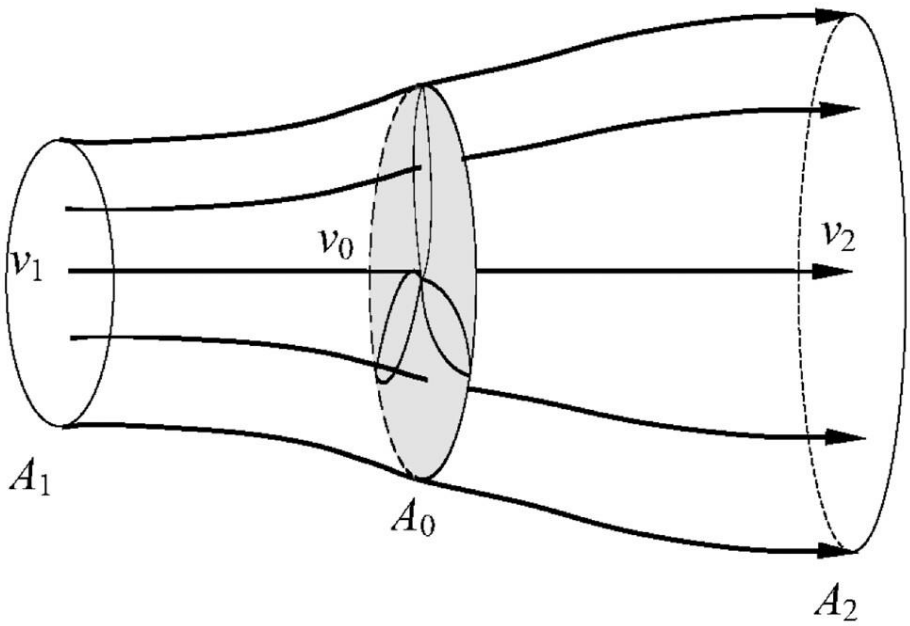

Figure 4.7 Streamtube around a fluid turbine (Coelho,2022)

4.6 Cavitation

The origin of cavitation comes from the Latin word “Cavitas”, which can be translated as pit or cavity. It can be defined as the phenomenon of vapor bubbles forming and collapsing inward in areas where sudden pressure changes occur in a fluid. The increase in the velocity of the fluid causes a drop in pressure, which causes the fluid to transition to the gas phase at that point and increase its volume. Cavitation is usually associated with a solid object surrounded by liquid, where the liquid reaches high speeds, as in devices such as submarine thrusters, water pump systems, or water turbines. When the pressure increases again, these bubbles collapse inwards, creating the potential to damage the device accompanied by shock waves spreading around. It is of great importance to consider the presence of cavitation in designs to prevent negative effects (Silva et al., 2017).

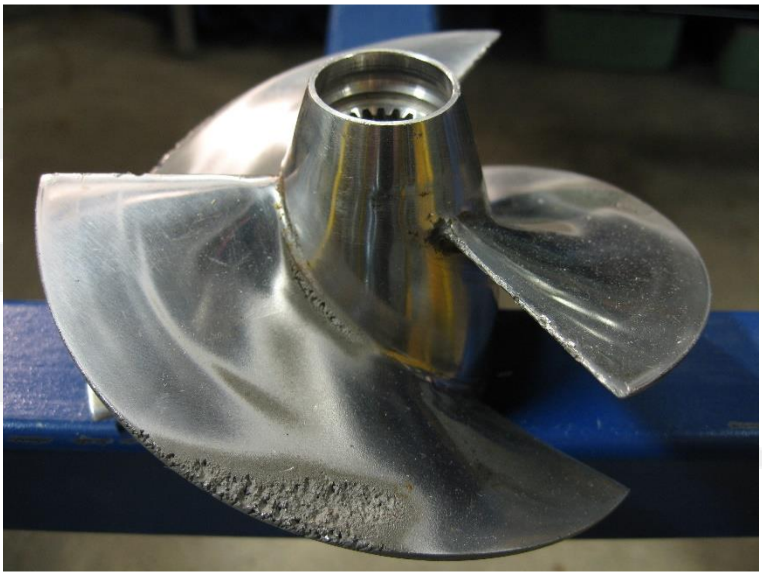

Figure 4.8 A propeller which is damaged by cavitation (Common license, 2006)

Anti-cavitation designs are used in engineering applications to prevent damage to devices. They consist of simple blades attached to the hydrofoil tip and help reduce cavitation erosion under flow conditions and on the wing (Lee et al., 2014).

It should be noted that the occurrence of cavitation depends on several factors, including the physical properties of the liquid such as density and viscosity, as well as factors such as flow rate, pressure and the amount of dissolved gas in the liquid. Considering that cavitation is often an undesirable event, it is important for the device to be designed to take preventive measures against cavitation during the design phase.

Figure 4.9 Cavitation of propeller (http://www.dt.navy.mil)

Cavitation has been studied at different stages throughout history, but advanced research primarily began in the early 20th century. The first observations date back to the 17th century, when scientists observed wear and damage to the turbine blades of water turbines. This phenomenon was associated with the formation and collapse of bubbles due to the rapid flow of liquid. However, the mechanism of cavitation is still not fully understood. The emergence of the term 'cavitation' as a technical term occurred in the scientific literature in the middle of the 19th century. Scientists have discovered that bubbles form and collapse due to pressure drops during high-speed flow of liquids. This incident was taken into consideration because it caused damage to hydraulic systems and water turbines. The first studies on cavitation were made in this period.

In the early 20th century, scientists began to investigate cavitation in more detail. Studies have been conducted on factors such as properties of fluids, flow rate, pressure drop, bubble formation, and collapse mechanisms. Experimental and theoretical studies have contributed to a better understanding of the causes and effects of cavitation. Advanced experimental methods, numerical modeling techniques, and imaging technologies have helped to better understand the complex nature of cavitation. However, cavitation is still an active area of research and more studies are needed.

4.7 Rotor Solidity

Solidity is a dimensionless parameter in turbine designs. The solidity value in a turbine can be expressed as the ratio of the total length of all the blades of the turbine to the environment created by the tips of the turbine blades during rotation. While the increase in the number of blades or relative chord length increases the solidity value, the geometric shape of the circle formed during the rotation of the turbine reduces this value. In short, solidity value is a parameter depending on the width of the turbine blade and the gaps between it and other blades on the rotor.

$$\sigma = \frac{Nc}{2r} \qquad (4.13)$$

σ: Solidity

N: Number of blades

c: Chord length

r:Radius of rotor

Solidity value affects factors such as turbine efficiency, high-speed operating capacity and noise production. The increase in solidity helps the turbine potentially convert more power and be more effective at high speeds, as it increases the speed of the surrounding fluid in accordance with the continuity equations (Carrigan et al., 2012). However, high solidity values also cause increased noise production in the turbine. It is also stated that with high Solidity values, the possibility of turbines starting to rotate on their own may decrease (Twidell and Weil, 2006).

Solidity is a parameter that should be taken into account in turbine design, and the optimum value can vary directly depending on the intended use, fluid speed and design factors. When higher power generation is targeted, the solidity value is typically increased, while turbines operating at lower speeds may prefer lower solidity values.

4.8 Tip Speed Ratio

Tip Velocity Ratio (TSR) is a design parameter that depends on the rotation speed of the turbine in the fluid and the fluid velocity perpendicular to the turbine. It can be expressed as the ratio of the tip speed of the turbine blades to the fluid speed perpendicular to the turbine. Tip Speed Ratio, or TSR, as shown in Figure 4.10, also relates to the turbulent flows produced with the rotation of the turbine. If the rotor speed is significantly higher than the incoming fluid velocity, it causes turbulent flows behind the turbine blades, causing interference with other turbine blades. Turbine blades passing through turbulent flow may not produce the desired aerodynamic effects, which causes the power coefficient to decrease.

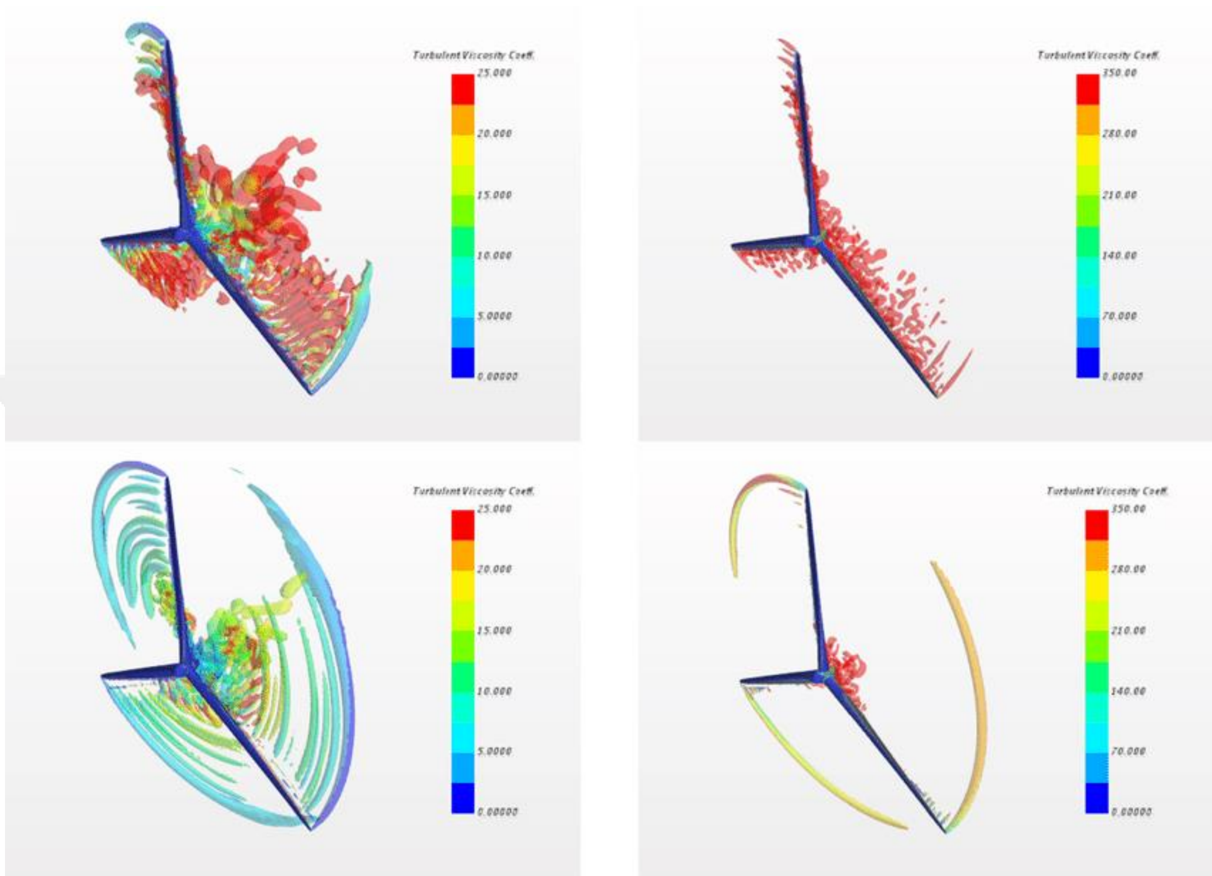

Figure 4.10 Tip speed ratio illustration on CFD. (Pinto et al, 2020)

Tip Speed Ratio (TSR) is a very important parameter in the design phase. The aerodynamic performance and power production of the turbine may vary at different TSR values. It is important to optimize TSR to achieve maximum power output. When the TSR parameter is not designed and adjusted appropriately, most of the energy turns into other types of energy without being converted into mechanical energy. To increase the power coefficient, the TSR parameter must be well designed.

It can be considered that there is a proportional relationship between Tip Speed Ratio (TSR) and turbulence. Turbulence has been described as a flow condition in which there are fluctuations in the speed and orientation of the fluid. It has been noted that turbulence affects turbine performance in rotary blade systems such as hydrokinetic turbines. Turbulence can create random fluctuations in the fluid, changing its speed and direction. These fluctuations can affect blade performance depending on the incoming flow. High levels of turbulence can cause serious damage to the blades, create aerodynamic loads, cause energy conversion losses and reduce turbine efficiency. Therefore, it is very important to find a balance between TSR value and turbulence. Ideally, high TSR values as well as design features that reduce turbulence should be taken into account when optimizing turbines. For example, airfoil profiles and turbine casing design can be optimized to reduce the negative effects of turbulence. Moreover, experimental studies and numerical simulations can be used to evaluate turbine performance in turbulent environments.

The term Tip Speed Ratio (TSR) is also frequently used in vertical axis turbines (VAWTs). However, it is calculated differently than horizontal axis turbines. In VAWTs, TSR can be expressed as the ratio between rotor speed and wind speed. In VAWTs, as the rotor blades rotate, the rotation speed changes under the influence of the fluid velocity. Therefore, it is almost impossible to use a single fixed TSR value. However, in VAWTs an average TSR value is usually calculated for a specific rotation speed or range of rotation speeds. In order to design the system in the best way, different TSR values at variable rotor speeds can be examined by looking at the power coefficient (Zhe Chen et al., 2009).

For VAWTs, the average TSR is the ratio of the average rotor speed to the wind speed and can be calculated as follows:

Average Tip Speed Ratio = (Average Rotor Speed) / (Wind Speed)

In that average tip speed ratio equation, “Average Rotor Speed” is the average value of the rotor's rotational speed over time or a rotation cycle.

4.9 Power Coefficient

Hydrokinetic turbines are devices that generate energy from water flow. The power coefficient, denoted as “Cp”, is a very important parameter that measures the efficiency turbines. The power coefficient (Cp) is calculated with the following equation:

$$Cp = P/(0.5 * \rho * A * V^3) \tag{4.14}$$

Cp: Power coefficient

P: Power output of turbine (Watt)

ρ: Density of water (kg/m^3)

A: Cross-section area of hydrofoil (m^2)

V: Velocity of water (m/s)

The equation stated in 4.14 can be used to evaluate the performance of hydrokinetic turbines. Cp value is a useful parameter that shows how efficient the turbine is. Ideally, for a hydrokinetic turbine, the Cp value is around 0.59 at maximum. However, in practice, this value varies depending on the design of the turbine, operating conditions and the environment in which it is placed. To increase the power coefficient of hydrokinetic turbines, the following factors can be taken into account:

- Turbine Design: Geometric features of the turbine are a parameter that affects the Cp value. Factors such as the turbine blade type, surface design, cross-sectional area and length of the blade profile affect the performance of the turbine. Well-designed blades can provide higher Cp values.
- Flow Velocity: Higher water speeds can help the turbine generate more power. However, excessively fast water flow can negatively affect the power coefficient of the turbine.
- Turbine Location: The characteristics of the environment in which hydrokinetic turbines are placed can affect their performance. Parameters such as water depth in which the turbine is located, flow speed and direction are among the many factors that must be taken into account for turbine placement.
- Turbine Maintenance: Regular maintenance can improve the performance and extend the life of the turbine.

Local conditions and design must be taken into account when hydrokinetic wind turbines perform the same in all conditions, unlike wind turbines. Continuous improvement efforts are being carried out to increase the power rates of hydrokinetic turbines and make them more efficient.

CHAPTER V

MESHING

5.1 The Development of the Finite Element Method

The finite element method is a technique developed to obtain approximate solutions of partial differential equations of elements with boundary conditions. The main purpose of this method is to approach the final solution by dividing the complex structure into relatively smaller components. The starting point of finite element analysis is thought to be the studies on natural vibration frequencies studied by John William Strutt in the late 1800s. With the development of numerical methods in the following years, the origins of specific and focused scientific studies aimed at solving complex problems in aviation and building sciences date back to the scientific articles published by A. Hrennikoff in 1941 and R. Courant in 1943 (Hrennikoff, 1941; Courant, 1943).

Finite element method; It emerged as a method for solving problems in fluid mechanics, thermodynamics, aviation and various engineering disciplines. The method came to prominence with the publication of Gilbert Strang and George Fix's book "Analysis of the Finite Element Method" in 1973 (Strang and George Fix, 1973). The finite element method enables the observation of behavior under stresses and forces at the theoretical design stage, without actually producing the models. At the same time, the Finite Element Method is necessary for designs that can be optimized before production and save time and production costs. It also eliminates the difficulty of testing how designs will behave under relatively high forces, very high or low temperatures, and under these effects, before they are actually manufactured.

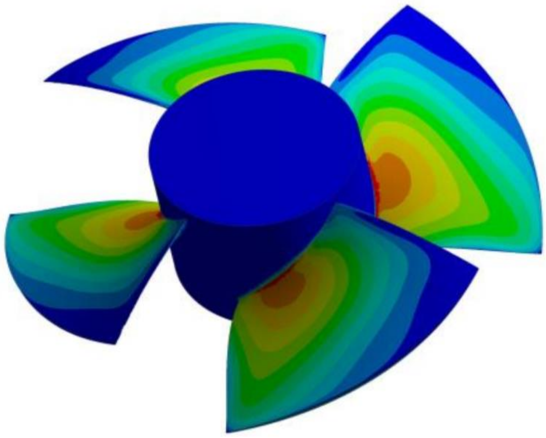

Figure 5.1 Tubular Pump Impeller (Wang et al., 2021)

5.2 Working Principle of the Finite Element Method

After relatively large components are divided into smaller parts without losing their material behavior properties, points are defined to follow the behavior of these small parts. These determined points are specifically called "Nodes". Each node is programmed to contain material and structural data of its location. Meshing is a step used when obtaining an accurate simulation using the finite element method. A mesh consists of elements containing nodes that represent the shape of the geometry. The meshing process transforms irregular volumes into pieces called "Elements", making equations solvable and meaningful. In the thesis, within the scope of the examination and analysis of the turbine, some terminologies related to meshing techniques have been researched in order to explain the meshing techniques used.

5.3 Terminology

Meshing is widely used in computational fluid dynamics solutions. Although it has simple definitions in terms of content, the results may deviate from the ideal solution if the technique is not used correctly. The geometric shapes to be analyzed can be combined in 2D or 3D under certain conditions. In 2D meshing, it can be divided into small pieces as "Rectangular" or "Triangle". Rectangular pieces can consist of squares or irregular quadrilaterals of different sizes and proportions. The area between the edges of the quadrilaterals is called "Cell". The midpoint of the cell between the edges can be called "Cell Center", and the intersecting corners of these quadrilaterals can be called "Nodes". Geometry meshes as Triangles have the same definitions for Cell, cell center, and nodes as in Quadrangles.

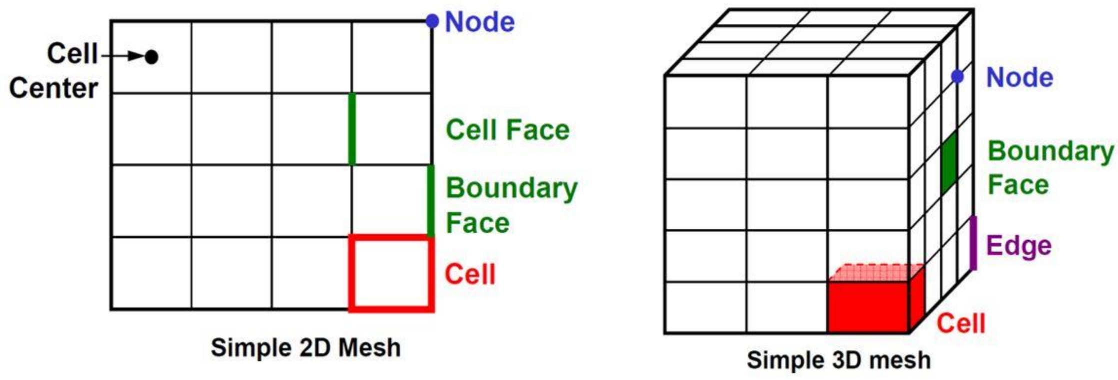

Figure 5.2 Simple 2D and 3D Mesh Basic Definitions (Manchester-cfd)

5.4 Mesh Methods

When creating a mesh, the choice of element properties should be based on the geometry and the behaviors to be observed. As mentioned, in 2D, there are two types of elements: triangles and quadrilaterals. These types can be further subdivided into TRI3, TRI6 for triangles, and QUAD4, QUAD8 for quadrilaterals. TRI3 is a triangle mesh element type with 3 nodes. Additionally, TRI6 is a triangle mesh type with 6 nodes, while QUAD4 and QUAD8 mesh types are quadrilateral meshes with 4 and 8 nodes, respectively. In 3D, meshes can be categorized into five main groups: Hex Dominant, Tetrahedrons, Sweep, Multizone, and Cartesian.

In the thesis study, quadrilateral mesh type and triangular type mesh were used in some places for 2-dimensional analysis. The purpose of using this technique is to make the solution relatively close to reality due to the high number of nodes in the equations used in the analysis phase. However, due to the large number of nodes, this technique caused the duration of the meshing phase and analysis phase to increase and the total number of equations to be solved to be higher. In addition to the technique used, there are also various mesh techniques;

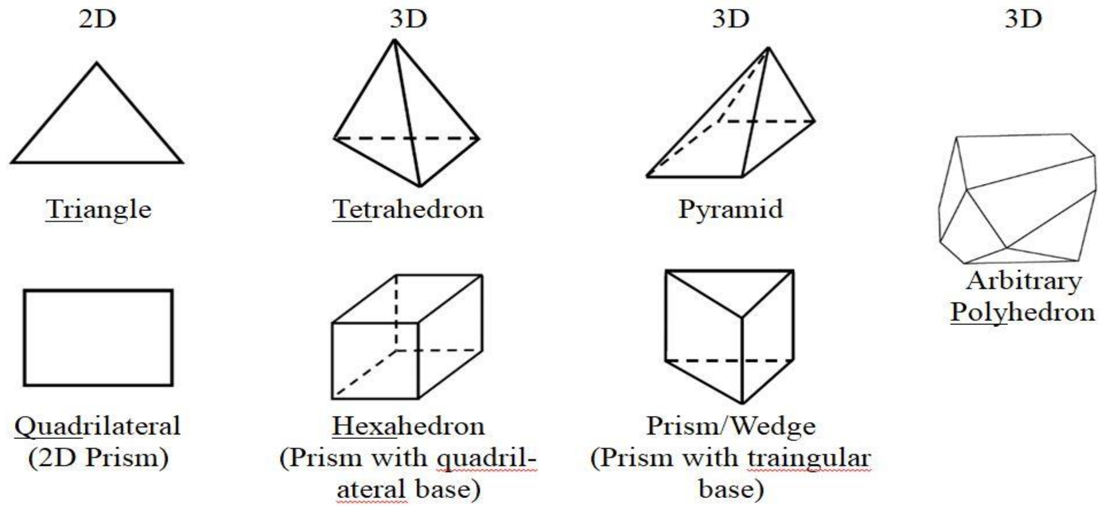

Figure 5.3 Mesh techniques according to their shapes (manchestercfd.co.uk)

5.4.1 Hex Dominant

Hex-dominant dominant meshing uses "Hexahedron" elements as the element type. This method is created by recombining the triangles of the initial network into rectangles. Therefore, using this method does not require that all elements have six sides. Many triangular or prismatic elements may still be present in the mesh geometry.

5.4.2 Tetrahedrons

Tetrahedral elements can be thought of as 2D three-dimensional counterparts of the triangular mesh type. Tetrahedral elements are typically formed equilaterally in systems with circular curvature. When a system has asymmetry, it can form as an isosceles tetrahedron. It has much higher accuracy than a simple 3D cubic mesh element or 2D square mesh element in terms of approximating the final results of the solution. This method is more suitable for polyhedral and relatively complex geometries.

5.4.3 Swept Mesh

Swept mesh can be defined as a mesh creation method that takes its name from the geometric creation technique used when creating geometry. This geometry creation option, called sweeping, continues regular geometries along a curve or along an axis. In other words, the sweep method is a modeling tool that relies on curved shapes or straight shapes to create the volume of a model.

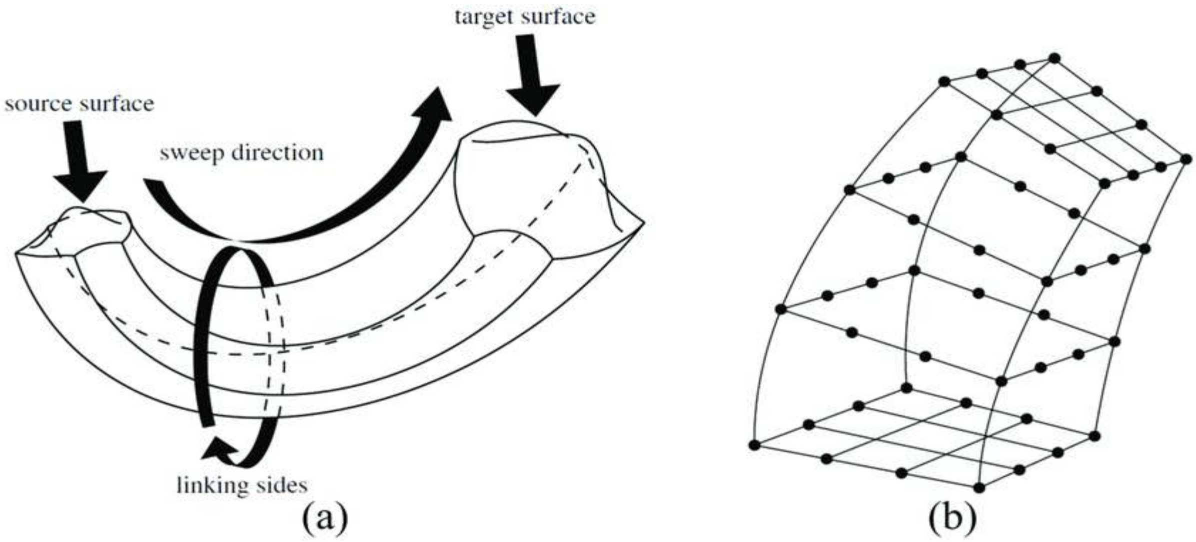

Figure 5.4 Swept Mesh Visulalisation. (Cai and Shengyong, 2015)

5.4.4 Multizone Mesh

If a shape is too complex to be created by the sweeping method, Multizone Mesh is used. It is a mesh method used especially when connecting body parts. It separates areas that can be swept from those that cannot. In this way, it combines the desired network into multiple regions.

5.4.5 Cartesian Mesh

Cartesian Mesh divides a geometry into Cartesian grids during meshing. Thus, a square-shaped grid pattern is formed. It takes its name from the square pattern formed. The advantage of this network method is that it can be created very quickly (Tucket and Pan, 2000).

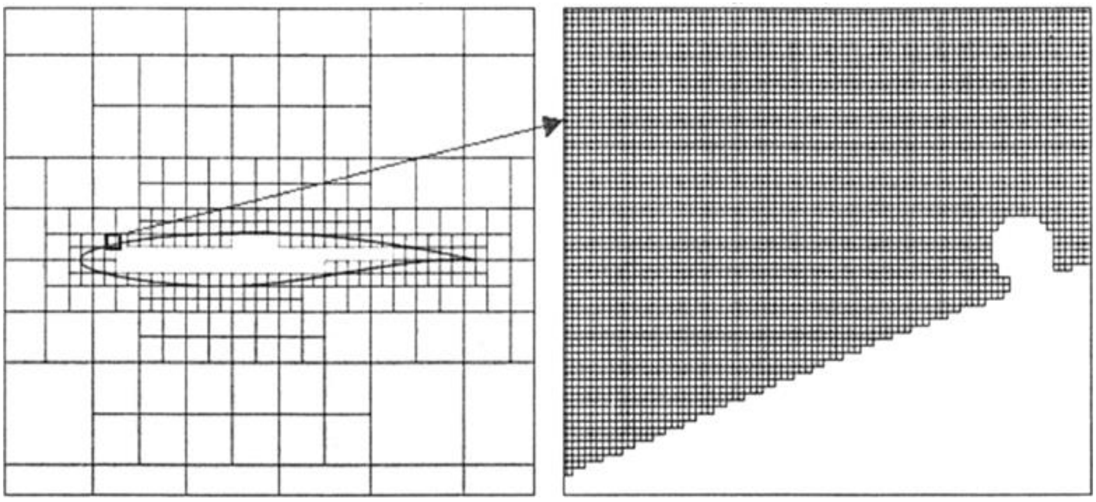

Figure 5.5 Mesh Finess (Kim et al, 2007)

5.5 Mesh Metrics

After the meshes are created, it is necessary to control the created mesh using some reference values and methods. These are called "Mesh Metrics". There are 8 main mesh metrics created by different methods. This is an important step in the pre-solution phase, as the quality of the mesh in a geometry directly affects the solution.

These mesh metrics are:

- Orthogonal Quality
- Element Quality
- Warping Factor
- Parallel Deviation
- Aspect Ratio
- Jacobian Ratio
- Maximum Corner Angle
- Skewness

The selection of mesh metrics is made specific to the geometry. When adding mesh to the geometry, if mesh metrics are not selected according to the meshing method used, deviations occur in the simulation results. In computational fluid dynamics solutions, especially in blade design, closely watched metrics include Orthogonal Quality, Element Quality, Jacobian Ratio and Skewness. In the thesis study, mesh metrics were carefully examined.

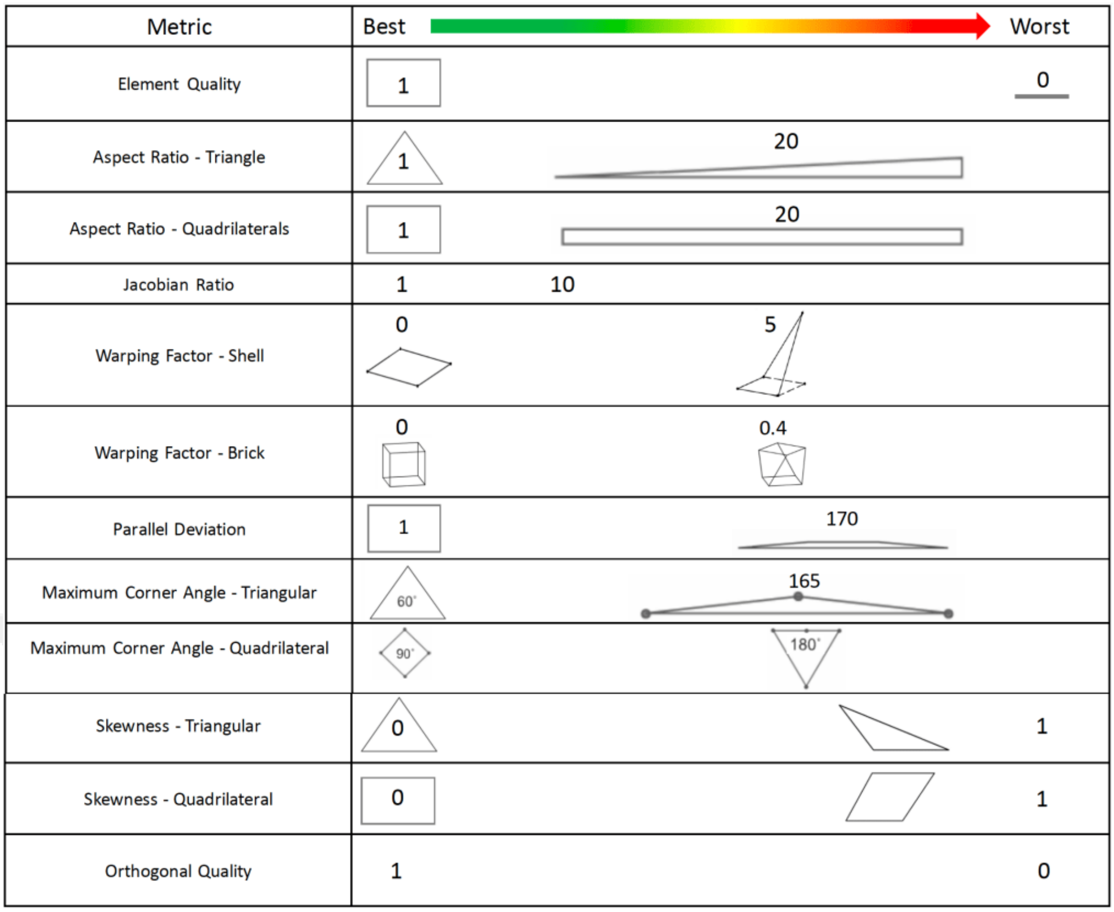

Figure 5.6 Mesh Metric reference values (Ansys User guide)

CHAPTER VI
TURBULANCE MODELS

6.1 Turbulence Models In CFD

Turbulence models are approaches used in fluid mechanics to describe and analyze turbulent flows mathematically through equations. It was stated that turbulence can be defined as irregular, random and complex movements of a fluid. Therefore, turbulent flows are quite complex to fully solve and predict. Turbulence models were developed to represent the effects of turbulence with simpler mathematical equations (Wilcox, 1998). These models are often based on statistical and numerical data to capture the fundamental characteristics of turbulence and produce accurate results.

6.2 K-ε Model

The K-ε model is one of the most widely used and oldest turbulence models (Nagano and Tagawa, 1990). This model is employed for the mathematical modeling of turbulent flows. The K-ε model utilizes two turbulence variables called turbulence kinetic energy (K) and turbulence scale (ε). The fundamental idea behind the K-ε model is based on the concept that turbulence scale controls the energy transfer, and turbulence kinetic energy feeds this energy transfer. The model calculates the effects of turbulence by using turbulence kinetic energy equations and turbulence scale equations. There are 2 parts of the K-ε equation, one of them is "Kinetic Energy Equation (K Equation)". This equation explains the change in turbulence kinetic energy. The velocity of the flow is influenced by factors such as pressure gradient, viscosity, and turbulence production. The other part of the equation is "Scale Equation (ε Equation)". This equation explains the change in turbulence scale. It is influenced by factors such as viscous dissipation, turbulence production, and turbulence diffusion.

These equations include terms such as turbulence generation, turbulence dispersion and viscous shear. Turbulence production represents the increase in turbulent energy due to velocity gradients in the flow. Turbulence dissipation expresses the decrease in turbulent energy due to viscous shear.

The K-ε model is a turbulence model that allows simple and computationally efficient modeling of turbulent flows. The K-ε model is a method used in various applications of turbulent flows, especially in sectors such as aviation and shipbuilding. The K-ε model produces accurate results in many cases. It is better to use more advanced equations instead of the K-ε model, especially when complex turbulence structures and local effects of flows are wanted to be investigated. The most commonly used isotropic two-equation turbulence model is the standard turbulence model (Launder and Spalding, 1974).

6.3 K-ω Model

The K-ω model is another widely used turbulence model. The K-ω model is used for mathematical modeling of turbulence and is particularly effective in complex flow conditions such as boundary layer flows and swirling flows. The K-ω model uses a new variable, Specific Dissipation Rate (ω), instead of Kinetic Energy (K). While kinetic energy is analyzed as in the K-ε model, the new variable related to kinetic energy is used as "ω" in order to obtain more accurate results. This model also performs well in low Reynolds number flows (Zheng et al., 1998).

The k-ω equation has 2 parts. The first chapter is about "Kinetic Energy Equation (K Equation)". This equation describes the change in turbulence kinetic energy. Gradients of flow rate are affected by factors such as pressure gradient and viscous shear. The second part of the equation is the "New Variable Equation (ω Equation)". This equation explains the change in the new variable related to kinetic energy. This variable is affected by factors such as viscous shear, kinetic energy production, and the distribution of the new variable related to kinetic energy. The K-ω model can be used in a variety of flow conditions, especially in boundary layer flows, rotating flows, and complex geometries. The k-ω model can better capture the effects of rotation-related turbulence in rotating flows and predict the results more accurately. However, the K-ω model has some limitations, like K-ε. More advanced models may be necessary, especially for situations involving high Reynolds number flows and large-scale turbulence structures.

6.4 Reynolds-averaged Navier-Stokes (RANS) Model

Reynolds-Averaged Navier-Stokes (RANS) is another turbulence modeling approach used for mathematical modeling of turbulent flows. RANS consists of a set of equations used to capture the average effects of turbulence. This model takes the time average of the flow variables and combines them with turbulence effects to produce a new equation. The RANS model is basically the Navier-Stokes equations averaged over time. In RANS equations, turbulence effects are expressed using several parameters. These are; terms related to viscous friction and terms related to Reynolds number. These terms arise from factors such as turbulence generation, turbulence dissipation, and turbulent viscosity. It is calculated according to turbulence variables such as turbulence energy and turbulence scale.

RANS models can often be viewed as simpler and computationally faster. Therefore, they are widely used in practical engineering applications. RANS models have applications in various industrial and academic environments, such as aircraft hydrofoils, automotive aerodynamics, turbine blades, etc. It may have difficulty accurately capturing large-scale turbulence structures and may not fully reflect the time-varying characteristics of turbulence, which imposes some limitations when modeling real-time turbulence events.

6.5 Large Eddy Simulation (LES) Model

Large Eddy Simulation (LES) is another turbulence model used to directly solve turbulent flows and accurately model large-scale structures. After calculating large-scale turbulence structures, LES identifies small-scale structures using a subgrid model. The basic idea behind LES is based on the concept that large-scale structures of turbulent flows should be solved directly, but small-scale structures should be modeled due to computational costs. Therefore, LES accurately resolves large-scale turbulent structures while representing small-scale structures using a subgrid model.

LES provides more detailed and realistic results by accurately capturing large-scale structures of the flow. Large-scale structures are fundamental components of energy transfer and are an important parameter in determining the properties of the flow. Small-scale structures have more local and random fluctuations. Therefore, LES uses the assumption that the energy transfer of turbulence is characterized by large-scale structures. LES models are often used in complex flow conditions and produce relatively good results, especially in cases involving large-scale turbulence structures and local effects of flow. However, on the other hand, LES is a computationally expensive method because a finer mesh is required both to directly solve large-scale structures and to model small-scale structures.

6.6 Direct Numerical Simulation (DNS) Model

Direct Numerical Simulation, or DNS, is a turbulence modeling method that solves turbulent flows in the most detailed and accurate way. DNS solves the Navier-Stokes equations directly. The next stage calculates all scales and structures of turbulence in the flow. The working logic of DNS is to proceed by precisely resolving all turbulent movements at every scale of the flow. In this method, Navier-Stokes equations calculate exact solutions for all flow variables with respect to time and three-dimensional space. This allows every detail of the flow, all turbulent movements and energy transfer to be accurately captured. The advantages of DNS include obtaining completely accurate results and a comprehensive understanding of the turbulence structure. Therefore, it enables detailed analysis of the nature of turbulence, energy transfer, flow properties and turbulence structure by providing access to information covering all scales and all-time scales of the flow.

DNS is also a suitable method for detailed analysis of small-scale turbulence structures and energy transfer. A high-resolution computational grid is required to accurately observe in realistic circumstance, turbulence events at every point and moment in the flow. DNS requires significant computational resources and high processing power because a very fine grid must be used to resolve the details of turbulence at all scales. Therefore, DNS is often used for low Reynolds number flows or small-scale research studies. In practical engineering applications, DNS results can be used as a reference to understand the effects of large-scale turbulence structures and to determine their parameters.

6.7 Shear Stress Transport Model

Shear Stress Transport (SST) model is known as a turbulence modeling method used in mathematical modeling of turbulence. It aims to achieve better performance in different regions of the flow by combining the "k-ω" and "k-ε" models (Menter, 2009). The SST model uses Reynolds-averaged Navier-Stokes (RANS) equations to resolve turbulence effects. These equations describe the average behavior of the flow. By including turbulence effects, it ensures more realistic results. The SST model offers an optimal solution for 2 cases. One of these is in low Reynolds number flows, where the k-ω model performs well near walls. The other is in high Reynolds number flows, where the k-ε model performs better in free flow regions. The combination of these two models allows for more accurate results in different regions of the flow. The SST model combines information from the k-ω and k-ε equations to describe the turbulence structure within the flow. On the other hand, the k-ε model is used to capture large-scale turbulence structures in free flow regions. The SST model uses various turbulent transport equations to calculate the turbulent viscosity of the flow. These equations express turbulence formation, turbulence distribution and turbulent viscosity. In this way, turbulence effects are calculated accurately and the turbulence structure in the flow is represented more realistically. The advantage of the SST model lies in its ability to perform well in both low Reynolds number near-wall regions and high Reynolds number free flow regions. It is a widely accepted turbulence model that is frequently used in practical engineering applications. However, the SST model has some disadvantages, especially in capturing the full complexity of the turbulence structure. Therefore, its suitability for each application must be evaluated. In conclusion, the Shear Stress Transport (SST) model is a turbulence modeling method that aims to achieve better performance in different regions of the flow by combining k-ω and k-ε models (Rahman, 2022).

CHAPTER VII
BLADE SECTION SELECTION

7.1 Selection of Hydrofoil

In hydrokinetic turbines, the blade profile holds a critical position as it directly influences efficiency and operational principles. If the designed blade profiles do not possess the desired characteristics, relatively low efficiency results can be obtained. NACA airfoil profiles can be categorized into various types, including flat-bottomed, cambered, and symmetric profiles. Within the scope of the study, 6 different blade structures have been examined, namely NACA-0011sc, NACA-0018, NACA-1412, NACA-2418, NACAchy, and NACA-M18. The selected blade profiles for use in the thesis have been determined to compare different blade structures. Blade structures can be classified as symmetric or non-symmetric. Various blade types have been selected, ensuring representation from at least one type within each hydrofoil category.

No	Hydrofoil Code	Hydrofoils
1	NACA-0018	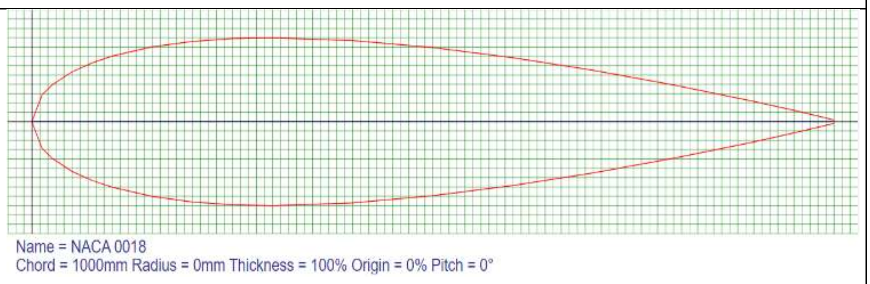
2	NACA-2418	

No	Hydrofoil Code	Hydrofoils
3	NACA-0011sc	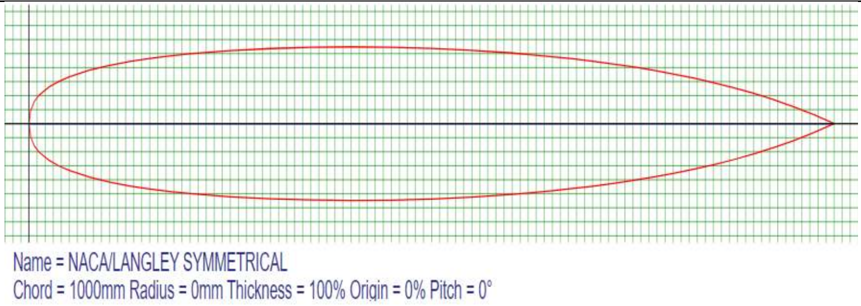
4	NACA-1412	
5	NACA-M18	
6	NACA-CHY	

Angle of attack is related to the position of rotor blades in the fluid and has a significant impact on the efficiency and energy performance of the turbine. The attack angle determines the position and angle of the turbine blades in the fluid. The correct attack angle enables the blades to more effectively resist the movement of the fluid and convert more energy. With the correct AoA, the blades can capture more energy and can get higher power outputs. In hydrokinetic turbines, the AoA can help prevent undesired phenomena such as cavitation on the blades. The attack angle is a crucial factor in the design and operation of hydrokinetic turbines, influencing efficiency, energy production, and durability. Therefore, the selection and control of the correct attack angle are of great importance in turbine design and operation. In the design phase, 17 different attack angles (1°, 2°, 3°, 4°, 5°, 6°, 7°, 8°, 9°, 10°, 11°, 12°, 13°, 14°, 15°, 20°, 25°) have been modeled for 6 different blade types.

7.2 Pre-processing

7.2.1 Geometry

Before modeling, it is necessary to introduce the blade profiles to Ansys. Ansys geometry modules support various file formats. In the scope of the study, blade profiles were transferred to the Ansys geometry module by entering 3-axis coordinates as "X, Y, Z" in the coordinate plane. The geometry modeled around the blade represents the area where the fluid flows. Modeling the fluid too close to the blade can lead to undesired results. Therefore, in the modeled geometries, boundaries were set at a distance of at least 6 times the length of the blade. In the visual given in Figure 7.1; R4 dimension is modeled as 6 meters, H5 and H6 dimensions are modeled as 20 meters, and V7 dimension is modeled as 12 meters

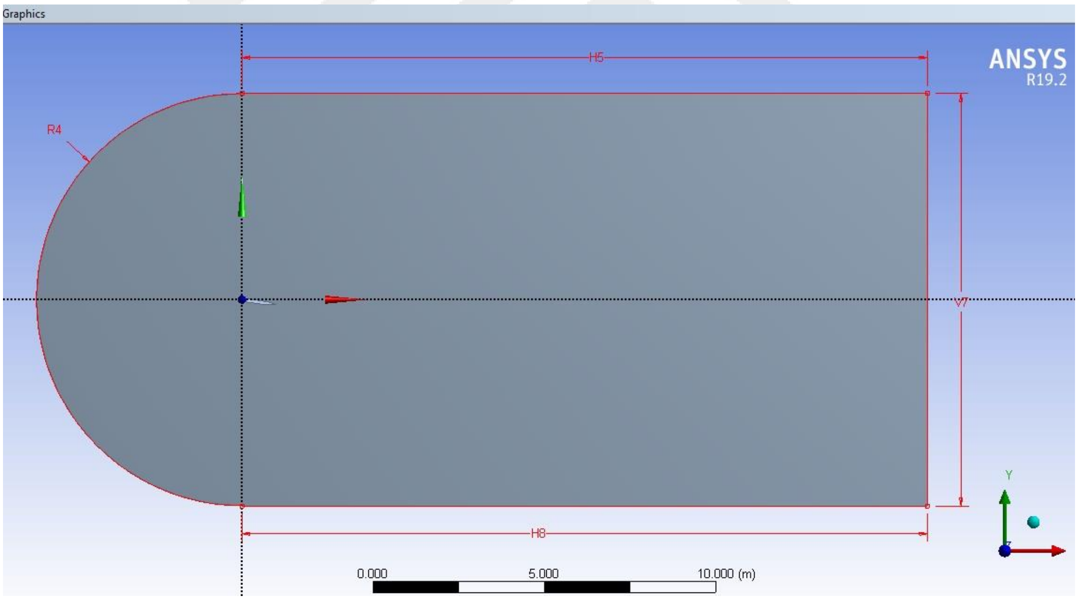

Figure 7.1 The geometry features to be used in the modeled hydrofoils

The lengths of the blade profiles are set to 1 meter. As mentioned in the theoretical section, the forces generated by the blades are directly proportional to their lengths. Setting the blade lengths to 1 meter is done to prevent potential issues in geometry and mesh quality. Since the blade length can affect the solidity value, at this stage, the results of standard 1-meter blade profiles will be compared against each other based on certain parameters to select the best blade profile. The data obtained from blades with a length of 1 meter is expected to exhibit parallel behavior with models having longer or shorter blade lengths.

7.2.2 Mesh Features of Hydrofoils

It was conveyed in the "Mesh" and "Theory" sections that mesh quality in CFD analyzes has a significant impact on the accuracy, stability and efficiency of calculations. Since mesh quality directly determines how close the results are to approximate or certain values, information was transferred again for the constitutive meshes at this design stage. Meshes created in low quality can produce misleading results, especially in models with sharp geometries or complex flow features. Good mesh quality simulates the effects of turbulence and flow details more accurately, allowing a more precise determination of the forces acting on the modeled geometry.

7.2.2.1 Boundary Conditions and Surface Interactions

The mesh quality assists in accurately simulating the interaction with the fluid's boundary surfaces. This is crucial for surface friction, flow separation, and other flow characteristics. The walls surrounding the blade have been divided into at least 1000 equal parts, creating a dense mesh network in this region.

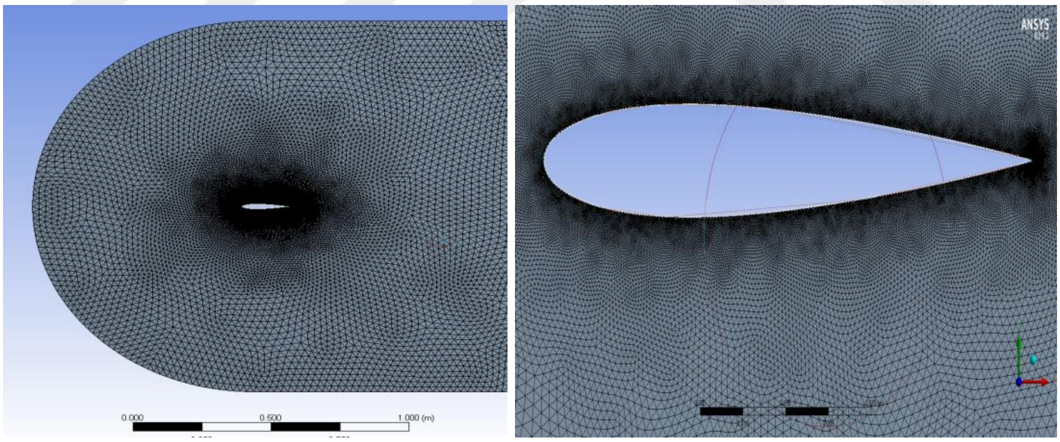

Figure 7.2 Mesh density used on hydrofoils

7.2.2.2 Time and Resource Efficiency

While calculations can take time to complete in a highly complex and detailed network structure, high-quality networks have a significant impact on the result accuracy despite the time disadvantages. Low-quality mesh structures may save time in the calculation phase, but may lead to less accurate results. When determining the mesh structure and type, paying attention to these two parameters is very important in terms of both result accuracy and required time. Using a dense mesh on 2D geometries does not require excessive computational power as it does not excessively increase the total number of meshes. Therefore, the network density used in the models is high for this stage.

Skewness Mesh Metrics Intervals					
Excellent	**Very good**	**Good**	**Acceptable**	**Bad**	**Unacceptable**
0-0.25	0.25-0.50	0.50-0.80	0.80-0.949	0.95-0.979	0.98-1.00
Orthogonal Quality Mesh Metrics Intervals					
Excellent	**Very good**	**Good**	**Acceptable**	**Bad**	**Unacceptable**
0-0.001	0.001-0.14	0.15-0.20	0.20-0.69	0.70-0.95	0.95-1.00

Figure 7.3 Mesh Metric Scale (Fatchurrohman and Chia, 2017)

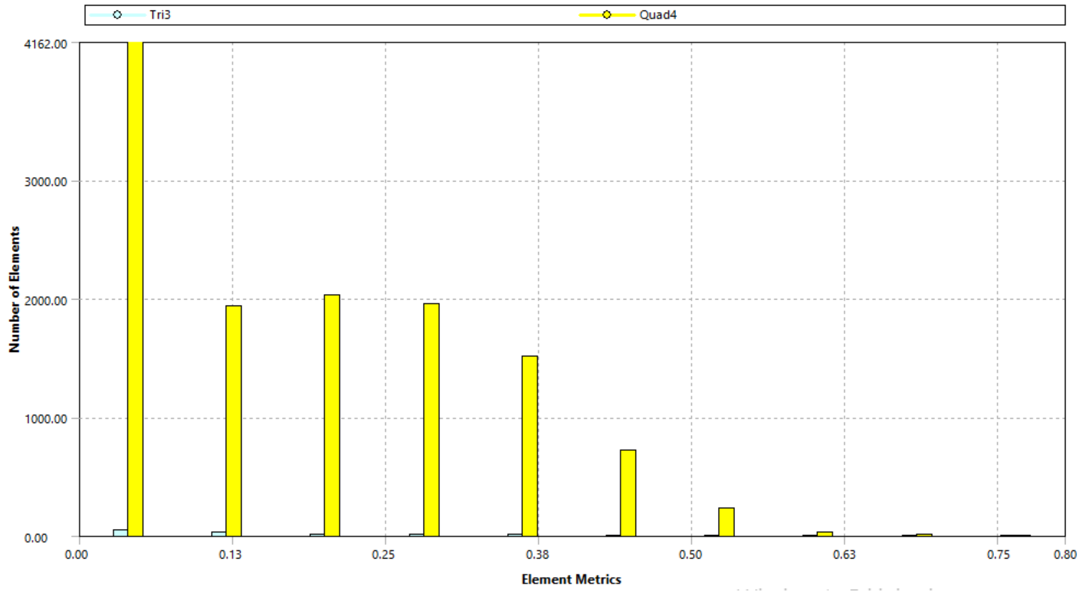

Figure7.4 Skewness table for mesh used in hydrofoil profiles

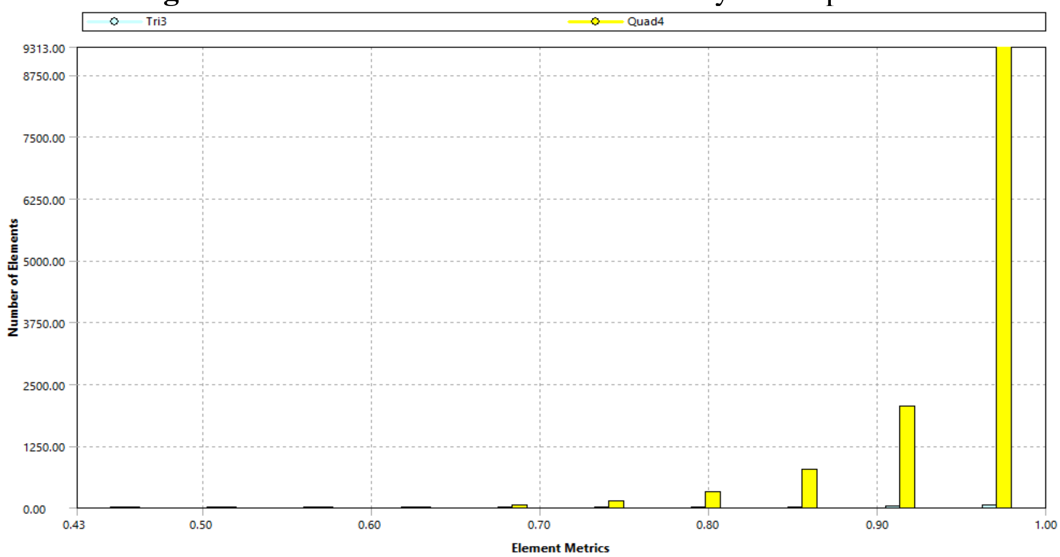

Figure7.5 Orthogonal quality table for mesh used in hydrofoil profiles

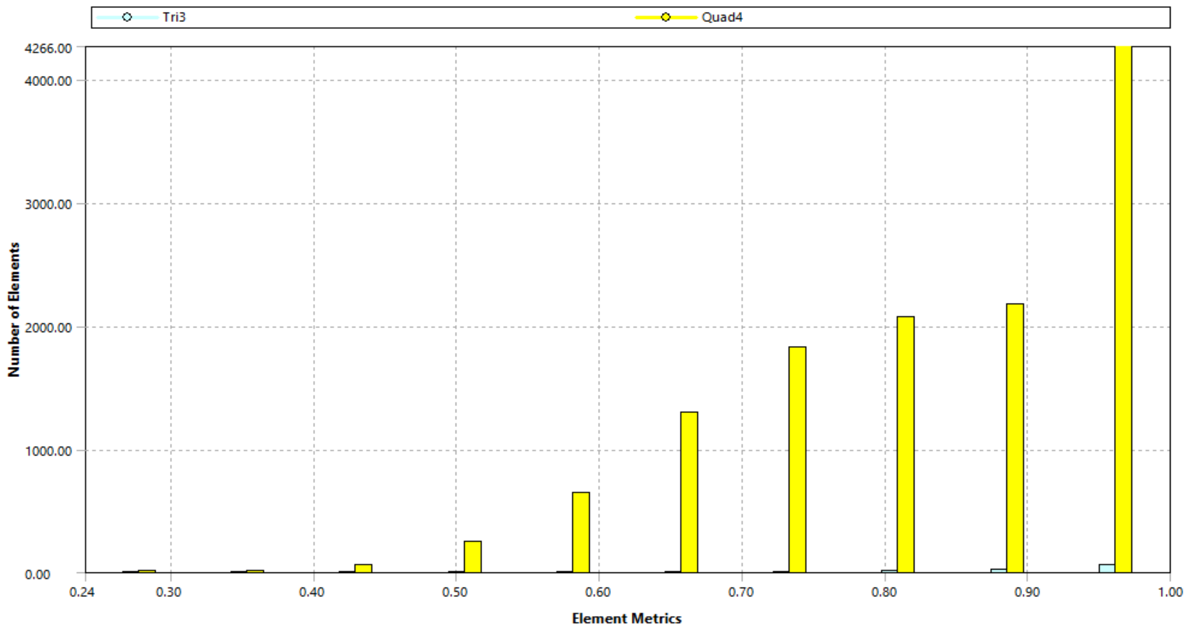

Figure7.6 Element quality table for mesh used in hydrofoil profiles

7.2.2.3 Geometric Complexity

High quality mesh should also be able to reveal the details in the modeled geometry. The hydrofoils used in the model have the feature of simple geometry. Turbulences that may occur during the movement of liquids around the model are important for the results. Since relatively small geometric additions in the model can cause turbulence, a mesh structure and count that reflects the geometry as much as possible was used. The curvature faces of the hydrofoils used are fixed to a certain degree, as seen in Figure 7.7, and no additional edges are allowed.

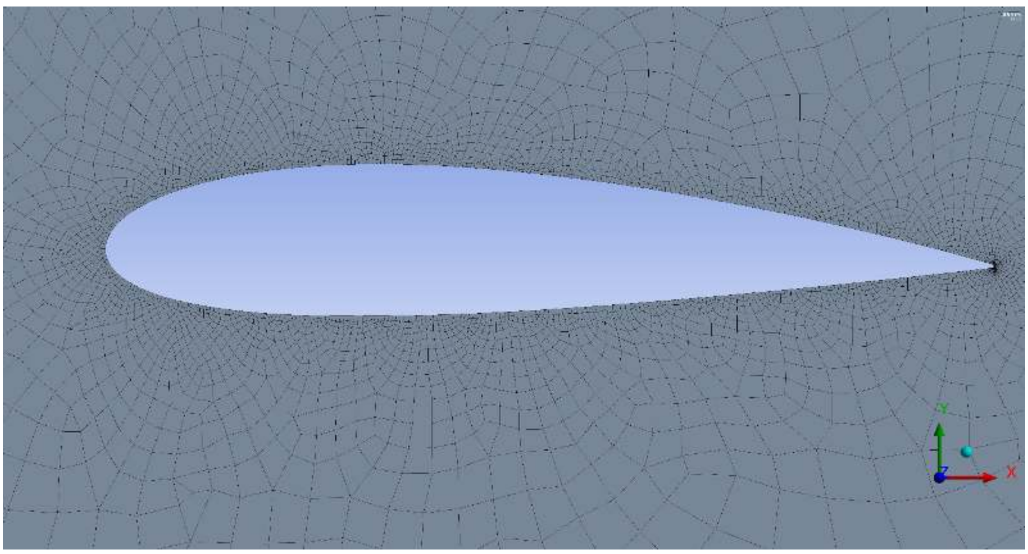

Figure 7.7 Curvature features in hydrofoil profiles

7.2.3 Analysis Setup of Hydrofoils

When configuring analysis settings, parameters should be added as realistic and close to reality as possible. There are several parameters in the analysis settings including 'Boundary Conditions', 'Viscous Models', 'Solution Methods' and 'Iteration Settings'.

7.2.3.1 Boundary conditions

Boundary conditions mathematically impose limits on the system being analyzed. It describes how the fluid will interact with these boundaries. It has parameters such as inlet conditions, outlet conditions, surface conditions.

Inlet Conditions: Inlet boundary conditions address the conditions at which the fluid enters the system. In general, in fluid studies; Features such as speed, temperature, pressure is stated in the introduction section. These conditions determine the starting point of the analysis and how the fluid enters the system. In the models created, entry speeds were set to 1 m/s.

Outlet Conditions: Exit boundary conditions consist of parameters that define how the fluid will exit the analysis area. This defines parameters such as velocity, pressure or temperature of the fluid at the outlet. Outlet conditions have a great impact on how the fluid will be separated from the analysis area and how the analysis results will be evaluated. In the created model, the outlet condition is set as pressure condition.

Wall Conditions: Wall boundary conditions are concerned with how the fluid should behave in that region when it encounters a surface or wall. The fluid velocity can be set to zero or a certain value perpendicular to the wall. The surface properties of the walls directly affect fluid surface friction and heat transfer. In the modeled geometries, hydrophilic blade edges were modeled with a non-slip condition.

Symmetry Conditions: Symmetry conditions are a parameter used in case there is symmetry in the geometry of the model. Since most of the hydrofoils used in the study were not symmetrical, this feature was not defined in the analyses. However, they can be used for geometries containing symmetry as they provide time economy.

Boundary conditions are important factors that affect the realism and accuracy of the analysis. Therefore, before analysis is carried out, the problem and the purpose of the analysis must be well defined. Only in this way will it be possible to create appropriate boundary conditions. Incorrect boundary conditions can adversely affect the accuracy of analysis results in representing a practical scenario.

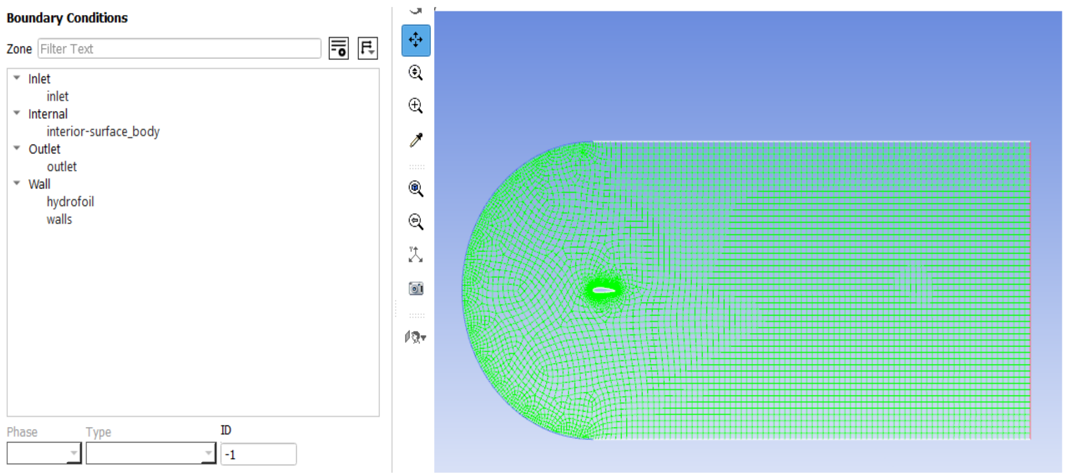

Figure 7.8 Boundary conditions of models

7.2.3.2 Viscous Model

Turbulence models are explained in detail in the relevant section. In this section, we will focus on the turbulence model used. Taking into account the complexity of the model, computational resources and the purpose of the analysis, the turbulence model was determined as SST k-omega. Complex turbulence models with higher computational costs can be used to obtain more accurate results. However, at this stage, it is seen that using SST k-omega equations with its simple geometry and good mesh quality will not affect the results much.

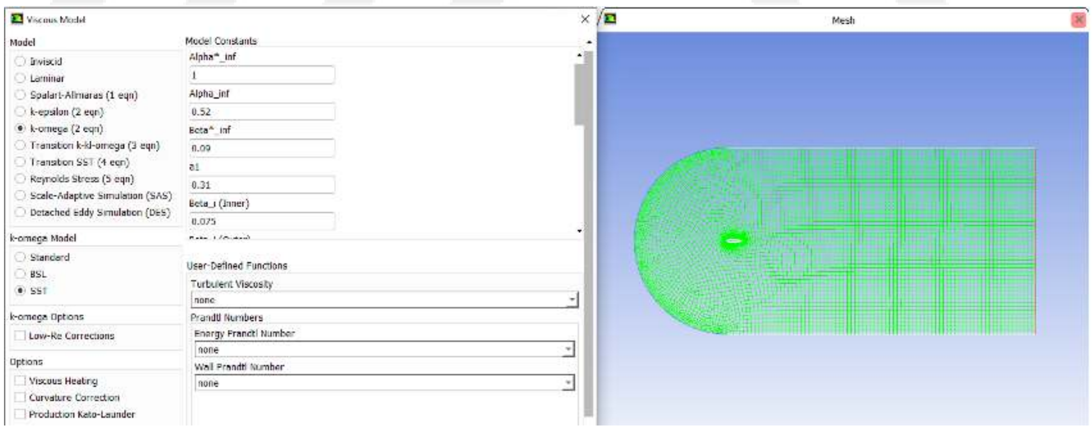

Figure 7.9 K-omega SST turbulence model parameters

7.2.3.3 Solution Methods

The separate section on Solvers is not mentioned. Basic level about solvers; They can be defined as the basic components used in Computational Fluid Dynamics (CFD) analyzes to simulate the movement of fluids by solving mathematical equations. Solvers represent numerical algorithms used to determine properties such as velocity, pressure, and temperature of fluids. Navier-Stokes equations are equations that mathematically describe fluid motion. Solvers solve these equations using numerical methods and calculate the variables of the flow. Solvent selection greatly affects the accuracy of analysis results. More complex solvers have the potential to produce more accurate results but may require additional computational resources.

Advanced solvers may be needed to model complex fluid behavior and more effectively address phenomena such as turbulence, heat transfer, and multiphase flows. In designs where turbulence needs to be actively taken into consideration, it is a good option to use second order energy equations as much as possible. A good solver helps achieve faster and more reliable convergence in the analysis. Solvers designed to operate under different physical conditions allow the flow to adapt to changing conditions.

Solvers are a fundamental phenomenon of CFD analysis. The correct selection of a solvent significantly affects the accuracy, reliability and analysis time of the results. In the models, parameters such as energy, loss rate, turbulence kinetic energy and momentum are solved in the second order.

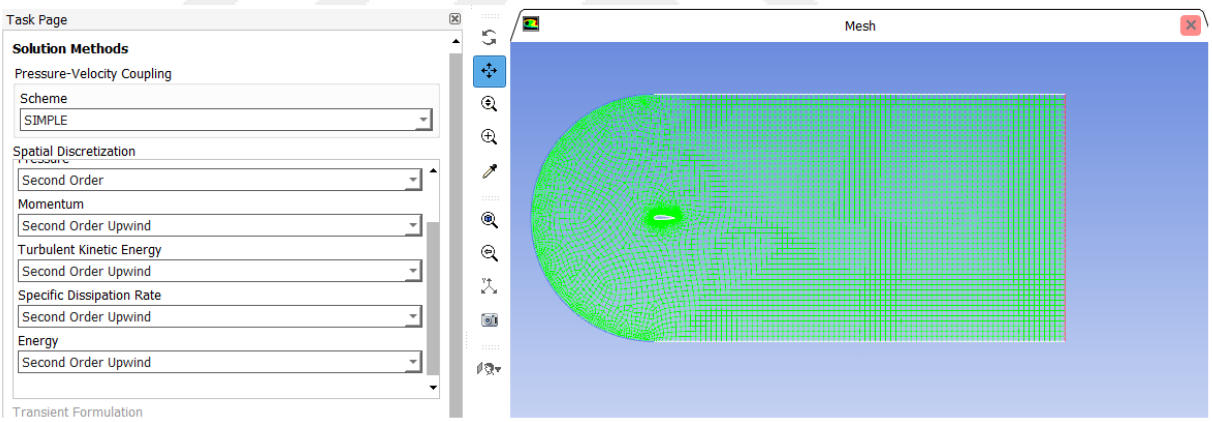

Figure 7.10 Solution methods features of modelled hydrograph

7.2.3.4 Number of Iterations

The number of iterations used in their analysis is an important variable for the accuracy of the results. It is directly related to the stability of the solution. Iterations mean how many times that equation is repeated in the process of solving mathematical equations representing fluid motion. In numerical methods; There are equations solved for each mesh cell. The results obtained from these equations are used as an input when solving the next equation, and this process ends with the convergence of the output parameter to the input parameter. Iterations continue until the analysis reaches the desired result.

Convergence in analysis allows results to be obtained with a certain level of precision and stability. Insufficient iterations may prevent analysis from convergence. It is inevitable to use a different number of iterations for each geometry and analysis setting. As simple iteration stages; Initially, flow rates, pressures, and other variables in the analysis area are estimated. These initial guesses determine the starting point for iterations. The closeness of the initial estimates to the certain values increases the convergence rate, and when the result converges, the final solution is reached. Various solver and turbulence model choices affect the convergence of the analysis. Some solvers or models may converge faster or slower. Stricter criteria may require slower convergence. Complex turbulent flows or intense fluid interactions may require more iterations. The nature of the flow and the purpose of the analysis affect the number of iterations.

Although a higher number of iterations produces a more accurate solution, after a certain point the solutions start to become very convergent. After this point, increasing the number of iterations only increases the need for processing power and does not significantly change the results. In general, the number of iterations is crucial for the reliability and accuracy of the analysis. A well-defined iteration strategy ensures that the analysis produces the desired results. Therefore, a balance appropriate to the purpose and complexity of the problem must be sought. 800 iterations were used in the models and it was observed that RSM values reached 10^-4.

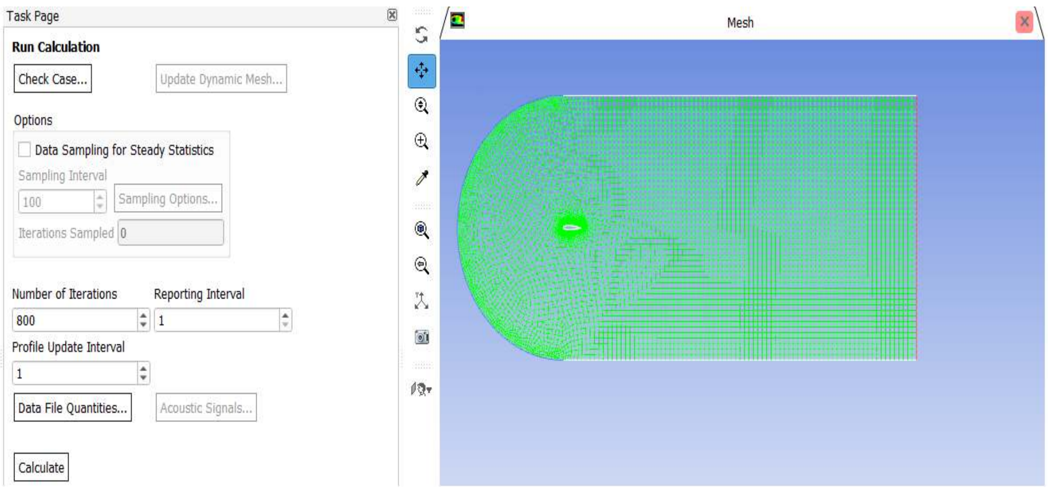

Figure 7.11 Number of iteration parameter in modelled hydrofoils.

7.3 Post-processing

The hydrofoil profiles were analyzed at different angles of attack, and the output included velocity and pressure contours, drag forces, lift forces, and Cl/Cd values.

7.3.1 Velocity and Pressure Counters

Velocity and pressure contours are an important monitoring tool used in fluid dynamics and aerodynamic studies. They provide important information, especially by showing moving or stagnant areas of the liquid and pressure changes. These contours can be used to examine and optimize the aerodynamic effects on hydrofoils during the design phase. It simplifies visual understanding of complex fluid dynamics topics and enhances the design process. Changes in velocity and pressure contours at different angles of attack are shown. Pressure and velocity curves for each hydrofoil at various angles of attack are presented sequentially.

NACA-0011SC		
AoA	**Pressure Counter**	**Velocity Counter**
1°	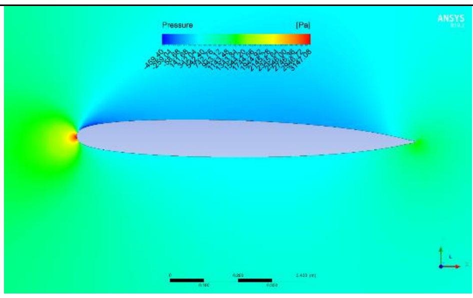	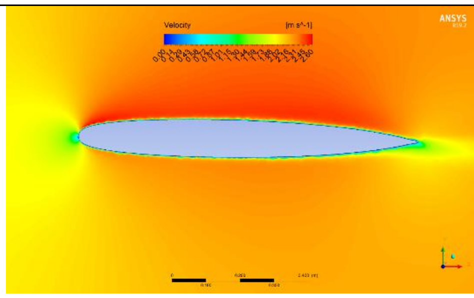
2°	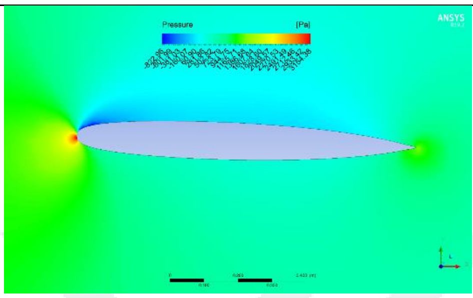	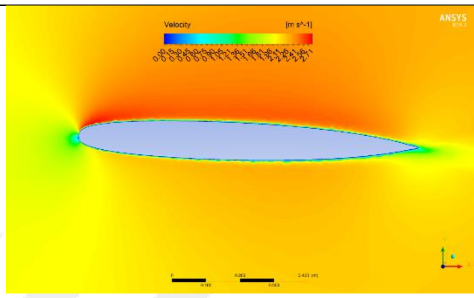
3°	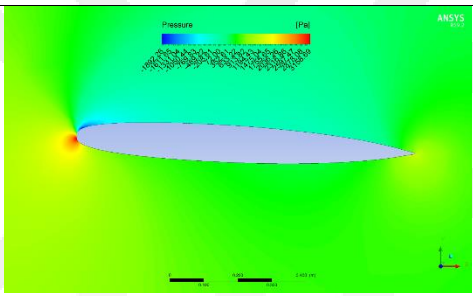	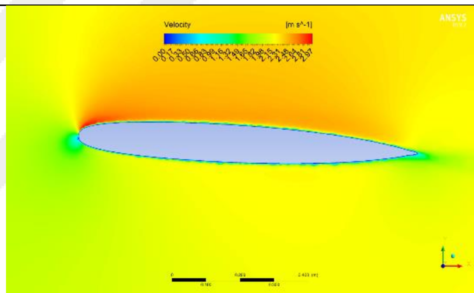
4°	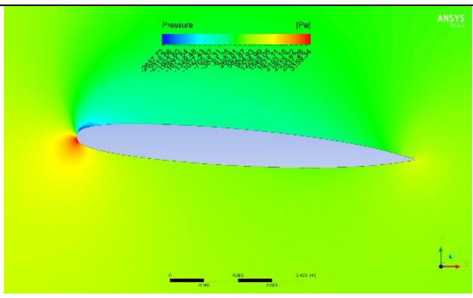	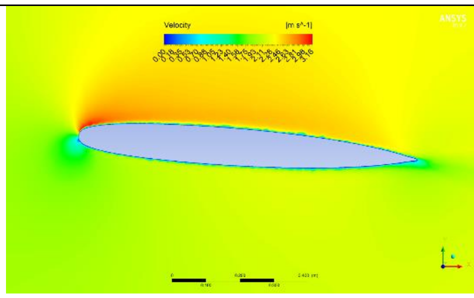
5°	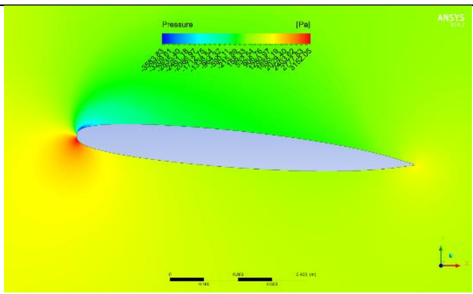	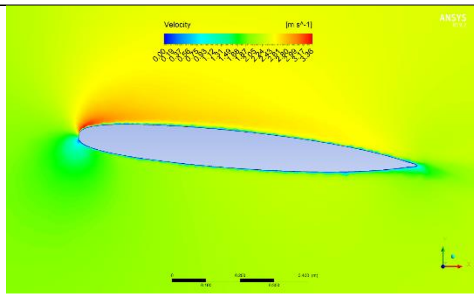

NACA-0011SC		
AoA	**Pressure Counter**	**Velocity Counter**
6°	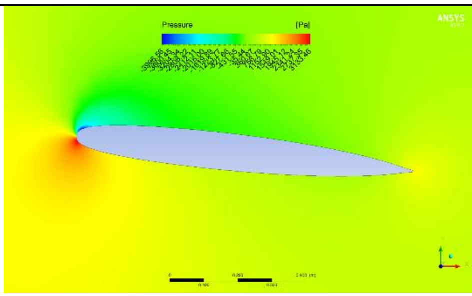	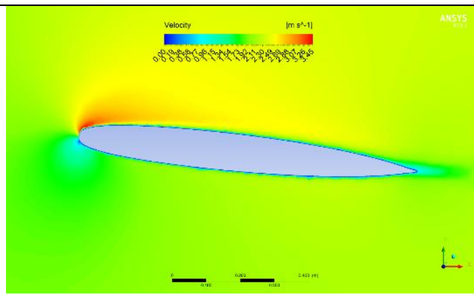
7°	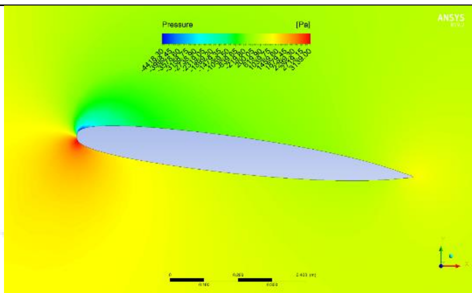	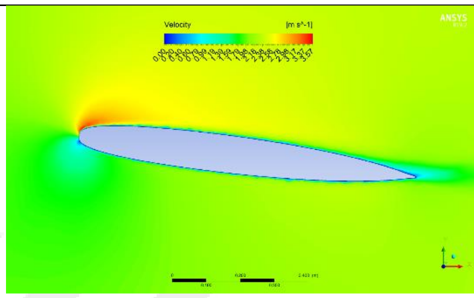
8°	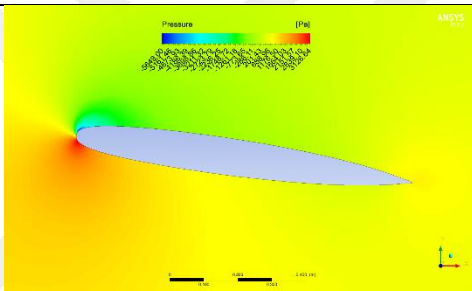	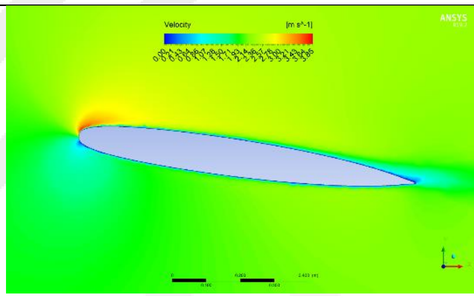
9°	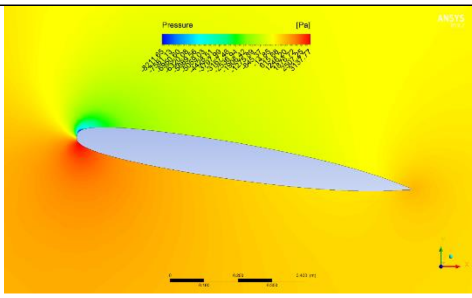	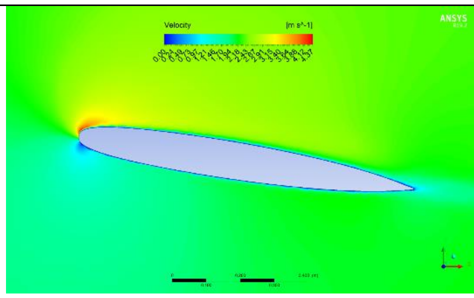
10°	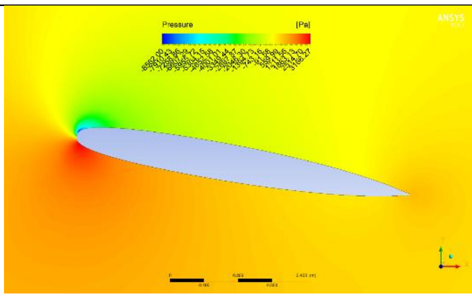	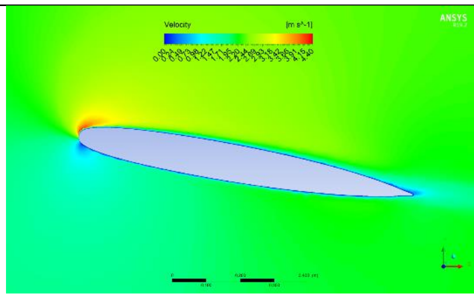

NACA-0011SC		
AoA	**Pressure Counter**	**Velocity Counter**
11°	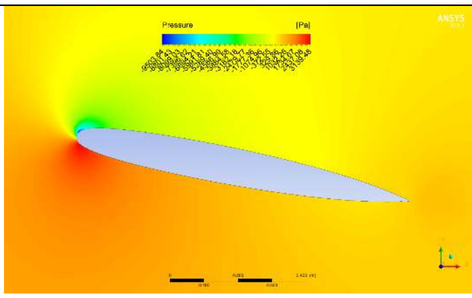	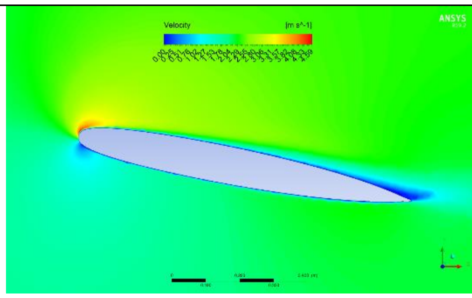
12°	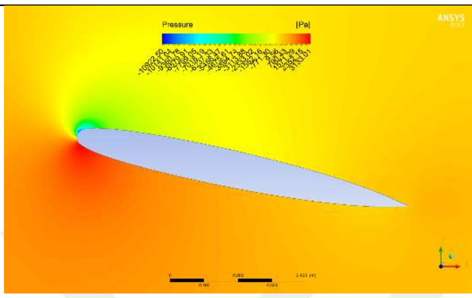	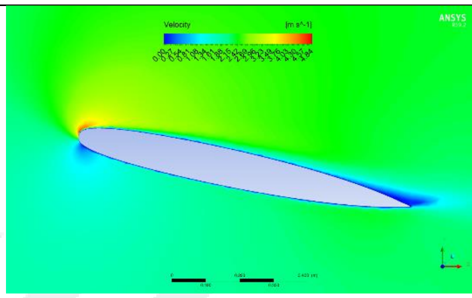
13°	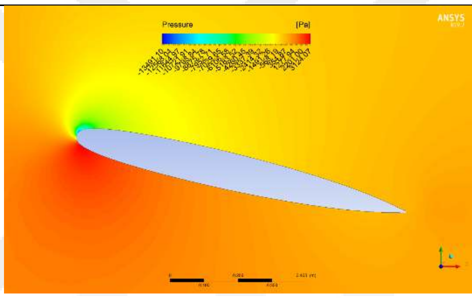	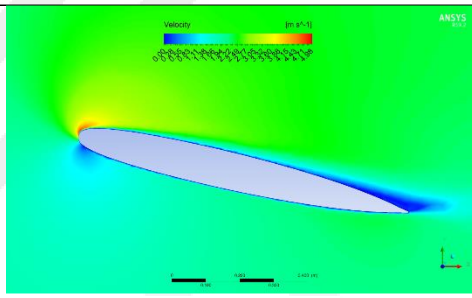
14°	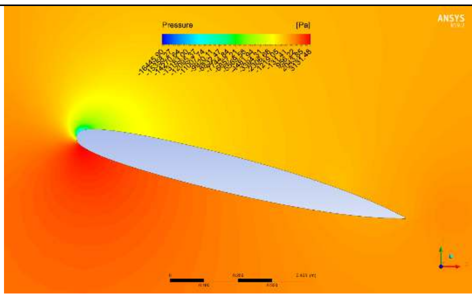	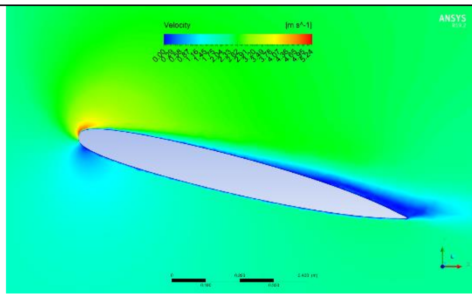
15°	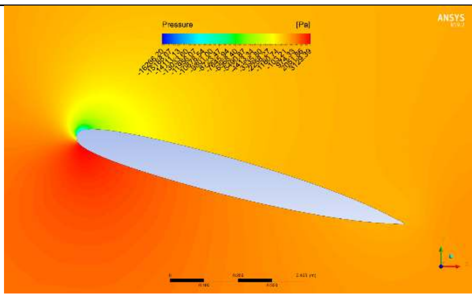	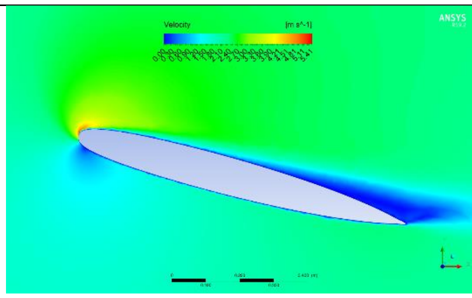

NACA-0011SC		
AoA	**Pressure Counter**	**Velocity Counter**
20°	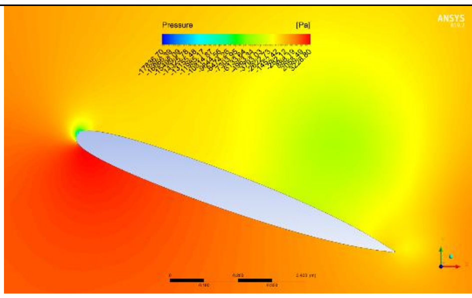	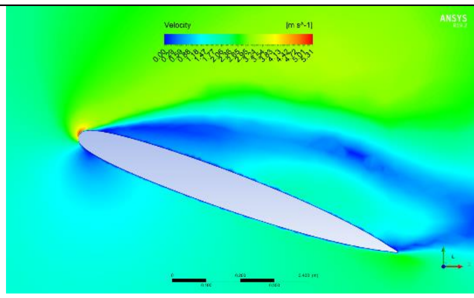
25°	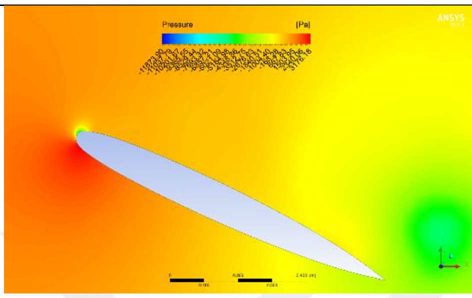	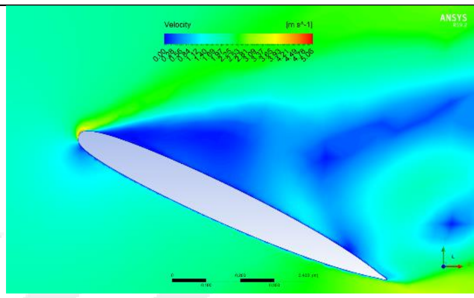

NACA-0018		
AoA	**Pressure Counter**	**Velocity Counter**
1°	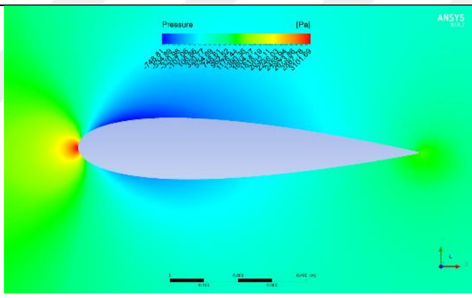	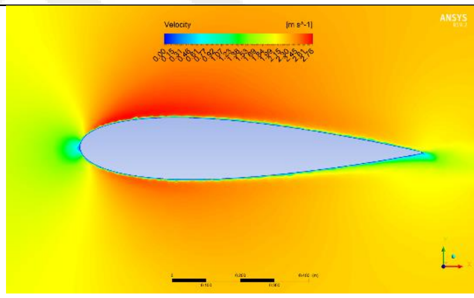
2°	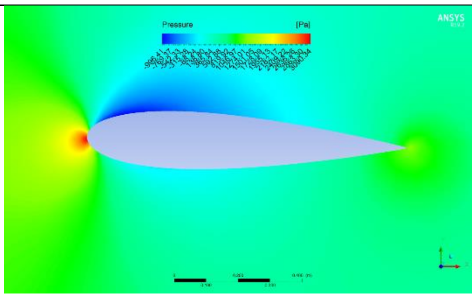	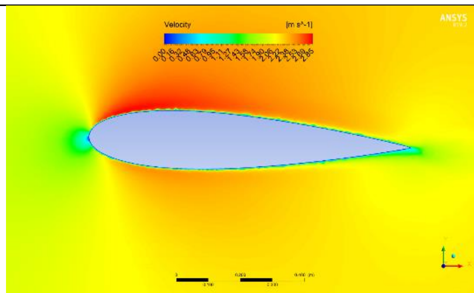
3°	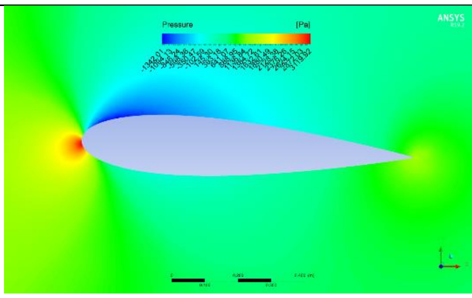	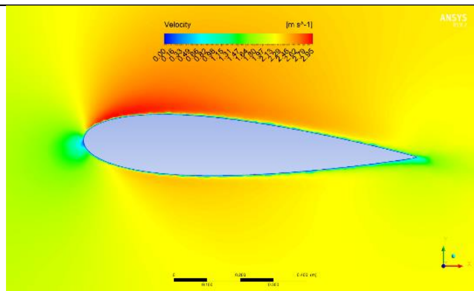

NACA-0018		
AoA	**Pressure Counter**	**Velocity Counter**
4°	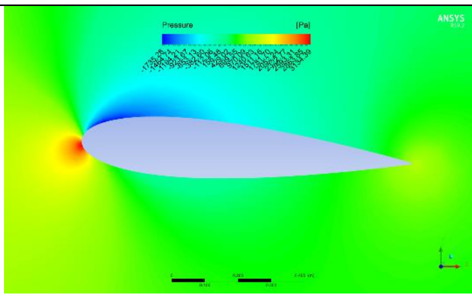	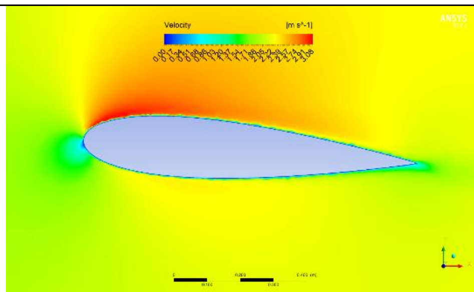
5°	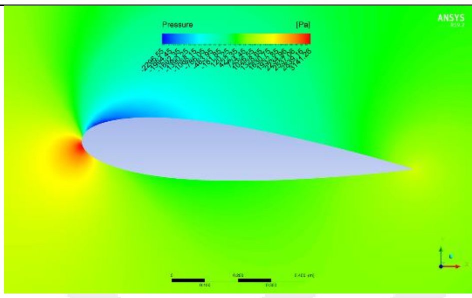	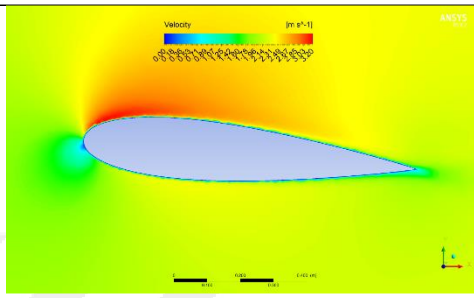
6°	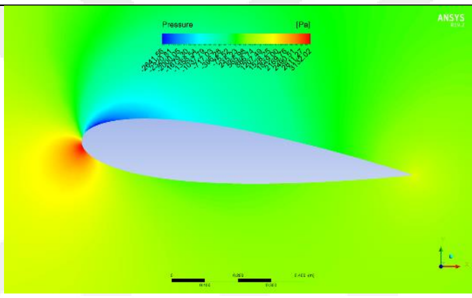	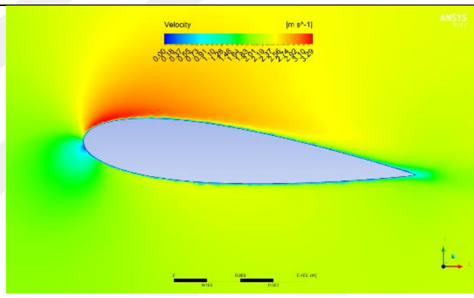
7°	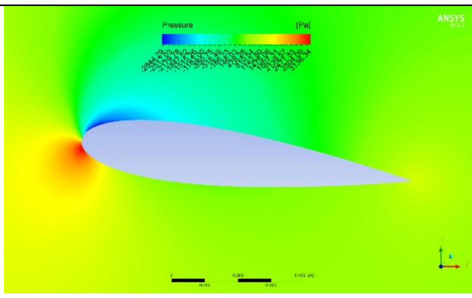	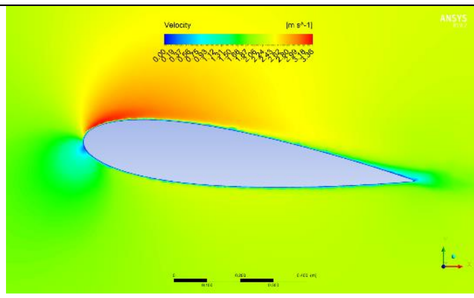
8°	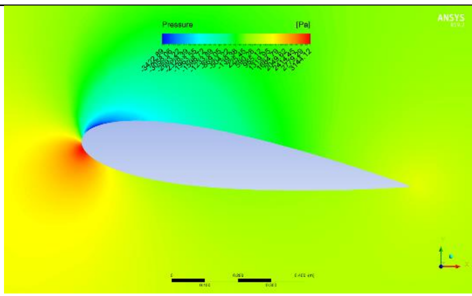	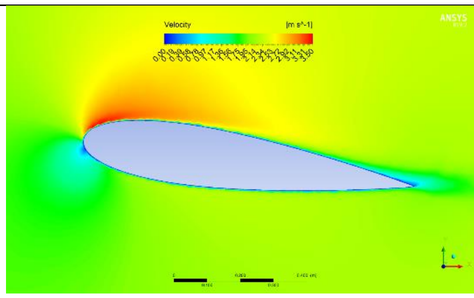

NACA-0018		
AoA	**Pressure Counter**	**Velocity Counter**
9°	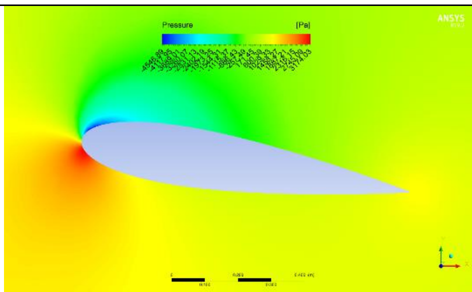	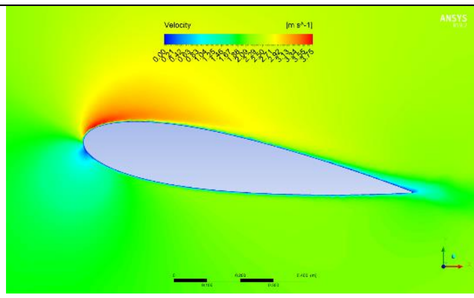
10°	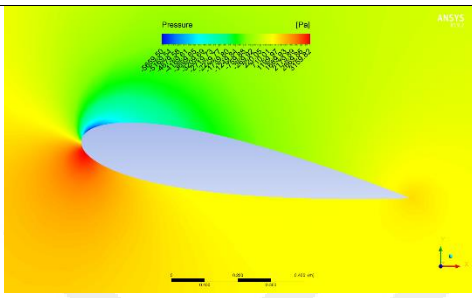	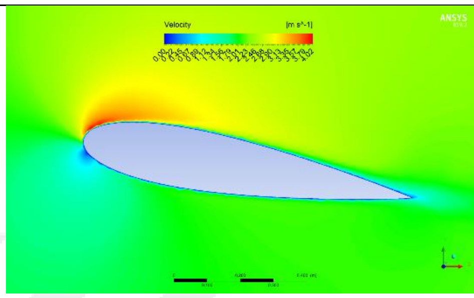
11°	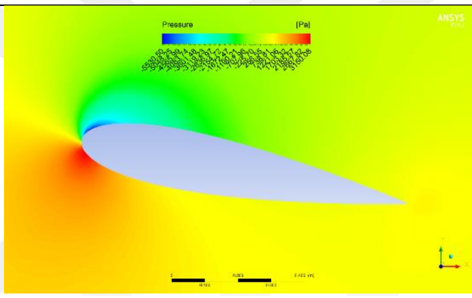	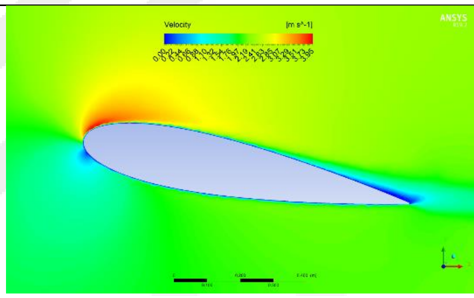
12°	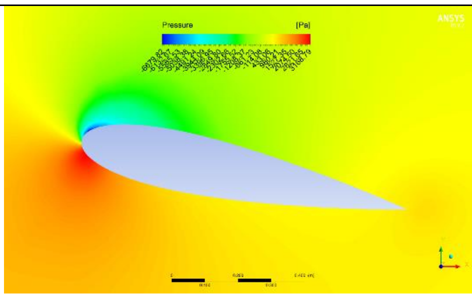	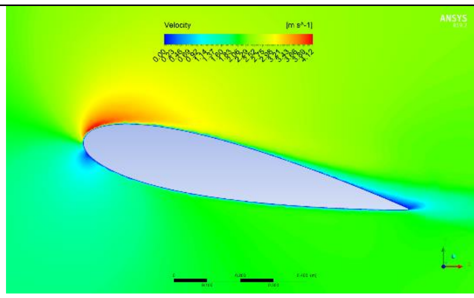
13°	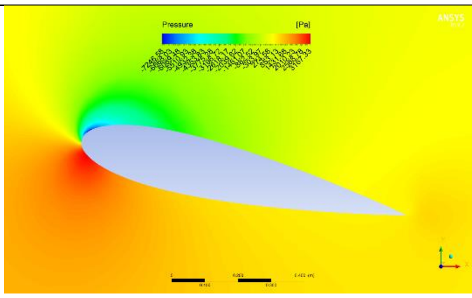	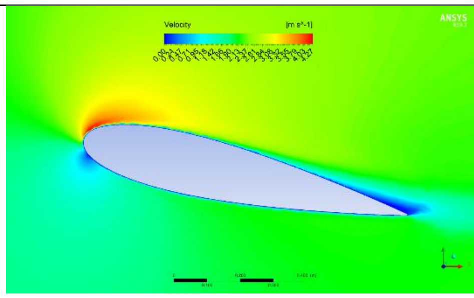

NACA-0018		
AoA	**Pressure Counter**	**Velocity Counter**
14°	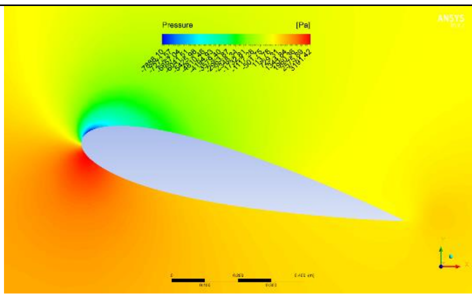	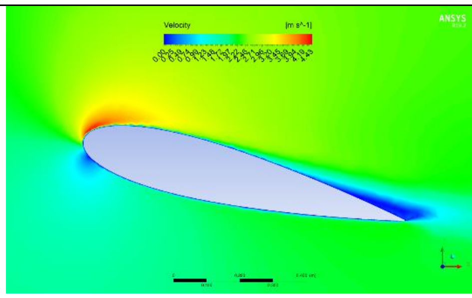
15°	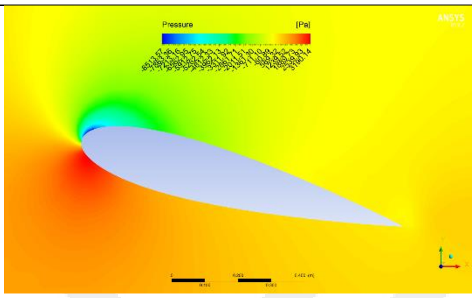	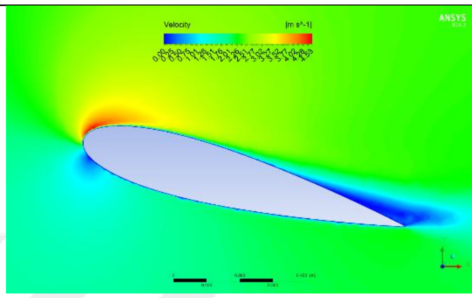
20°	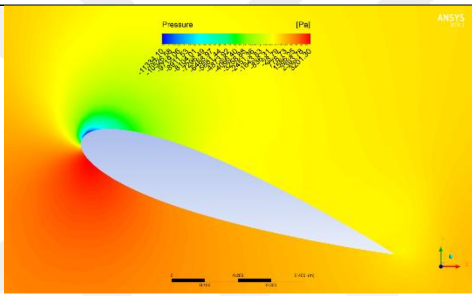	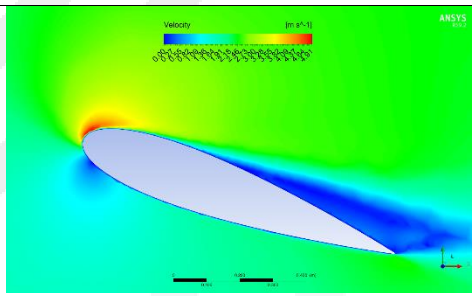
25°	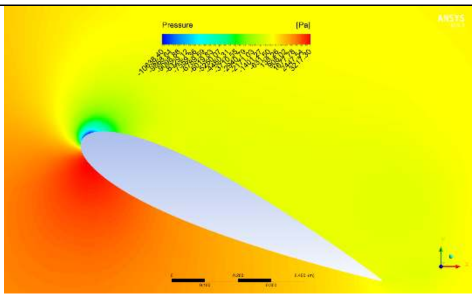	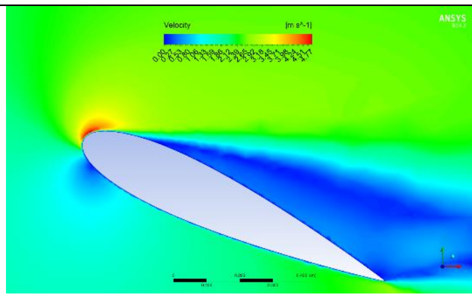

NACA-1412		
AoA	**Pressure Counter**	**Velocity Counter**
1°	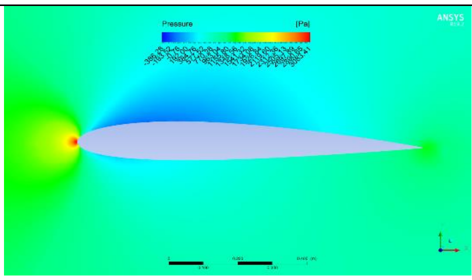	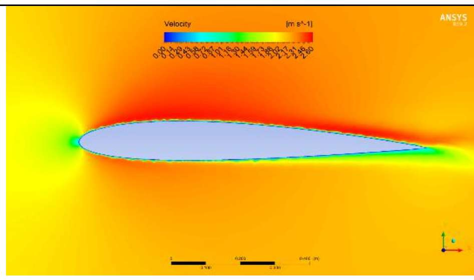
2°	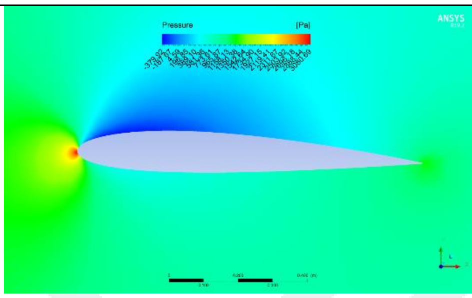	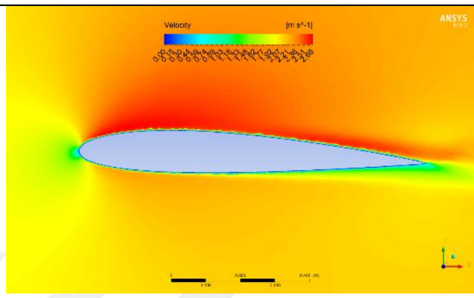
3°	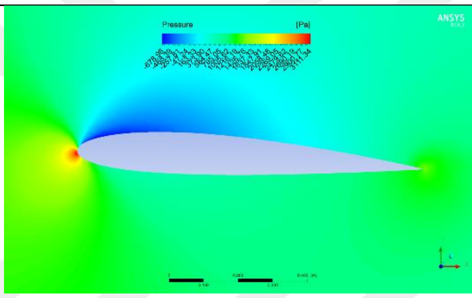	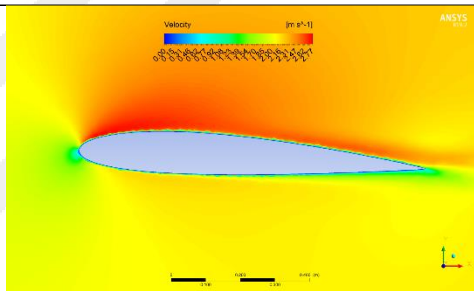
4°	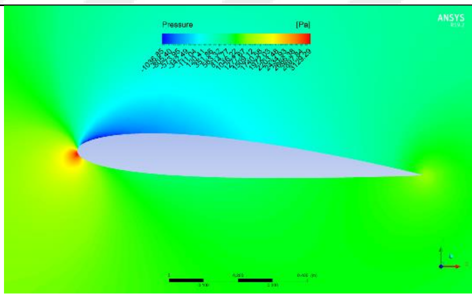	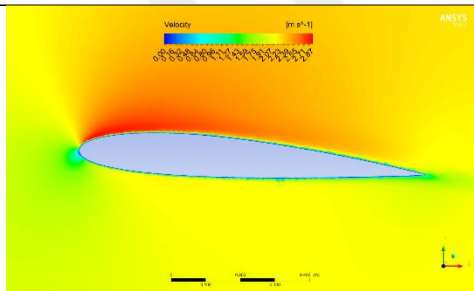
5°	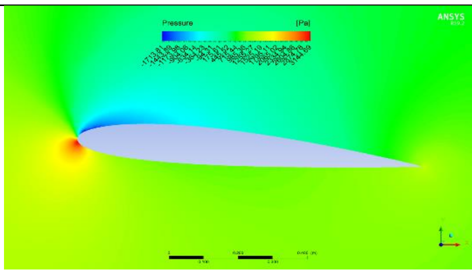	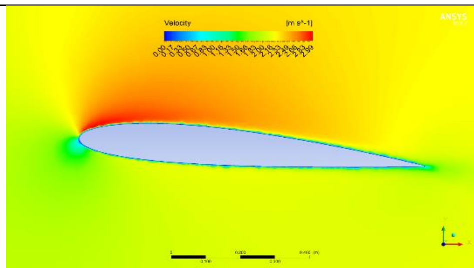
6°	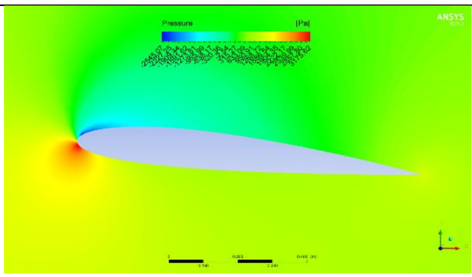	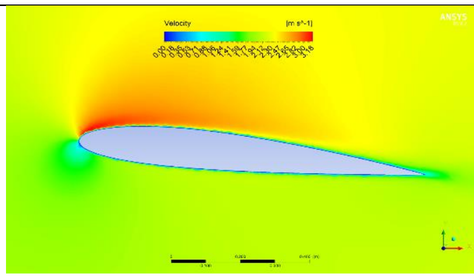

NACA-1412		
AoA	**Pressure Counter**	**Velocity Counter**
7°	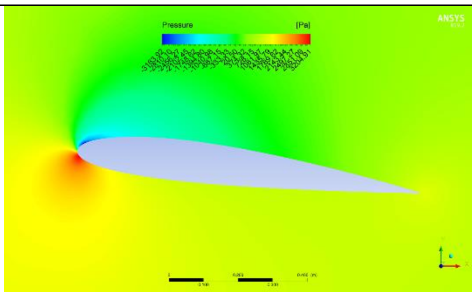	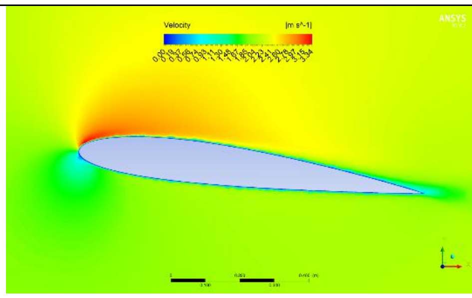
8°	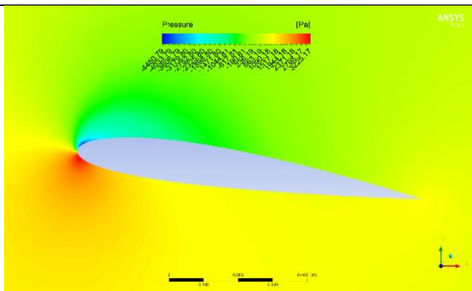	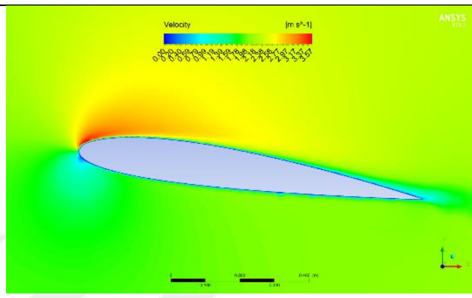
9°	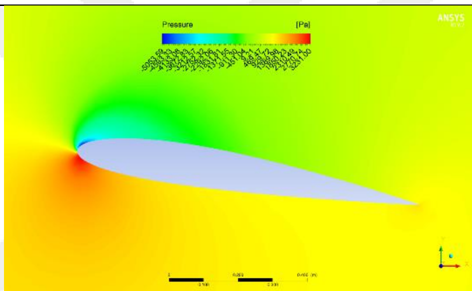	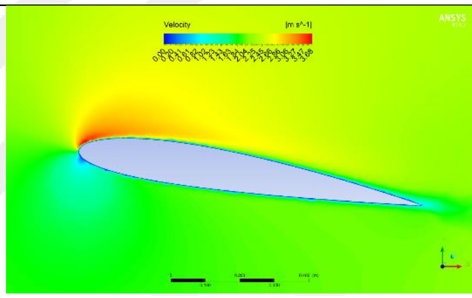
10°	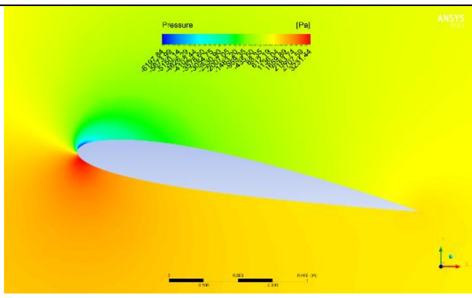	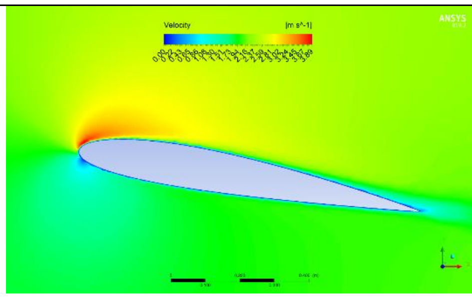
11°	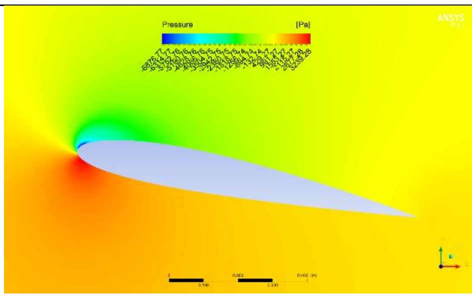	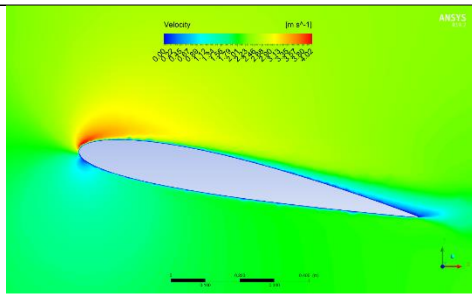

NACA-1412		
AoA	**Pressure Counter**	**Velocity Counter**
12°	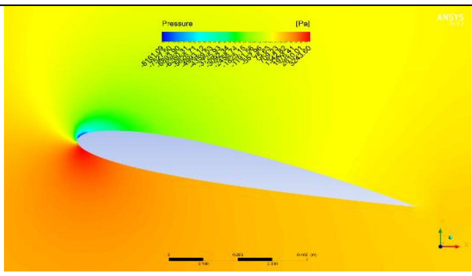	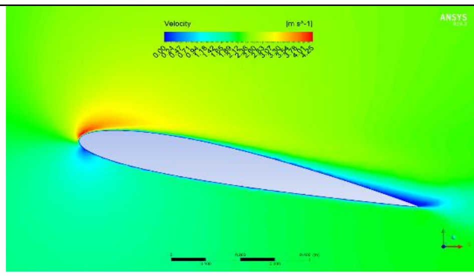
13°	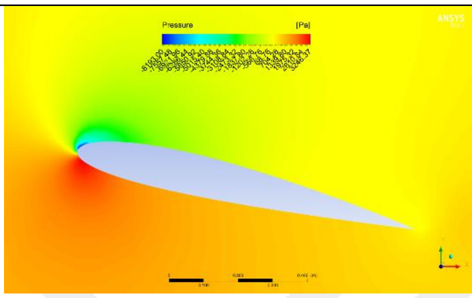	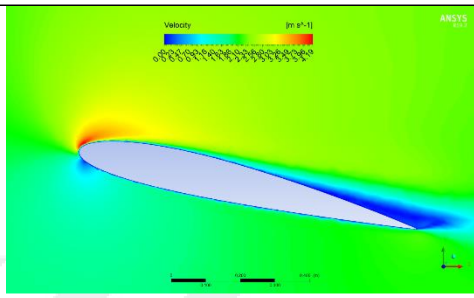
14°	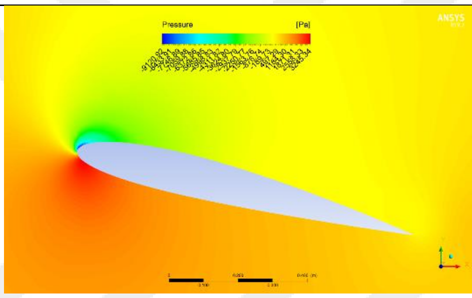	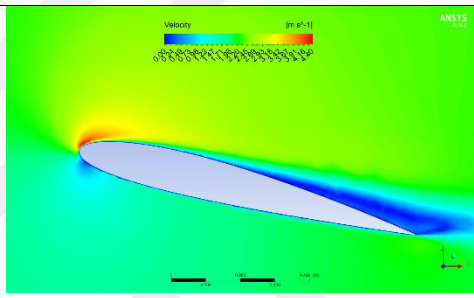
15°	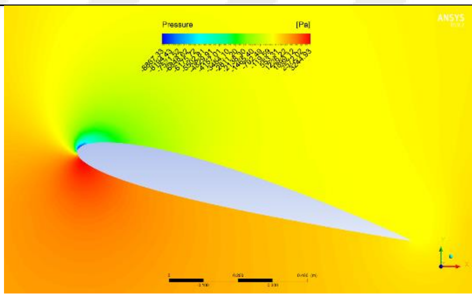	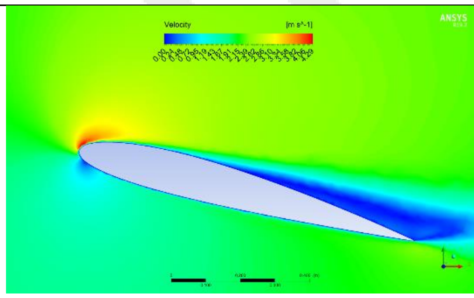
20°	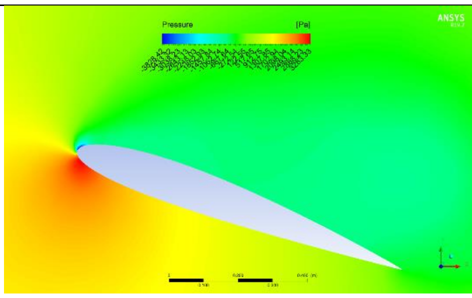	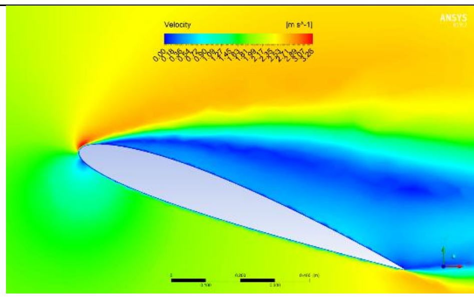
25°	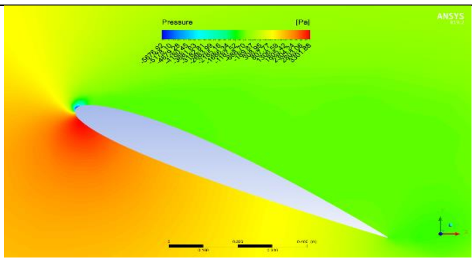	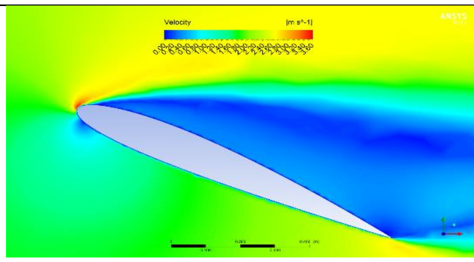

NACA-2418		
AoA	**Pressure Counter**	**Velocity Counter**
1°	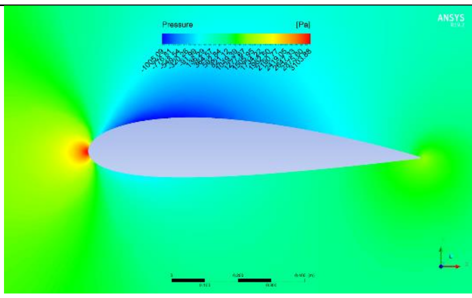	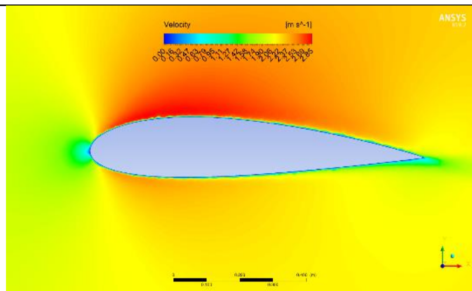
2°	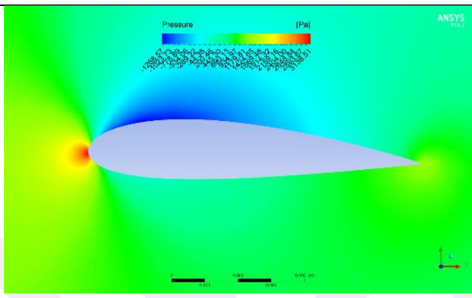	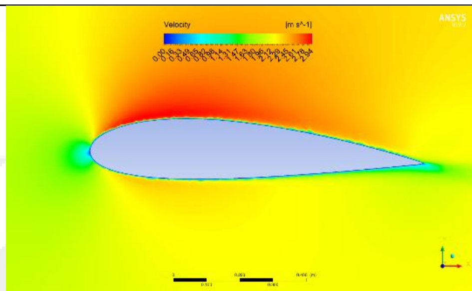
3°	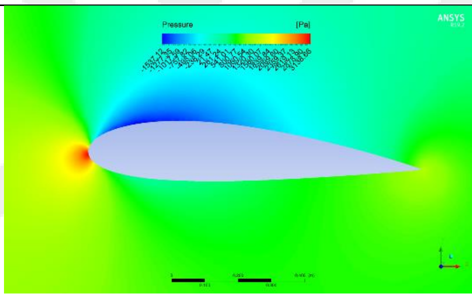	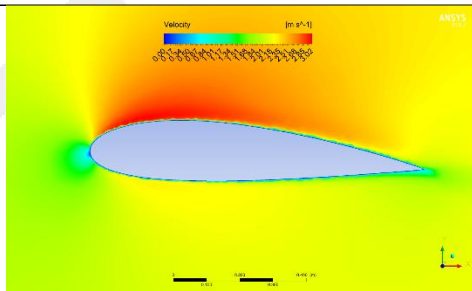
4°	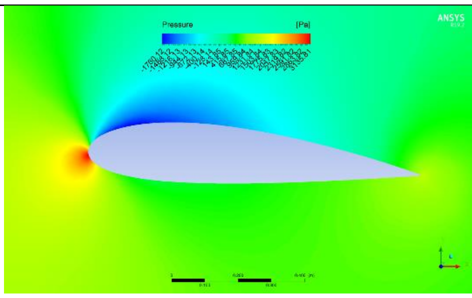	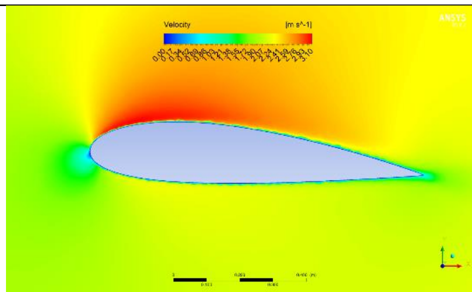
5°	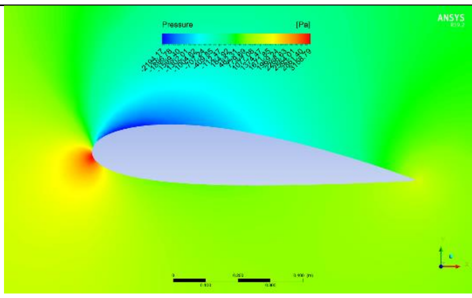	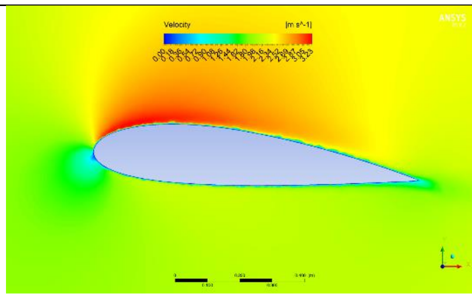

NACA-2418		
AoA	**Pressure Counter**	**Velocity Counter**
6°	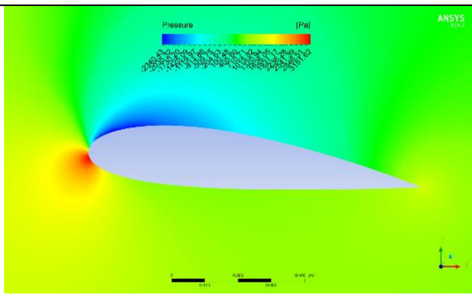	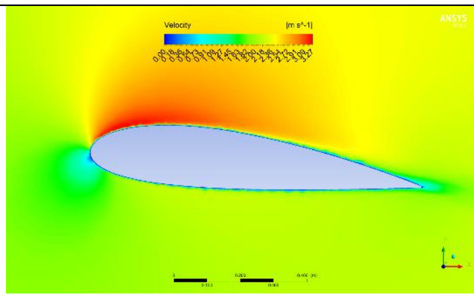
7°	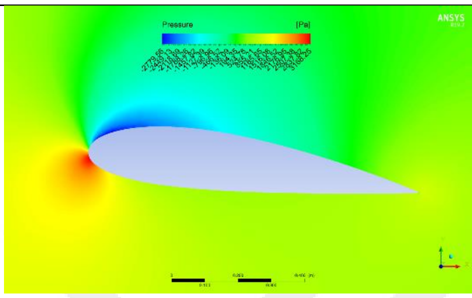	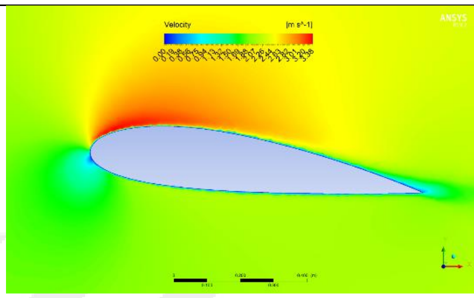
8°	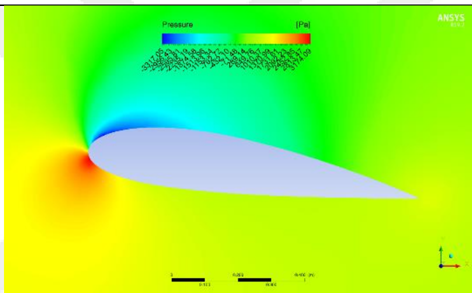	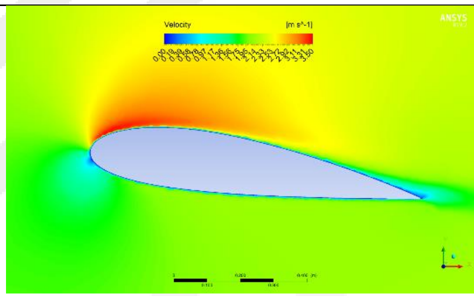
9°	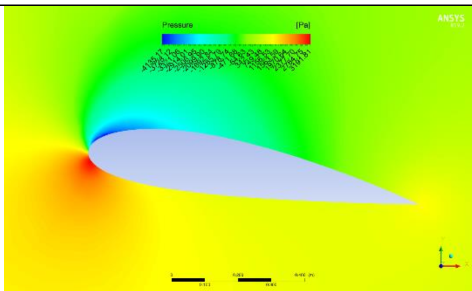	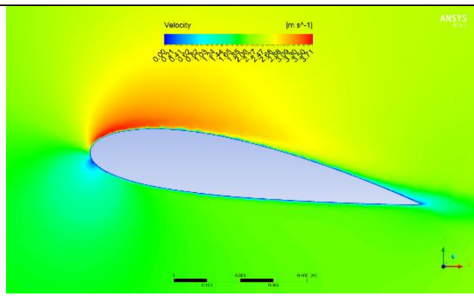
10°	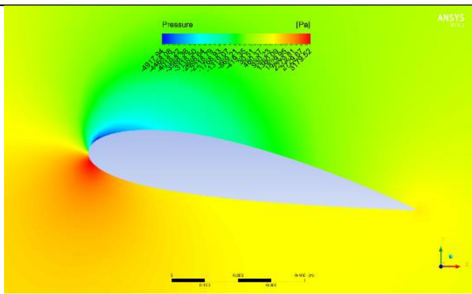	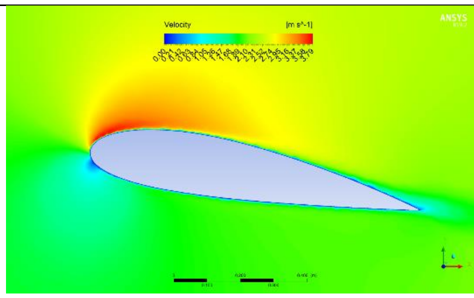

NACA-2418		
AoA	**Pressure Counter**	**Velocity Counter**
11°	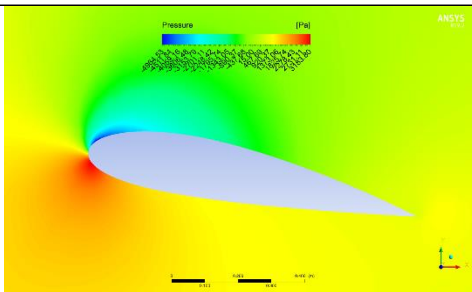	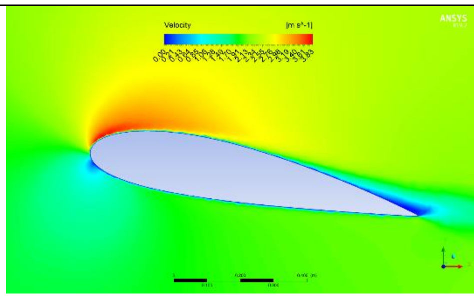
12°	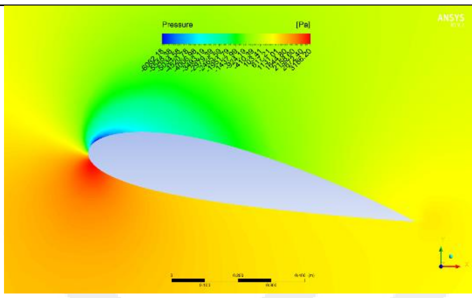	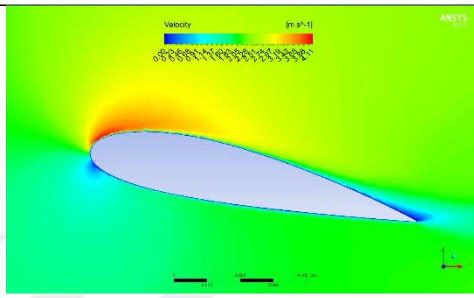
13°	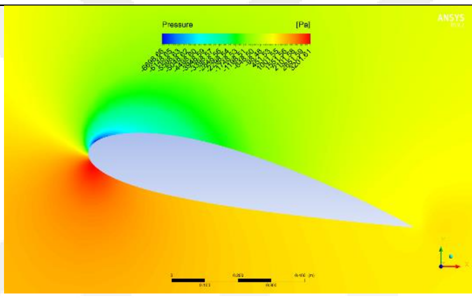	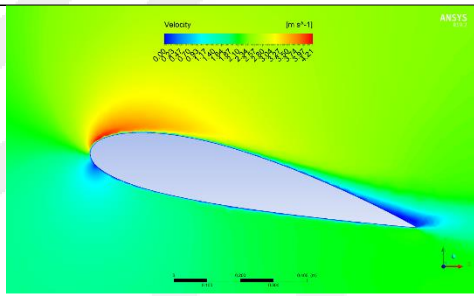
14°	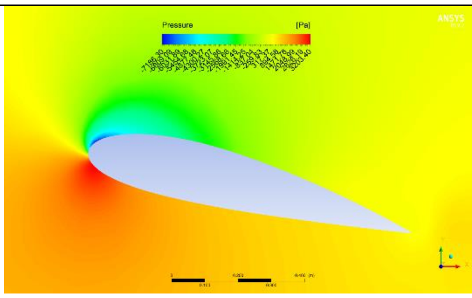	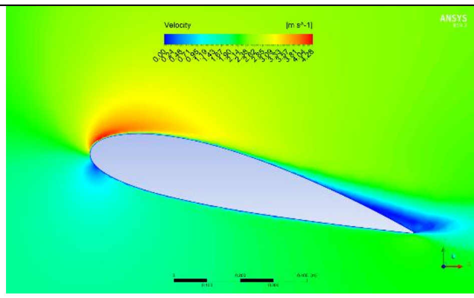
15°	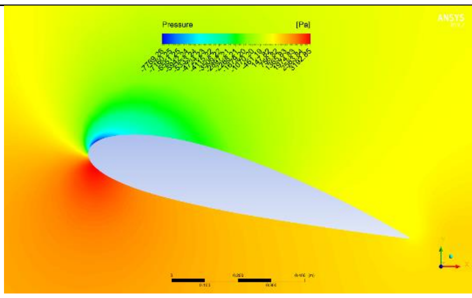	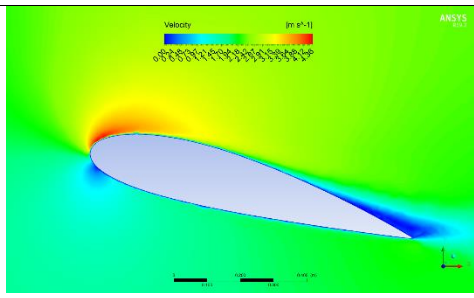

20°	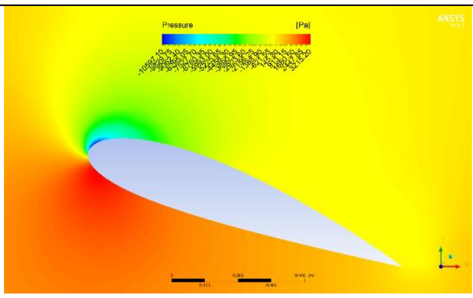	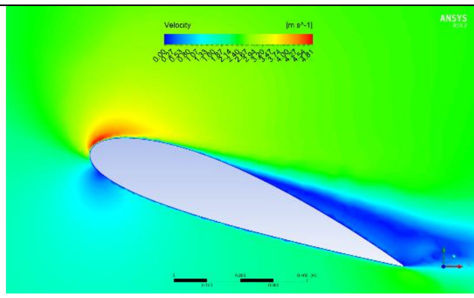
25°	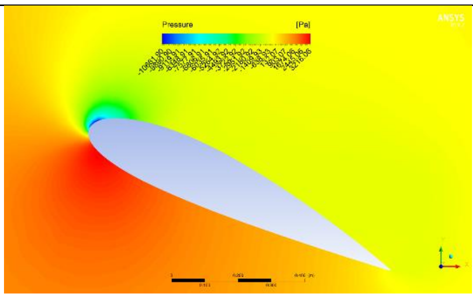	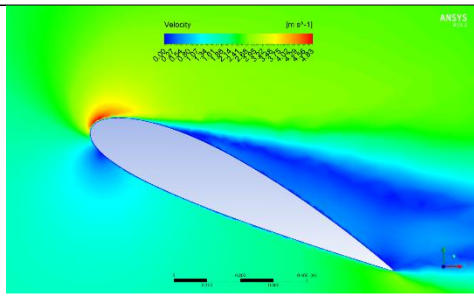

NACA-CHY		
AoA	**Pressure Counter**	**Velocity Counter**
1°	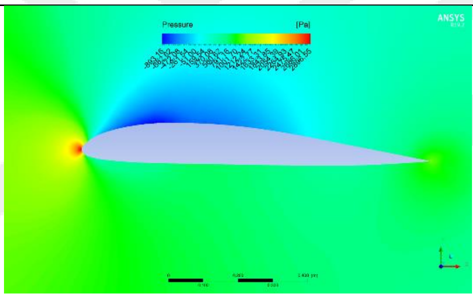	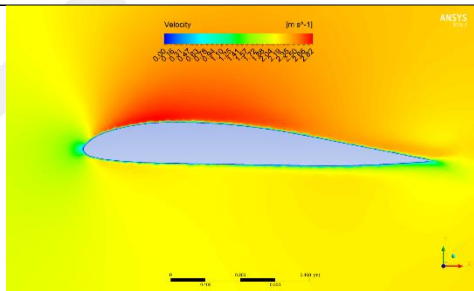
2°	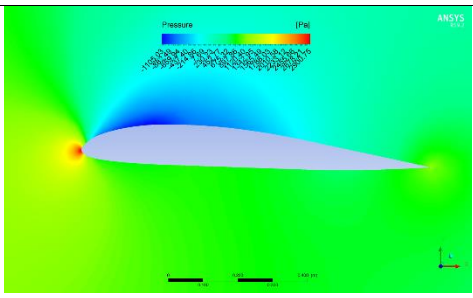	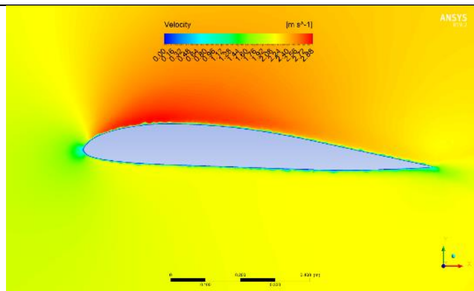
3°	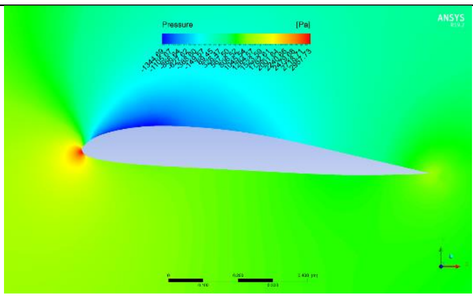	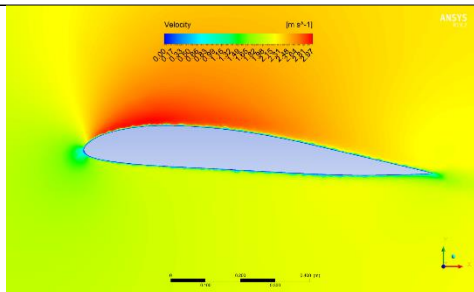

NACA-CHY		
AoA	**Pressure Counter**	**Velocity Counter**
4°	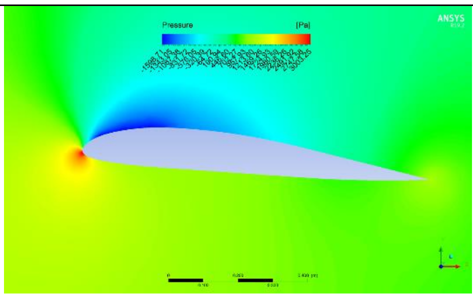	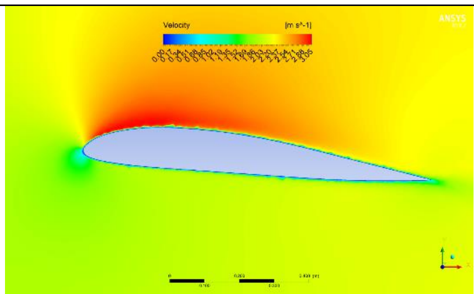
5°	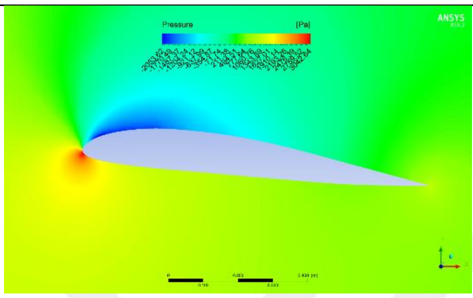	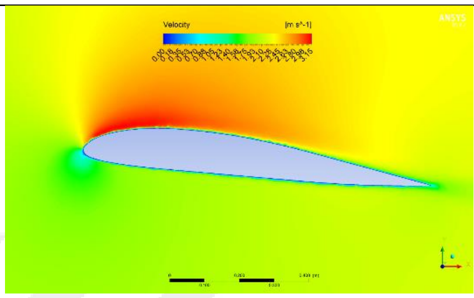
6°	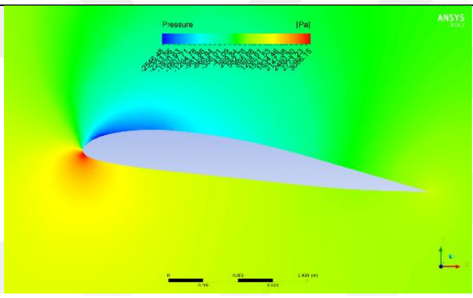	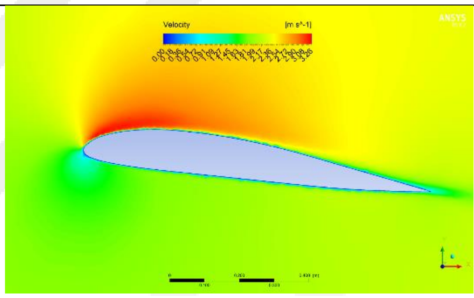
7°	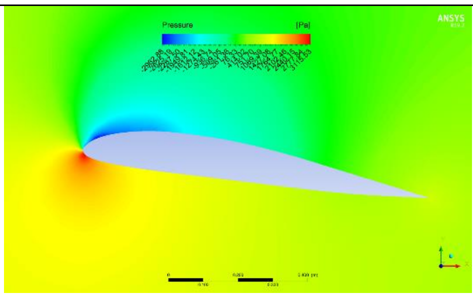	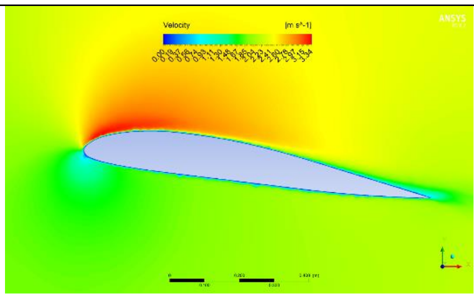
8°	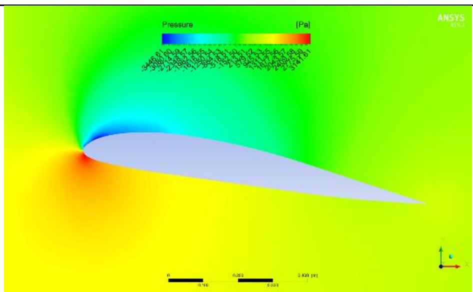	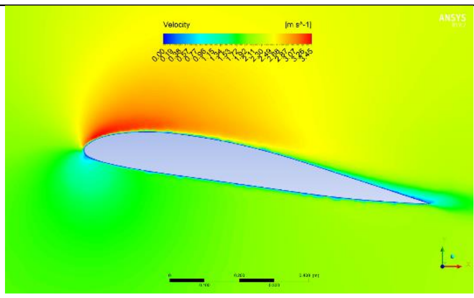

NACA-CHY		
AoA	**Pressure Counter**	**Velocity Counter**
9°	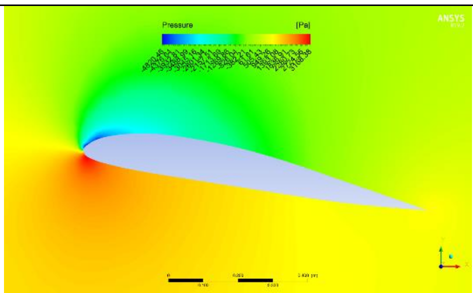	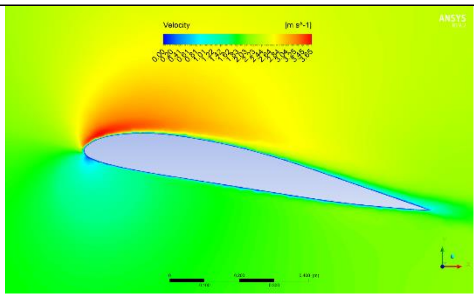
10°	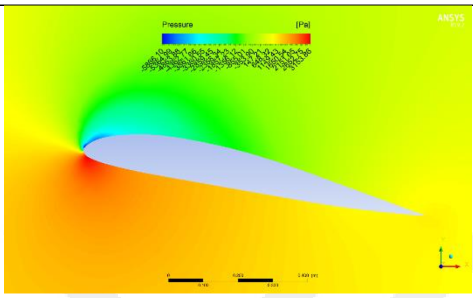	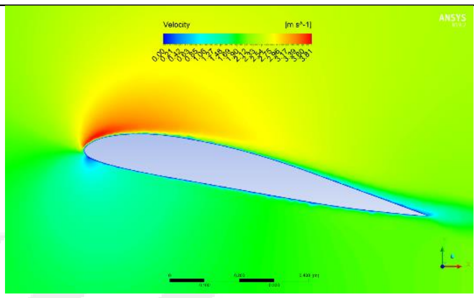
11°	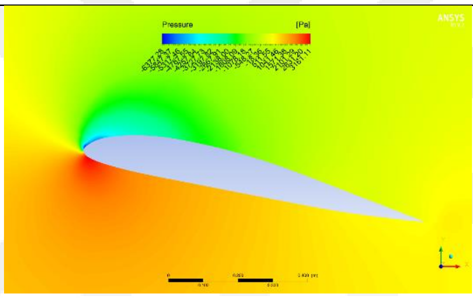	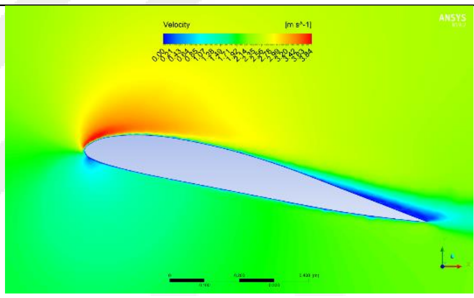
12°	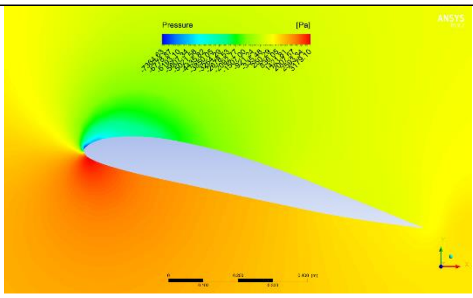	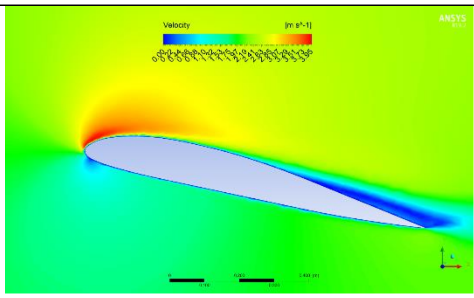
13°	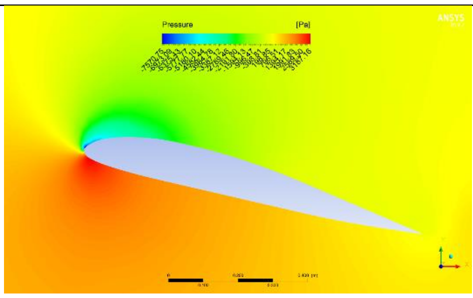	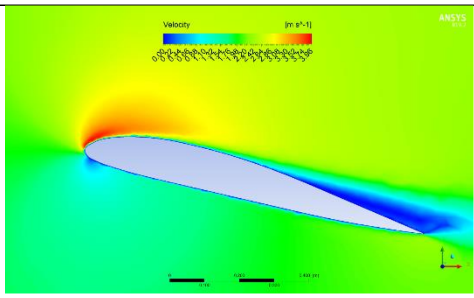

NACA-CHY		
AoA	**Pressure Counter**	**Velocity Counter**
14°	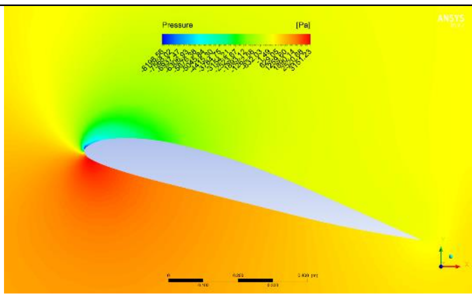	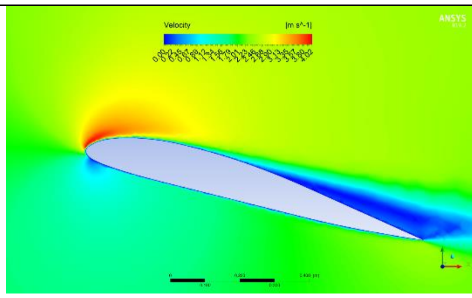
15°	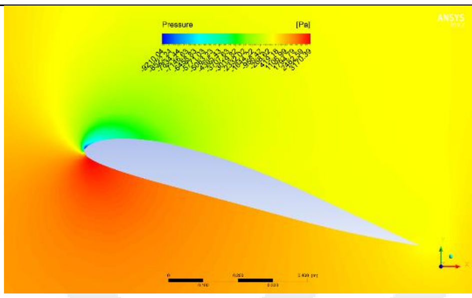	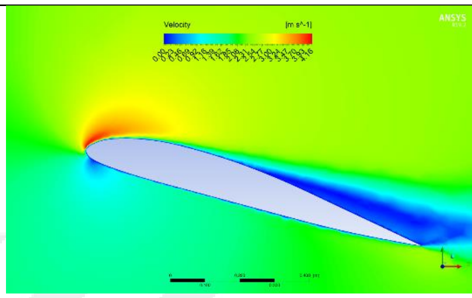
20°	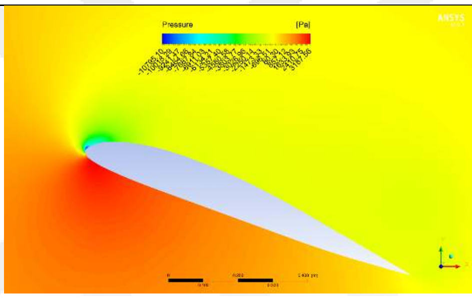	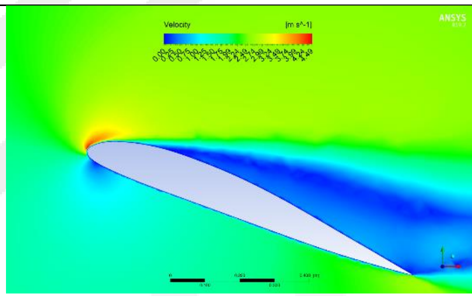
25°	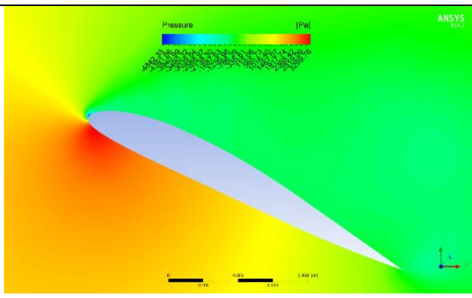	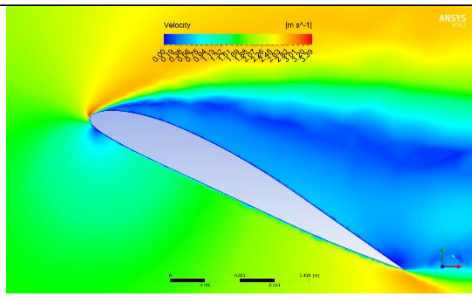

NACA-M18		
AoA	**Pressure Counter**	**Velocity Counter**
1°	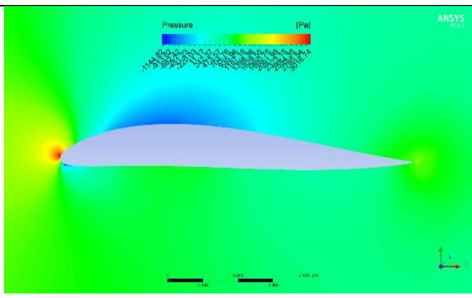	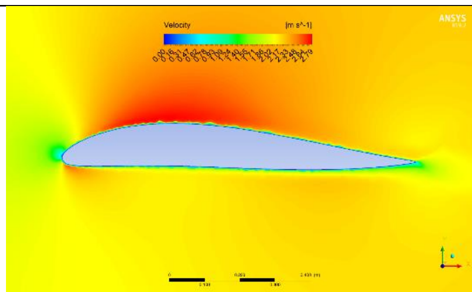

NACA-M18		
AoA	**Pressure Counter**	**Velocity Counter**
2°	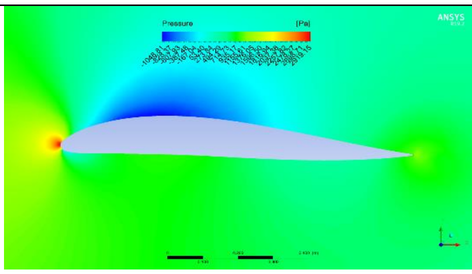	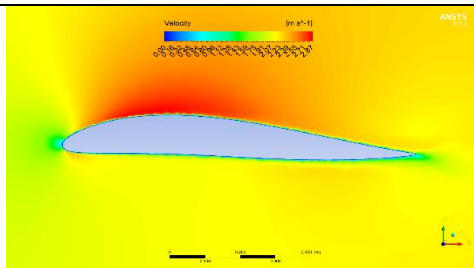
3°	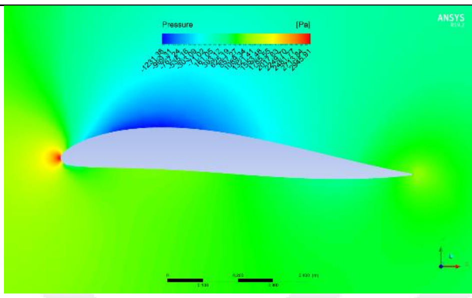	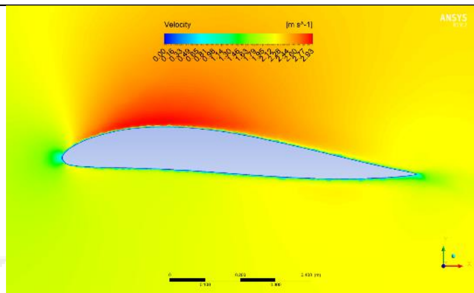
4°	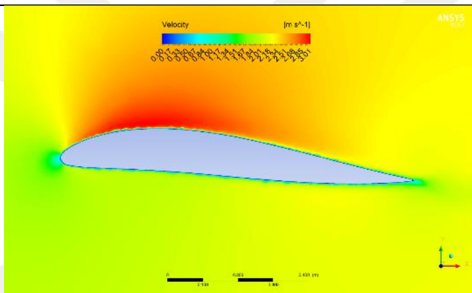	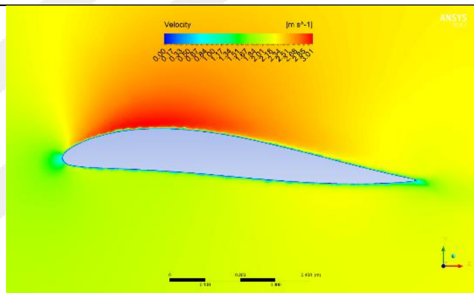
5°	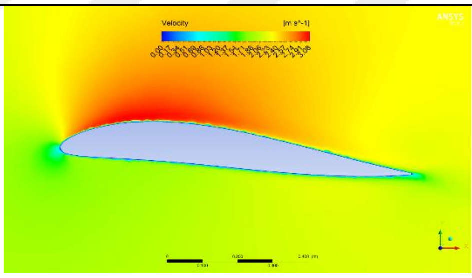	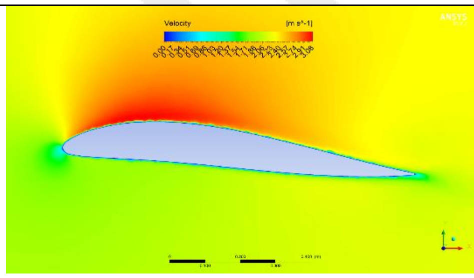
6°	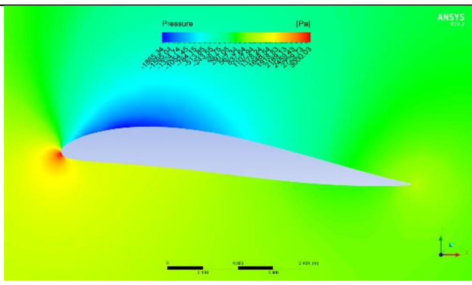	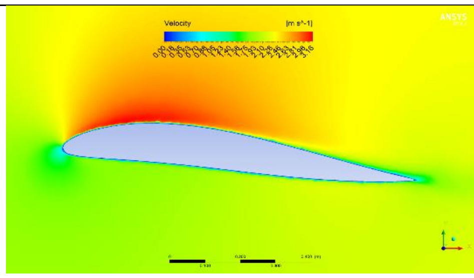
7°	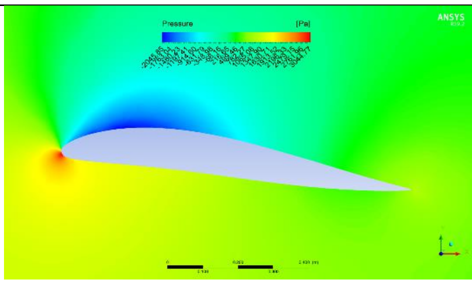	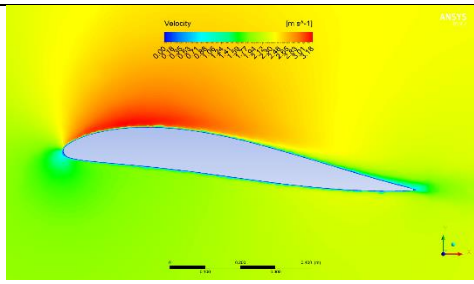

NACA-M18		
AoA	**Pressure Counter**	**Velocity Counter**
8°	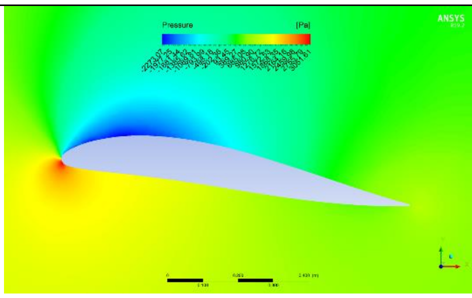	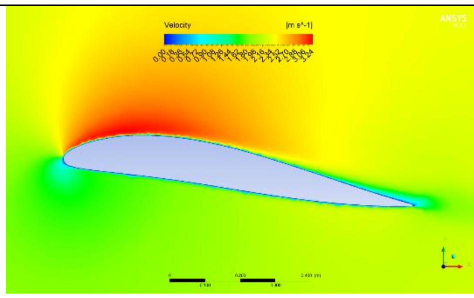
9°	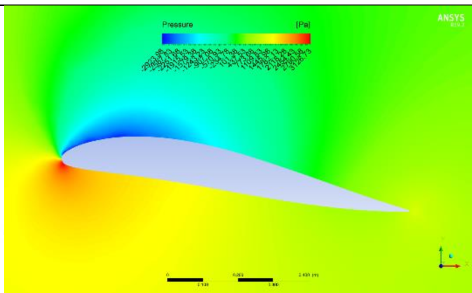	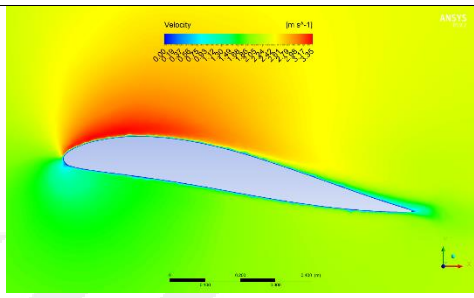
10°	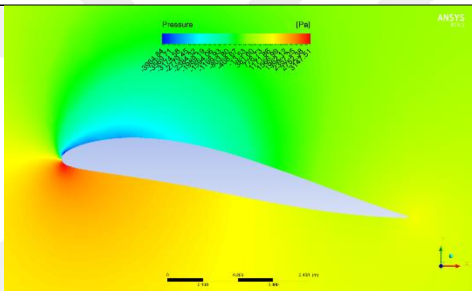	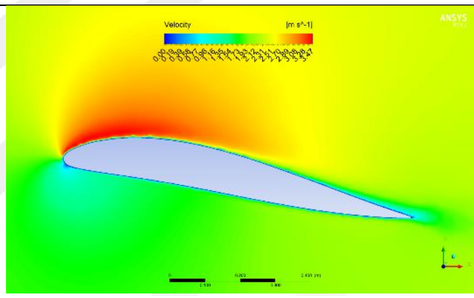
11°	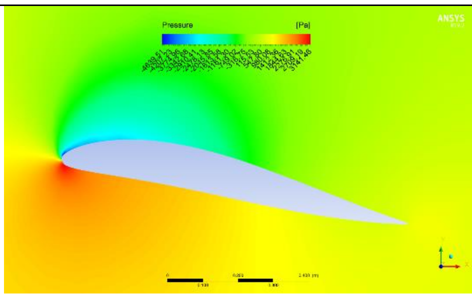	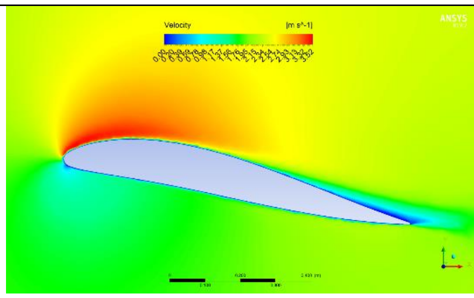
12°	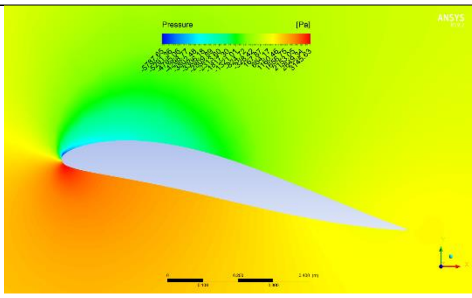	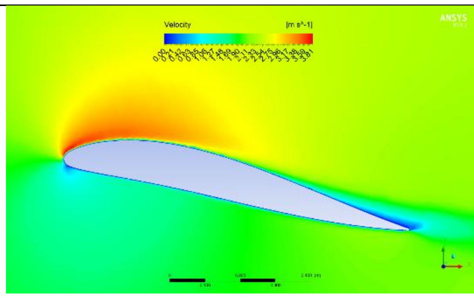

NACA-M18		
AoA	**Pressure Counter**	**Velocity Counter**
13°	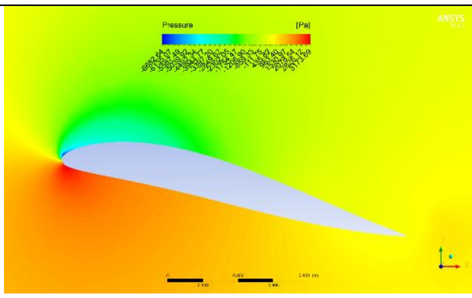	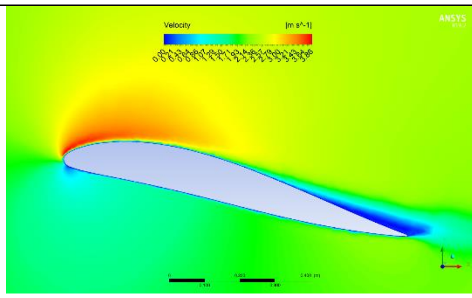
14°	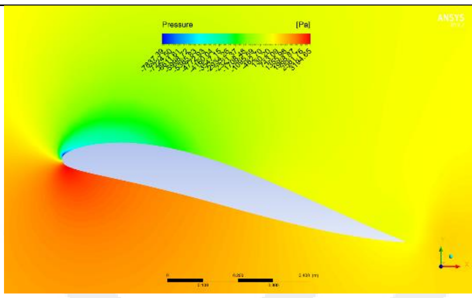	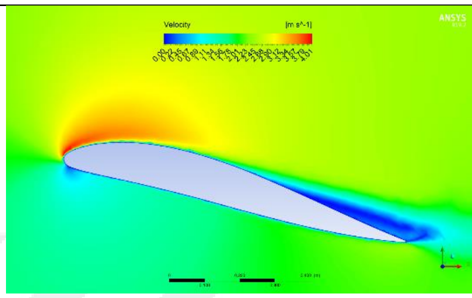
15°	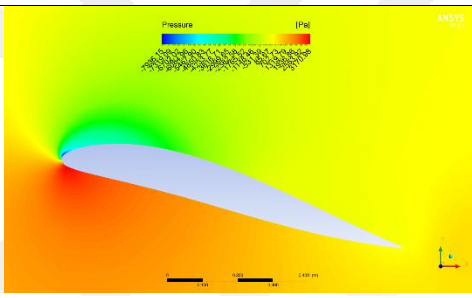	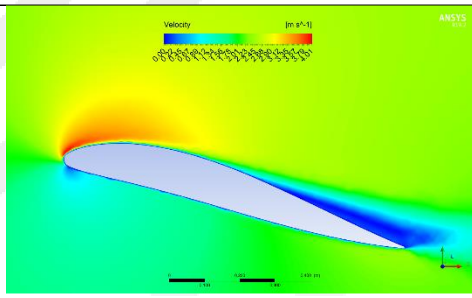
20°	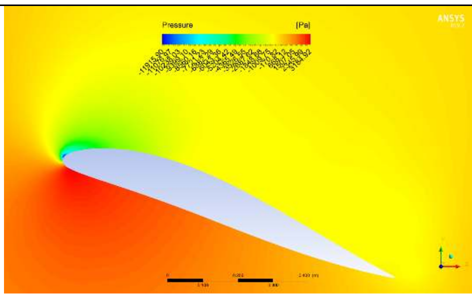	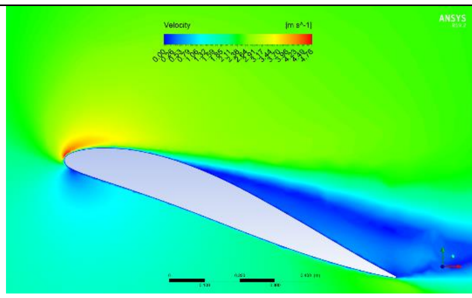
25°	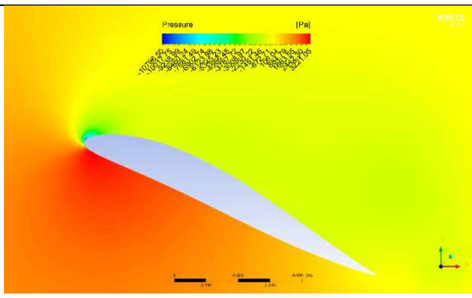	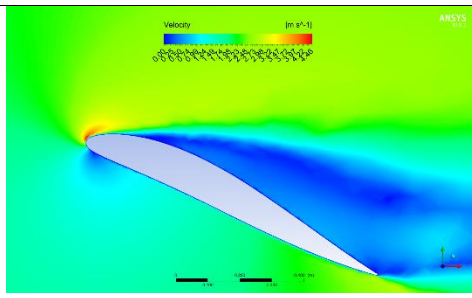

7.3.2 Drag Force

When studying drag forces, an increase in angles of attack has led to an augmentation in drag forces.

Table 7.1 Drag forces at different angles of attack

Drag Force (N)						
AoA(°)	**N0011-SC**	**NACA-0018**	**NACA-1412**	**NACA-2418**	**NACA-CHY**	**NACA-M18**
1	66.000	87.391	57.063	99.628	155.167	151.266
2	68.644	90.626	63.153	106.952	171.855	162.456
3	77.562	96.680	67.717	115.903	188.328	174.804
4	86.197	104.655	80.389	120.349	207.927	192.029
5	93.131	112.658	91.222	134.311	230.998	211.201
6	101.638	120.494	101.446	140.315	265.569	231.410
7	101.068	124.311	107.883	142.759	283.346	248.829
8	108.701	130.125	127.831	152.576	311.790	274.392
9	131.999	147.666	162.202	175.604	382.805	314.391
10	148.101	164.145	168.035	199.976	411.894	351.189
11	149.789	175.356	176.139	202.550	440.583	389.959
12	166.724	190.481	194.719	220.401	523.616	405.599
13	191.432	206.708	221.172	235.550	544.259	464.922
14	229.989	223.838	251.998	244.191	644.882	530.793
15	237.260	226.145	293.665	284.829	701.183	613.912
20	273.007	420.272	717.515	453.388	1307.972	1022.550
25	346.261	723.794	926.099	737.297	2255.445	1880.848

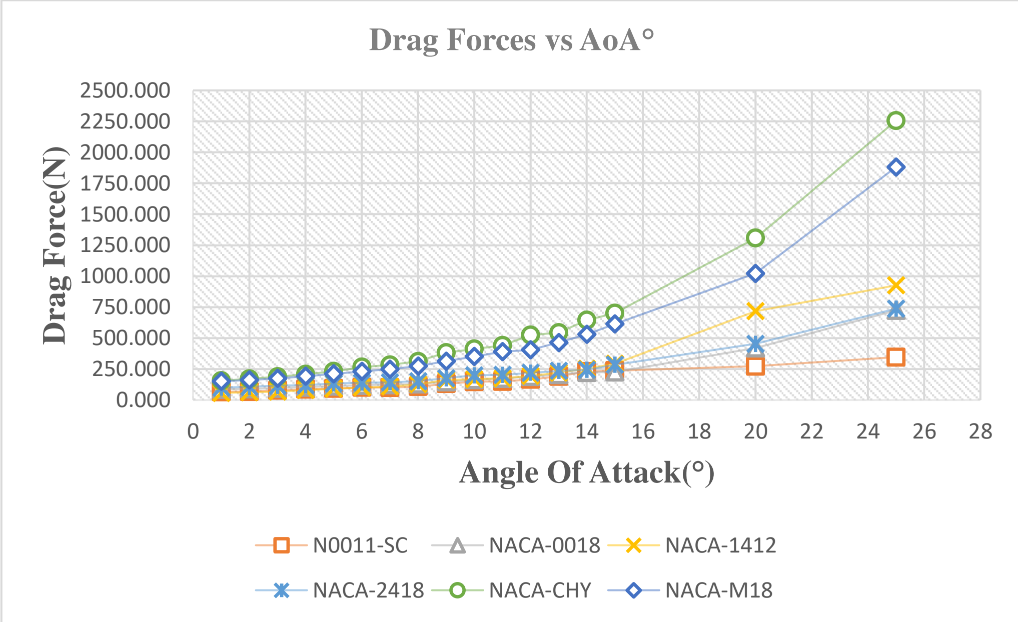

Figure 7.12 Variation of drag forces with angles of attack

7.3.3 Lift Forces

When examining lift forces, an increase in angles of attack resulted in an increase in lift forces.

Table 7.2 Lift forces at different angles of attack

	Lift Force (N)					
AoA(°)	**N0011-SC**	**NACA-0018**	**NACA-1412**	**NACA-2418**	**NACA-CHY**	**NACA-M18**
1	132.000	174.783	114.126	199.256	77.583	75.633
2	136.885	181.251	126.306	213.904	85.927	81.228
3	146.029	193.359	135.434	231.807	94.164	87.402
4	158.075	209.310	160.779	240.698	103.964	96.015
5	170.164	225.316	182.443	268.621	115.499	105.601
6	181.999	240.988	202.892	280.630	132.785	115.705
7	187.764	248.622	215.766	285.518	141.673	124.414
8	196.545	260.249	255.662	305.153	155.895	137.196
9	223.040	295.332	324.405	351.208	191.402	157.196
10	247.932	328.290	336.070	399.952	205.947	175.594
11	264.865	350.713	352.277	405.100	220.292	194.980
12	287.710	380.961	389.437	440.803	261.808	202.799
13	312.220	413.415	442.344	471.099	272.130	232.461
14	338.094	447.676	503.996	488.382	322.441	265.397
15	341.579	452.290	587.331	569.658	350.591	306.956
20	634.796	840.544	1435.030	906.775	653.986	511.275
25	1093.248	1447.588	1852.199	1474.594	1127.723	940.424

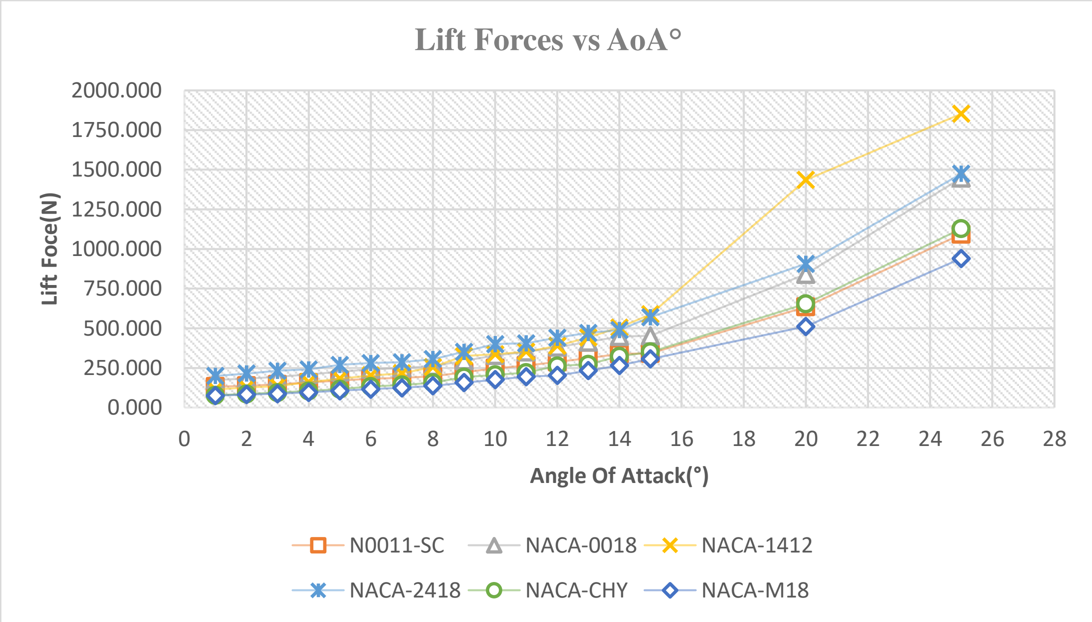

Figure 7.13 Variation of lift forces with angles of attack

7.3.4 C_L/C_D values

When analyzed under different angles of attack with the same geometric conditions and mesh quality, the "C_L/C_D" value for each hydrofoil is given in the table below. The outputs show that NACA-1412 has a better Cl/Cd value when used at a 7-degree angle of attack. The NACA-1412 hydrofoil has a lift force 15.806 times higher than the drag force at a 7-degree angle of attack.

Table 7.3 Ratios of Cl/Cd values at different angles of attack

CL/CD Values in different angle of attacks						
	Hydrofoil Type					
AoA	***NACA-0011sc***	***NACA-0018***	***NACA-1412***	***NACA-2418***	***NACA-CHY***	***NACA-M18***
0	0.920	0.276	4.093	4.851	7.781	4.224
1	3.460	2.150	7.114	6.379	9.628	6.857
2	6.000	4.734	10.000	7.997	11.598	9.231
3	9.053	6.583	12.087	9.667	12.897	11.331
4	11.002	8.744	13.607	10.728	14.078	12.642
5	12.315	9.458	14.910	11.582	14.431	13.558
6	12.889	10.771	15.396	12.090	14.567	14.531
7	13.801	11.345	***15.806***	12.316	14.598	14.497
8	13.676	11.941	15.264	12.638	14.022	14.269

(Continues.). CL/CD Values in different angle of attacks						
	Hydrofoil Type					
AoA	***NACA-0011sc***	***NACA-0018***	***NACA-1412***	***NACA-2418***	***NACA-CHY***	***NACA-M18***
9	13.479	12.095	14.571	12.460	13.577	14.000
10	12.598	12.284	13.705	12.174	12.970	13.130
11	12.955	12.454	12.450	11.954	12.290	13.195
12	11.831	12.168	11.235	11.849	11.053	12.409
13	10.966	11.879	9.840	11.961	9.867	11.590
14	10.425	11.622	9.129	11.691	8.803	10.994
15	9.448	11.021	8.046	11.095	7.891	9.855
20	3.093	6.886	2.715	7.387	4.118	5.617
25	2.789	3.677	2.283	4.177	2.060	3.102

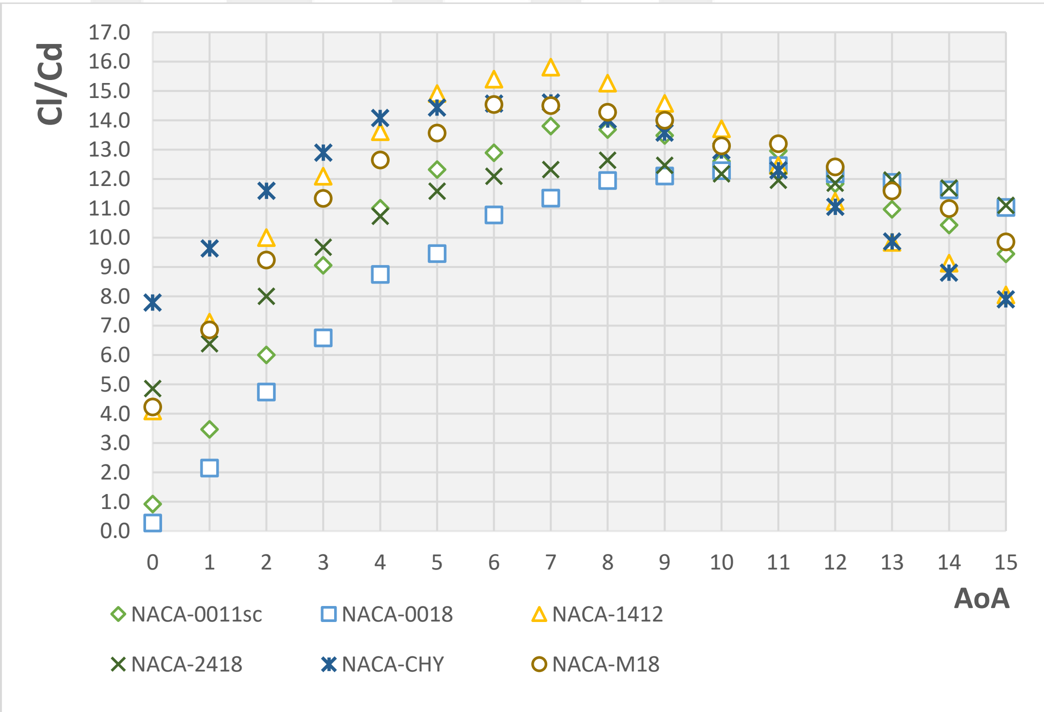

Figure 7.14 Variation of Cl/Cd values with angles of attack

When the values are examined, it is determined that the NACA-1412 hydrofoil profile performs better than the other hydrofoil profiles at the same hydrofoil angle of attack. Therefore, it is decided to choose the NACA-1412 hydrofoil profile. Based on the modeled designs, the NACA-1412 is selected for its highest Cl/Cd value at a 7-degree angle of attack.

Table 7.4 Forces for Different Hydrofoil Profiles at AoA=7

Comparison of Blades at AoA=7°				
No	***Hydrofoil Type***	***Drag Force (N)***	***Lift Force (N)***	***C_L/C_D***
1	NACA0011SC	90.634	1250.868	13.801
2	NACA0018	115.158	1306.440	11.345
3	NACA1412	94.354	1491.402	15.806
4	NACA2418	138.751	1708.889	12.316
5	NACACHY	131.261	1916.182	14.598
6	NACAM18	114.287	1656.832	14.497

CHAPTER VIII

CHORD LENGTH & BLADE NUMBERS SELECTION

8.1 Solidity and Power Coefficient

It was mentioned that the solidity value depends on the length and number of the blade. Typically, a longer blade diameter means more surface area, which means a higher potential for capturing energy from water flow. While longer blade, diameters perform better at energy capture, they also require more material costs, larger and more complex turbine design. Solidity will be examined in detail in Chapter 8. In hydrokinetic turbines, solidity is the ratio of how much the rotor blades cover around the rotor diameter. In other words, the rotor solidity indicates how "Occupied" the space around it is by the blades. A higher solidity rate means more blades can be used. However, an excessively high solidity ratio may increase the turbine's resistance to water flow and reduce efficiency. An attempt will be made to find a balance between the parameters explained in the section.

The solidity value will be examined in this section using two parameters as the number of blades and the chord length of the blades vary. The NACA1412-coded blade profile obtained as output in Chapter 7 will be used as an input parameter in Chapter 8 with a 7° angle of attack obtained from the outputs. Three different numbers of blades, namely 4, 5, and 6, will be used, along with five different chord lengths: 10 cm, 15 cm, 20 cm, 25 cm, and 30 cm, resulting in a total of 15 different geometry models.

8.2 Pre-processing

The steps present in Chapter 7 will be repeated in Chapter 8. In the first stage, geometry modeling will be performed, followed by detailed examinations for the mesh section in the subsequent stage. Afterward, the analysis setup will be completed, and the outputs will be examined.

8.2.1 Geometry

In the geometry section, 2D models have been defined. Three different numbers of blades were considered: 4 blades, 5 blades, and 6 blades. Additionally, a total of 15 different geometry models were created with 5 different chord lengths: 10 cm, 15 cm, 20 cm, 25 cm, and 30 cm. The created geometries were written to different Fluent files, and the results were obtained independently. The rotor domain diameter was assumed to be 1 meter, and the outer domain was prepared to be at least 15 times the diameter of the rotor domain.

Figure 8.1 General view of dimensions of model

8.2.2 Meshing

The mesh outputs are shown in Figures 8.2, 8.3, and 8.4. Mesh outputs consist of 2 different domains. To ensure the accuracy of the analysis, the boundaries between the domains were divided and meshed.

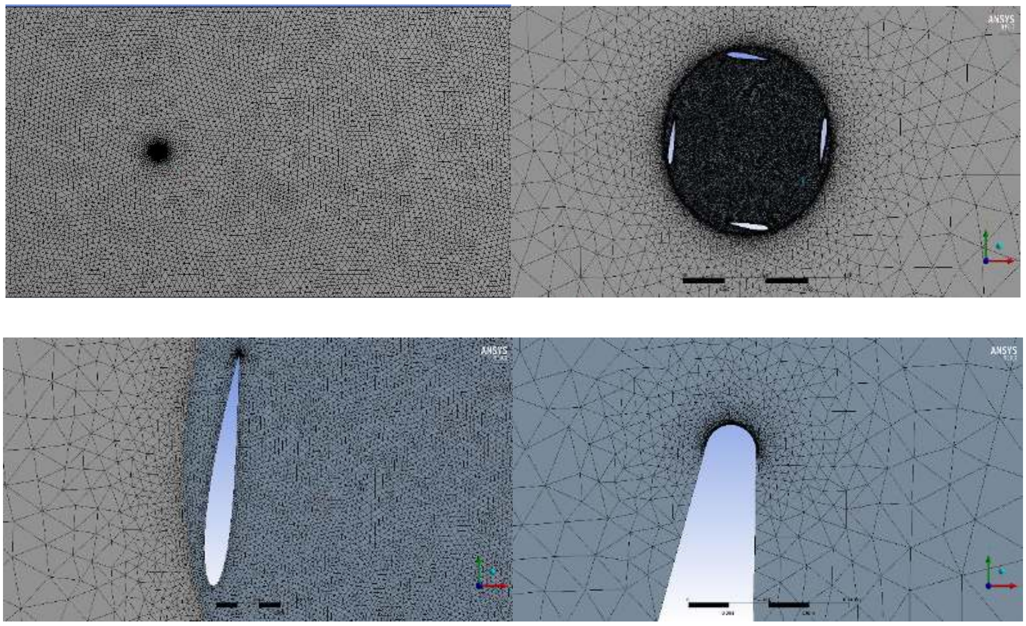

Figure 8.2 Mesh features of modelled geometries

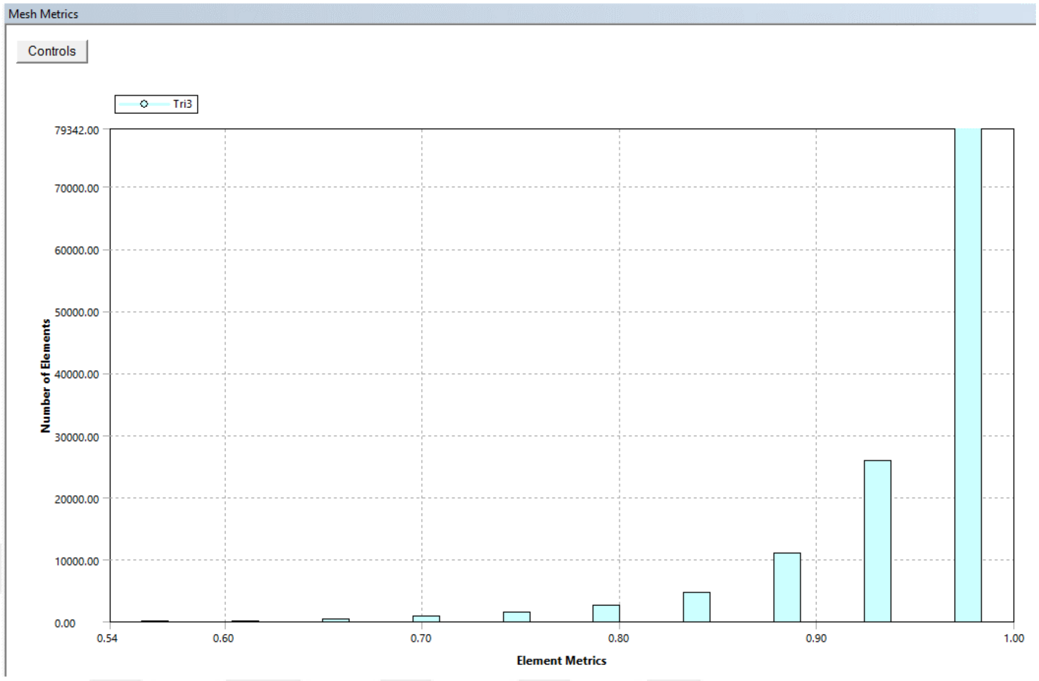

Figure 8.3 The average "Element quality" mesh metric for the geometries.

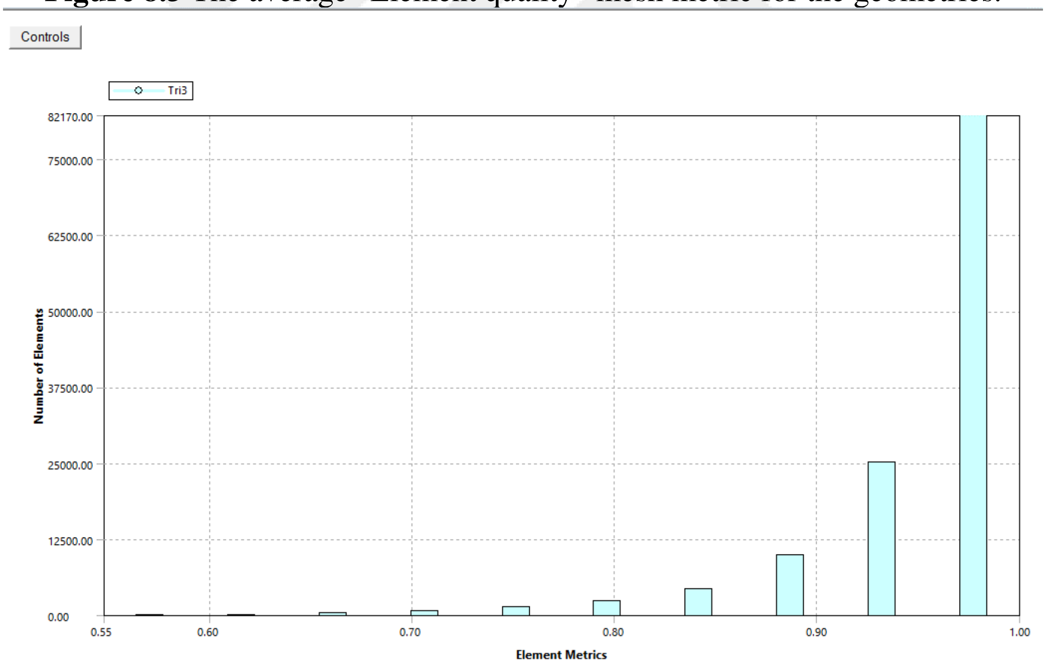

Figure 8.4 The average "Orthogonal quality" mesh metric for the geometries.

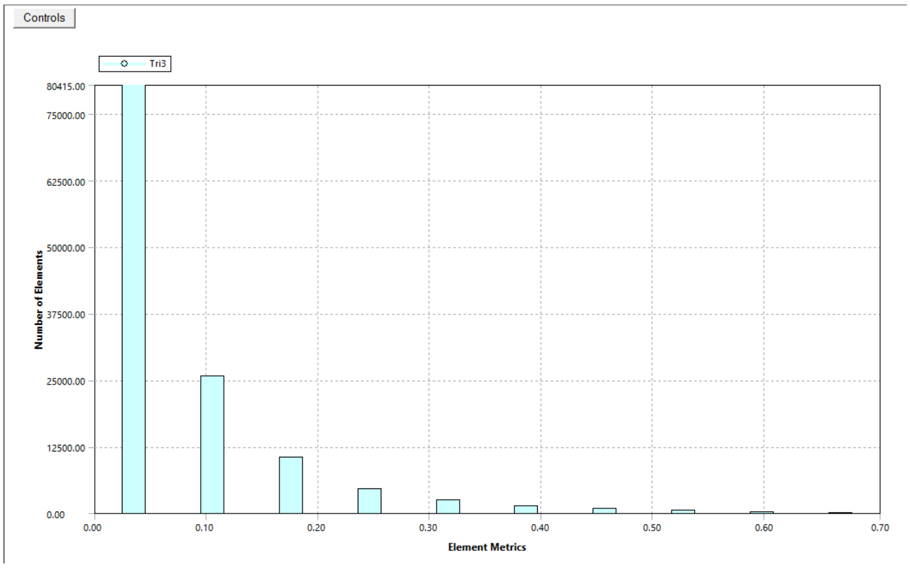

Figure 8.5 The average “Skewness” mesh metric for the geometries.

8.2.2.1 Mesh Figures

At each stage, mesh qualities have been checked, and mesh metrics have been obtained on a scale ranging from good to very good. Chord lengths of 0.10, 0.15, 0.20, 0.25, and 0.30 cm are presented in separate tables based on the number of blades.

0.10 m Chord Length Mesh		
4 blades	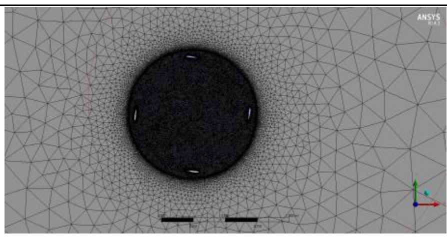	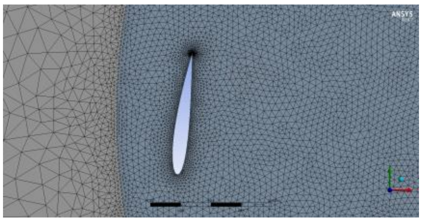
5 blades	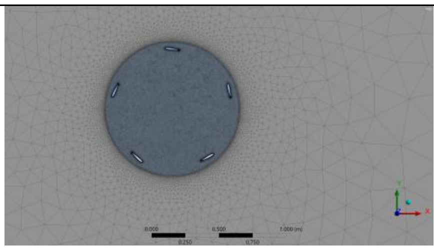	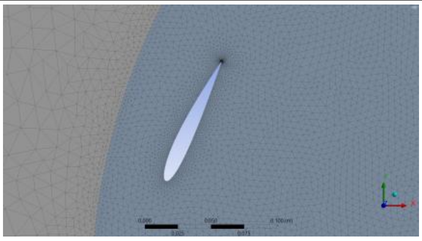
6 blades	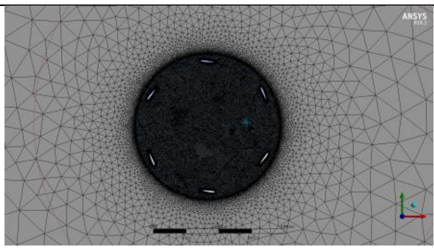	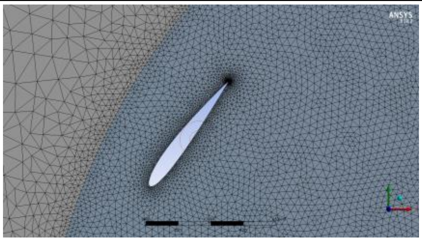

0.15 m Chord Length Mesh		
4 blades	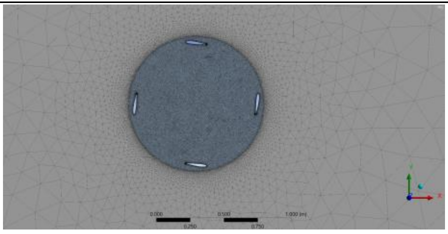	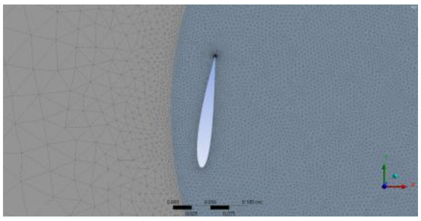
5 blades	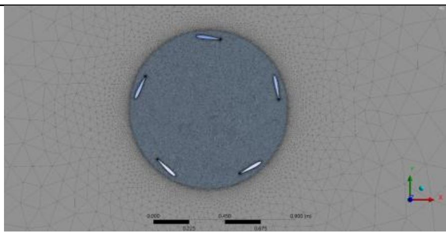	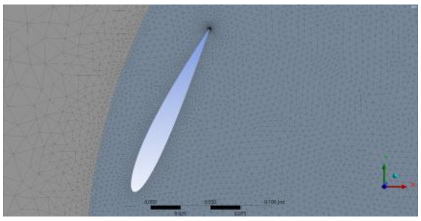
6 blades	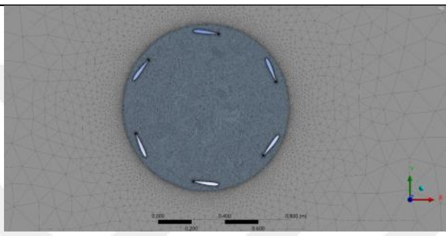	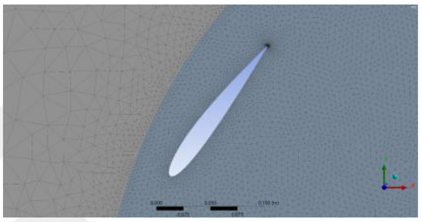

0.20 m Chord Length		
4 blades	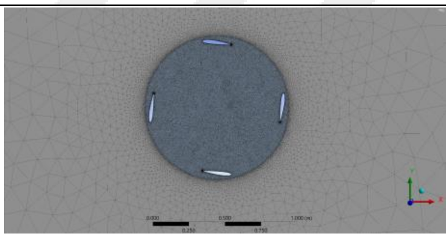	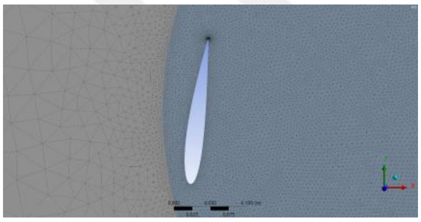
5 blades	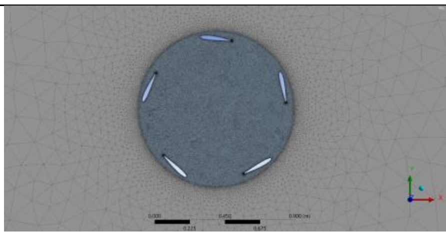	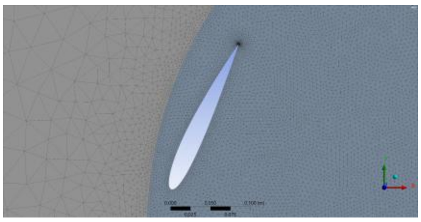
6 blades	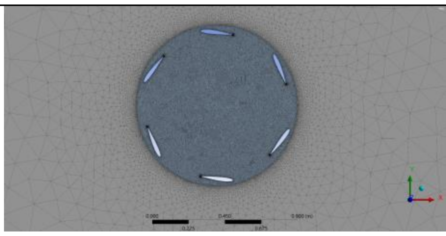	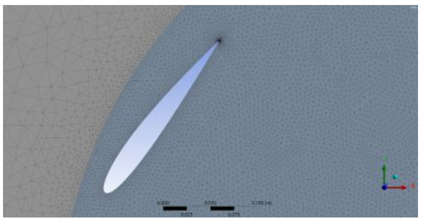

0.25 m Chord Length		
4 blades	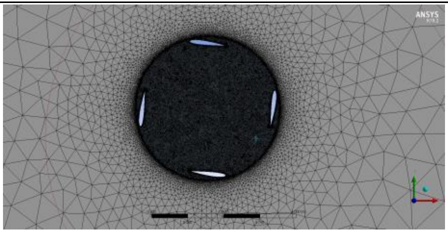	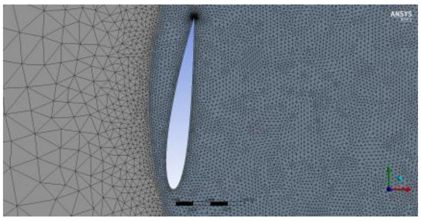
5 blades	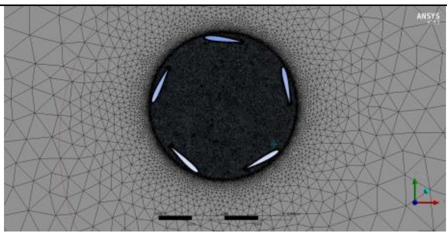	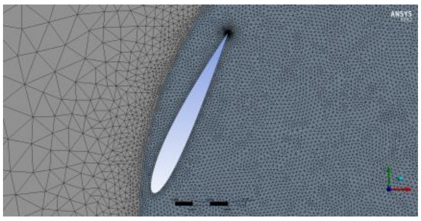
6 blades	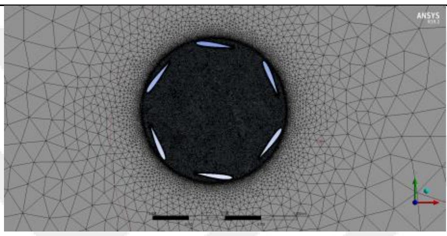	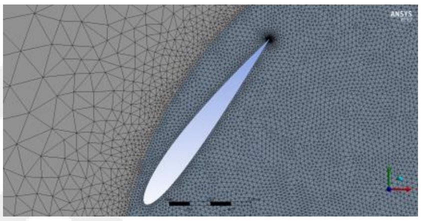

0.30 m Chord Length		
4 blades	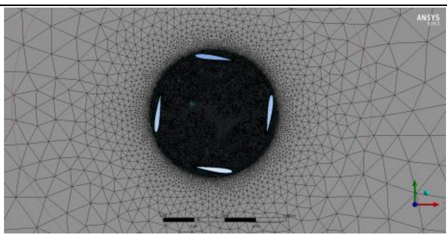	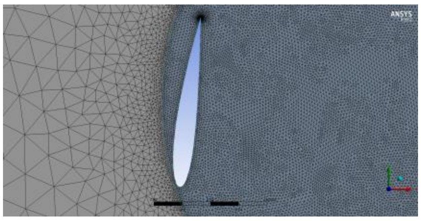
5 blades	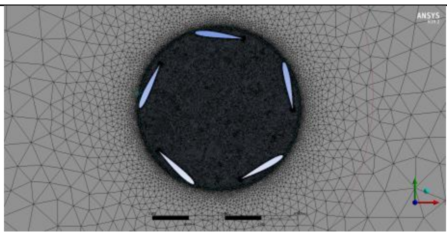	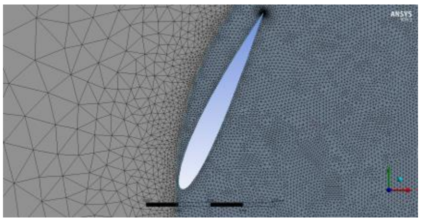
6 blades	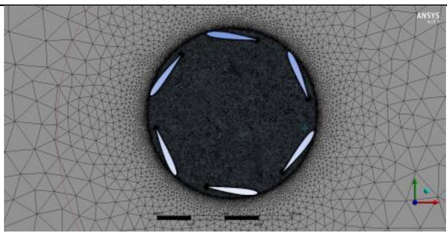	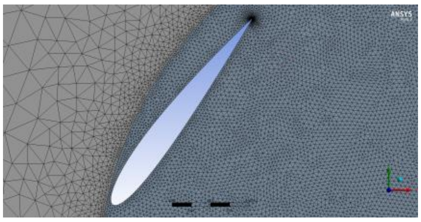

Due to variations in geometries, the mesh numbers differ for each model.

8.2.3 Analysis Setup

Modeling includes 15 different models with 4 blades, 5 blades, 6 blades, and chord lengths of 0.10 m, 0.15 m, 0.20 m, 0.25 m, and 0.30 m, respectively. The chord lengths of the models are arranged according to solidity, and the goal is to obtain the highest power coefficient output without exceeding a maximum solidity value of 0.35. In the simulations, a water flow rate of 2 m/s is used as the input parameter. It is mentioned that the solution consists of 2 different domains. For the outer domain, a relatively sparse mesh is applied to save time. The inner domain has a rotational angle. The rotational angle of the inner domain is assigned as a variable and tested at speeds of 0 rad/s, 2 rad/s, 4 rad/s, 6 rad/s, 8 rad/s, 10 rad/s, 12 rad/s, 14 rad/s, 16 rad/s, 18 rad/s, 20 rad/s, 22 rad/s, 24 rad/s, 26 rad/s, 28 rad/s, and 30 rad/s. As a result of the tested speeds, power coefficients corresponding to different TSR values will be calculated and compared.

8.2.3.1 Turbulence Model

While setting up the models, the Transition SST turbulence model with 4 equation sets has been used. The model equations involve a high number of meshes, allowing for high-accuracy simulations; however, it has proven to be computationally expensive in terms of time.

8.2.3.2 Iteration

During the simulations, the iteration count was set to 1000. It has been observed that the solutions are convergent.

8.2.3.3 Solver settings

Second-degree equations were carefully employed in the parameters, and the solutions were conducted with high precision.

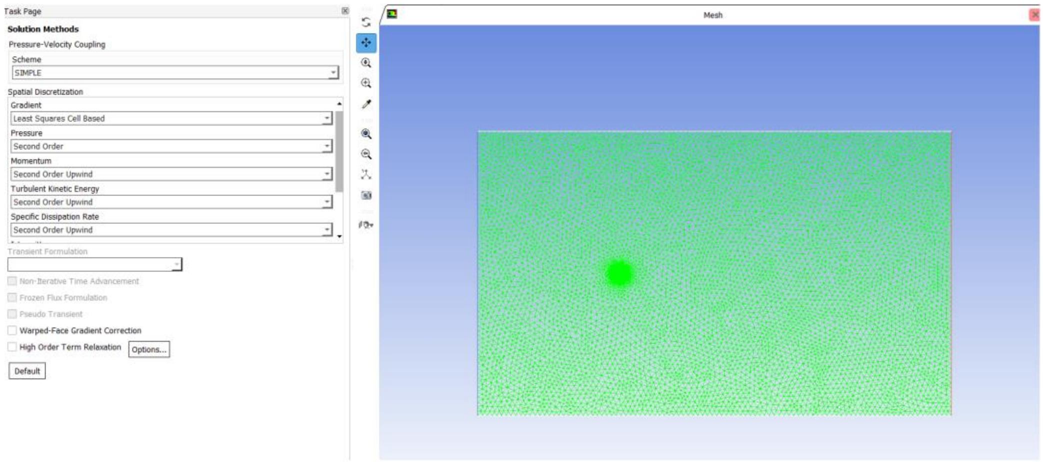

Figure 8.6 General solution method for modelled geometries

8.3 Post-processing

The results of the analyses were obtained, and graphs were utilized for easier examination.

8.3.1 Results

As a result of the analyses, turbines with 4, 5, and 6 blades were tested with different chord lengths, and the results were presented in tables. Since higher chord lengths correspond to higher solidity, turbines with higher solidity were observed to achieve a higher power coefficient.

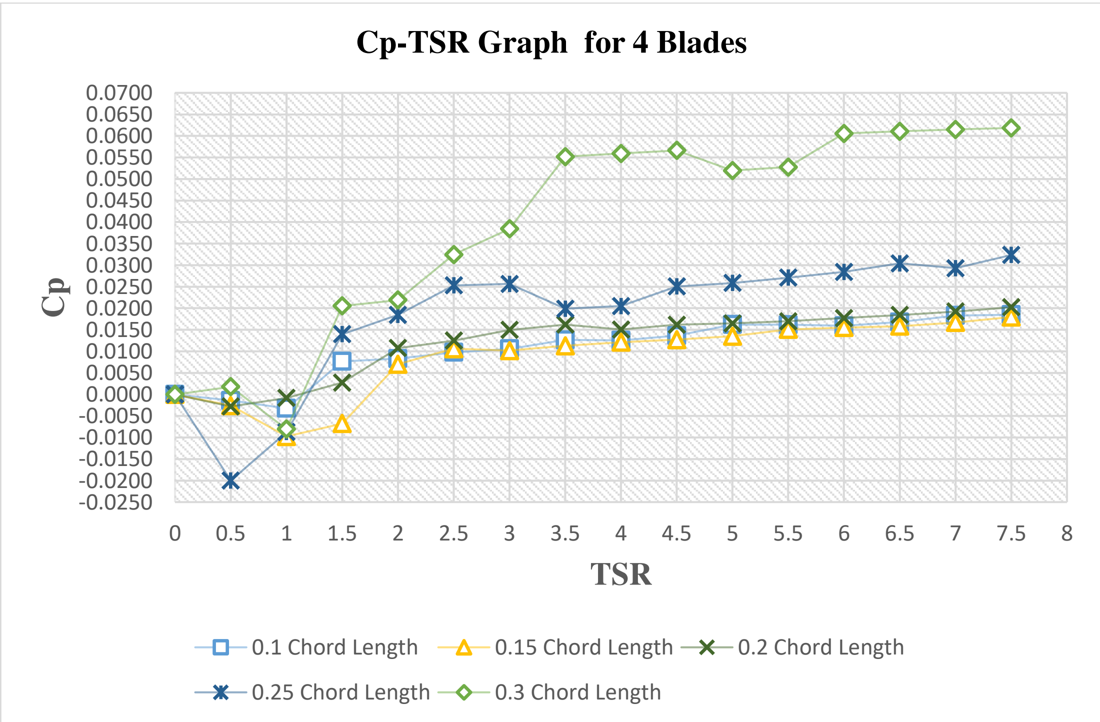

Figure 8.7 Cp vs. TSR Graph for 4 Blades

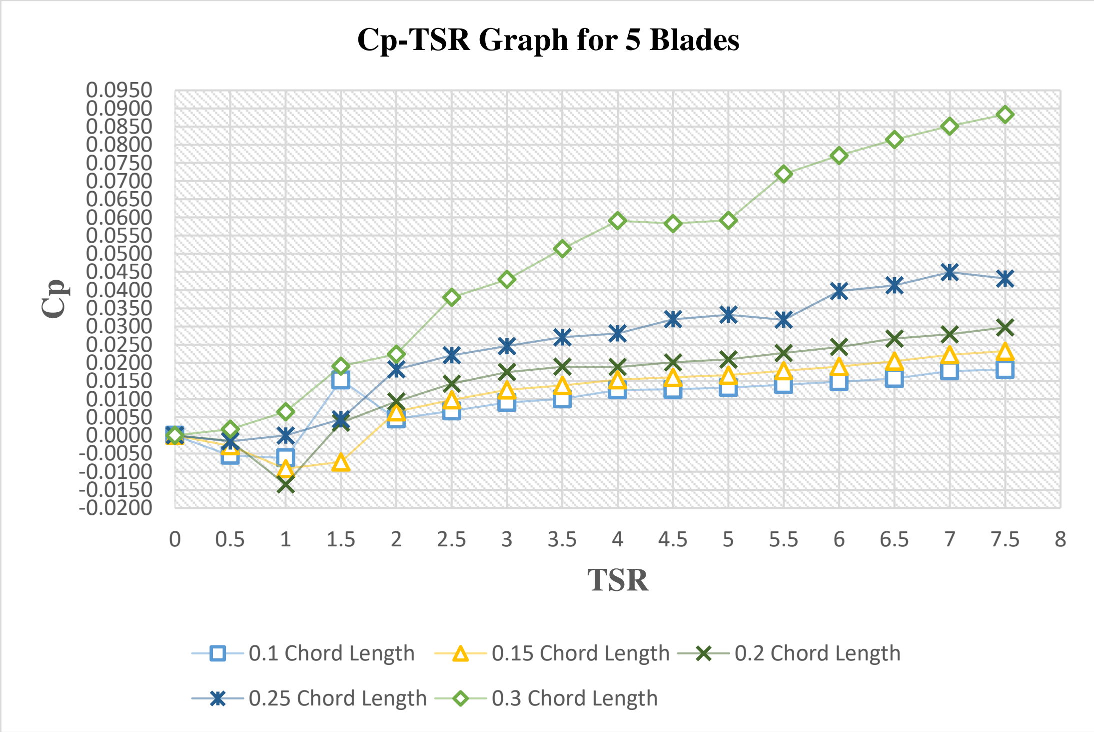

Figure 8.8 Cp vs. TSR Graph for 5 Blades

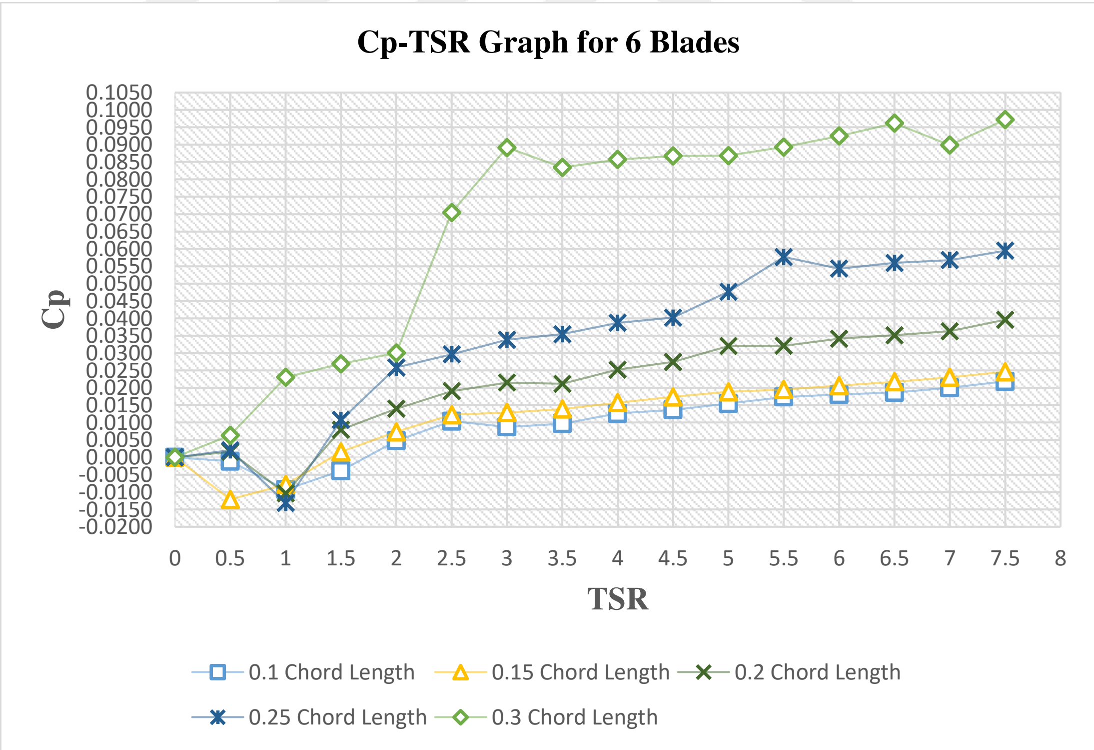

Figure 8.9 Cp vs. TSR Graph for 6 Blades

Turbines with 4, 5, and 6 blades had the average power coefficients calculated, and they were compared with solidity values. Each point seen in the graph represents a different chord length, while curves with different colors represent different blade numbers.

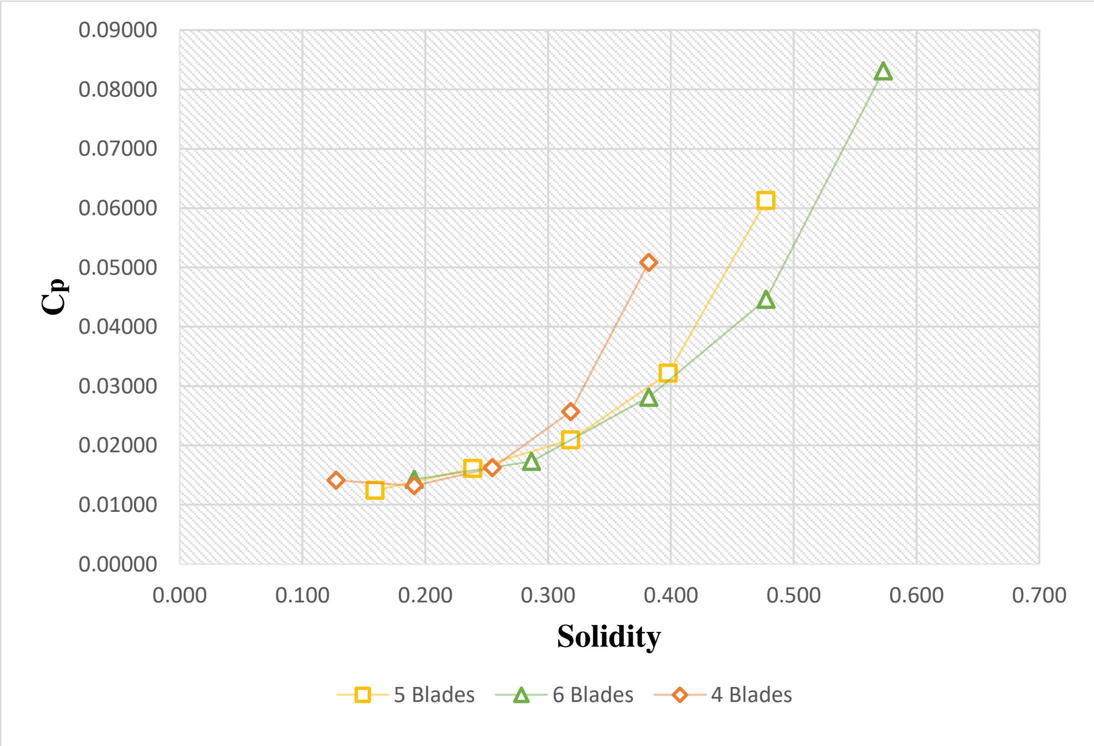

Figure 8.10 Cp vs. Solidity Graph for 4-5-6 number of blades

According to the analysis, the turbine with 4 blades and a chord length of 25cm has the highest power coefficient at a solidity value that does not impede the turbine's operation. Visuals of velocity, pressure, and eddy viscosity counters indicate the turbine with the best output.

The negative Cp values given as a percentage suggest that the turbine is not operating in the desired direction at its current rotational speed. Blade designs are made to ensure that the turbine rotates in the intended direction. Based on the current analyses, it can be concluded that at low rotational speeds, the turbine rotates in the opposite direction, indicating that the designed Cl/Cd value does not take effect at that speed. Instead, it moves based solely on the drag force effect and the flow direction.

Table 8.6 Output results for σ and Cp for the 4 number of blade turbine.

Model No	Number of Blades	Angular velocity	Chord Length (Meters)	Solidity	Cp (%)
1	4	0	0.1	0.1286	0
2	4	2	0.1	0.1286	-0.142
3	4	4	0.1	0.1286	-0.324
4	4	6	0.1	0.1286	0.7678
5	4	8	0.1	0.1286	0.83
6	4	10	0.1	0.1286	0.9765
7	4	12	0.1	0.1286	1.0587
8	4	14	0.1	0.1286	1.2656
9	4	16	0.1	0.1286	1.2556
10	4	18	0.1	0.1286	1.3635
11	4	20	0.1	0.1286	1.6205
12	4	22	0.1	0.1286	1.618
13	4	24	0.1	0.1286	1.5927
14	4	26	0.1	0.1286	1.6809
15	4	28	0.1	0.1286	1.8308
16	4	30	0.1	0.1286	1.85
17	4	0	0.15	0.1929	0
18	4	2	0.15	0.1929	-0.2571
19	4	4	0.15	0.1929	-0.975
20	4	6	0.15	0.1929	-0.6774
21	4	8	0.15	0.1929	0.7021
22	4	10	0.15	0.1929	1.0613
23	4	12	0.15	0.1929	1.0157
24	4	14	0.15	0.1929	1.1286
25	4	16	0.15	0.1929	1.2122
26	4	18	0.15	0.1929	1.2698
27	4	20	0.15	0.1929	1.3516
28	4	22	0.15	0.1929	1.51
29	4	24	0.15	0.1929	1.553
30	4	26	0.15	0.1929	1.5826
31	4	28	0.15	0.1929	1.6704
32	4	30	0.15	0.1929	1.7968
33	4	0	0.2	0.2572	0
34	4	2	0.2	0.2572	-0.2798
35	4	4	0.2	0.2572	-0.0821
36	4	6	0.2	0.2572	0.2744
37	4	8	0.2	0.2572	1.0769
38	4	10	0.2	0.2572	1.2486
39	4	12	0.2	0.2572	1.4979
40	4	14	0.2	0.2572	1.6221

Model No	Number of Blades	Angular velocity	Chord Length (Meters)	Solidity	Cp (%)
41	4	16	0.2	0.2572	1.5072
42	4	18	0.2	0.2572	1.6184
43	4	20	0.2	0.2572	1.649
44	4	22	0.2	0.2572	1.6986
45	4	24	0.2	0.2572	1.7708
46	4	26	0.2	0.2572	1.843
47	4	28	0.2	0.2572	1.9231
48	4	30	0.2	0.2572	2.0226
49	4	0	0.25	0.3215	0
50	4	2	0.25	0.3215	-2
51	4	4	0.25	0.3215	-0.875
52	4	6	0.25	0.3215	1.397
53	4	8	0.25	0.3215	1.8462
54	4	10	0.25	0.3215	2.5316
55	4	12	0.25	0.3215	2.5643
56	4	14	0.25	0.3215	1.9891
57	4	16	0.25	0.3215	2.0513
58	4	18	0.25	0.3215	2.5056
59	4	20	0.25	0.3215	2.5853
60	4	22	0.25	0.3215	2.7087
61	4	24	0.25	0.3215	2.8422
62	4	26	0.25	0.3215	3.0405
63	4	28	0.25	0.3215	2.9306
64	4	30	0.25	0.3215	3.2355
65	4	0	0.3	0.3858	0
66	4	2	0.3	0.3858	0.1779
67	4	4	0.3	0.3858	-0.8071
68	4	6	0.3	0.3858	2.0545
69	4	8	0.3	0.3858	2.1916
70	4	10	0.3	0.3858	3.2446
71	4	12	0.3	0.3858	3.843
72	4	14	0.3	0.3858	5.5171
73	4	16	0.3	0.3858	5.5925
74	4	18	0.3	0.3858	5.6623
75	4	20	0.3	0.3858	5.1974
76	4	22	0.3	0.3858	5.2752
77	4	24	0.3	0.3858	6.055
78	4	26	0.3	0.3858	6.1057
79	4	28	0.3	0.3858	6.1486
80	4	30	0.3	0.3858	6.1856

Table 8.7 Output results for σ and Cp for the 5 number of blade turbine

Model No	Number of Blades	Angular velocity	Chord Length (Meters)	Solidity	Cp (%)
1	5	0	0.1	0.1608	0
2	5	2	0.1	0.1608	-0.5501
3	5	4	0.1	0.1608	-0.6251
4	5	6	0.1	0.1608	1.5265
5	5	8	0.1	0.1608	0.4535
6	5	10	0.1	0.1608	0.6736
7	5	12	0.1	0.1608	0.9035
8	5	14	0.1	0.1608	1.0032
9	5	16	0.1	0.1608	1.2515
10	5	18	0.1	0.1608	1.2697
11	5	20	0.1	0.1608	1.3162
12	5	22	0.1	0.1608	1.3981
13	5	24	0.1	0.1608	1.4773
14	5	26	0.1	0.1608	1.5655
15	5	28	0.1	0.1608	1.771
16	5	30	0.1	0.1608	1.8112
17	5	0	0.15	0.2411	0
18	5	2	0.15	0.2411	-0.287
19	5	4	0.15	0.2411	-0.9183
20	5	6	0.15	0.2411	-0.7308
21	5	8	0.15	0.2411	0.6503
22	5	10	0.15	0.2411	0.9786
23	5	12	0.15	0.2411	1.2543
24	5	14	0.15	0.2411	1.3763
25	5	16	0.15	0.2411	1.534
26	5	18	0.15	0.2411	1.5974
27	5	20	0.15	0.2411	1.6589
28	5	22	0.15	0.2411	1.7803
29	5	24	0.15	0.2411	1.8957
30	5	26	0.15	0.2411	2.0423
31	5	28	0.15	0.2411	2.2202
32	5	30	0.15	0.2411	2.3203
33	5	0	0.2	0.3215	0
34	5	2	0.2	0.3215	-0.1498
35	5	4	0.2	0.3215	-1.349
36	5	6	0.2	0.3215	0.3499
37	5	8	0.2	0.3215	0.9327
38	5	10	0.2	0.3215	1.4218
39	5	12	0.2	0.3215	1.7412
40	5	14	0.2	0.3215	1.8882
41	5	16	0.2	0.3215	1.8803

Model No	Number of Blades	Angular velocity	Chord Length (Meters)	Solidity	Cp (%)
42	5	18	0.2	0.3215	2.0095
43	5	20	0.2	0.3215	2.0908
44	5	22	0.2	0.3215	2.267
45	5	24	0.2	0.3215	2.4326
46	5	26	0.2	0.3215	2.6645
47	5	28	0.2	0.3215	2.7834
48	5	30	0.2	0.3215	2.9724
49	5	0	0.25	0.4019	0
50	5	2	0.25	0.4019	-0.164
51	5	4	0.25	0.4019	-0.0025
52	5	6	0.25	0.4019	0.4458
53	5	8	0.25	0.4019	1.8158
54	5	10	0.25	0.4019	2.204
55	5	12	0.25	0.4019	2.4569
56	5	14	0.25	0.4019	2.6999
57	5	16	0.25	0.4019	2.8092
58	5	18	0.25	0.4019	3.1973
59	5	20	0.25	0.4019	3.3231
60	5	22	0.25	0.4019	3.1827
61	5	24	0.25	0.4019	3.9708
62	5	26	0.25	0.4019	4.13
63	5	28	0.25	0.4019	4.4919
64	5	30	0.25	0.4019	4.3164
65	5	0	0.3	0.4823	0
66	5	2	0.3	0.4823	0.1714
67	5	4	0.3	0.4823	0.65
68	5	6	0.3	0.4823	1.9059
69	5	8	0.3	0.4823	2.234
70	5	10	0.3	0.4823	3.7995
71	5	12	0.3	0.4823	4.2908
72	5	14	0.3	0.4823	5.1362
73	5	16	0.3	0.4823	5.9083
74	5	18	0.3	0.4823	5.83
75	5	20	0.3	0.4823	5.9211
76	5	22	0.3	0.4823	7.1935
77	5	24	0.3	0.4823	7.7064
78	5	26	0.3	0.4823	8.1409
79	5	28	0.3	0.4823	8.5135
80	5	30	0.3	0.4823	8.8365

Table 8.8 Output results for σ and Cp for the 6 number of blade turbine

Model No	Number of Blades	Angular velocity	Chord Length (Meters)	Solidity	Cp (%)
1	6	0	0.1	0.1929	0
2	6	2	0.1	0.1929	-0.1112
3	6	4	0.1	0.1929	-0.9303
4	6	6	0.1	0.1929	-0.387
5	6	8	0.1	0.1929	0.4767
6	6	10	0.1	0.1929	1.0415
7	6	12	0.1	0.1929	0.8748
8	6	14	0.1	0.1929	0.9658
9	6	16	0.1	0.1929	1.2649
10	6	18	0.1	0.1929	1.3653
11	6	20	0.1	0.1929	1.5457
12	6	22	0.1	0.1929	1.735
13	6	24	0.1	0.1929	1.8071
14	6	26	0.1	0.1929	1.8654
15	6	28	0.1	0.1929	2.0009
16	6	30	0.1	0.1929	2.1868
17	6	0	0.15	0.2894	0
18	6	2	0.15	0.2894	-1.2103
19	6	4	0.15	0.2894	-0.7833
20	6	6	0.15	0.2894	0.1568
21	6	8	0.15	0.2894	0.7313
22	6	10	0.15	0.2894	1.2253
23	6	12	0.15	0.2894	1.2901
24	6	14	0.15	0.2894	1.3881
25	6	16	0.15	0.2894	1.5727
26	6	18	0.15	0.2894	1.74
27	6	20	0.15	0.2894	1.8858
28	6	22	0.15	0.2894	1.9517
29	6	24	0.15	0.2894	2.0605
30	6	26	0.15	0.2894	2.1723
31	6	28	0.15	0.2894	2.3036
32	6	30	0.15	0.2894	2.4616
33	6	0	0.2	0.3858	0
34	6	2	0.2	0.3858	0.1599
35	6	4	0.2	0.3858	-1.0392
36	6	6	0.2	0.3858	0.7948
37	6	8	0.2	0.3858	1.3976
38	6	10	0.2	0.3858	1.9056
39	6	12	0.2	0.3858	2.1487
40	6	14	0.2	0.3858	2.1152

Model No	Number of Blades	Angular velocity	Chord Length	Solidity	Cp (%)
41	6	16	0.2	0.3858	2.5244
42	6	18	0.2	0.3858	2.7451
43	6	20	0.2	0.3858	3.2027
44	6	22	0.2	0.3858	3.2103
45	6	24	0.2	0.3858	3.4141
46	6	26	0.2	0.3858	3.5128
47	6	28	0.2	0.3858	3.6281
48	6	30	0.2	0.3858	3.9591
49	6	0	0.25	0.4823	0
50	6	2	0.25	0.4823	0.2022
51	6	4	0.25	0.4823	-1.31
52	6	6	0.25	0.4823	1.0735
53	6	8	0.25	0.4823	2.5835
54	6	10	0.25	0.4823	2.963
55	6	12	0.25	0.4823	3.3848
56	6	14	0.25	0.4823	3.5453
57	6	16	0.25	0.4823	3.8719
58	6	18	0.25	0.4823	4.0207
59	6	20	0.25	0.4823	4.7662
60	6	22	0.25	0.4823	5.765
61	6	24	0.25	0.4823	5.4298
62	6	26	0.25	0.4823	5.5969
63	6	28	0.25	0.4823	5.6757
64	6	30	0.25	0.4823	5.947
65	6	0	0.3	0.5787	0
66	6	2	0.3	0.5787	0.6342
67	6	4	0.3	0.5787	2.3055
68	6	6	0.3	0.5787	2.6913
69	6	8	0.3	0.5787	3.004
70	6	10	0.3	0.5787	7.0466
71	6	12	0.3	0.5787	8.9169
72	6	14	0.3	0.5787	8.3444
73	6	16	0.3	0.5787	8.5714
74	6	18	0.3	0.5787	8.6721
75	6	20	0.3	0.5787	8.6842
76	6	22	0.3	0.5787	8.9319
77	6	24	0.3	0.5787	9.2477
78	6	26	0.3	0.5787	9.6164
79	6	28	0.3	0.5787	8.9865
80	6	30	0.3	0.5787	9.7202

For better clarity of the analysis results presented in the table, the average Cp values for different pitch angles of each blade count have been calculated and compared with the solidity values.

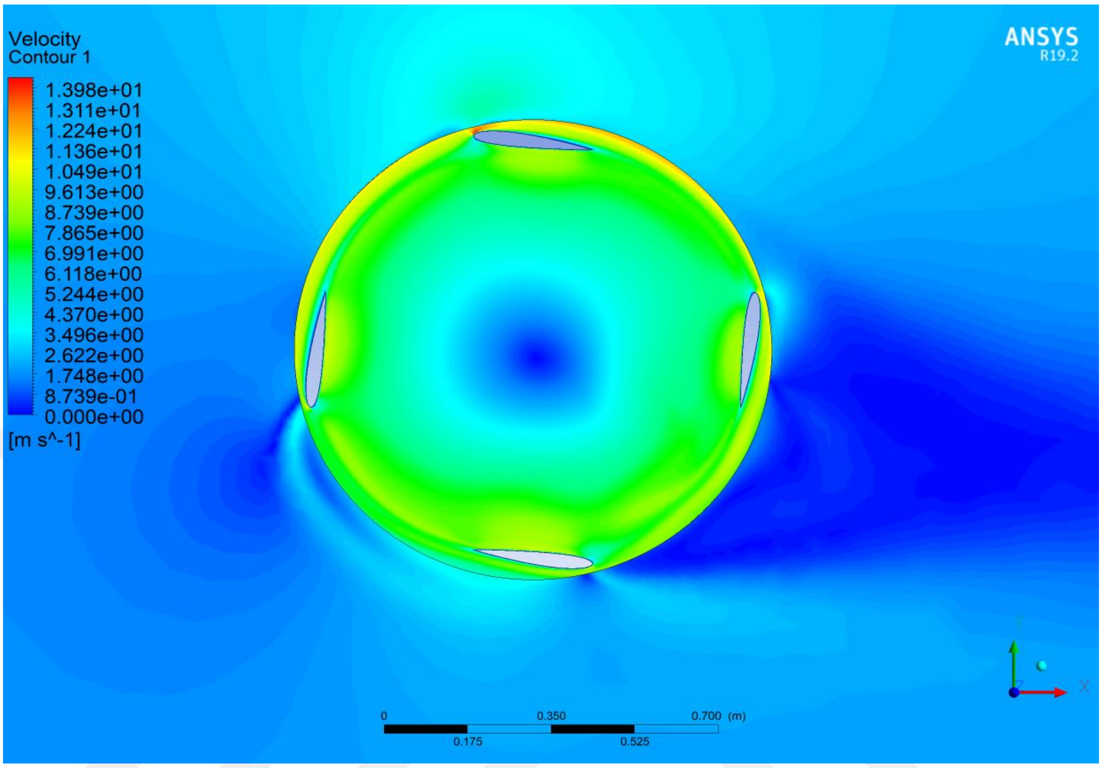

Figure 8.11 Velocity counter for optimized turbine

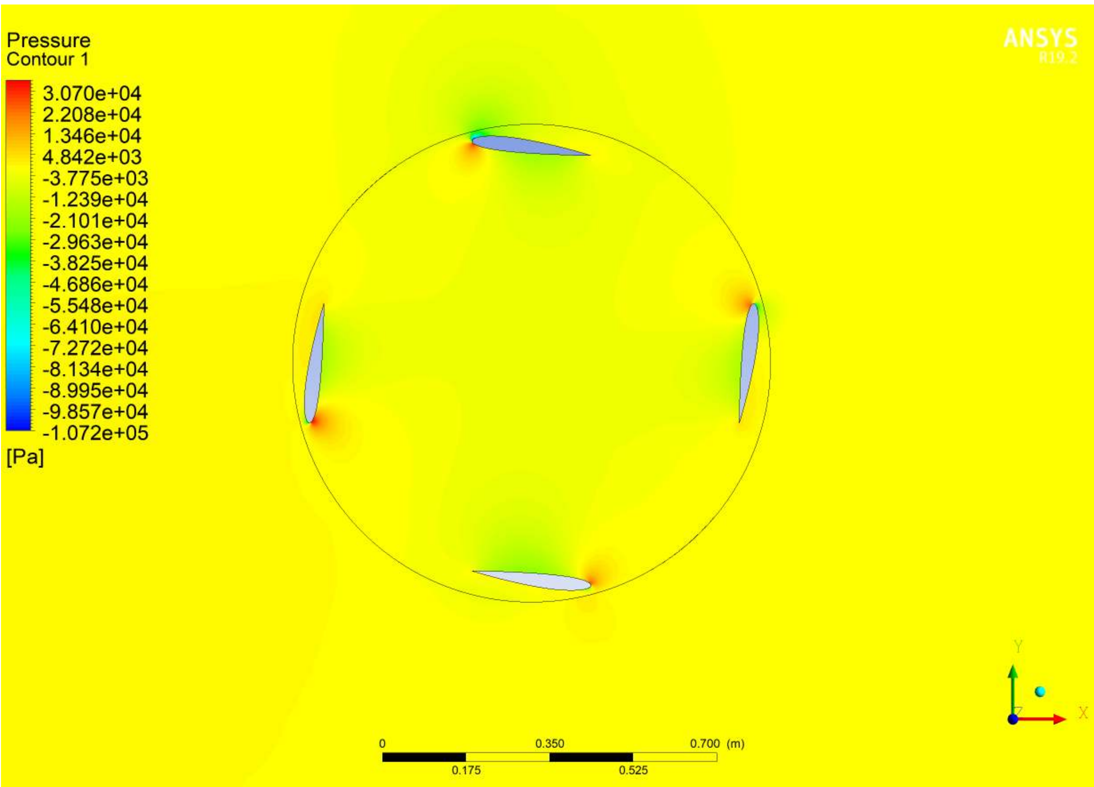

Figure 8.12 Pressure counter for optimized turbine

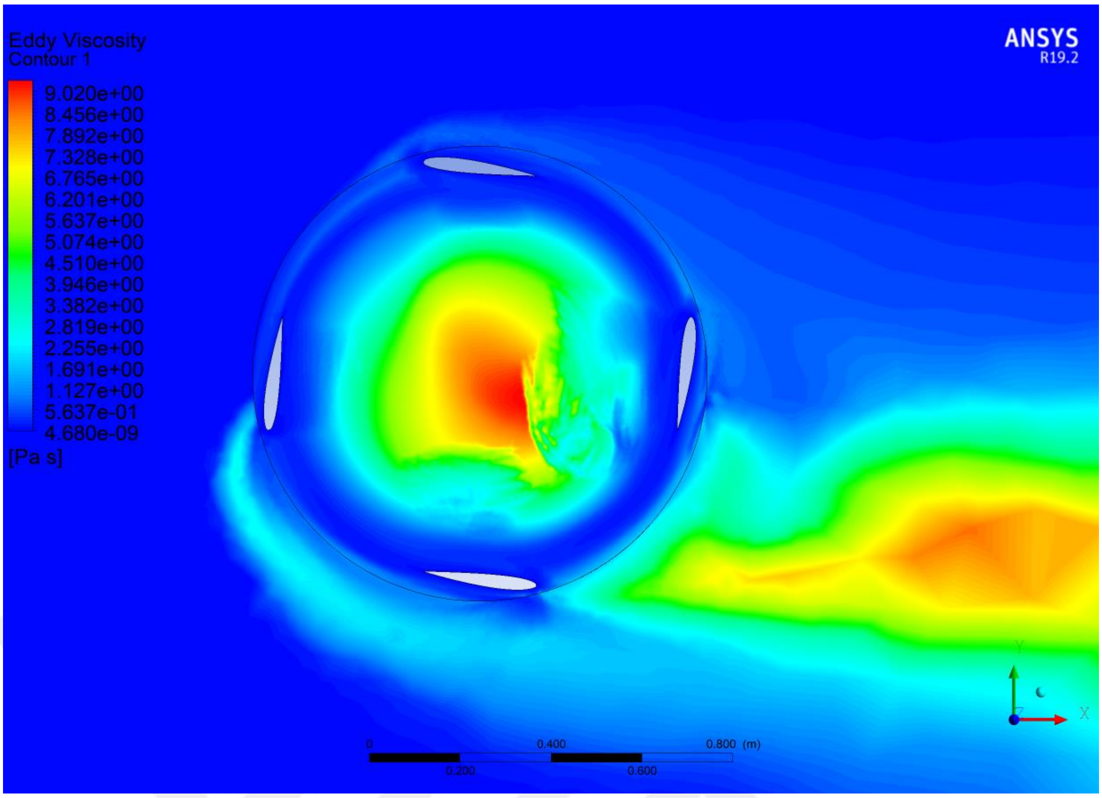

Figure 8.13 Eddy viscosity counter for optimized turbine

Counter printouts were taken for all analyses. It is divided into 3 main groups to be examined in more detail. These are Velocity counters, Pressure counters and eddy viscosity counters.

8.3.1.1 Velocity Counters Results

<table>
<tr><td colspan="3">0.10 m Chord Length Velocity Counter</td></tr>
<tr><td></td><td>All Domain</td><td>Rotor Domain</td></tr>
<tr><td>4
Blades</td><td>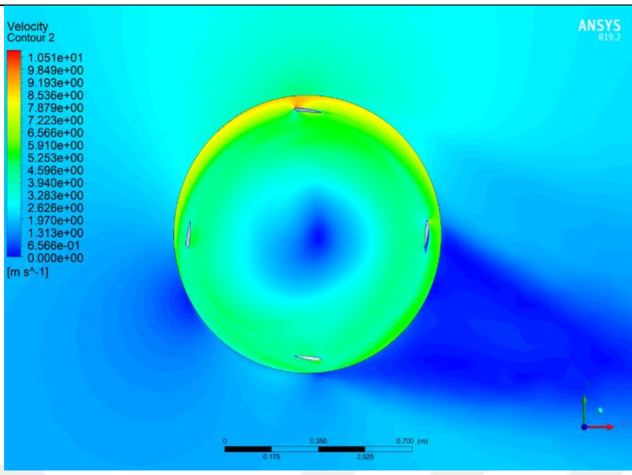
</td><td>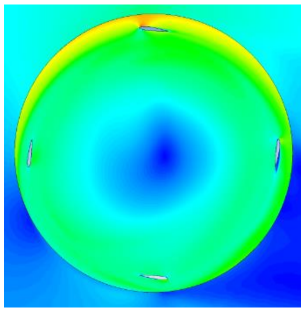</td></tr>
<tr><td>5
Blades</td><td>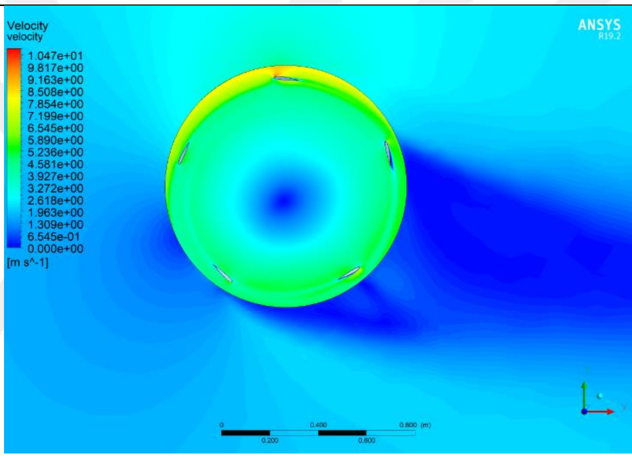
</td><td>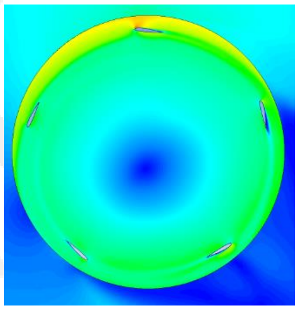</td></tr>
<tr><td>6
Blades</td><td>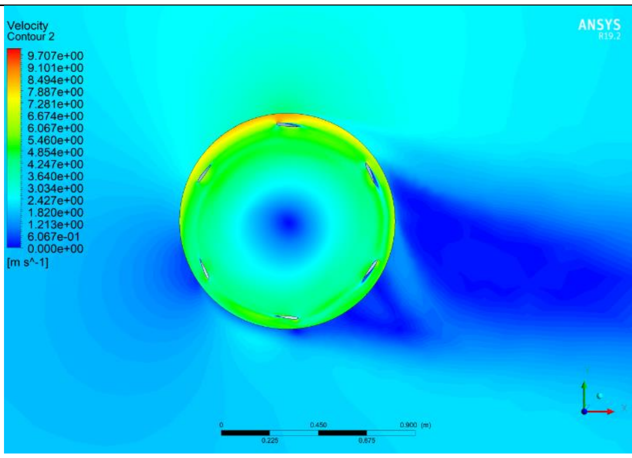
</td><td>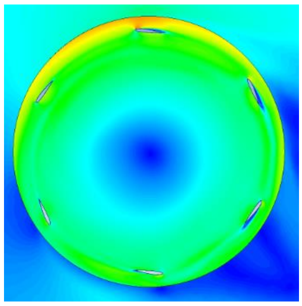</td></tr>
</table>

<table>
<tr><td colspan="3">0.15 m Chord Length Velocity Counter</td></tr>
<tr><td></td><td>All Domain</td><td>Rotor Domain</td></tr>
<tr><td>4 Blades</td><td>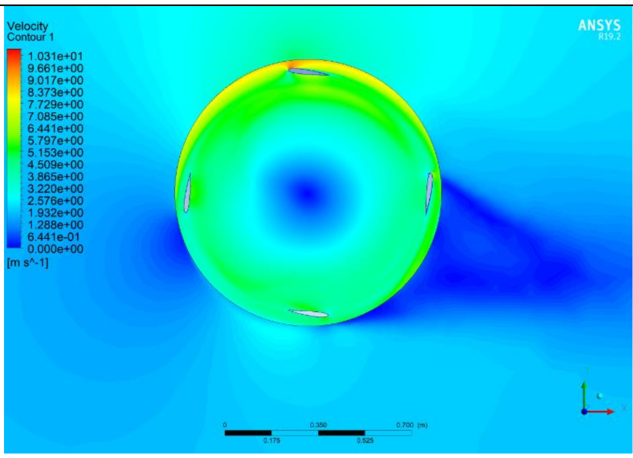
</td><td>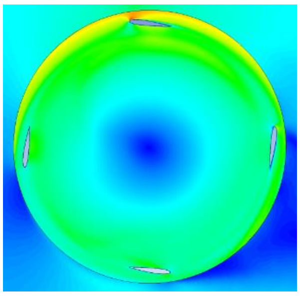</td></tr>
<tr><td>5 Blades</td><td>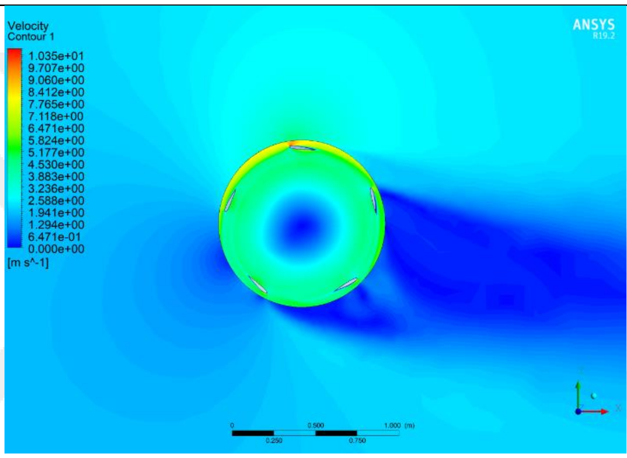
</td><td>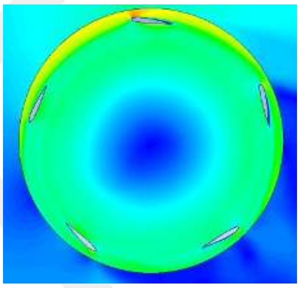</td></tr>
<tr><td>6 Blades</td><td>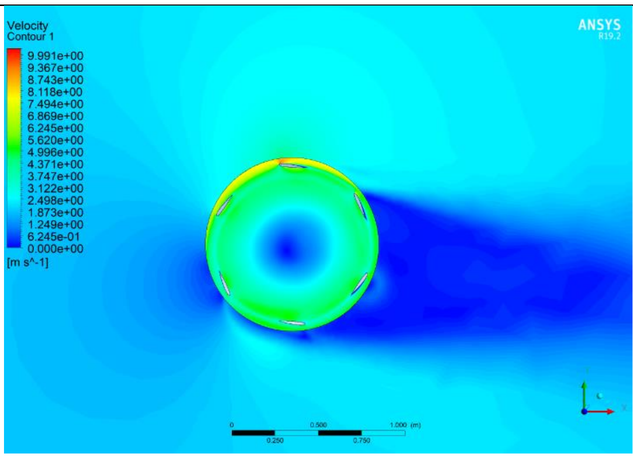
</td><td>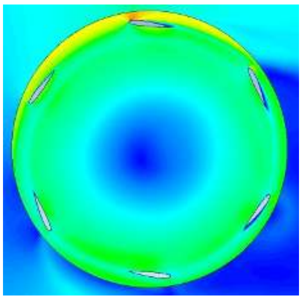</td></tr>
</table>

<table>
<tr><td colspan="3">0.20 m Chord Length Velocity Counter</td></tr>
<tr><td></td><td>All Domain</td><td>Rotor Domain</td></tr>
<tr><td>4
Blades</td><td>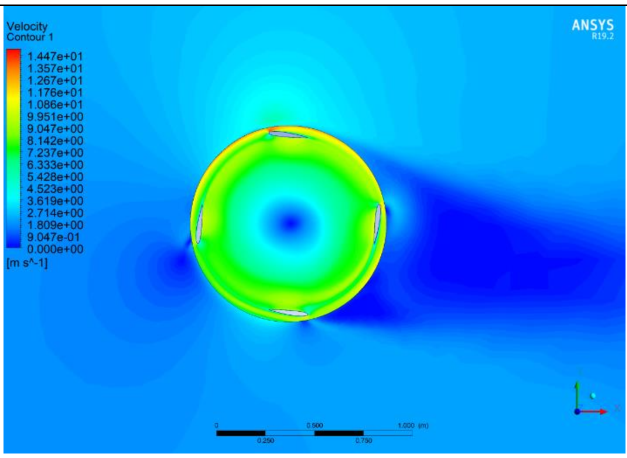
</td><td>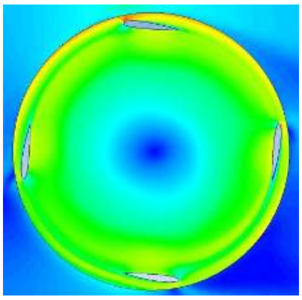</td></tr>
<tr><td>5
Blades</td><td>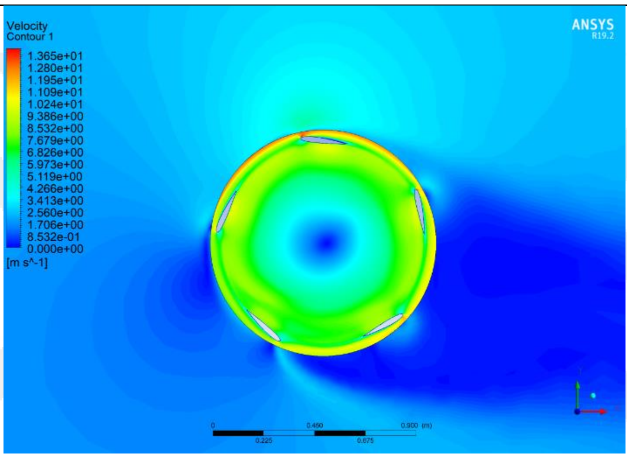
</td><td>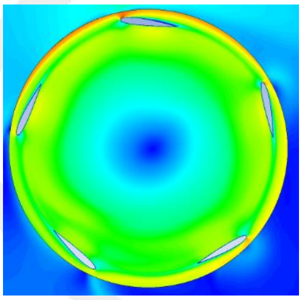</td></tr>
<tr><td>6
Blades</td><td>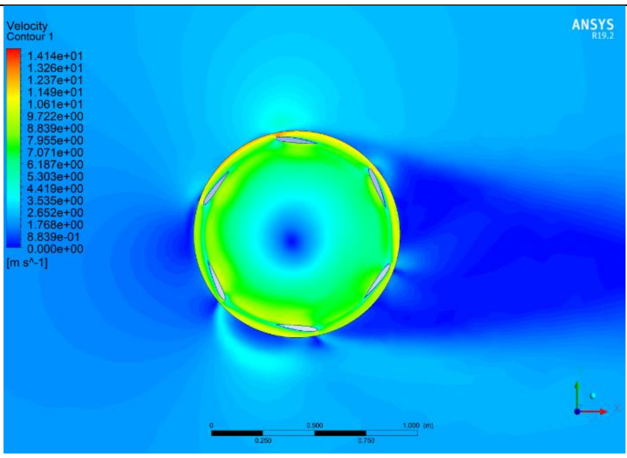
</td><td>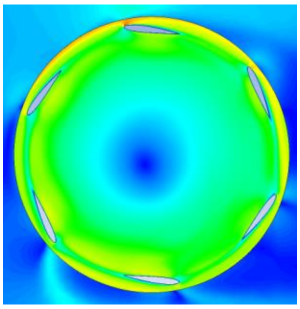</td></tr>
</table>

0.25 m Chord Length Velocity Counter		
	All Domain	**Rotor Domain**
4 Blades	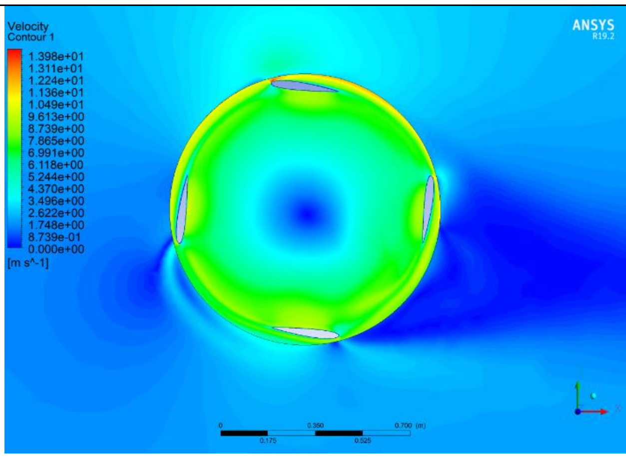	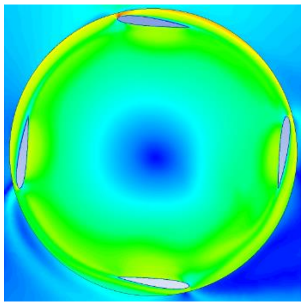
5 Blades	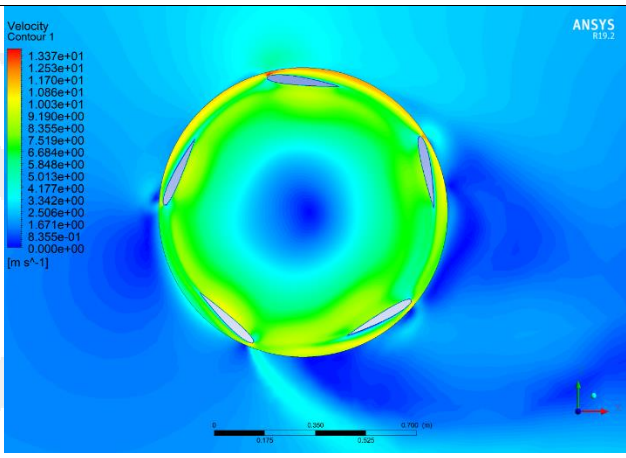	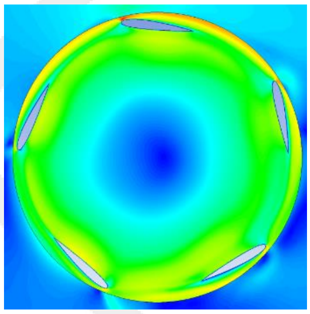
6 Blades	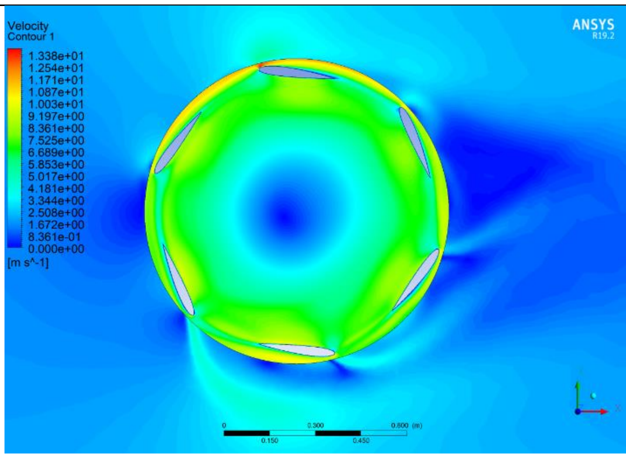	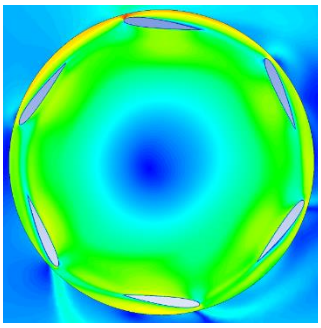

<table>
<tr><td colspan="3">0.30 m Chord Length Velocity Counter</td></tr>
<tr><td></td><td>All Domain</td><td>Rotor Domain</td></tr>
<tr><td>4 Blades</td><td>
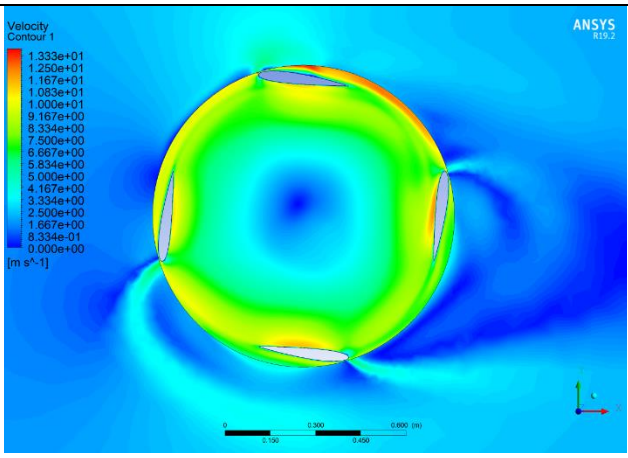

</td><td>
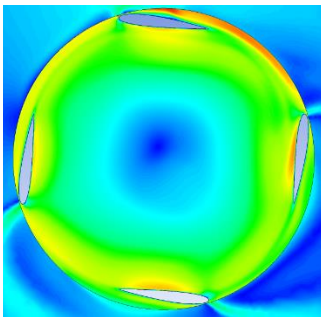
</td></tr>
<tr><td>5 Blades</td><td>
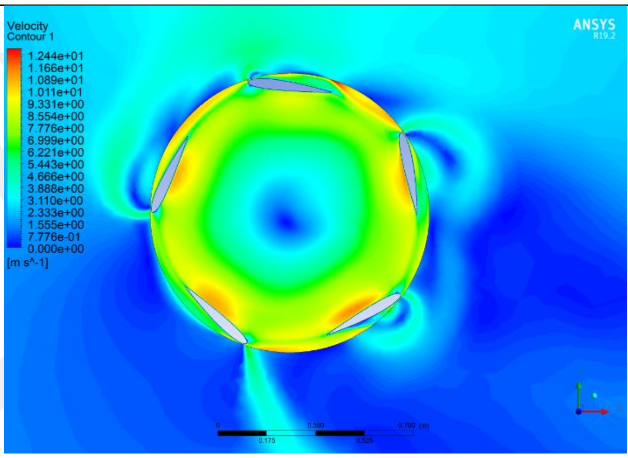

</td><td>
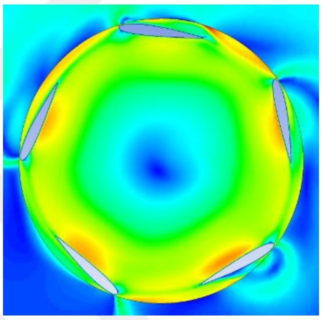
</td></tr>
<tr><td>6 Blades</td><td>
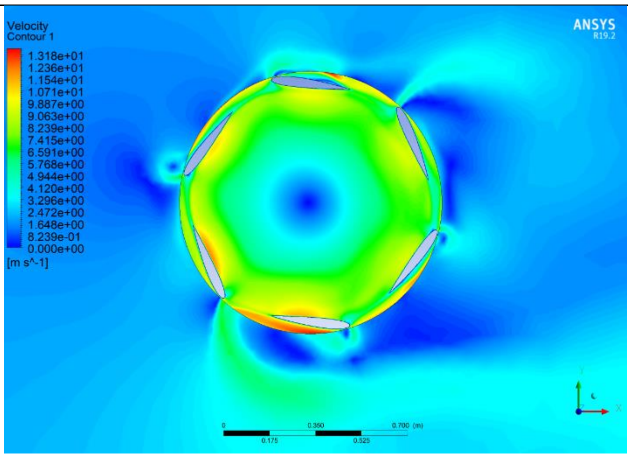

</td><td>
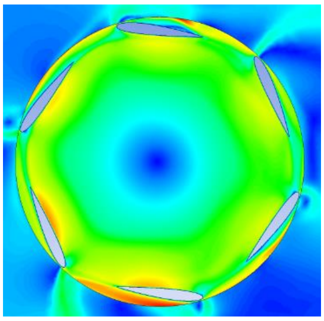
</td></tr>
</table>

8.3.1.2 Pressure Counters Results

0.10 m Chord Length Pressure Counter		
	All Domain	**Rotor Domain**
4 Blades	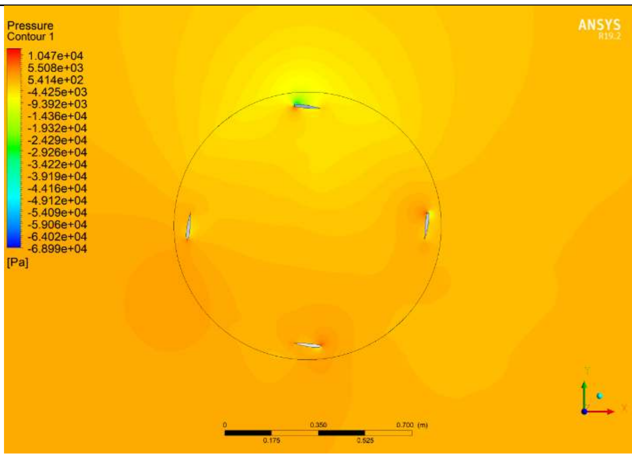	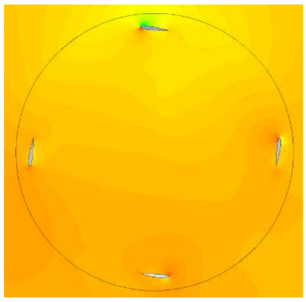
5 Blades	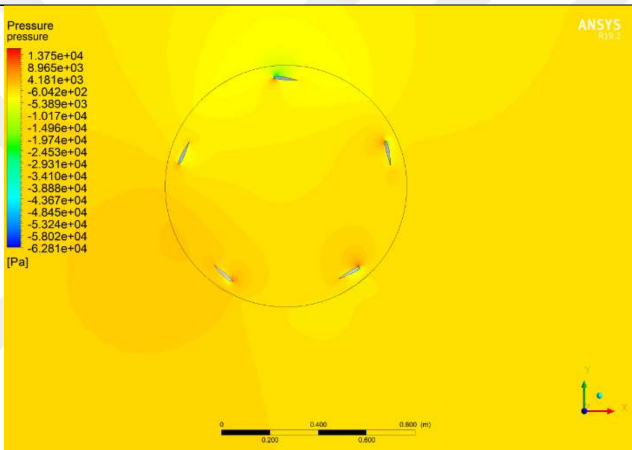	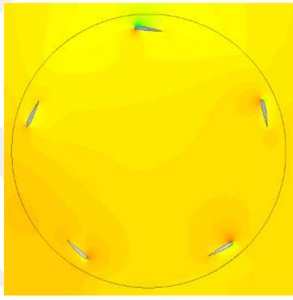
6 Blades	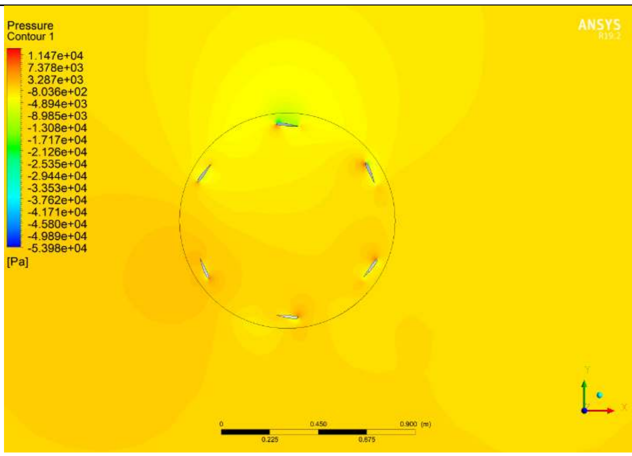	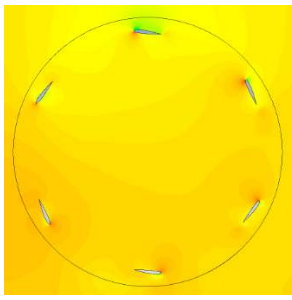

0.15 m Chord Length Pressure Counter		
	All Domain	**Rotor Domain**
4 Blades	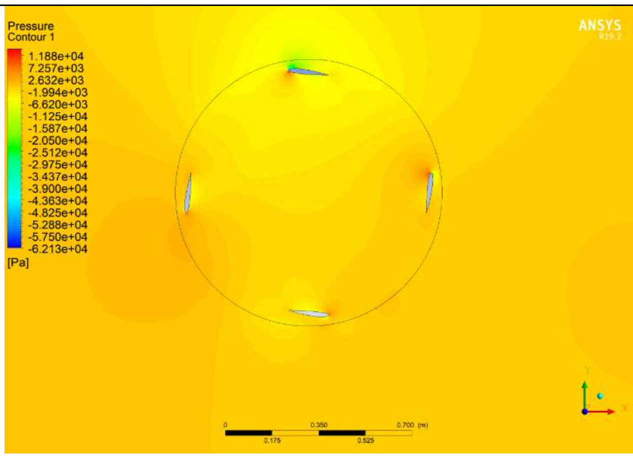	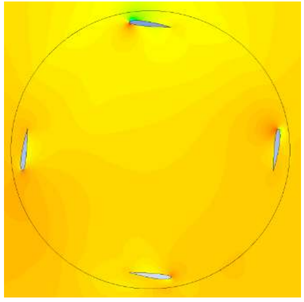
5 Blades	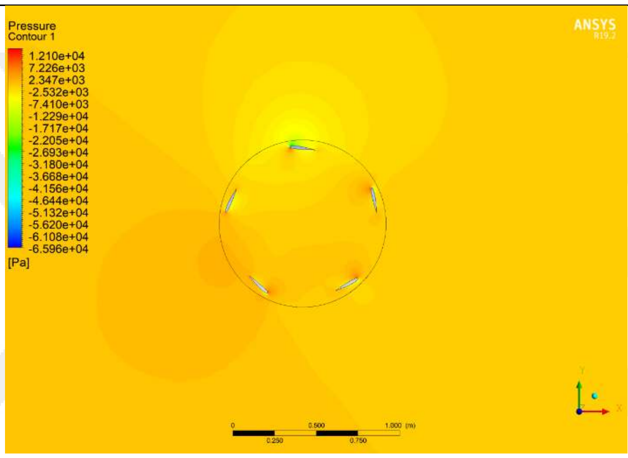	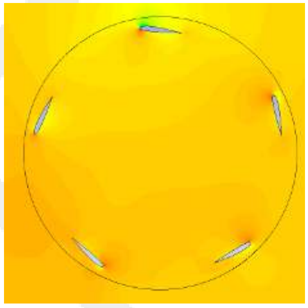
6 Blades	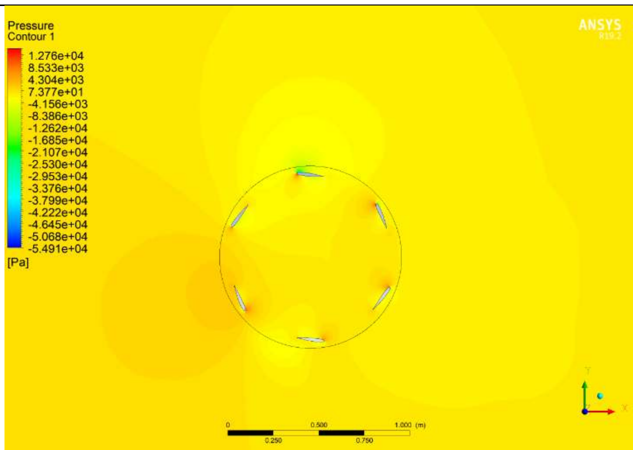	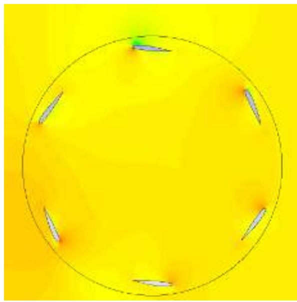

0.20 m Chord Length Pressure Counter		
	All Domain	**Rotor Domain**
4 Blades	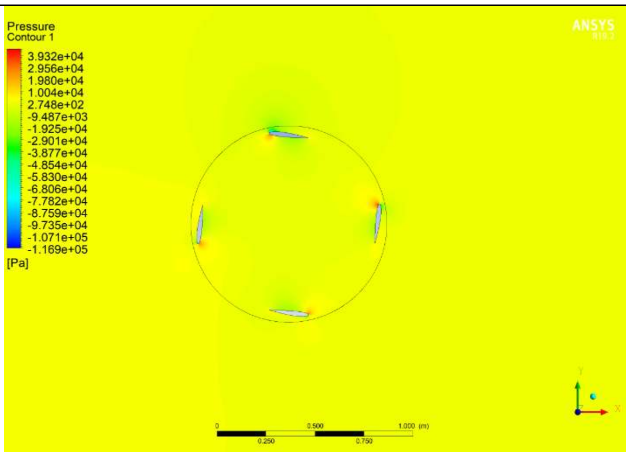	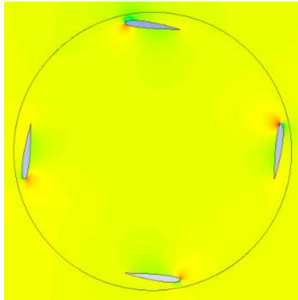
5 Blades	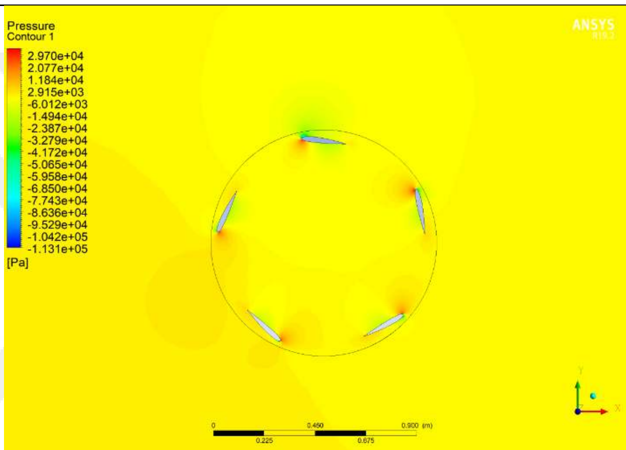	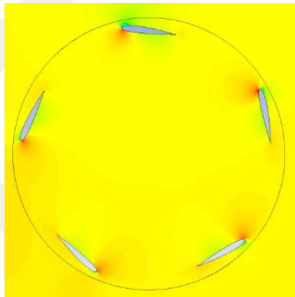
6 Blades	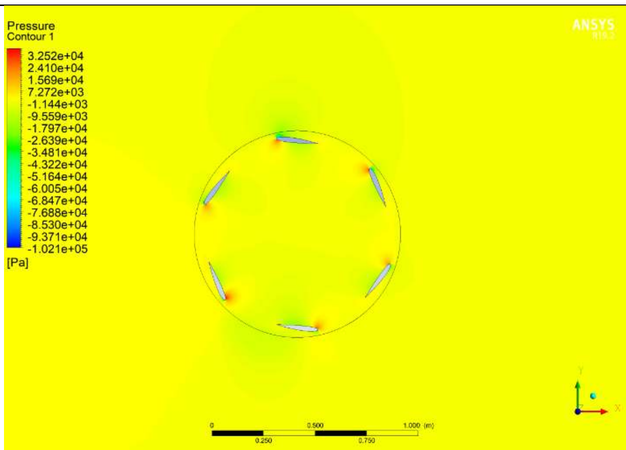	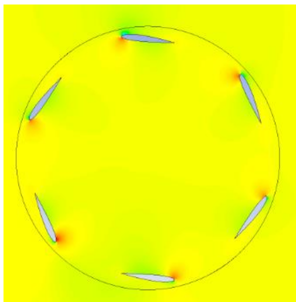

<table>
<tr><td colspan="3">0.25 m Chord Length Pressure Counter</td></tr>
<tr><td></td><td>All Domain</td><td>Rotor Domain</td></tr>
<tr><td>4 Blades</td><td>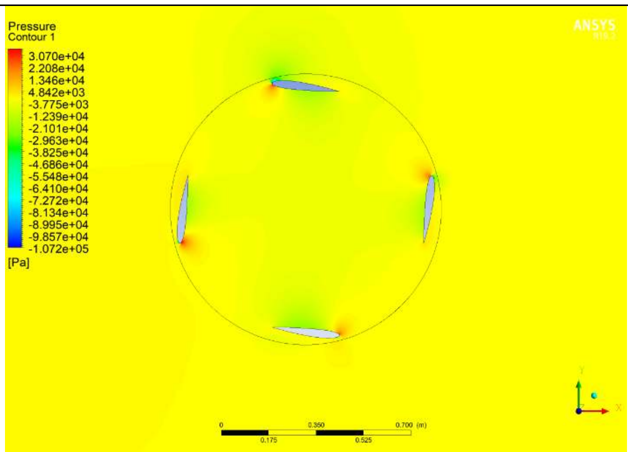
</td><td>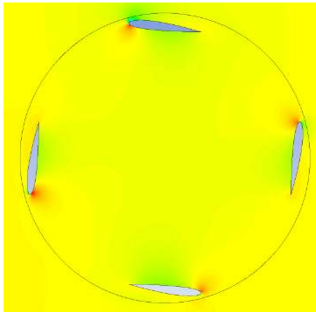</td></tr>
<tr><td>5 Blades</td><td>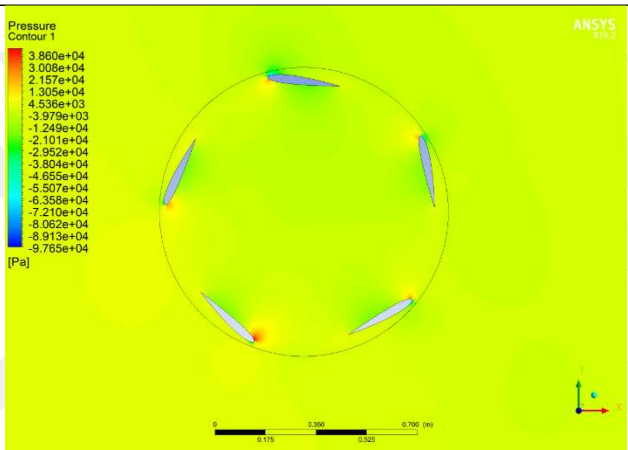
</td><td>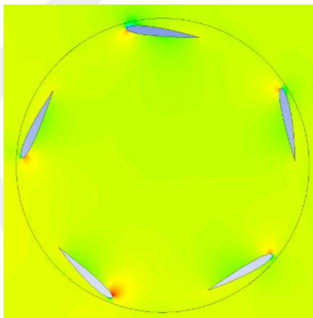</td></tr>
<tr><td>6 Blades</td><td>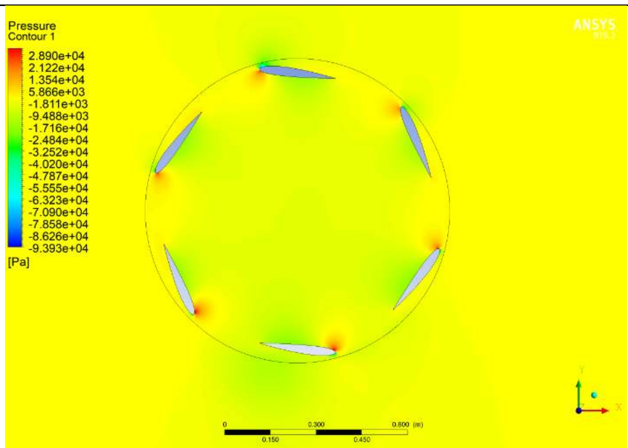
</td><td>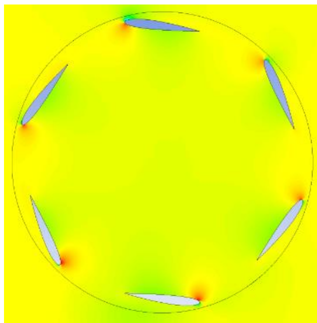</td></tr>
</table>

<table>
<tr><td colspan="3">0.30 m Chord Length Pressure Counter</td></tr>
<tr><td></td><td>All Domain</td><td>Rotor Domain</td></tr>
<tr><td>4 Blade s</td><td>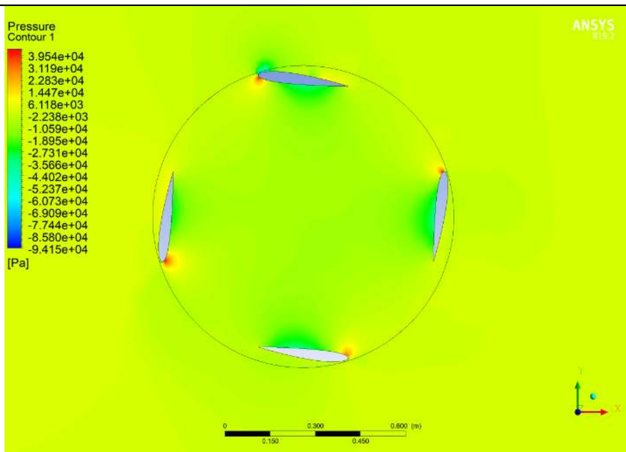
</td><td>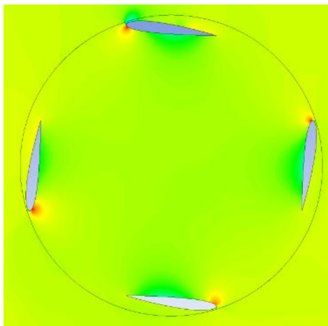</td></tr>
<tr><td>5 Blade s</td><td>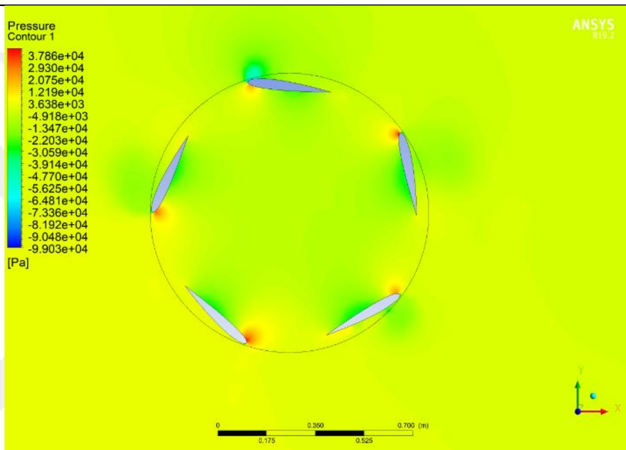
</td><td>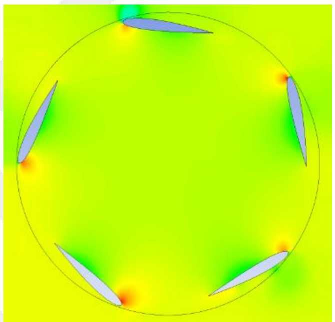</td></tr>
<tr><td>6 Blade s</td><td>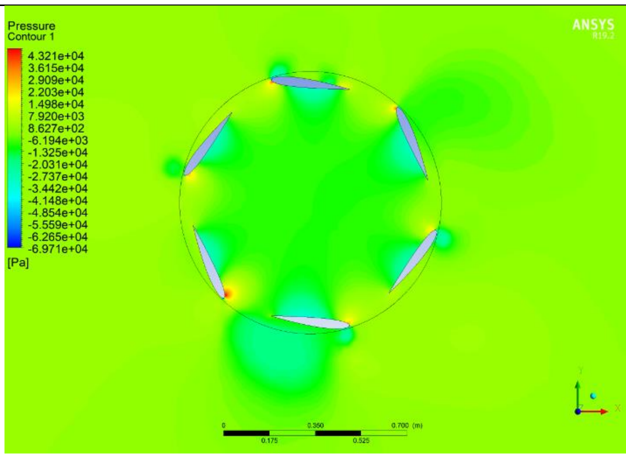
</td><td>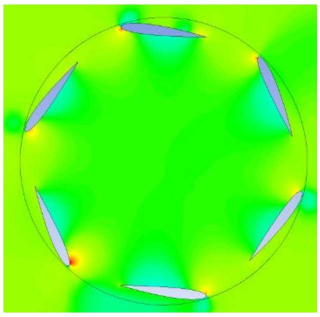</td></tr>
</table>

8.3.1.3 Eddy Viscosity Counters Results

0.10 m Chord Length Eddy Viscosity Counter		
	All Domain	**Rotor Domain**
4 Blades	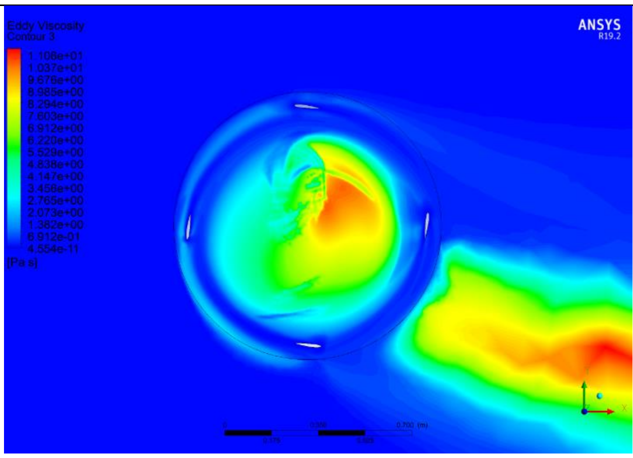	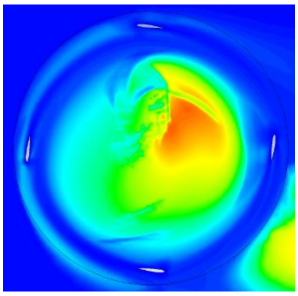
5 Blades	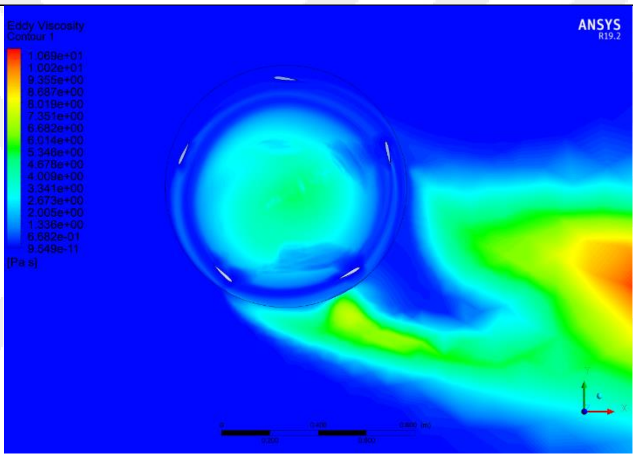	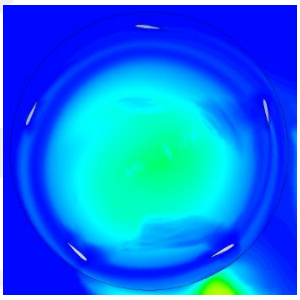
6 Blades	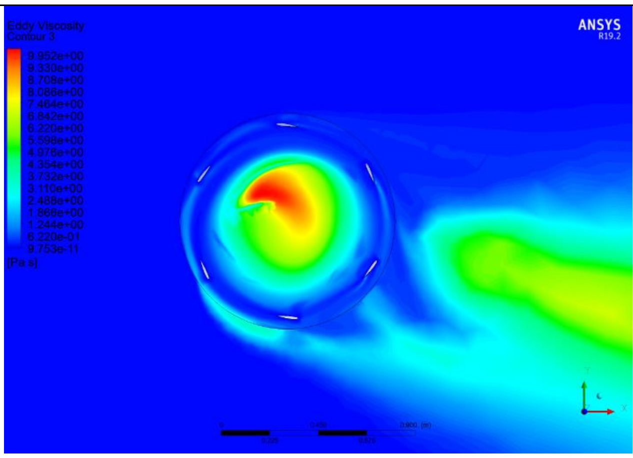	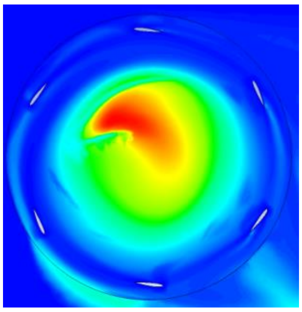

0.15 m Chord Length Eddy Viscosity Counter		
	All Domain	**Rotor Domain**
4 Blades	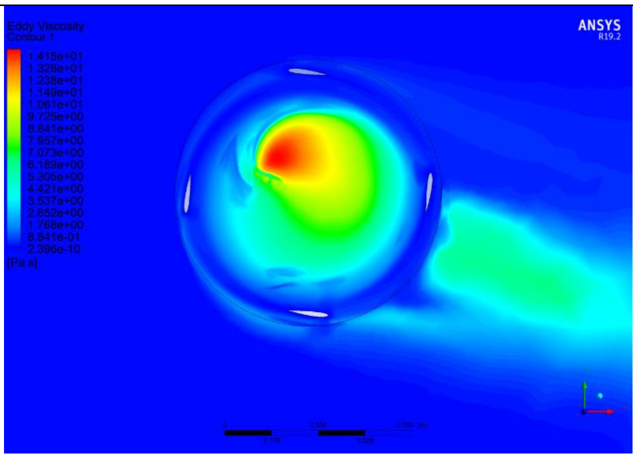	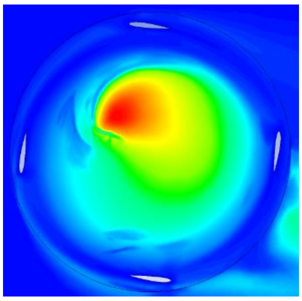
5 Blades	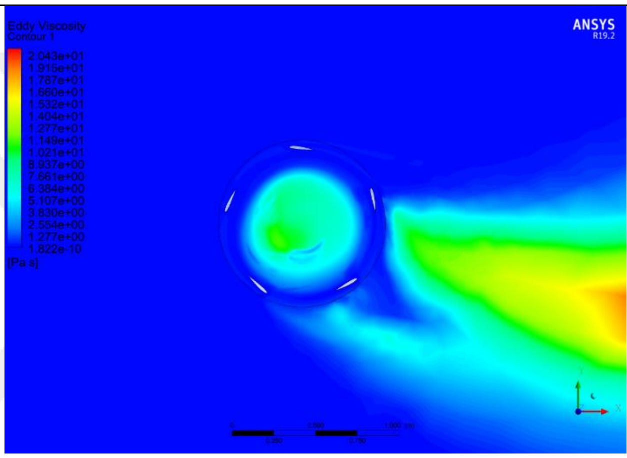	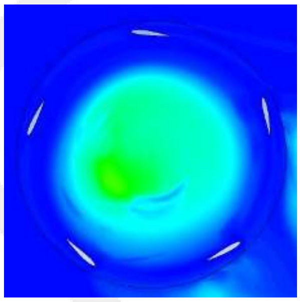
6 Blades	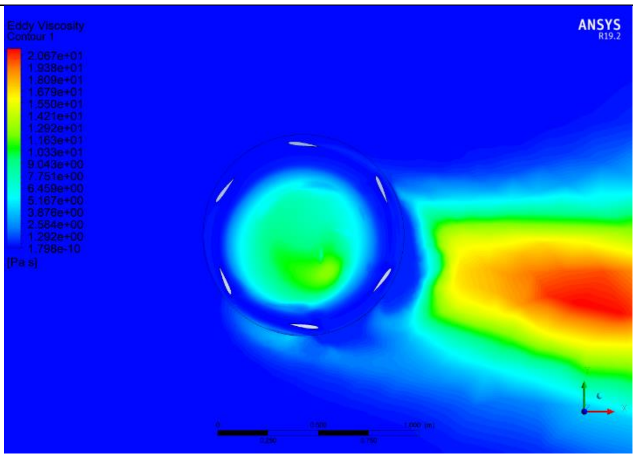	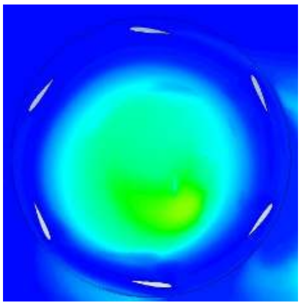

0.20 m Chord Length Eddy Viscosity Counter		
	All Domain	**Rotor Domain**
4 Blades	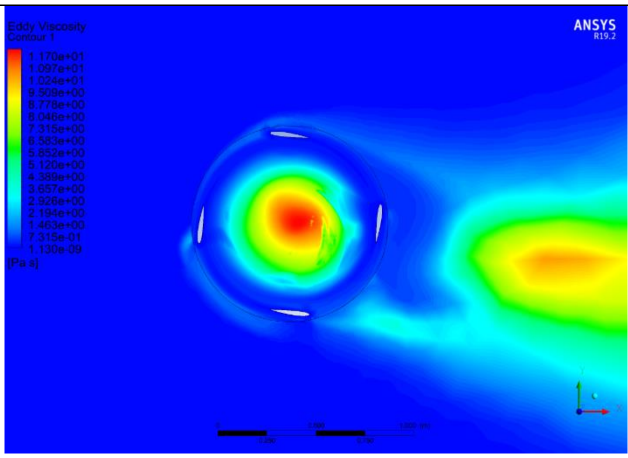	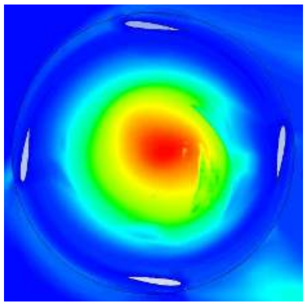
5 Blades	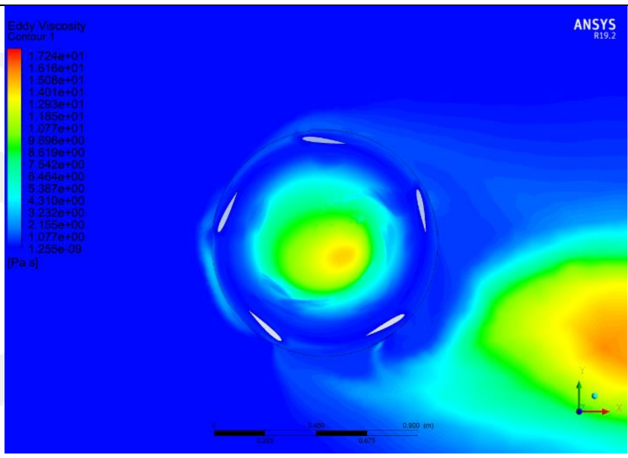	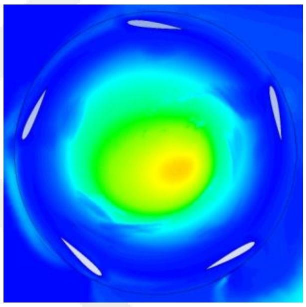
6 Blades	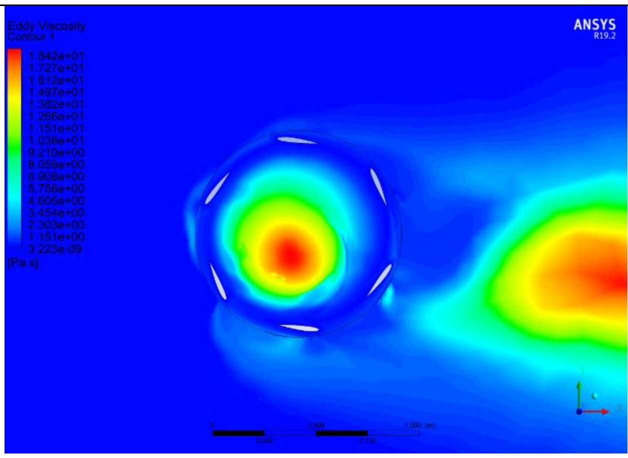	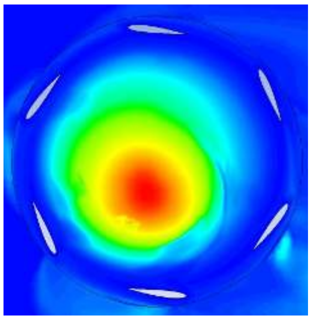

0.25 m Chord Length Eddy Viscosity Counter		
	All Domain	**Rotor Domain**
4 Blades	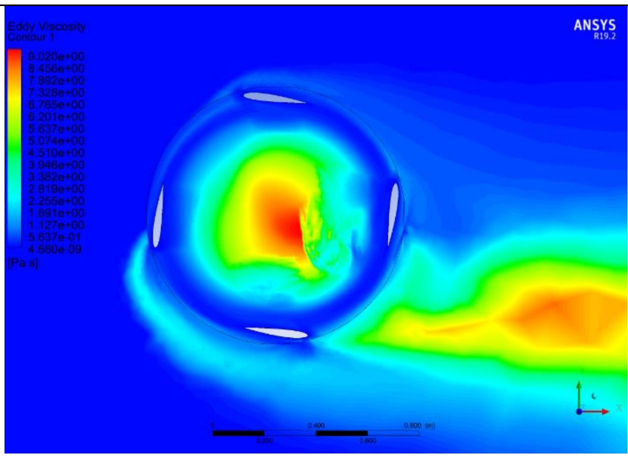	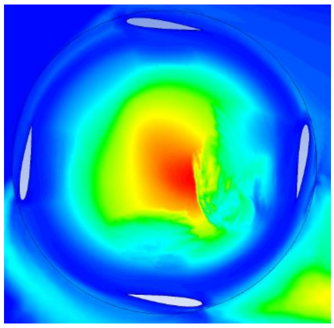
5 Blades	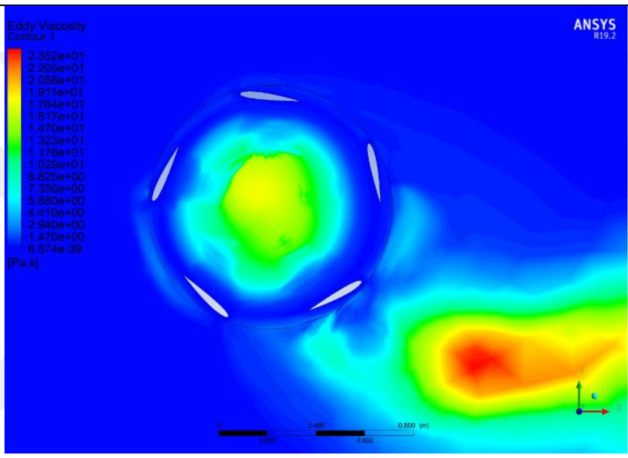	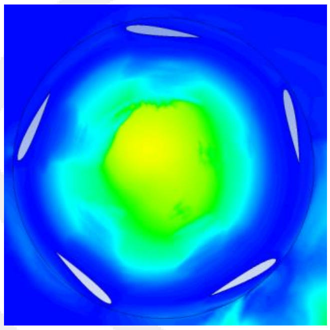
6 Blades	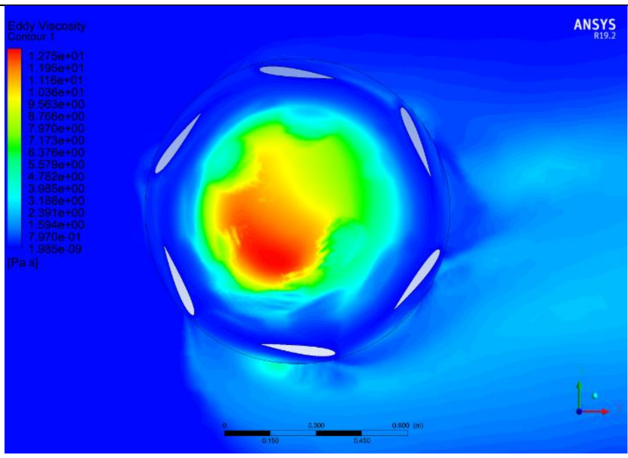	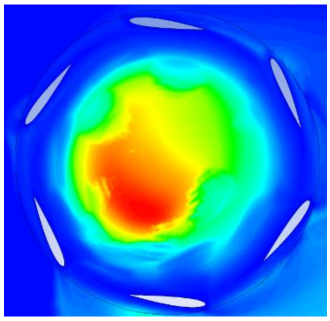

0.30 m Chord Length Eddy Viscosity Counter		
	All Domain	**Rotor Domain**
4 Blades	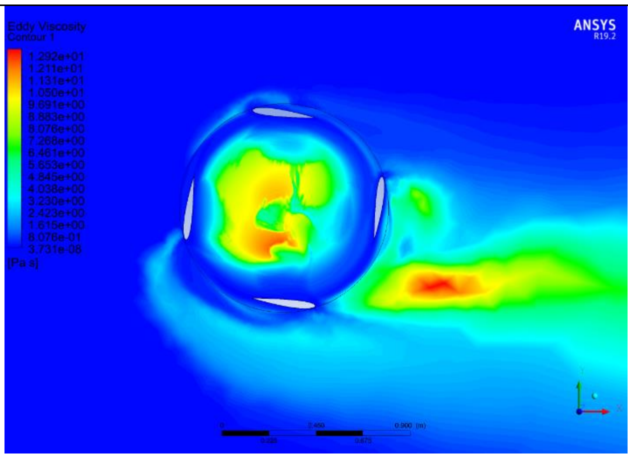	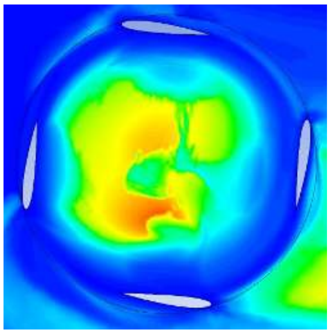
5 Blades	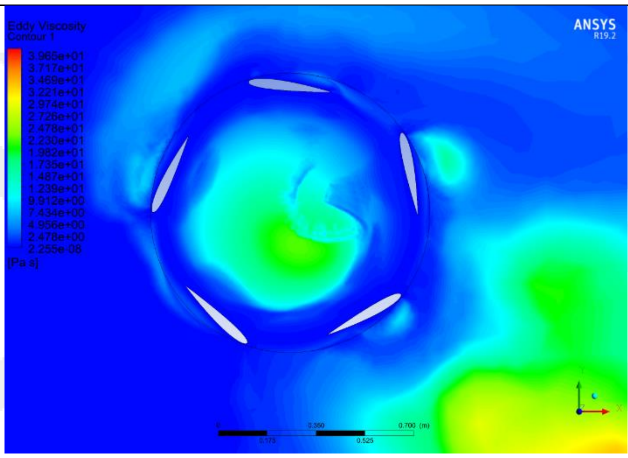	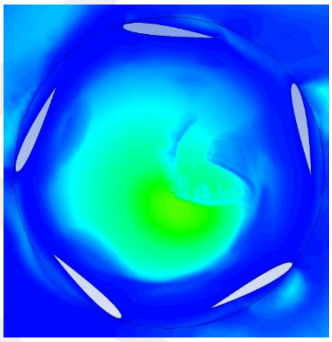
6 Blades	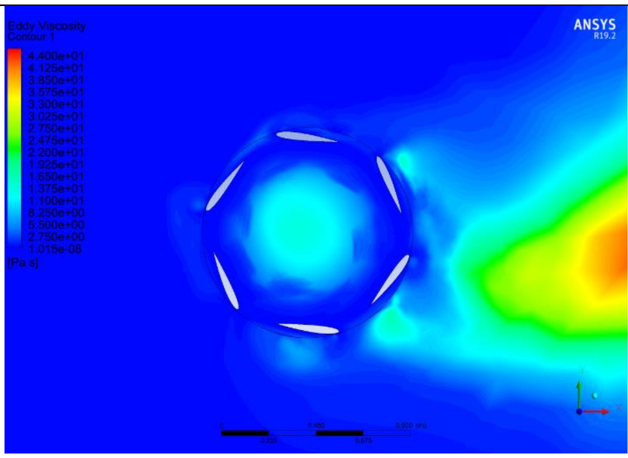	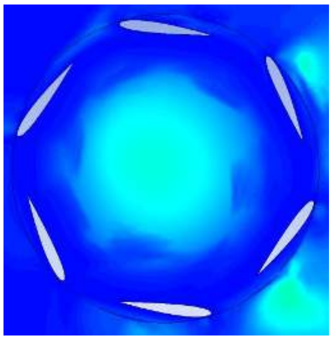

CHAPTER IX
TWIST ANGLE SELECTION

9.1 Selection of Twist Angle

In Chapter 7, the selection of hydrofoil types and parameters such as attack angles were employed to determine the optimal hydrofoil and attack angle. In Chapter 8, with the identified hydrofoil type and attack angle, various hydrofoil numbers and chord lengths were specified, and analyses were conducted. As a result of these analyses, a final model emerged, consisting of 4 hydrofoils with a NACA 1412 hydrofoil profile, a 7-degree attack angle, and a 25 cm chord length. In this chapter, twist angle analyses, an important parameter in axial turbines, will be performed. Turbines with twist angles of 0 degrees, 10 degrees, 20 degrees, and 30 degrees will be modeled, and through three-dimensional CFD analyses, the turbine with the optimal twist angle will be determined.

9.2 Pre-processing

9.2.1 Geometry

Based on the results obtained from 2-dimensional analyses, a turbine with 4 blades, a 7-degree attack angle, and a 25 cm chord length, using the NACA1412 hydrofoil profile, was designed with a diameter of 1 meter. For the twist angle parameter in axial turbines, four different rotation angles were specified: 0, 10, 20, and 30 degrees. As the rotation angles increase, the useful length of the hydrofoils decreases to prevent angular distortion of the existing geometry.

The geometric modeling process began with 2-dimensional drawing as a rough draft. Three-dimensional drawings were then modeled in AutoCAD and SolidWorks.

9.2.1.1 AutoCAD

The AutoCAD outputs are detailed in Figure 9.1 with dimensions.

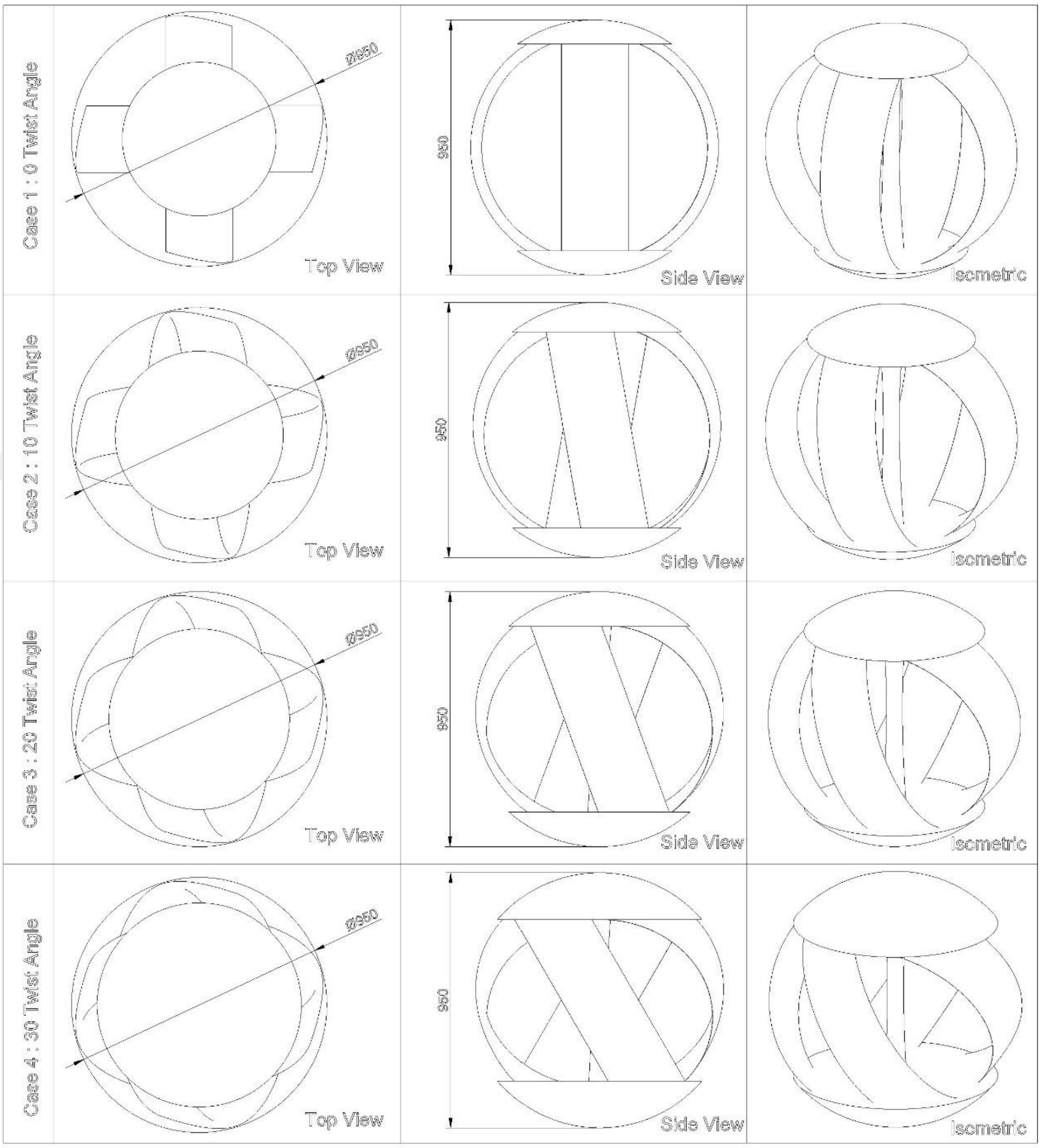

Figure 9.1 AutoCAD Geometries of Spherical Turbine

9.2.1.2 SolidWorks modelling

SolidWorks is a 3D computer-aided design (CAD) and computer-aided engineering (CAE) software. To use the Ansys Fluent plugin, models need to be created in SolidWorks. SolidWorks solid models provide better results in terms of curvature features. As indicated in the visuals, a visual representation is available for each model with twist angles of 0, 10, 20, and 30 degrees. For Ansys analyses, two different models were created in SolidWorks, consisting of an external domain and an internal domain. The models were named 'Rotor' for the rotating part of the turbine and 'Ex-Domain' for the stationary part. Separate modeling of the rotating part of the turbine is important for steady-state analyses.

Twist Angle	**Visual 1**	**Visual 2**
0	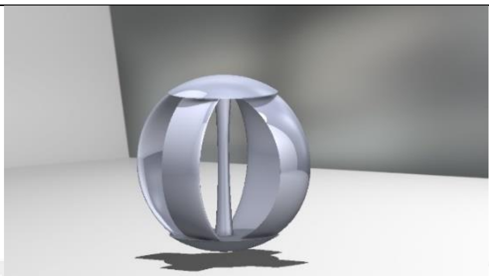	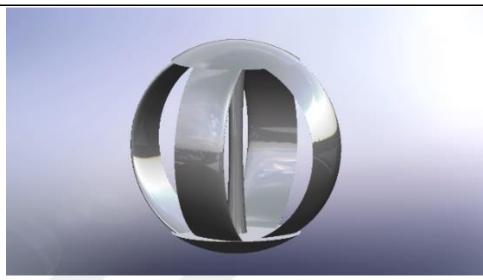
10	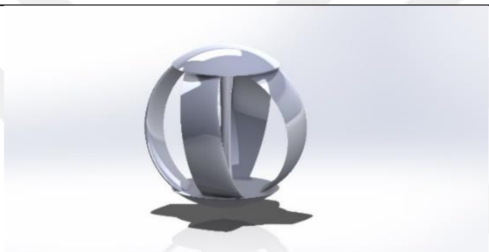	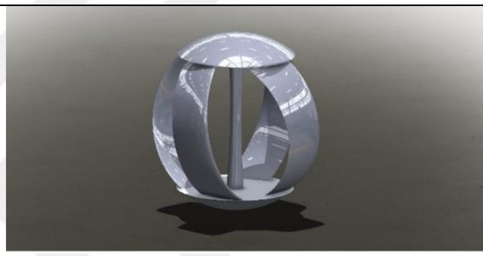
20	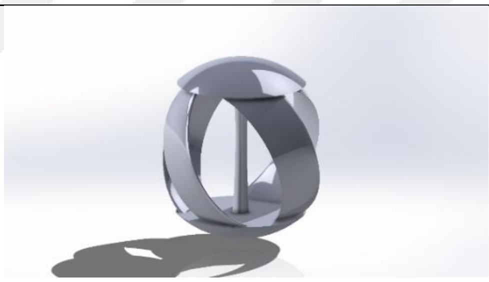	
30	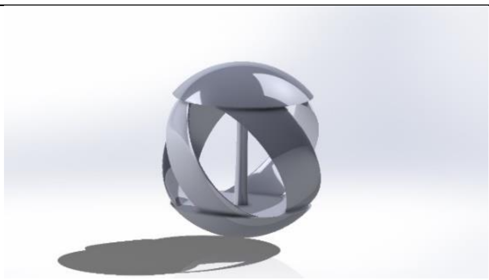	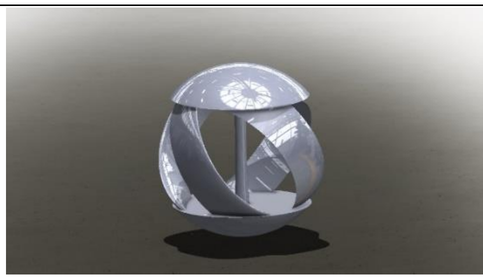

Figure 9.2 SolidWorks Geometries of Spherical Turbine

9.2.2 Meshing

The importance and necessity of mesh quality have been explained in the previous chapters. When examining the mesh numbers created in geometries prepared prior to 3D analyses, it is demonstrated that the mesh quality is good when considering the qualities of "Element quality," "orthogonal quality," and "skewness quality.

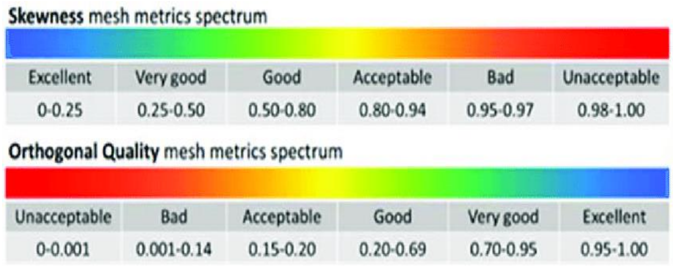

Skewness mesh metrics spectrum

Excellent	Very good	Good	Acceptable	Bad	Unacceptable
0-0.25	0.25-0.50	0.50-0.80	0.80-0.94	0.95-0.97	0.98-1.00

Orthogonal Quality mesh metrics spectrum

Unacceptable	Bad	Acceptable	Good	Very good	Excellent
0-0.001	0.001-0.14	0.15-0.20	0.20-0.69	0.70-0.95	0.95-1.00

Figure 9.3 Mesh Metrics Scales (Fatchurrohman and Chia, 2017)

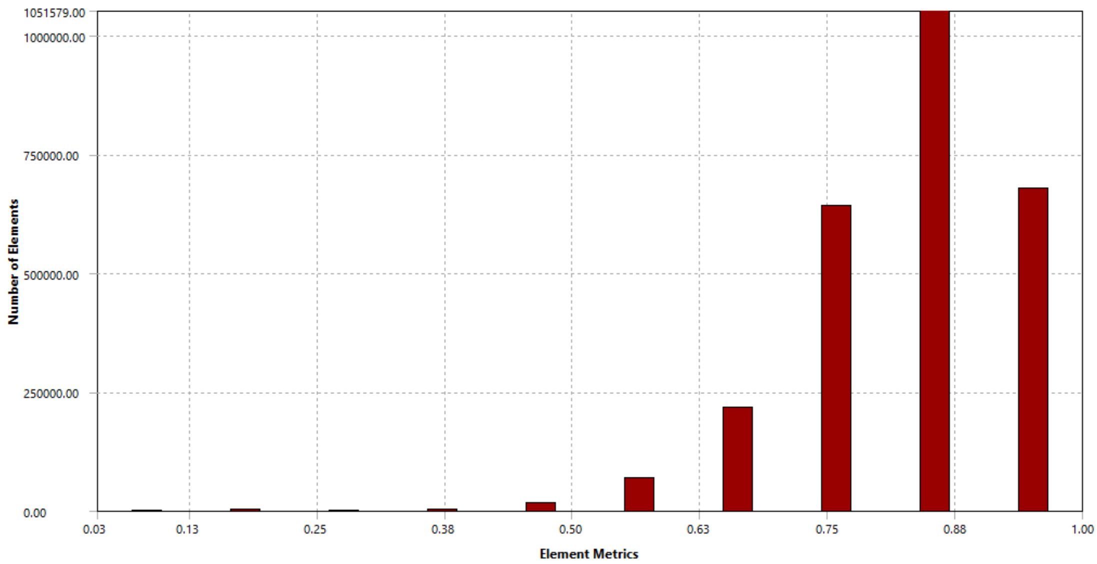

Figure 9.4 “Element Quality” Mesh metric of modelled geometries

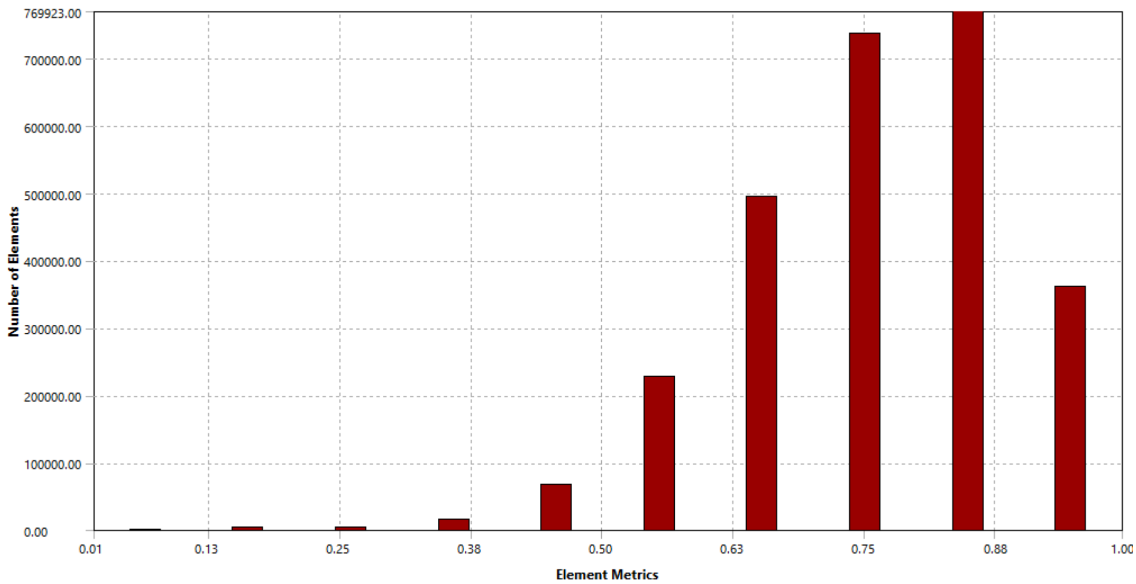

Figure 9.5 “Orthogonal Quality” Mesh metric of modelled geometries

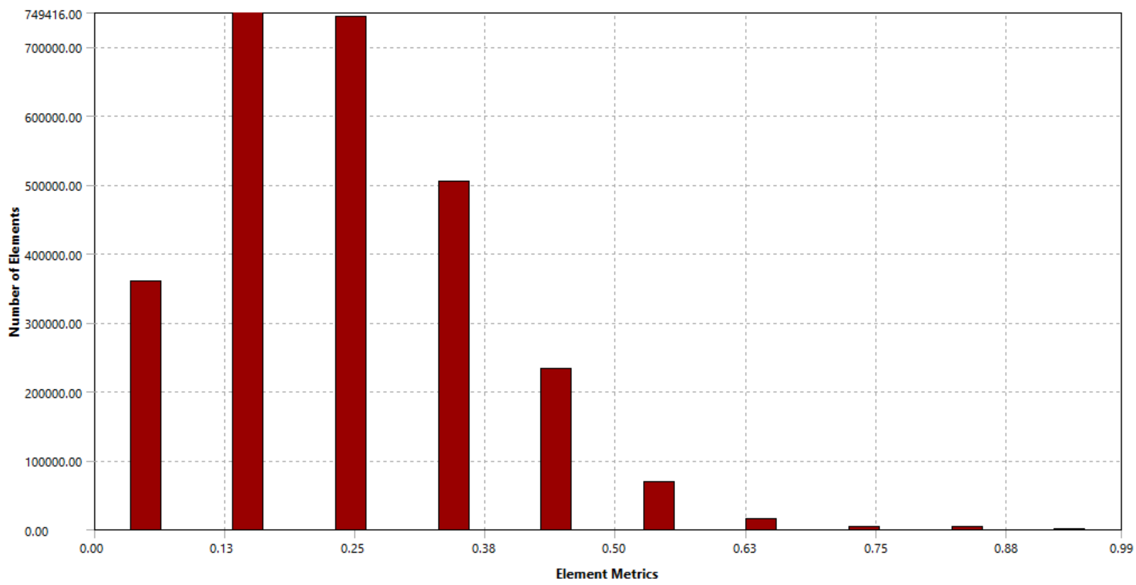

Figure 9.6 “Skewness” Mesh metric of modelled geometries

As seen in the visuals, mesh refinements are created much more densely in the area where the effects of the fluid are to be examined.

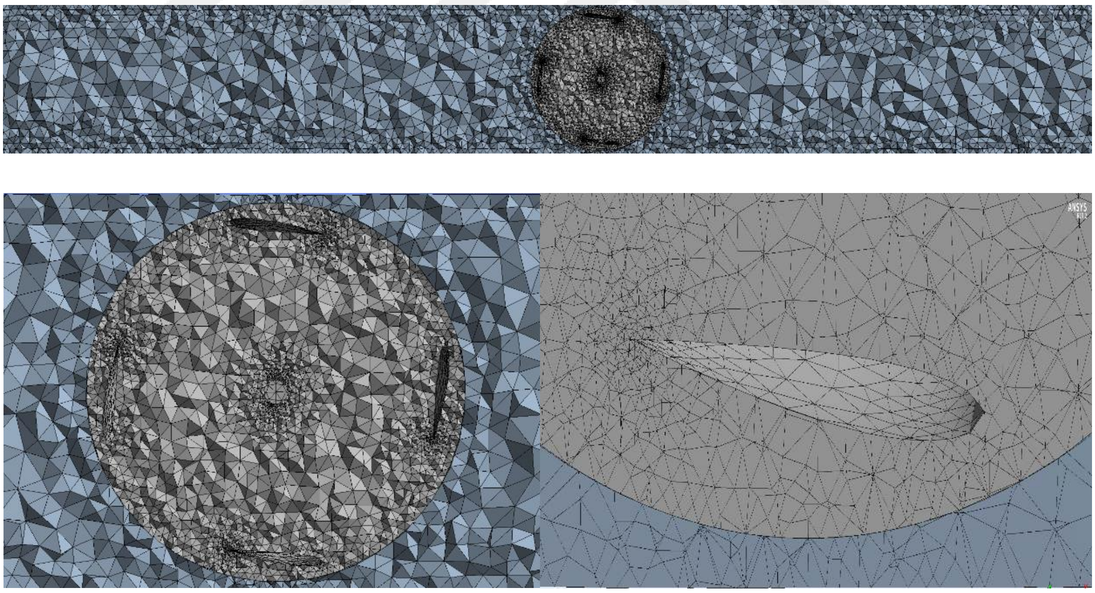

Figure 9.7 General view of meshes of models

9.2.3 Analysis Setup

The Ansys analysis setup section specifies the analysis parameters and settings. In the analysis settings, it should be determined which turbulence model the analysis will be conducted on, and the turbulence models are detailed in Chapter 6. The sst-e model has been utilized as the turbulence model. The convergence of the iteration count has been taken into account, ensuring the results converge.

9.3 Post-processing

9.3.1 Results

When examining the table supported by graphics, it is observed that the turbine with a 0-degree twist angle reaches maximum efficiency at a TSR (Tip Speed Ratio) value of 11.25. When examining the model with a 0-degree twist angle, the velocity vectors appear as shown in Figure 9.8. The velocity vector formed at the bottom of the model can be expressed as the composition of the turbine's rotational speed and the incoming fluid velocity.

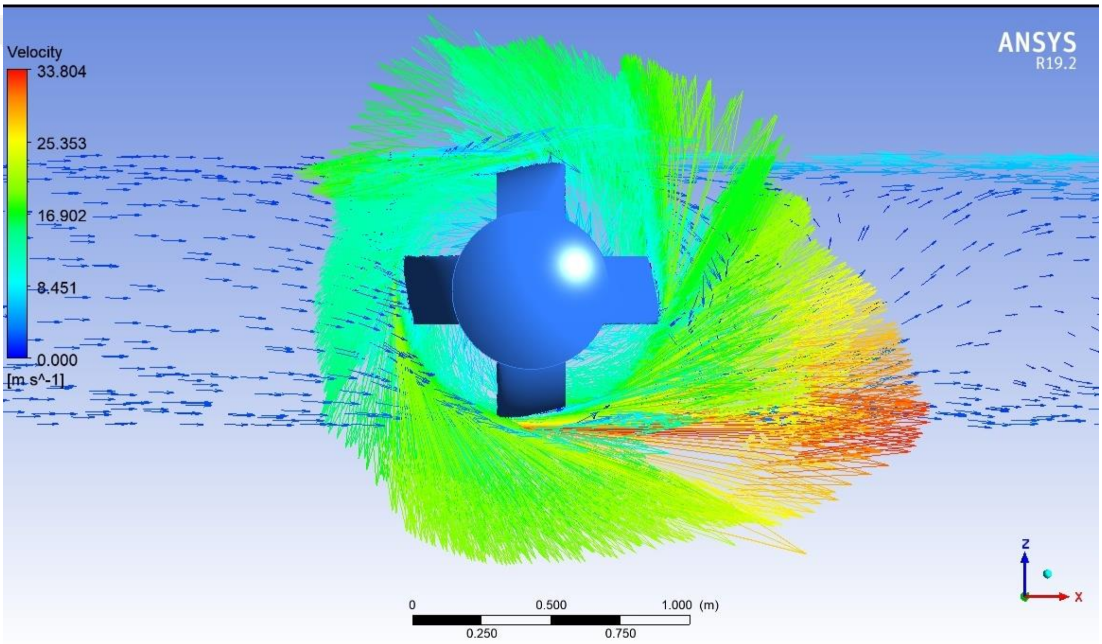

Figure 9.8 Velocity Arrow for 0-degree modelled geometry

The velocity vectors generated in the 10-degree model are illustrated in Figure 9.9. Observing the blade positions of the turbine, it can be noted that the velocity vectors are distributed, and there is no excessive increase in velocity at any specific location.

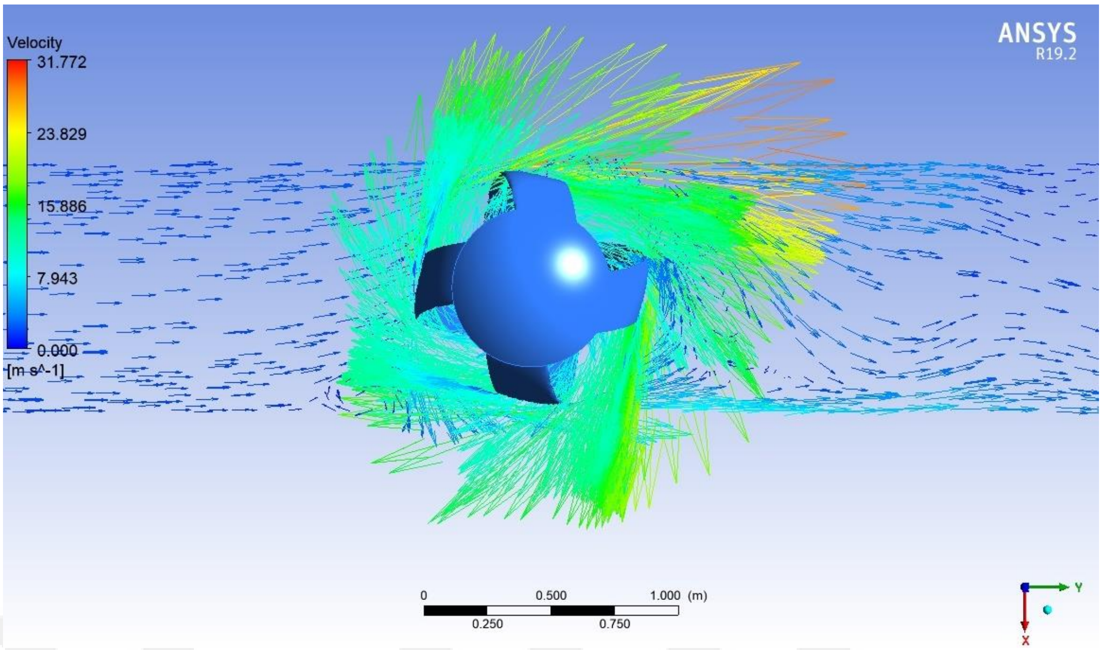

Figure 9.9 Velocity Arrow for 10-degree modelled geometry

In Figure 9.10, the velocity vectors in the model with a 20-degree twist angle exhibit a distribution similar to Figure 9.8. Upon closer inspection, it can be observed that there is not as focused a velocity as in the model with a 0-degree twist angle.

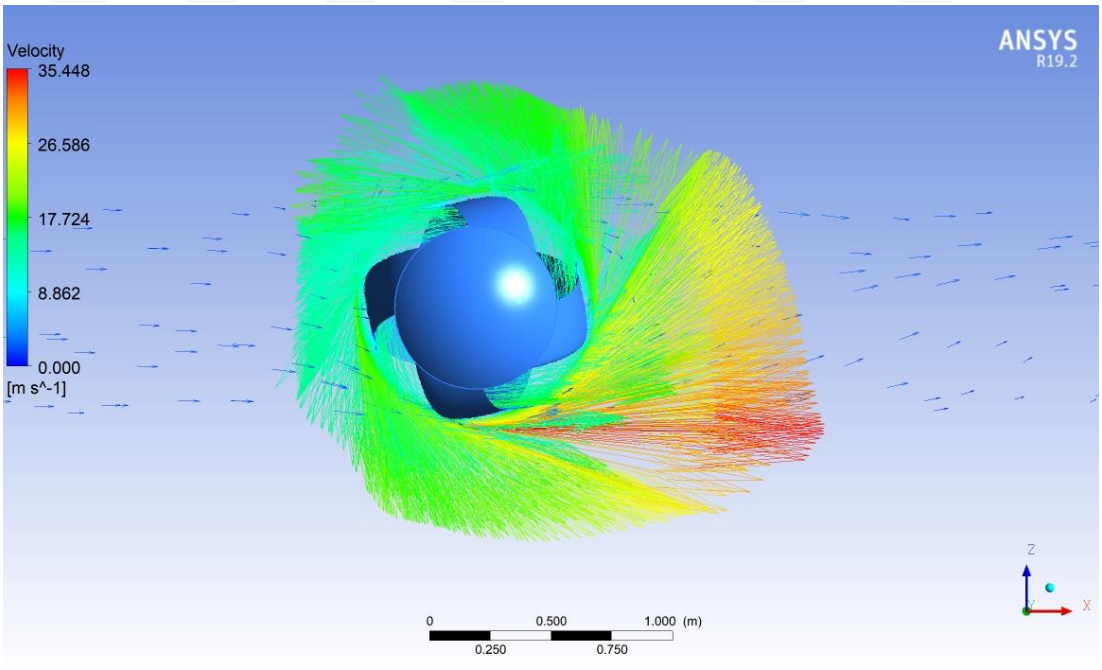

Figure 9.10 Velocity Arrow for 20-degree modelled geometry

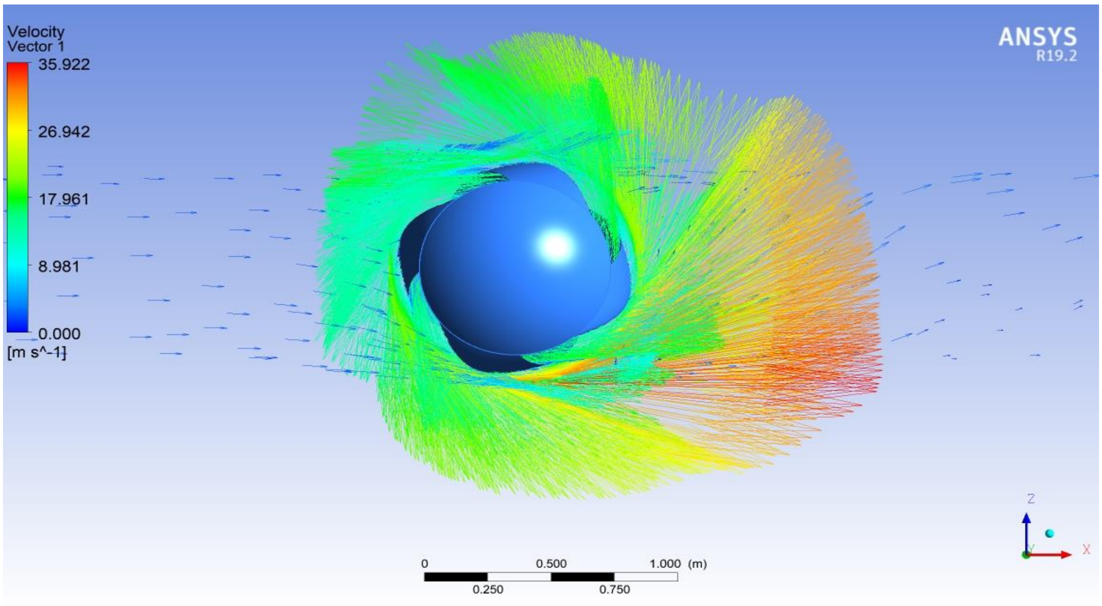

Figure 9.11 Velocity Arrow for 30-degree modelled geometry

Table 9.1 TSR vs Power Coefficient Table For 0°,10°,20°,30°

TSR	**Cp for Twist Angle=0°**	**Cp for Twist Angle=10°**	**Cp for Twist Angle=20°**	**Cp for Twist Angle=30°**
0	0.000	0.000	0.000	0.0000
1.25	0.021	0.014	0.017	0.0077
2.5	0.027	0.015	0.015	0.0147
3.75	0.049	0.026	0.024	0.0387
5	0.062	0.047	0.039	0.0481
6.25	0.073	0.072	0.046	0.0575
7.5	0.077	0.078	0.062	0.0606
8.75	0.089	0.069	0.057	0.0570
10	0.098	0.066	0.052	0.0570
11.25	**0.099**	0.062	0.050	0.0504
12.5	0.085	0.060	0.047	0.0484
13.75	0.079	0.056	0.048	0.0462
15	0.070	0.053	0.048	0.0446
16.25	0.047	0.050	0.048	0.0424
17.5	0.051	0.044	0.048	0.0419
18.75	0.053	0.036	0.047	0.0426
20	0.072	0.035	0.045	0.0423

In Figure 9.12, a comparison of power coefficients for analysis at 0, 10, 20, and 30-degree twist angles has been conducted. The 0-degree angle, diverging positively, produced a higher power coefficient at the same TSR (Tip Speed Ratio) values.

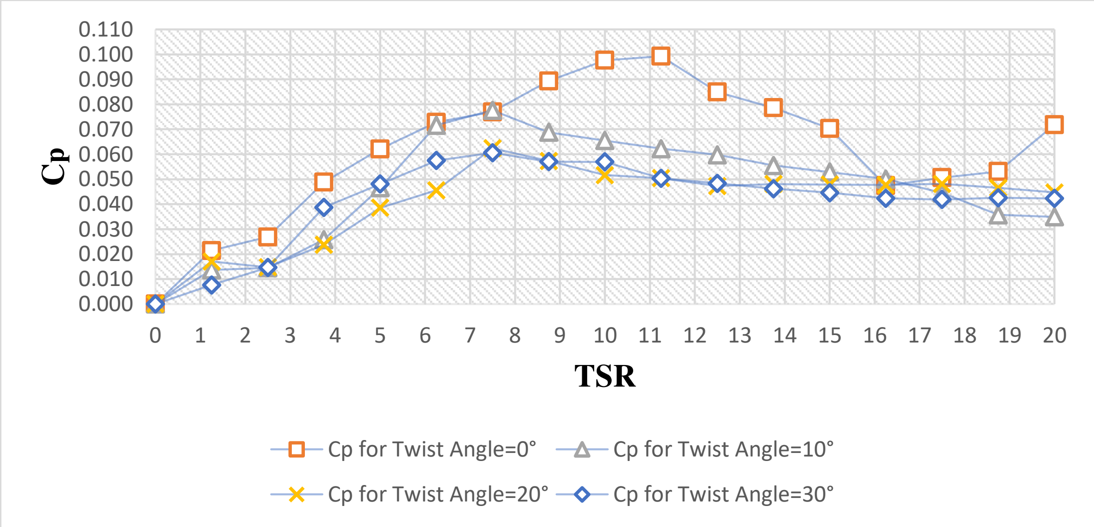

Figure 9.12 Cp vs. TSR graph for different twist angle

The results indicate that the power coefficient decreases in the area where the twist angle increases. This is because, as the twist angle increases to preserve the geometry, the useful length of the hydrofoil decreases. This results in a reduction in the drag/lift effects on the hydrofoil and, consequently, a decrease in the power coefficient. When evaluating the power coefficient as the twist angle increases, hydrofoil sections need to be examined in a three-dimensional manner, with hydrofoil lengths remaining the same as a whole. This implies that the attack angles should not be used as a parameter.

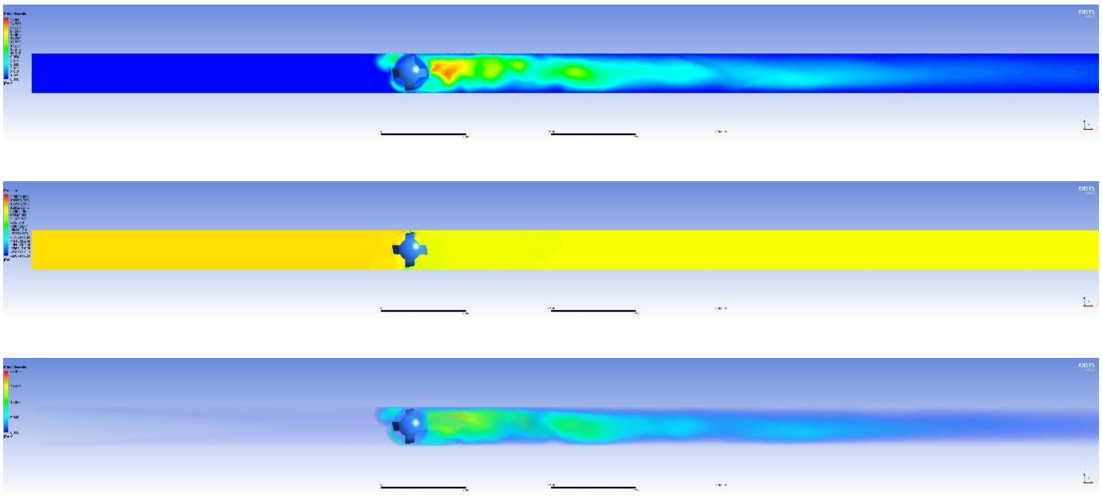

Figure 9.13 Velocity, Pressure and Eddy viscosity output for Optimized Turbine

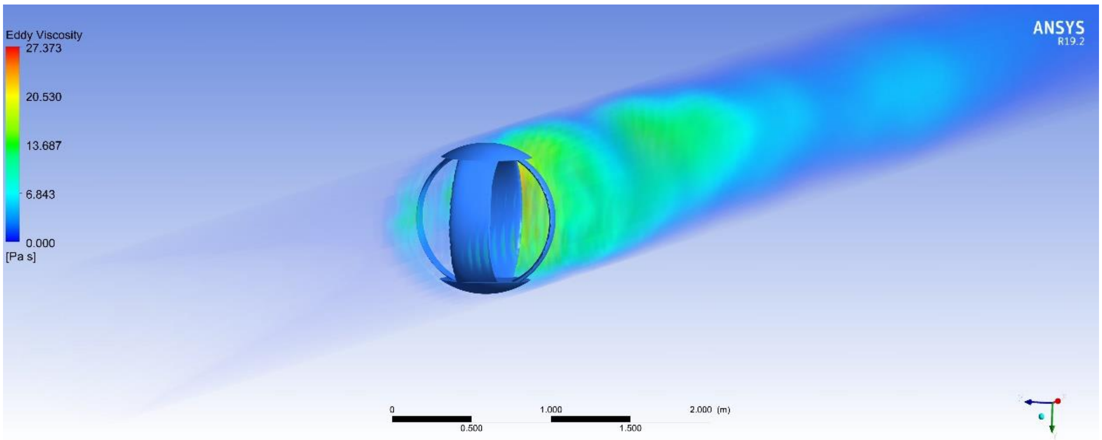

Figure 9.14 3D Eddy viscosity for optimized turbine

In Figure 9.15, when pressure changes are examined, it is observed that the pressure distribution on the hydrofoil is higher at surface points, as predicted. The sudden change in pressure can be explained by the decrease in the gap between the pipe and the hydrofoil.

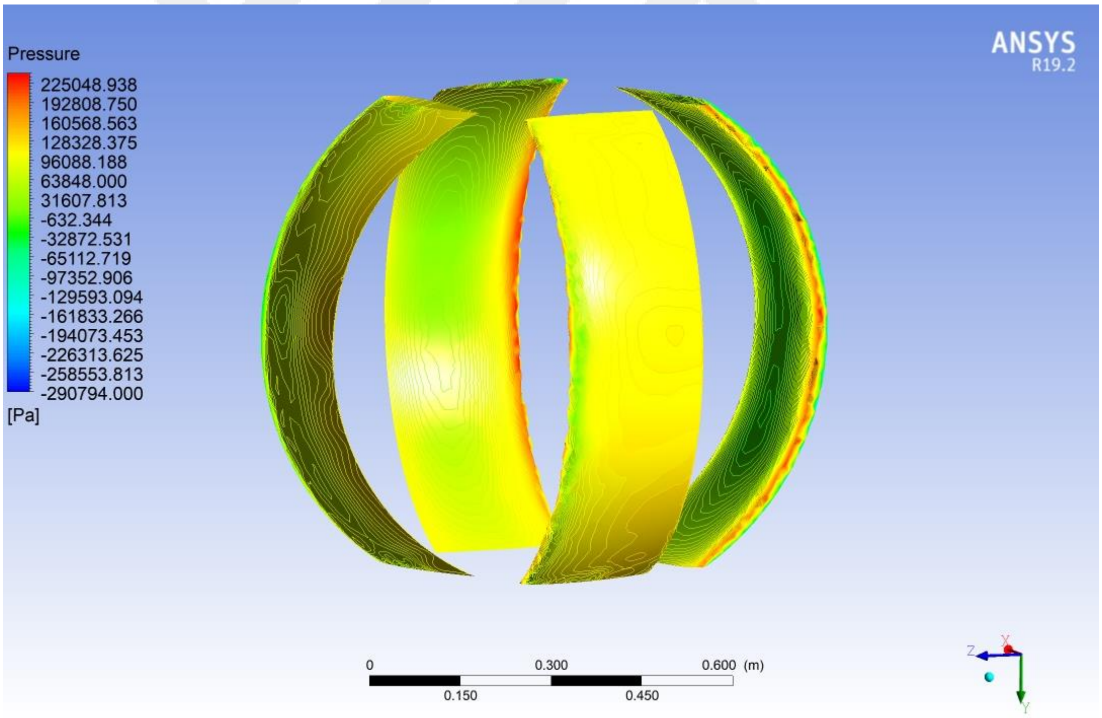

Figure 9.15 Pressure distribution on Turbine Blades

9.3.1.1 0° Twist Angle - Counter Outputs

0 Twist Angle			
	Velocity	**Pressure**	**Eddy Viscosity**
0 Rad/s	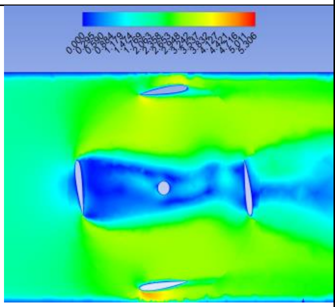	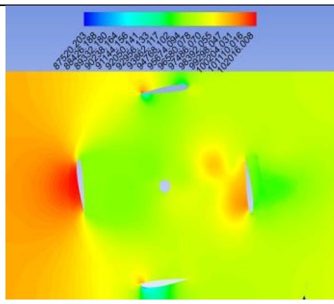	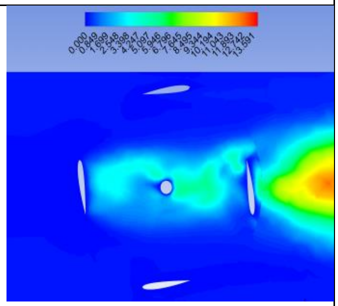
20 Rad/s	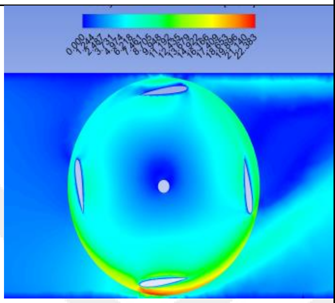	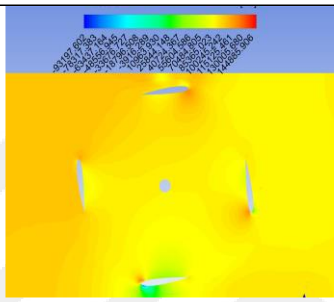	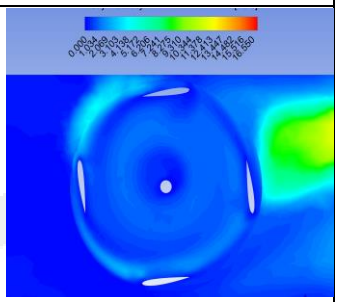
40 Rad/s	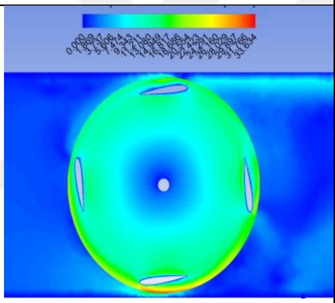	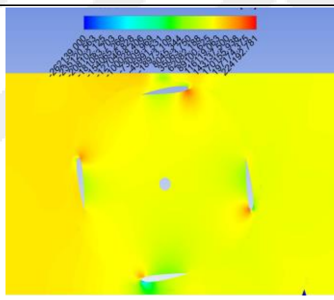	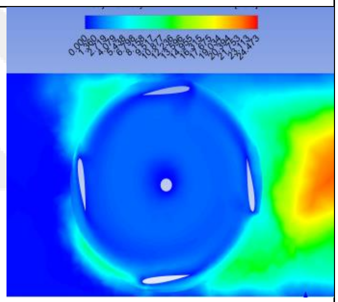
60 Rad/s	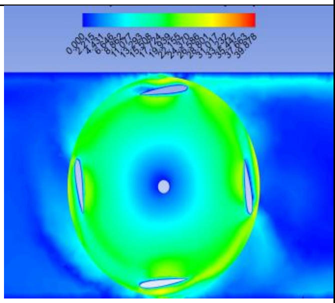	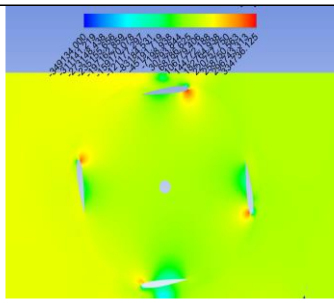	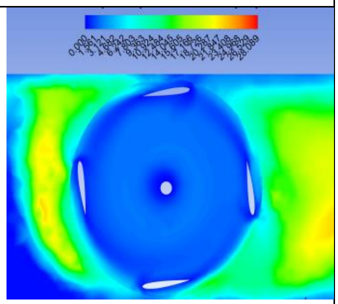
80 Rad/s	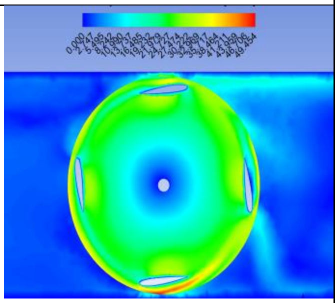	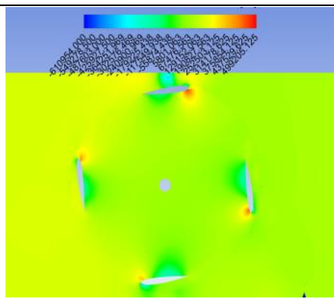	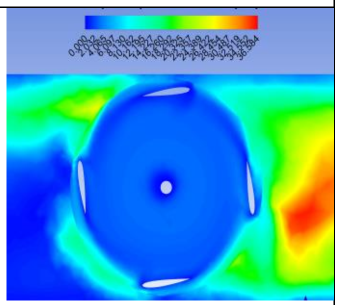

9.3.1.2 10° Twist Angle - Counter Outputs

10 Twist Angle			
	Velocity	**Pressure**	**Eddy Viscosity**
0 Rad/s	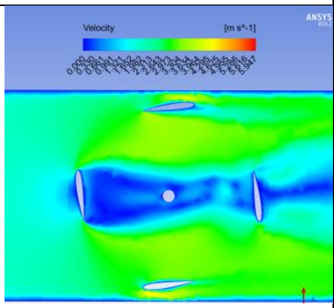	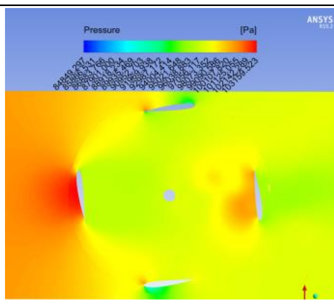	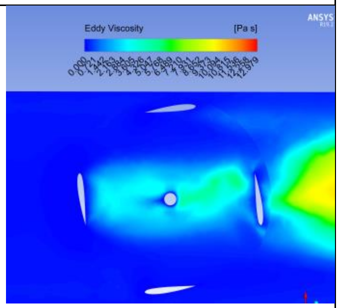
20 Rad/s	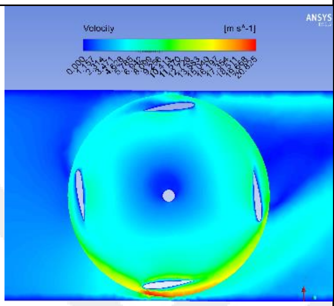	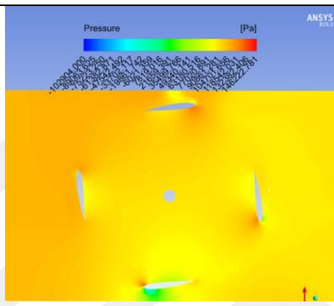	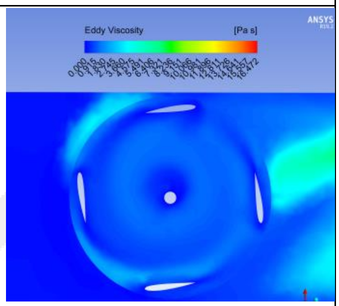
40 Rad/s	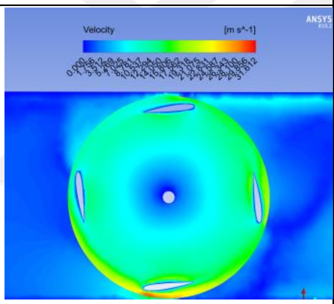	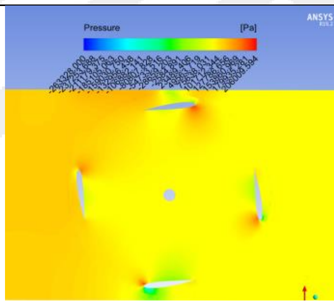	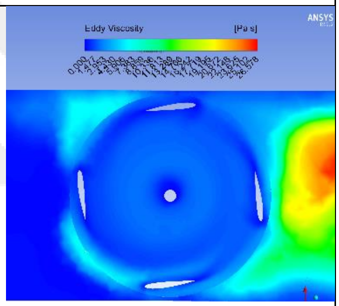
60 Rad/s	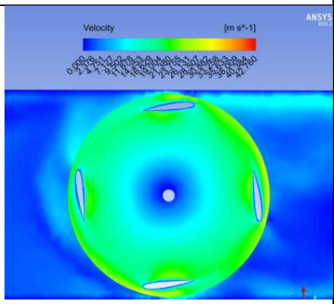	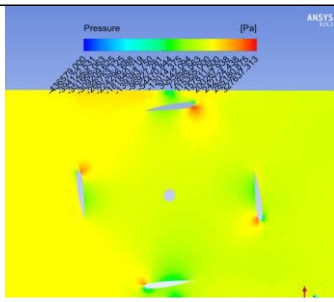	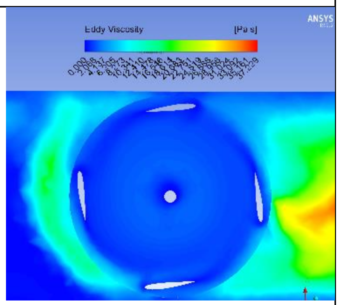
80 Rad/s	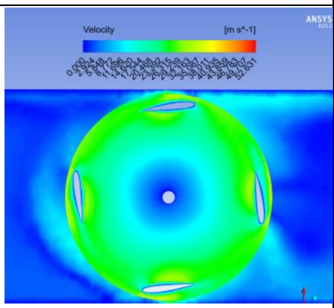	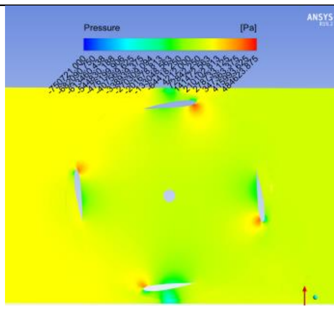	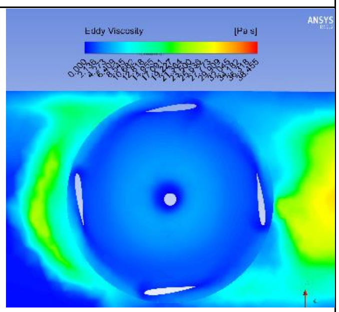

9.3.1.3 20° Twist Angle - Counter Outputs

20 Twist Angle			
	Velocity	**Pressure**	**Eddy Viscosity**
0 Rad/s	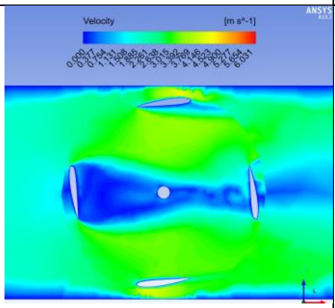	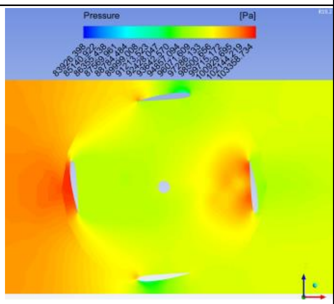	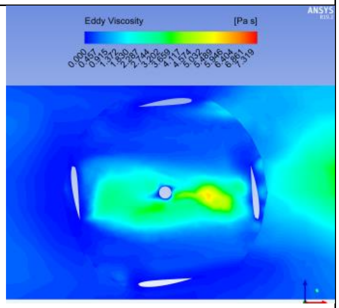
20 Rad/s	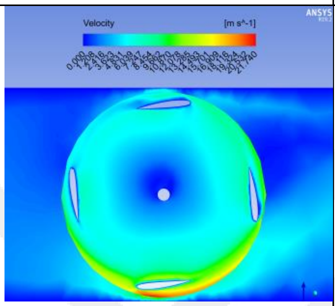	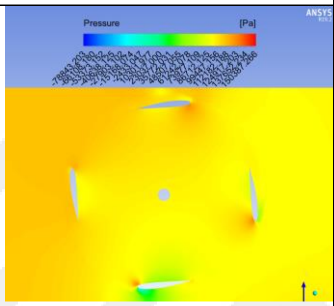	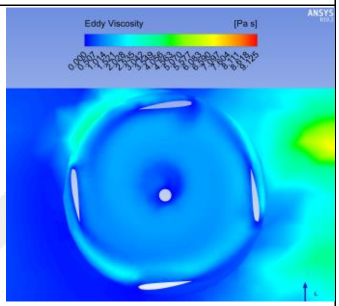
40 Rad/s	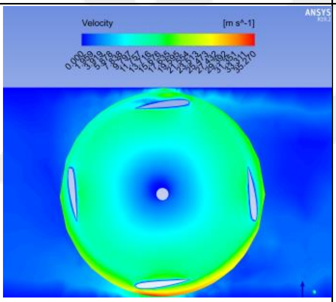	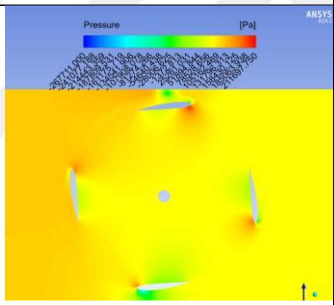	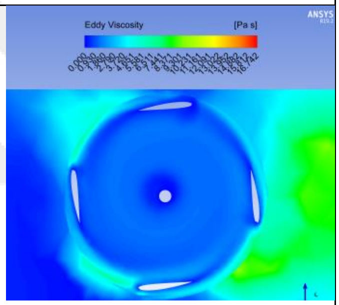
60 Rad/s	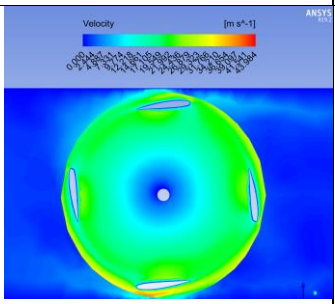	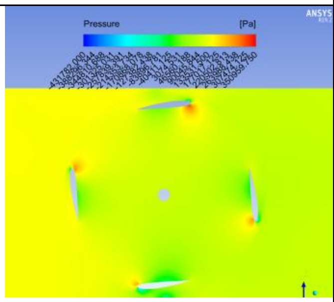	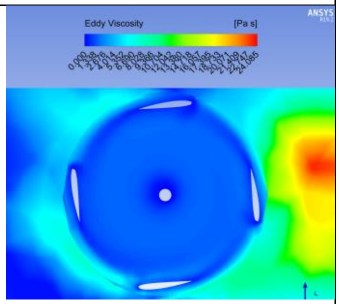
80 Rad/s	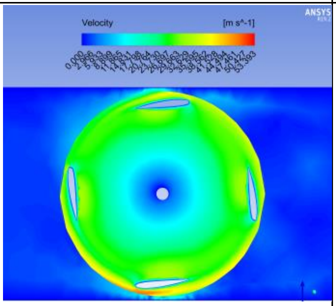	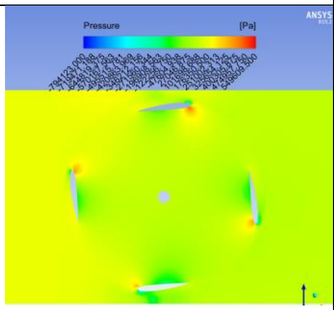	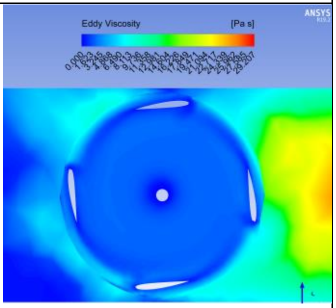

9.3.1.4 30° Twist Angle - Counter Outputs

30 Twist Angle			
	Velocity	**Pressure**	**Eddy Viscosity**
0 Rad/s	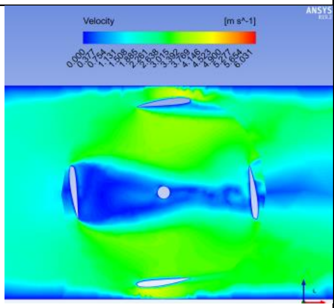	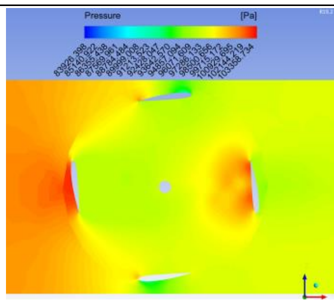	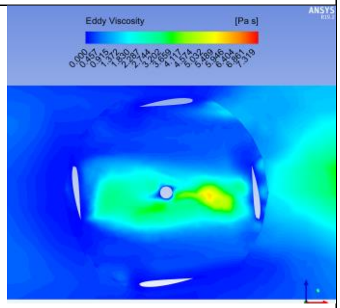
20 Rad/s	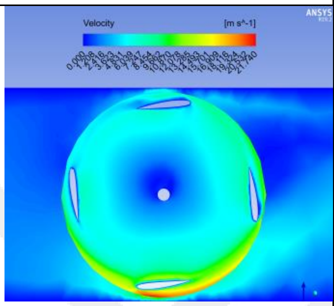	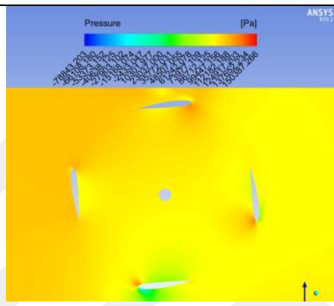	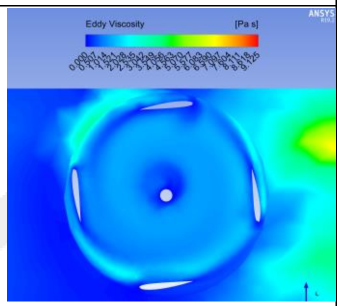
40 Rad/s	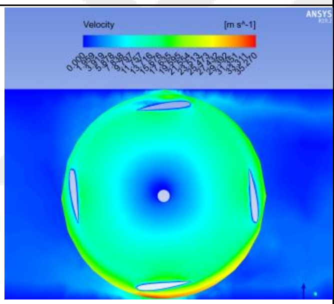	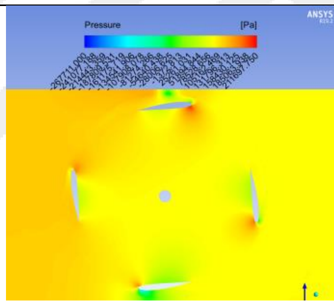	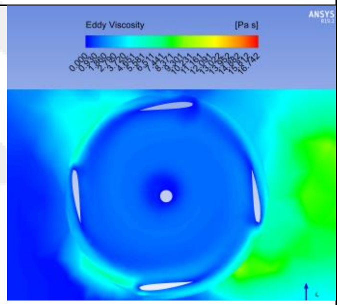
60 Rad/s	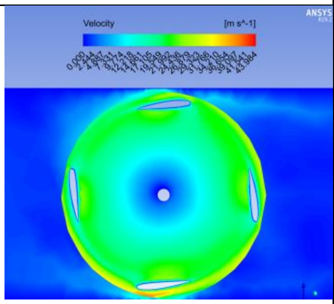	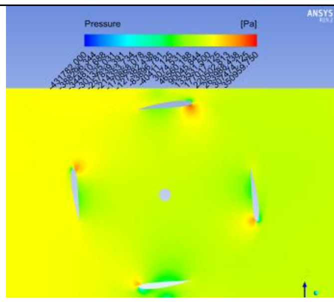	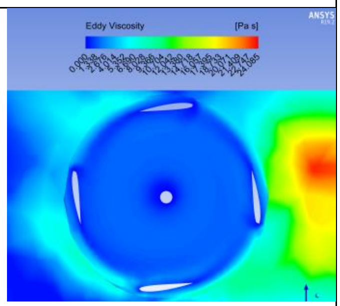
80 Rad/s	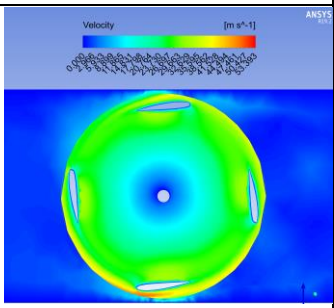	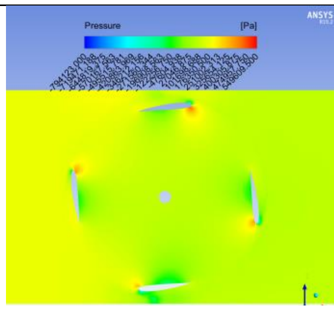	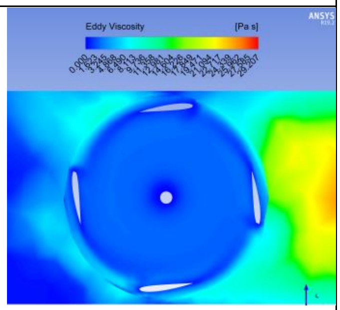

CHAPTER X
DISCUSSION &CONCLUSION

As the world population increases, energy demand increases rapidly and the need for clean, renewable energy sources also increases. Hydrokinetic energy is a relatively new energy source that encompasses many causes that have been addressed through research and development efforts. As a result of these reasons, research on hydrokinetic energy is gaining momentum and is of great importance. First of all, hydrokinetic energy has a significant potential for sustainable energy production. In addition, this technology promises to reduce the negative environmental effects of energy production based on fossil fuels. Moreover, hydrokinetic turbines offer flexibility that traditional hydroelectric power plants cannot provide. While traditional hydroelectric projects can damage ecosystems by creating reservoirs, hydrokinetic turbines minimize environmental impacts by using water flow. They can produce energy directly from water flows such as ocean currents, rivers, and tidal energy without the need for large dams or reservoirs. Hydrokinetic resources such as ocean currents and tidal energy have the potential to reduce carbon emissions while enabling environmentally friendly energy production.

Energy imports are becoming an economic problem in many countries. Hydrokinetic energy can also contribute to diversifying energy sources and reducing dependence on energy imports. Hydrokinetic energy research has the potential to help water-rich countries meet their future energy needs more sustainably and reliably by combining the goals of sustainable energy, environmental protection, and energy security. For this reason, it is thought that ongoing research on hydrokinetic energy will play an important role in the development of the energy sector.

There are many types of hydrokinetic turbines. Each type has the best efficiency in different operating conditions depending on where it is designed. At this point, design and optimization have a great place in hydrokinetic turbines. Although design and optimization methods vary, making simulations with CFD methods and redesigning according to output parameters are among the best options in terms of cost and time.

Among different types, Spherical hydrokinetic turbines have a different place in terms of usage area. The fact that spherical hydrokinetic turbines can be used instead of energy dispersions used in pressure pipes accelerates the research of this type of turbine. Since the designs of turbines must be made specifically for the operating conditions, these design conditions should be taken into consideration when designing spherical turbines.

The design parameters were determined to initiate the study. Questions were posed to obtain outputs for this work, such as:

- Why spherical Turbines?
- What hydrofoil type is suitable for a spherical turbine, and how can this be determined?
- At what angle of attack does the hydrofoil type provide the best performance?
- What should be the chord length of the hydrofoil to be used in the turbine?
- How many blades should be used in the turbine?
- Is a turbine shaft necessary, and what parameters should be considered?
- What should be the twist angle of the hydrofoils used in the spherical turbine?

While designing a spherical hydrokinetic turbine, as mentioned in the previous chapters, several crucial parameters need to be considered. During the geometric design phase, the most important aspect is geometric idealization. Idealizations can only be made by predicting how the turbine works against forces. The shaft, lower and upper covers, and blades of a spherical turbine constitute the main elements of the design. When the design transforms into a practical prototype, various factors may occur, such as weld marks, slight changes in angles, and the surface being rougher than anticipated. While these are foreseen during the design of a spherical turbine, neglecting them in the modeling and geometric design phase is necessary for time efficiency.

Turbines with designed geometric modeling are transferred to the Ansys Fluent module using the CFD method. This transfer stage involves various variables and challenges. It is necessary to transfer to this program in pre-defined file formats through the interface provided by Fluent. In the scope of this study, models created with the SolidWorks program worked smoothly with Ansys Fluent and did not pose any issues. The analyses consist of three main stages. In the first stage, 84 different analyses were performed with 6 different pre-defined hydrofoil geometries at 17 different angles of attack and various water speed conditions to select the hydrofoil type with the highest Cl/Cd value. The selected hydrofoil type is NACA1412 with a 7-degree angle of attack, obtained from the results of the first stage. In the second stage, a total of 24 different geometries were analyzed with 3 different hydrofoil blade counts (4, 5, 6) and 6 different chord lengths (0.10m, 0.15m, 0.20m, 0.25m, 0.30m). For each geometry, 15 different rotational speeds (0, 2, 4, 6, 8, 10, 12, 14, 16, 18, 20, 22, 24, 26, 28, 30) were determined, resulting in a total of 240 analyses. Number of hydrofoils in the turbine and chord length were determined to achieve the highest power coefficient at the same solidity value. The output of the second stage is a turbine consisting of 4 blades with a chord length of 0.25 m. In the third stage, the twist angle was determined. A total of 68 analyses were conducted with twist angles of 0°, 10°, 20°, and 30° at 17 different angular rotation speeds (0 rad/s, 5 rad/s, 10 rad/s, 15 rad/s, 20 rad/s, 25 rad/s, 30 rad/s, 35 rad/s, 40 rad/s, 45 rad/s, 50 rad/s, 55 rad/s, 60 rad/s, 65 rad/s, 70 rad/s, 75 rad/s, 80 rad/s). By examining the TSR & Cp graph, it was decided that the optimized turbine should have a twist angle of 0°. The final design is a spherical turbine with a diameter of 1 meter, consisting of 4 blades. The hydrofoil profile is NACA1412 with a 7-degree angle of attack, a chord length of 25 cm, and a twist angle of 0°. The shaft geometry is a cylindrical shaft thickening towards the center at the junction points.

In the studies conducted in the thesis, turbine parameters such as hydrofoil type, angle of attack, hydrofoil count, and hydrofoil length were investigated in a point-wise manner. These parameters are not continuous in the current study content. For example, in the analyses performed, angular rotation speeds could be within certain interval values rather than specific points. Such a study, conducted with an unlimited number of points, would allow performance outputs for each point. While peak points were determined between certain two values in the current analyses, in an analysis where continuous points are input, the peak point will yield a precise number. Beyond the parameters investigated in the thesis, research can be conducted on power coefficients depending on the diameter and radius in spherical turbines. Analyzing the power coefficient of the turbine designed with a diameter of 1 meter, in dimensions requiring less material and thus being more economical, could be attempted. This comparison of size/power coefficient could aim to achieve the most economical section with the highest power coefficient. The current turbine design considers the angle of attack as a parameter. The fact that the angle of attack is a parameter leads to a decrease in the useful hydrofoil length as the twist angle increases. If the angle of attack is not a parameter, and thus, twist angles can be tested without distorting the geometry with a 0° angle of attack, it could be explored. The current turbine design is intended to be integrated into pressurized and closed-system pipes. In today's conditions, it would be beneficial to look at and examine the open-channel performance of the same turbine. Technically, the analyses conducted are computationally intensive. At this point, in the design phase, considering mesh density and convergence conditions, a mesh metric scale between "Very Poor - Poor - Medium - Good - Very Good" levels in 2D analyses and within the "Good - Very Good" scale in 3D analyses was used for time economy. The current analyses were performed in a steady-state condition. Conducting transient analyses on workstations with high computing capacity and performing the time interval factor at 1/10000th of the desired simulation time in transient analyses will provide a good perspective for more detailed examination of the results.

REFERENCES

Akwa, J. V., Vielmo, H. A., & Petry, A. P. (2012). A review on the performance of Savonius wind turbines. *Renewable and Sustainable Energy Reviews*, *16*(5), 3054–3064. https://doi.org/10.1016/J.RSER.2012.02.056

Bachant, P., & Wosnik, M. (2015). Performance measurements of cylindrical- and spherical-helical cross-flow marine hydrokinetic turbines, with estimates of exergy efficiency. *Renewable Energy*, *74*, 318–325. https://doi.org/10.1016/J.RENENE.2014.07.049

Batten, W. M. J., Bahaj, A. S., Molland, A. F., & Chaplin, J. R. (2006). Hydrodynamics of marine current turbines. *Renewable Energy*, *31*(2), 249–256. https://doi.org/10.1016/J.RENENE.2005.08.020

Batten, W. M. J., Bahaj, A. S., Molland, A. F., & Chaplin, J. R. (2007). Experimentally validated numerical method for the hydrodynamic design of horizontal axis tidal turbines. *Ocean Engineering*, *34*(7), 1013–1020. https://doi.org/10.1016/J.OCEANENG.2006.04.008

Beck, M. W., Claassen, A. H., & Hundt, P. J. (2012). Environmental and livelihood impacts of dams: common lessons across development gradients that challenge sustainability. *International Journal of River Basin Management*, *10*(1), 73–92. https://doi.org/10.1080/15715124.2012.656133

Berkün, M., Aras, E., & Koç, T. (2008). Barajların ve hidroelektrik santrallerin nehir ekolojisi üzerinde oluşturduğu etkiler. Türkiye Mühendislik Haberleri, 452(6), 41-48.

Bilgili, M., Bilirgen, H., Ozbek, A., Ekinci, F., & Demirdelen, T. (2018). The role of hydropower installations for sustainable energy development in Turkey and the world. *Renewable Energy*, *126*, 755–764. https://doi.org/10.1016/J.RENENE.2018.03.089

Bryden, I. G., Naik, S., Fraenkel, P., & Bullen, C. R. (1998). Matching tidal current plants to local flow conditions. *Energy*, *23*(9), 699–709. https://doi.org/10.1016/S0360-5442(98)00021-8

Cai, S. (2015). *Algorithmic Improvements to Sweeping and Multi-Sweeping Volume Mesh Generation*.

Capik, M., Osman Ylmaz, A., & Cavusoglu, I. (2012). Hydropower for sustainable energy development in Turkey: The small hydropower case of the Eastern Black Sea Region. *Renewable and Sustainable Energy Reviews*, *16*(8), 6160–6172. https://doi.org/10.1016/J.RSER.2012.06.005

Çapik, M., Yilmaz, A. O., & Çavuşoĝlu, I. (2012). Present situation and potential role of renewable energy in Turkey. *Renewable Energy*, *46*, 1–13. https://doi.org/10.1016/J.RENENE.2012.02.031

Carrigan, T. J., Dennis, B. H., Han, Z. X., & Wang, B. P. (2012). Aerodynamic Shape Optimization of a Vertical-Axis Wind Turbine Using Differential Evolution. *ISRN Renewable Energy*, *2012*, 1–16. https://doi.org/10.5402/2012/528418

Cengel, Y. A., & Boles, M. A. (2015). Gas-vapor mixtures and air-conditioning. In Thermodynamics and Engineering Approach (pp. 725-729). McGraw Hill New York, NY, USA.

Chattot, J.-J. (2014). Actuator Disk Theory—Steady and Unsteady Models. *Journal of Solar Energy Engineering*, *136*(3). https://doi.org/10.1115/1.4026947

Chen, J., Shi, H., Sivakumar, B., & Peart, M. R. (2016). Population, water, food, energy and dams. *Renewable and Sustainable Energy Reviews*, *56*, 18–28. https://doi.org/10.1016/J.RSER.2015.11.043

Chen, Z., Guerrero, J. M., & Blaabjerg, F. (2009). A Review of the State of the Art of Power Electronics for Wind Turbines. *IEEE Transactions on Power Electronics*, *24*(8), 1859–1875. https://doi.org/10.1109/TPEL.2009.2017082

Coelho, P. (2023). The Betz limit and the corresponding thermodynamic limit. *Wind Engineering*, *47*(2), 491–496. https://doi.org/10.1177/0309524X221130109

Courant, R. (1943). Variational methods for the solution of problems of equilibrium and vibrations. *Bulletin of the American Mathematical Society*, *49*(1), 1 – 23.

Demirbas, M. F., & Balat, M. (2006). Recent advances on the production and utilization trends of bio-fuels: A global perspective. *Energy Conversion and Management*, *47*(15–16), 2371–2381. https://doi.org/10.1016/j.enconman.2005.11.014

Dominy, R., Lunt, P., Bickerdyke, A., & Dominy, J. (2007). Self-starting capability of a Darrieus turbine. *Proceedings of the Institution of Mechanical Engineers, Part A: Journal of Power and Energy*, *221*(1), 111–120. https://doi.org/10.1243/09576509JPE340

Elghali, S. E. Ben, Benbouzid, M. E. H., & Charpentier, J. F. (2007). Marine Tidal Current Electric Power Generation Technology: State of the Art and Current Status. *2007 IEEE International Electric Machines & Drives Conference*, 1407–1412. https://doi.org/10.1109/IEMDC.2007.383635

Elimelech, Y., Arieli, R., & Iosilevskii, G. (2007). Flow over NACA-0009 and Eppler-61 Airfoils at Reynolds Numbers 5000 and 60,000. *AIAA Journal*, *45*(10), 2414–2421. https://doi.org/10.2514/1.22376

Elosegi, A., & Sabater, S. (2013). Effects of hydromorphological impacts on river ecosystem functioning: a review and suggestions for assessing ecological impacts. *Hydrobiologia*, *712*(1), 129–143. https://doi.org/10.1007/s10750-012-1226-6

Eriksson, M. H., Moroso, A., & Fiorentino, A. (2006, March). The vertical axis Kobold turbine in the Strait of Messina–a case study of a full scale marine current prototype. In World maritime technology conference, London.

Fatchurrohman, N., & Chia, S. T. (2017). Performance of hybrid nano-micro reinforced mg metal matrix composites brake calliper: simulation approach. *IOP Conference Series: Materials Science and Engineering*, *257*, 012060. https://doi.org/10.1088/1757-899X/257/1/012060

Fridleifsson, I. B. (2001). Geothermal energy for the benefit of the people. *Renewable and Sustainable Energy Reviews*, *5*(3), 299–312. https://doi.org/10.1016/S1364-0321(01)00002-8

Güney, M. S., & Kaygusuz, K. (2010). Hydrokinetic energy conversion systems: A technology status review. *Renewable and Sustainable Energy Reviews*, *14*(9), 2996–3004. https://doi.org/10.1016/j.rser.2010.06.016

Jayaram, V., & Bavanish, B. (2021). A brief review on the Gorlov helical turbine and its possible impact on power generation in India. *Materials Today: Proceedings*, *37*, 3343–3351. https://doi.org/10.1016/j.matpr.2020.09.203

Jin, X., Zhao, G., Gao, K., & Ju, W. (2015). Darrieus vertical axis wind turbine: Basic research methods. *Renewable and Sustainable Energy Reviews*, *42*, 212–225. https://doi.org/10.1016/j.rser.2014.10.021

Kagazyo, T., Kaneko, K., Akai, M., & Hijikata, K. (1997). Methodology and evaluation of priorities for energy and environmental research projects. *Energy*, *22*(2–3), 121–129. https://doi.org/10.1016/S0360-5442(96)00132-6

Kaygusuz, K. (1999). The Viability of Thermal Energy Storage. *Energy Sources*, *21*(8), 745–755. https://doi.org/10.1080/00908319950014489

Kaygusuz, K. (2010). Sustainable energy, environmental and agricultural policies in Turkey. *Energy Conversion and Management*, *51*(5), 1075–1084. https://doi.org/10.1016/J.ENCONMAN.2009.12.012

Khan, M., Iqbal, M., & Quaicoe, J. (2006). A Technology Review and Simulation Based Performance Analysis of River Current Turbine Systems. *2006 Canadian Conference on Electrical and Computer Engineering*, 2288–2293. https://doi.org/10.1109/CCECE.2006.277821

Khan, M. J., Bhuyan, G., Iqbal, M. T., & Quaicoe, J. E. (2009). Hydrokinetic energy conversion systems and assessment of horizontal and vertical axis turbines for river and tidal applications: A technology status review. *Applied Energy*, *86*(10), 1823–1835. https://doi.org/10.1016/J.APENERGY.2009.02.017

Killingtveit, Å. (2019). Hydropower. *Managing Global Warming: An Interface of Technology and Human Issues*, 265–315. https://doi.org/10.1016/B978-0-12-814104-5.00008-9

Kim, L. S., Nakahashi, K., Jeong, H. K., & Ha, M. Y. (2007). High-density mesh flow computations by building-cube method. *Journal of Mechanical Science and Technology*, *21*(8), 1306–1319. https://doi.org/10.1007/BF03179047

Kumar, R., & Sarkar, S. (2023). Performance analysis of spherical-shaped Darrieus hydrokinetic turbine for an in-pipe hydropower system. *Energy Conversion and Management*, *294*, 117600. https://doi.org/10.1016/j.enconman.2023.117600

Lago, L. I., Ponta, F. L., & Chen, L. (2010). Advances and trends in hydrokinetic turbine systems. *Energy for Sustainable Development*, *14*(4), 287–296. https://doi.org/10.1016/j.esd.2010.09.004

Lee, A. K., Lewis, D. M., & Ashman, P. J. (2015). Microalgal cell disruption by hydrodynamic cavitation for the production of biofuels. *Journal of Applied Phycology*, *27*(5), 1881–1889. https://doi.org/10.1007/s10811-014-0483-3

Lissaman, P. B. S. (1983). Low-Reynolds-number airfoils. *Annual Review of Fluid Mechanics*, *15*(1), 223–239.

Mahmuddin, F. (2017). Rotor Blade Performance Analysis with Blade Element Momentum Theory. *Energy Procedia*, *105*, 1123–1129. https://doi.org/10.1016/j.egypro.2017.03.477

Manwell, J. F., McGowan, J. G., & Rogers, A. L. (2010). *Wind energy explained: theory, design and application*. John Wiley & Sons.

Marsh, G. (2004). Tidal turbines harness the power of the sea. *Reinforced Plastics*, *48*(6), 44–47. https://doi.org/10.1016/S0034-3617(04)00344-3

Menter, F. R. (2009). Review of the shear-stress transport turbulence model experience from an industrial perspective. *International Journal of Computational Fluid Dynamics*, *23*(4), 305–316. https://doi.org/10.1080/10618560902773387

Mertens, S., van Kuik, G., & van Bussel, G. (2003). Performance of an H-Darrieus in the Skewed Flow on a Roof1. *Journal of Solar Energy Engineering*, *125*(4), 433–440. https://doi.org/10.1115/1.1629309

Midilli, A., Dincer, I., & Ay, M. (2006). Green energy strategies for sustainable development. *Energy Policy*, *34*(18), 3623–3633. https://doi.org/10.1016/j.enpol.2005.08.003

Mohan Kumar, P., Sivalingam, K., Lim, T.-C., Ramakrishna, S., & Wei, H. (2019). Strategies for Enhancing the Low Wind Speed Performance of H-Darrieus Wind Turbine—Part 1. *Clean Technologies*, *1*(1), 185–204. https://doi.org/10.3390/cleantechnol1010013

Molland, A. F., & Turnock, S. R. (2022). Hydrofoils. In *Marine Rudders, Hydrofoils and Control Surfaces* (pp. 57–89). Elsevier. https://doi.org/10.1016/B978-0-12-824378-7.00005-6

Muratoglu, A., & Yuce, M. I. (2015). Performance analysis of hydrokinetic turbine blade sections. *Journal ISSN*, *2*, 1–10.

Myers, L., & Bahaj, A. S. (2006). Power output performance characteristics of a horizontal axis marine current turbine. *Renewable Energy*, *31*(2), 197–208. https://doi.org/10.1016/j.renene.2005.08.022

Nagano, Y., & Tagawa, M. (1990). An Improved k-ε Model for Boundary Layer Flows. *Journal of Fluids Engineering*, *112*(1), 33–39. https://doi.org/10.1115/1.2909365

Noyes, C., Qin, C., & Loth, E. (2018). Pre-aligned downwind rotor for a 13.2 MW wind turbine. *Renewable Energy*, *116*, 749–754. https://doi.org/10.1016/j.renene.2017.10.019

Ostos, I., Ruiz, I., Gajic, M., Gómez, W., Bonilla, A., & Collazos, C. (2019). A modified novel blade configuration proposal for a more efficient VAWT using CFD tools. *Energy Conversion and Management*, *180*, 733–746. https://doi.org/10.1016/j.enconman.2018.11.025

Panwar, N. L., Kaushik, S. C., & Kothari, S. (2011). Role of renewable energy sources in environmental protection: A review. *Renewable and Sustainable Energy Reviews*, *15*(3), 1513–1524. https://doi.org/10.1016/j.rser.2010.11.037

Pinto, M. L., Franzini, G. R., & Simos, A. N. (2020). A CFD analysis of NREL's 5MW wind turbine in full and model scales. *Journal of Ocean Engineering and Marine Energy*, *6*(2), 211–220. https://doi.org/10.1007/s40722-020-00162-y

Qazi, A., Hussain, F., Rahim, N. A., Hardaker, G., Alghazzawi, D., Shaban, K., & Haruna, K. (2019). Towards Sustainable Energy: A Systematic Review of Renewable Energy Sources, Technologies, and Public Opinions. *IEEE Access*, *7*, 63837–63851. https://doi.org/10.1109/ACCESS.2019.2906402

Quinn, R., Schepers, G., & Bulder, B. (2016). A Parametric Investigation Into the Effect of Low Induction Rotor (LIR) Wind Turbines on the Levelised Cost of

Electricity for a 1 GW Offshore Wind Farm in a North Sea Wind Climate. *Energy Procedia*, *94*, 164–172. https://doi.org/10.1016/j.egypro.2016.09.213

Raadal, H. L., Gagnon, L., Modahl, I. S., & Hanssen, O. J. (2011). Life cycle greenhouse gas (GHG) emissions from the generation of wind and hydro power. *Renewable and Sustainable Energy Reviews*, *15*(7), 3417–3422. https://doi.org/10.1016/j.rser.2011.05.001

RAHMAN, M. M. (2023). Capturing transition and non-transition flows with a new shear stress transport model. *Chinese Journal of Aeronautics*, *36*(3), 121–136. https://doi.org/10.1016/j.cja.2022.08.013

Roberts, A., Thomas, B., Sewell, P., Khan, Z., Balmain, S., & Gillman, J. (2016). Current tidal power technologies and their suitability for applications in coastal and marine areas. *Journal of Ocean Engineering and Marine Energy*, *2*(2), 227–245. https://doi.org/10.1007/s40722-016-0044-8

Saini, G., & Saini, R. P. (2019). A review on technology, configurations, and performance of cross-flow hydrokinetic turbines. *International Journal of Energy Research*, er.4625. https://doi.org/10.1002/er.4625

Schlager, N., & Weisblatt, J. (2006). *Alternative Energy-Volume 1*. Thomson Gale.

Selig, M. S., & Guglielmo, J. J. (1997). High-Lift Low Reynolds Number Airfoil Design. *Journal of Aircraft*, *34*(1), 72–79. https://doi.org/10.2514/2.2137

Shi, L., Zhu, J., Wang, L., Chu, S., Tang, F., Jiang, Y., Xu, T., & Yu, J. (2021). Analysis of Strength and Modal Characteristics of a Full Tubular Pump Impeller Based on Fluid-Structure Interaction. Research Square Platform LLC. https://doi.org/10.21203/rs.3.rs-627588/v1

Siciliano, G., Urban, F., Tan-Mullins, M., & Mohan, G. (2018). Large dams, energy justice and the divergence between international, national and local developmental needs and priorities in the global South. *Energy Research & Social Science*, *41*, 199–209. https://doi.org/10.1016/J.ERSS.2018.03.029

Silva, P. A. S. F., Shinomiya, L. D., de Oliveira, T. F., Vaz, J. R. P., Amarante Mesquita, A. L., & Brasil Junior, A. C. P. (2017). Analysis of cavitation for the optimized design of hydrokinetic turbines using BEM. *Applied Energy*, *185*, 1281–1291. https://doi.org/10.1016/j.apenergy.2016.02.098

Sobieczky, H., & Seebass, A. R. (1984). Supercritical Airfoil and Wing Design. *Annual Review of Fluid Mechanics*, *16*(1), 337–363. https://doi.org/10.1146/annurev.fl.16.010184.002005

Strang, G., & Fix, G. J. (1973). An analysis of the finite element method(Book- An analysis of the finite element method.). *Englewood Cliffs, N. J., Prentice-Hall, Inc., 1973. 318 P.*

Talukdar, P. K., Sardar, A., Kulkarni, V., & Saha, U. K. (2018). Parametric analysis of model Savonius hydrokinetic turbines through experimental and computational investigations. *Energy Conversion and Management*, *158*, 36–49. https://doi.org/10.1016/j.enconman.2017.12.011

Tucker, P. ., & Pan, Z. (2000). A Cartesian cut cell method for incompressible viscous flow. *Applied Mathematical Modelling*, *24*(8–9), 591–606. https://doi.org/10.1016/S0307-904X(00)00005-6

Twidell, J., & Weir, T. (2006). Renewable energy resources. by taylor and francis. *Newyork, USA*.

Wilcox, D. C., & others. (1998). *Turbulence modeling for CFD* (Vol. 2). DCW industries La Canada, CA.

Xu, C., & Khoo, B. C. (2022). Numerical investigation on the cloud cavitating flow over a Clark Y foil under free surface effect. *Ocean Engineering*, *266*, 112953. https://doi.org/10.1016/j.oceaneng.2022.112953

Yilanci, A., Dincer, I., & Ozturk, H. K. (2009). A review on solar-hydrogen/fuel cell hybrid energy systems for stationary applications. *Progress in Energy and Combustion Science*, *35*(3), 231–244. https://doi.org/10.1016/j.pecs.2008.07.004

Youssef, K. M., El Kholy, A. M., Hamed, A. M., Mahmoud, N. A., El Baz, A. M., & Mohamed, T. A. (2020). An innovative augmentation technique of savonius wind turbine performance. *Wind Engineering*, *44*(1), 93–112. https://doi.org/10.1177/0309524X19849860

Yuce, M. I., & Muratoglu, A. (2015). Hydrokinetic energy conversion systems: A technology status review. *Renewable and Sustainable Energy Reviews*, *43*, 72–

82. https://doi.org/10.1016/j.rser.2014.10.037

Zheng, X., Liu, C., Liu, F., & Yang, C.-I. (1998). Turbulent transition simulation using thek-ω model. *International Journal for Numerical Methods in Engineering*, *42*(5), 907–926. https://doi.org/10.1002/(SICI)1097-0207(19980715)42:5<907::AID-NME393>3.0.CO;2-T

Zhou, J., Erdem, E., Li, G., & Shi, J. (2010). Comprehensive evaluation of wind speed distribution models: A case study for North Dakota sites. *Energy Conversion and Management*, *51*(7), 1449–1458. https://doi.org/10.1016/j.enconman.2010.01.020

CURRICULUM VITAE

FETİHHAN UĞUR

EDUCATION

Master-graduate: Gaziantep University / Civil Engineering & Hydraulic Engineering (02/2021-Ongoing)

University Gaziantep University / Civil Engineering (08/2015-01/2020)

High School IMKB Anatolia High School (09/2010-06/2015)

WORK EXPERIENCE

Research Assistance Gaziantep University (02/2021-Working)

PROJECTS

Kopula Fonksiyonları Kullanılarak Orta Fırat, Kızılırmak ve Yeşilırmak Havzalarının Kuraklık Risk Haritalarının Çıkarılması (Prof. Dr. Mehmet İshak YÜCE TUJJB-TÜMEHAP-2020-02)

ARTICLES

1-YÜCE, M. İ., AKSOY, H., AYTEK, A., EŞİT, M., ŞİMŞEK, A., YAŞA, İ., . . . UĞUR, F. (2022/10/15). Kuraklik Parametreleri İçin Spi Ve Spei İndislerini Kullanarak Uygun Dağilimlarin Hesaplanmasi. 11. Ulusal Hidroloji Kongresi, (s. 547 562).

2-YÜCE, M. İ., AKSOY, H., AYTEK, A., EŞİT, M., ŞİMŞEK, A., YAŞA, İ., . . . UĞUR, F. (2022/10/15). Meteorolojik Kuraklik Değerlendirmesi İçin Spi, Spei Ve Rdi İndislerinin Karşilaştirilmasi. 11. Ulusal Hidroloji Kongresi, (s. 607-615).

3-YÜCE, M. İ., AKSOY, H., AYTEK, A., EŞİT, M., UĞUR, F., YAŞA, İ., . . . DEĞER, İ. H. (2022/9/3). SPI ve SPEI ile Samsun İli Kuraklık Analizi. Kahramanmaraş Sütçü İmam Üniversitesi Mühendislik Bilimleri Dergisi, 25(3), 285-2

4- YUCE, M. I., UGUR, F., & SIK, I. (2020/10/15). Hidrokinetik Dikey Eksenli Türbinlerde Debi Değişimlerinin Güç Katsayısına Etkisi. 11. Ulusal Hidroloji Kongresi.. (s.591-597).

5- DEGER, H.I., YUCE, M. I., AYTEK, A., ESIT, M., UGUR, F., SIK, I. (2020/10/15). GAZİANTEP İLİ İÇİN YAĞIŞ ŞİDDET-SÜRE-TEKERRÜR EĞRİLERİNİN TESPİTİ. 11. Ulusal Hidroloji Kongresi. (S.335-341)